Pristine and modified nanoparticles:

Complement activation and immunomodulation

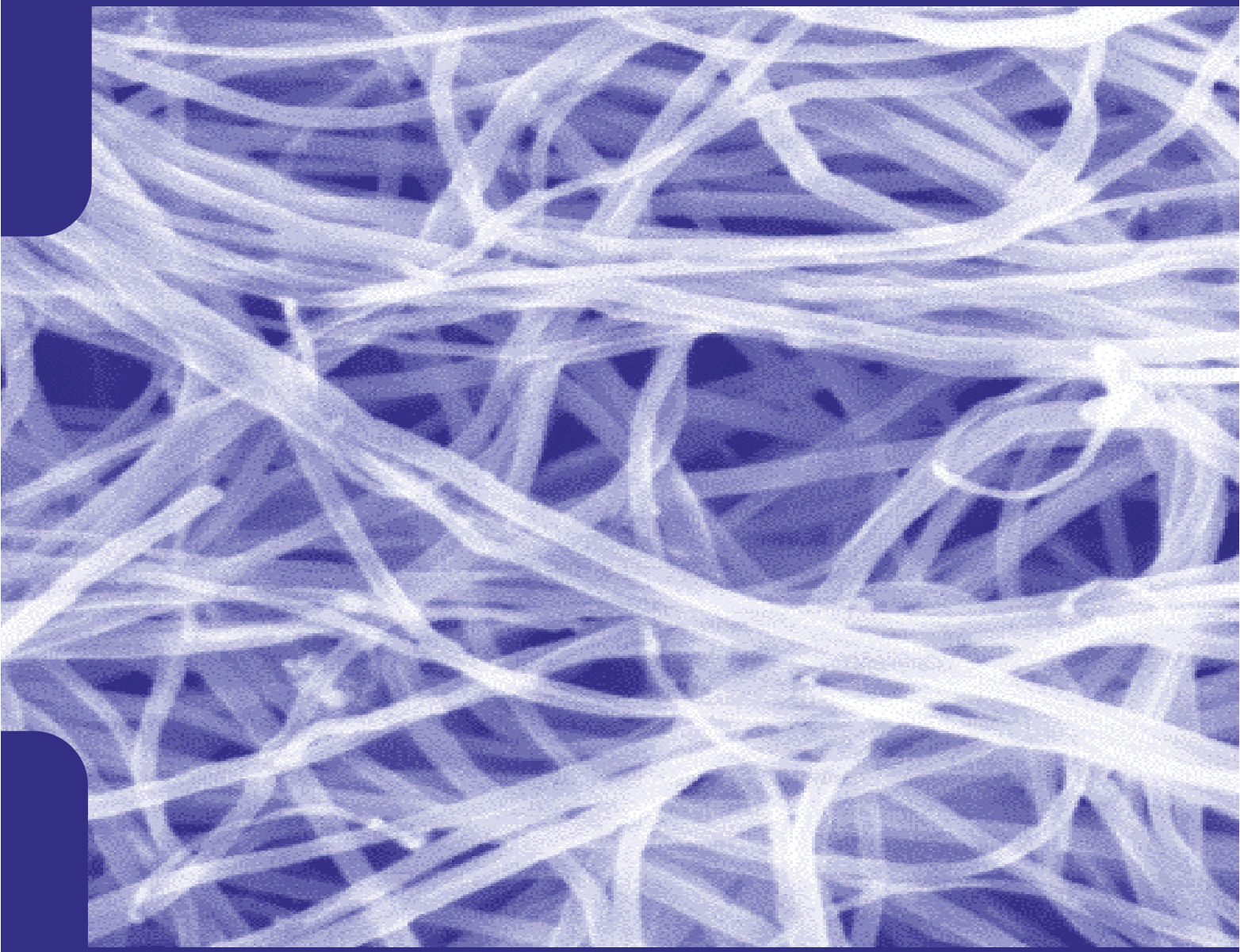

Kirsten Pondman

PRISTINE AND MODIFIED NANOPARTICLES:

COMPLEMENT ACTIVATION AND IMMUNOMODULATION

K.M.Pondman

PhD committee

Prof. dr. ir. J.W.M. Hilgenkamp (voorzitter)	Universiteit Twente
Prof. dr. ir. J.E. ten Elshof (promotor)	Universiteit Twente
Prof. dr. R.B. Sim (promotor)	Oxford University
Dr. ir. B. ten Haken (assistant promotor)	Universiteit Twente
Prof. dr. A. Brinkman	Universiteit Twente
Prof. dr. L. Abelmann	Universiteit Twente
Dr. U. Kishore	Brunel University
Dr. E. Flahaut	Université de Toulouse

Cover page:
High resolution scanning electron microscopy image of pristine multi walled carbon nanotubes. Image obtained by Mark Smithers.

The work described in this thesis was carried out at the faculty of Science and Technology, University of Twente, P.O. Box 217, 7500 AE Enschede, The Netherlands. Part of this research was carried out in the group of professor Robert Sim at Oxford University, Oxford, United Kingdom and the group of Dr. Uday Kishore at Brunel University, London, United Kindom.

K.M.Pondman
Pristine and modified nanoparticles: Complement activation and immunomodulation

PhD Thesis, University of Twente, Enschede, The Netherlands

ISBN: 978-90-365-3728-5
DOI: 10.3990/1.9789036537285
Printed by: Gildeprint drukkerijen (Enschede, The Netherlands)

PRISTINE AND MODIFIED NANOPARTICLES:

COMPLEMENT ACTIVATION AND IMMUNOMODULATION

PROEFSCHRIFT

ter verkrijging van
de graad van doctor aan de Universiteit Twente,
op gezag van de Rector Magnificus, prof.dr. H. Brinksma,
volgens besluit van het College voor Promoties
in het openbaar te verdedigen
op woensdag 10 september 2014, 14.45 uur

door

Kirsten Milou Pondman

geboren op 27 januari 1987
te Utrecht

Dit proefschrift is goedgekeurd door de promotoren
en de assistent-promotor:

Prof. Dr. J.E. ten Elshof
Prof. Dr. R.B. Sim
Dr. B. ten Haken

Contents

Chapter 1

General introduction

1.1 Nanomedicine

Nanomedicine is one of the buzzwords in modern research. The wide field can be roughly split between two extremes, the first are the nano-enthusiastics; who exaggerate the benefits giving the impression that everything will (soon) be possible and every disease will be curable with the use of nanotechnology. The other group are the nano-cautionists; who are very concerned about the risks of nanotechnology, study the harmful effects and try to avoid the widespread use of nanotechnology in medicine until all possible (long term) risks are fully known. The truth lies somewhere in between. Nanotechnology offers many new opportunities in medicine, but in order to implement a technology in clinics the risks should be known and carefully balanced with the benefits of the new technology.

To discuss the possibilities and risks, first a definition of nanomedicine is needed. Although the term nanomedicine has been used for over two decades, only in 2005 was a definition agreed upon in a consensus conference, when the European Science Foundation's (ESF) defined "nanomedicine"[1]:

> *"Nanomedicine uses nano-sized tools for the diagnosis, prevention and treatment of disease and to gain increased understanding of the complex underlying patho-physiology of disease. The ultimate goal is improved quality-of-life."*

This definition however does not define "nano-sized" which is another source of ongoing debate, although the generally accepted definition is that at least one dimension of the structure should be between 1 and 100 nm. Therefore there are nanofilms (1 dimension), nanowires (2 dimensions) and nanoparticles (3 dimensions). With this definition nanoparticles are similar in size to the dimensions of cells, proteins and DNA and are therefore able to perform

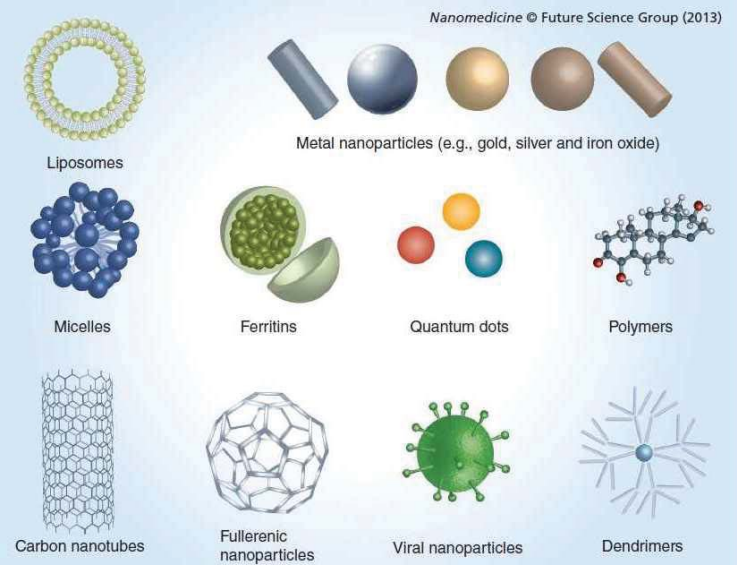

Figure 1.1: Examples of nanoparticles used and proposed for use in biomedical applications. Reproduced from [2].

functions at the very basic levels of biology. This enables for example the delivery of therapeutics at an intracellular level.

Nanoparticles used in biomedicine (figure 1.1) can be divided into hard, solid particles, soft particles and "others". The first category includes all metal and ceramic particles: most famous are gold nanoparticles, magnetic nanoparticles (superparamagnetic iron oxide, SPIO), and carbon nanotubes or fullerenes. Soft particles are formed of polymers, lipids or proteins: examples are liposomes, proteosomes and virus like particles, but also dendrimers can be considered soft nanoparticles. The third category consists of antibody-drug conjugates and composite nanoparticles [3].

In drug delivery the use of nanoparticles continues to grow rapidly. When the nanoparticle/drug complex is optimised, they offer better pharmacokinetic properties, controlled and sustained release and targeting to specific organs, tissues, cells and cell compartments [5]. The main aim in nanotherapeutics is to improve the efficacy of therapeutic agents which are dose-limiting (e.g. toxic) or poorly bioavailable (e.g. poor water solubility or difficult transport through membranes). The treatment of cancer is the main target for nanomedicine, as the disease is usually localised and many of the therapeutics applicable in tumor treatment are highly toxic to the human body, making systemic therapy undesirable.

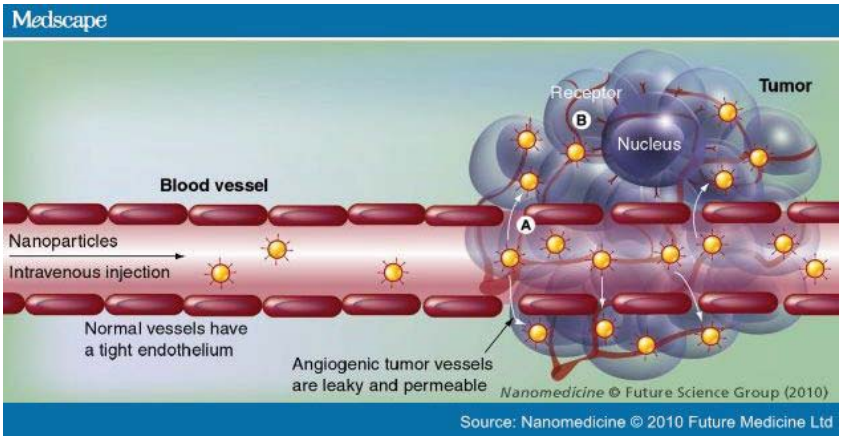

Figure 1.2: Nanoparticle drug targeting to solid tumors. (A) Passive targeted delivery. Nanoparticles accumulate in tumors through permeable tumor vasculature.(B) Active targeted delivery. Ligand-coated nanoparticles bind to a cancer cell receptor (image reproduced from [4]).

Targeting in nanomedicine can be achieved by passive or active strategies (figure 1.2). The passive strategy makes use of the enhanced permeability and retention effect (EPR) caused by tumor angiogenesis, which can also be found in inflammatory diseases. The EPR effect makes the vessels more permeable, allowing passive targeting of diseased areas. There is no set size limit for particles to be used in this method, as fenestrations vary between tumor types, vessel types and the age of the vessels. The reported targeting efficiencies vary between 1-15%, which is similar to reported for random diffusion [6]. A higher efficiency is found in smaller tumors. The reduced effect in larger tumors is related to the closing of fenestrations in aged vessels, or the presence of necrotic regions [7].

Active targeting can be achieved by receptor mediated targeting. This strategy is often considered to "revolutionize cancer treatment" [8], but so far no targeted drug product has been released on the market [3, 9]. Popular receptors for targeting are epidermal growth factor receptors (EGFR). Most famous is the use of HER2; a receptor present in certain breast cancers [10], and the folate receptor (FR) which is often over expressed on tumorous cells [11, 12]. The lack of success of the receptor based strategies can be attributed to the barriers which a particle has to overcome before interaction with the receptor [5, 9]:

- Antibodies used as ligand for the receptor are activators of the immune system, causing the particles to be taken up by macrophages and other immune responsive cells.
- Some receptors are not expressed on the cells lining the vessels, but further inside the tumor tissue and hard to reach.

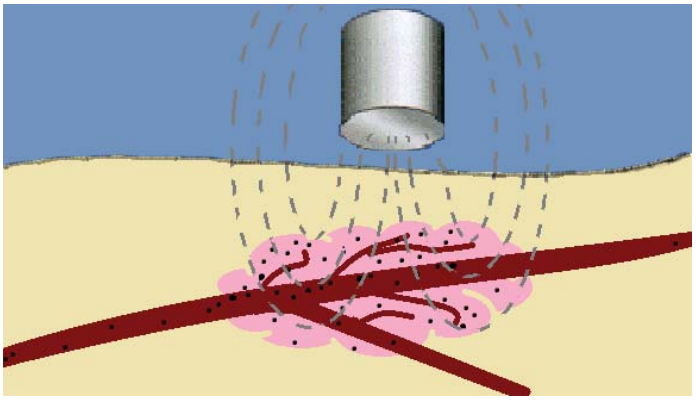

Figure 1.3: In magnetic drug delivery a therapeutic agent is coupled to a magnetic nanoparticle and withdrawn from the blood vessels into the tumor tissue at the target region by an external magnet.

- Receptors can be inhomogeneously distributed, and therefore only part of the tumor cells will be targeted.
- Receptors can be saturated with the ligand before the required drug dose is reached.

To avoid the difficulties with receptor-based strategies other methods are studied. Among these are physical methods to deliver a drug to the target location. An obvious method to achieve this is by injecting the nanoparticle/therapeutic suspension in the target region, but this is not always feasible. Another method is to use liposomes, which can freely flow through the bloodstream and be collapsed at the target location by a directed ultrasound pulse to release the therapeutic contents [13].

The targeting method studied in this thesis is magnetic drug delivery (figure 1.3). In this technique, a drug is coupled to a magnetic particle and injected into blood flow. A magnet located close to the target location is used to capture the particles and therapeutics in the target area. The method has promising results in modeling studies and also some in-vivo results have been published, but no magnetic drug delivery applications are used in clinics today [14–22].

1.2 Carbon nanotubes and nanowires

The majority of nanoparticles used in biomedical applications are spherical, which are the most easily produced. Most chemical synthesis procedures rely on the spontaneous formation of particles in the liquid phase, where spherical particles are most energetically favourable. But spherical nanoparticles have disadvantages, especially in magnetic drug delivery as will

be elaborated later in this thesis. Nanowires and nanorods, with their elongated shape and anisotropic properties, can be used to overcome some of the limitations of spherical particles. Therefore, nanowires are receiving growing attention in biomedicine [23–33].

Carbon nanotubes (CNT) are the most well known elongated nanoparticles. These one-dimensional allotropes of carbon, were first described by Iijima in 1991 [34]. In principle CNTs are rolled hexagonal carbon networks capped by half fullerene molecules. Depending on the number of carbon walls they can be divided in single walled (SWNT), double walled (DWNT) and multi walled (MWNT) CNTs. They come in a variety of lengths and diameters, purities (catalyst contaminants), chiralities (way of rolling of the carbon sheets), and can be coated with a range of different compounds to render them dispersible in liquids.

Due to their many advantageous properties, CNTs have been extensively explored for biological and biomedical applications [35–38], which range from drug delivery, [31, 36–44] to in vivo imaging [45, 46]. At the same time CNTs are considered high risk nanoparticles due to their high aspect ratio and fiber like appearance, similar to asbestos fibers. According to the World Health Organisation (WHO) (1997) definition of fibers, only the longest among CNTs can be classified as a fiber; longer than 5 μm, thinner than 3 μm and with an aspect ratio greater than 3:1. Due to their length, macrophages might not be able to engulf the particles. This can lead to frustrated phagocytosis, or formation of a granuloma around the CNTs. Sometimes, macrophages fuse together to form giant cells that encapsulate the particle, but this strategy is not always sufficient [47].

1.3 Immune system

The effectiveness of nanoparticles as intravenous drug delivery platform is strongly influenced by the immune system. The main function of the immune system is to protect the body against parasites, viruses, fungi, bacteria and pathogens; also other foreign invaders including nanoparticles can be seen as targets. Recognition can lead to rapid elimination of the particles from the systemic circulation. In addition, other functional interactions with the immune system, such as inflammatory responses, should be avoided. Therefore, understanding the interactions between nanoparticles and the immune system is essential for their strategic and specific use in in-vivo delivery [48, 49].

The immune system consists of a complex network of interacting proteins, cells and various other components. The system is divided into the innate immune response (fast responding and with broader specificity) and adaptive immune response (slow responding and of narrower specificity) (figure 1.4). There is a delicate balance in the workings of the innate and adaptive immune system, to avoid the spread of dangerous substances through the body without initiating hypersensitivity or destroying tissue.

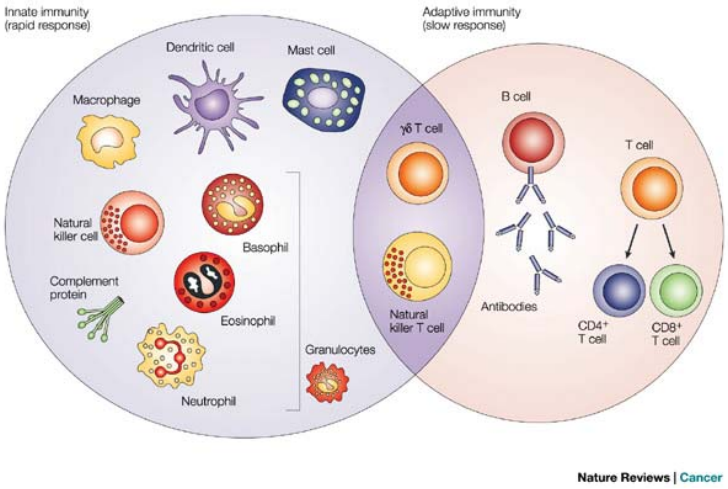

Figure 1.4: The immune system can be divided in two interacting parts, the innate (fast responding and with broader specificity) and adaptive (slow responding and of narrower specificity) immune response (image reproduced from [50]).

The innate immune response is described in detail in chapter 2. In short, the response is initialised by opsonisation of the foreign particle by proteins of the complement system, through one of three pathways (classical, alternative or lectin pathway). Recognition by the first immune cells leads to migration and activation of more phagocytic cells; leukocytes, macrophages and dendritic cells (DCs). Phagocytosis can occur after opsonisation, it can also be induced more directly through interactions of the foreign particle with Toll-like receptors (TLRs) on macrophages or neutrophils [47]. Phagocytosis can either be the end stage of the immune response, or it can initiate the directed activation and maturation of an immature DC towards antigen presenting cell (APC). APCs migrate towards lymph nodes where they activate T-lymphocytes, with the specific receptors for the presented epitope [51].

T-lymphocytes can be distinguished by the presence of CD4 and CD8 (cluster of differentiation) on the cell surface. CD8 positive cells are cytotoxic T-cells (Tc), specialized in killing cells. CD4 positive cells are helper T-cells (Th) , which help activate the Tc and immature B-lymphocytes to become antibody producing cells or memory B-cells. Th-cells and their cytokines can be subdivided into Th1 and Th2. Th1-cytokines induce pro-inflammatory responses, Th1 cells are triggered by interleukins (IL)-2 and IL-12 and produce IFN-α. Th2 cytokines include IL-4, IL-5 and IL-13 which promote synthesis of IgE and eosinophilic responses and IL-10 which has an anti-inflammatory response. Excessive pro-inflammatory responses can lead to tissue damage, and too much Th2 response leads to atopy (allergic

response). Therefore Th1 and Th2 response have to be well balanced to give a suited immune response [52].

Nanoparticle recognition and clearance by the immune system can occur almost everywhere in the body. In the bloodstream particles are taken up by monocytes, platelets, neutrophils and DCs. In tissues they can be filtered out by resident phagocytes in the liver (Kupffer cells), spleen (macrophages and B-cells) and lymph nodes (DCs and B-cells). Both innate and adaptive immune responses are involved in the clearance process. In this thesis mainly the interactions between nanoparticles and the innate immune system in the bloodstream are studied, because this part of the immune system will be the first to interact with nanoparticles and is likely to have the greatest influence.

1.4 Thesis scope and outline

This thesis combines the development of new nanoparticles for magnetic drug delivery, with the careful characterisation of the response of the immune system towards pristine and coated CNTs and magnetic nanowires. In the study of the immune system the focus lies with the innate immune system and the way the response of the complement system influences further immune response.

Chapter 2 provides an overview of the available literature on interactions between the innate immune system and CNTs. This overview gives an insight in the extent of activation of the innate immune system and its possible effects on inflammation and application of CNTs in biomedical applications. In **chapter 3** we study the pathways involved in the activation of the complement system by pristine and functionalized CNTs. As described above, activation of the complement system is generally considered to have an adverse effect. However, we show that complement activation by CNTs can have a positive effect on their uptake by phagocytes and subsequent immune response of the cells.

In **chapter 4** a novel Au-Ni nanowire is developed which is optimised for use in magnetic drug delivery applications. The Au-Ni nanowire is fully characterised and tested for cytotoxicity. These Au-Ni nanowires activate complement very poorly as opposed to strongly complement activating CNTs. In **chapter 5** we show that this difference in complement activation impacts upon phagocytosis and immune response by U937 (macrophage), Raji (B-cell) and Jurkat (T-cell) cells. In order to understand the effects of individual complement proteins, in **chapter 6** we examine the effect of pre-coating CNTs with factor H, C1q, and its individual recombinant globular head regions on the immune response towards the CNTs. These results have implications on regulating complement activation prior to designing therapeutic strategies based on nanoparticles.

Chapter 7 is dedicated to an application of nanomedicine: magnetic drug delivery using elongated nanoparticles. First the properties of magnetic nanowires are examined in detail. Both the behaviour of the magnetisation of the particle and the forces needed to trap the particle using an external magnetic field are evaluated. This knowledge is used to develop a magnetic FePd nanowire in combination with a magnet able to trap the nanoparticles from the flow of blood. The FePd nanowire is optimised and tested for biocompatibility with respect to size, cytotoxicity and avoidance of complement activation. The designed magnet is applied in an animal study, but can also be scaled up to be used in a clinical setting.

Chapter 8 provides general conclusions and perspectives of the results presented in this thesis.

References

[1] ESF, "European Science foundation's forward look nanomedicine: an EMRC Concensus Opinion," 2005.

[2] Y. Ding, S. Li, and G. Nie, "Nanotechnological strategies for therapeutic targeting of tumor vasculature.," *Nanomedicine (London, England)*, vol. 8, pp. 1209–22, July 2013.

[3] C. A. Schütz, L. Juillerat-Jeanneret, H. Mueller, I. Lynch, and M. Riediker, "Therapeutic nanoparticles in clinics and under clinical evaluation.," *Nanomedicine (London, England)*, vol. 8, pp. 449–67, Mar. 2013.

[4] X. Dong and R. J. Mumper, "Nanomedicinal strategies to treat multidrug-resistant tumors: current progress.," *Nanomedicine (London, England)*, vol. 5, pp. 597–615, June 2010.

[5] Y. Malam, E. J. Lim, and A. M. Seifalian, "Current Trends in the Application of Nanoparticles in Drug Delivery.," *Current medicinal chemistry*, vol. 18, no. 7, pp. 1067–1078, 2011.

[6] M. A. Phillips, M. L. Gran, and N. A. Peppas, "Targeted nanodelivery of drugs and diagnostics," *Nano Today*, vol. 5, no. 2, pp. 143–159, 2010.

[7] K. J. Harrington, S. Mohammadtaghi, P. S. Uster, D. Glass, A. M. Peters, R. G. Vile, and J. S. Stewart, "Effective targeting of solid tumors in patients with locally advanced cancers by radiolabeled pegylated liposomes," *ACS Clinical cancer research*, vol. 7, pp. 243–254, 2001.

[8] J. D. Byrne, T. Betancourt, and L. Brannon-Peppas, "Active targeting schemes for nanoparticle systems in cancer therapeutics," *Advanced Drug Delivery Reviews*, vol. 60, pp. 1615–1626, 2008.

[9] R. Duncan and R. Gaspar, "Nanomedicine(s) under the microscope," *Molecular pharmaceutics*, vol. 8, pp. 2101–41, 2011.

[10] H. Wartlick, K. Michaelis, S. Balthasar, K. Strebhardt, J. Kreuter, and K. Langer, "Highly specific HER2-mediated cellular uptake of antibody-modified nanoparticles in tumour cells.," *Journal of drug targeting*, vol. 12, pp. 461–471, 2004.

[11] B. Stella, S. Arpicco, M. T. Peracchia, D. Desmaële, J. Hoebeke, M. Renoir, J. D'Angelo, L. Cattel, and P. Couvreur, "Design of folic acid-conjugated nanoparticles for drug targeting.," *Journal of pharmaceutical sciences*, vol. 89, pp. 1452–1464, 2000.

[12] S. A. Kularatne and P. S. Low, "Targeting of nanoparticles: folate receptor.," *Methods in molecular biology*, vol. 624, pp. 249–265, 2010.

[13] A. Schroeder, J. Kost, and Y. Barenholz, "Ultrasound, liposomes, and drug delivery: principles for using ultrasound to control the release of drugs from liposomes,"

Chemistry and Physics of Lipids, vol. 162, pp. 1–16, 2009.

[14] Y. Hirota, Y. Akiyama, Y. Izumi, and S. Nishijima, "Fundamental study for development magnetic drug delivery system," *Physica C: Superconductivity*, vol. 469, pp. 1853–1856, Oct. 2009.

[15] H. Xu, T. Song, X. Bao, and L. Hu, "Site-directed research of magnetic nanoparticles in magnetic drug targeting," *Journal of Magnetism and Magnetic Materials*, vol. 293, pp. 514–519, May 2005.

[16] O. Mykhaylyk, N. Dudchenko, and A. Dudchenko, "Doxorubicin magnetic conjugate targeting upon intravenous injection into mice: High gradient magnetic field inhibits the clearance of nanoparticles from the blood," *Journal of Magnetism and Magnetic Materials*, vol. 293, pp. 473–482, May 2005.

[17] C. Alexiou, W. Arnold, R. J. Klein, F. G. Parak, P. Hulin, C. Bergemann, W. Erhardt, S. Wagenpfeil, and a. S. Lübbe, "Locoregional cancer treatment with magnetic drug targeting.," *Cancer research*, vol. 60, pp. 6641–8, Dec. 2000.

[18] C. Alexiou, R. Jurgons, R. Schmid, A. Hilpert, C. Bergemann, F. Parak, and H. Iro, "In vitro and in vivo investigations of targeted chemotherapy with magnetic nanoparticles," *Journal of Magnetism and Magnetic Materials*, vol. 293, pp. 389–393, 2005.

[19] S. Goodwin, C. Peterson, C. Hoh, and C. Bittner, "Targeting and retention of magnetic targeted carriers (MTCs) enhancing intra-arterial chemotherapy," *Journal of Magnetism and Magnetic Materials*, vol. 194, pp. 132–139, Apr. 1999.

[20] A. S. Lübbe, C. Bergemann, W. Huhnt, T. Fricke, and H. Riess, "Predinical Experiences Drug Targeting : Tolerance and Efficacy," *Cancer research*, vol. 56, pp. 4694–4701, 1996.

[21] Y. Yoshida, S. Fukui, S. Fujimoto, F. Mishima, S. Takeda, Y. Izumi, S. Ohtani, Y. Fujitani, and S. Nishijima, "Ex vivo investigation of magnetically targeted drug delivery system," *Journal of Magnetism and Magnetic Materials*, vol. 310, pp. 2880–2882, Mar. 2007.

[22] J. . A. Dobson, "Magnetic Nanoparticles for Drug Delivery," *Drug development research*, vol. 60, pp. 55–60, 2006.

[23] A. Hultgren, M. Tanase, C. S. Chen, G. J. Meyer, D. H. Reich, and L. A. Bauer, "Cell manipulation using magnetic nanowires," *Journal of Applied Physics*, vol. 93, no. 10, pp. 7275–7280, 2003.

[24] A. Prina-Mello, Z. Diao, and J. M. D. Coey, "Internalization of ferromagnetic nanowires by different living cells.," *Journal of nanobiotechnology*, vol. 4, p. 9, Jan. 2006.

[25] A. O. Fung, V. Kapadia, E. Pierstorff, D. Ho, and Y. Chen, "Induction of cell death by magnetic actuation of nickel nanowires internalized by fibroblasts," *Journal of Physical Chemistry C*, vol. 112, no. 39, pp. 15085–15088, 2008.

[26] F. K. Keating, M. K. Fung, and D. J. Schneider, "Induction of platelet white blood cell (WBC) aggregate formation by platelets and WBCs in red blood cell units," *Transfusion*, vol. 48, no. 6, pp. 1099–1105, 2008.

[27] Q. I. N. Hu, Y. Q. I. LIU, N. Li, C. Cheng, S. G. Xu, N. Wang, W. E. I. Qin, and B. Z. E. N. Z. TANG, "Ni-NTA-Coated nanowire materials for protein enrichment and the application in a medical device used for blood glucose degradation," *Nano*, vol. 8, no. 3, p. 1350029, 2013.

[28] K. M. Pondman, A. W. Maijenburg, F. B. Celikkol, A. A. Pathan, U. Kishore, B. ten Haken, and J. E. ten Elshof, "Au coated Ni nanowires with tuneable dimensions for biomedical applications.," *Journal of Materials Chemistry B*, vol. 1, pp. 6129–6136, 2013.

[29] N. Sinha and J. T. Yeow, "Carbon nanotubes for biomedical applications," *IEEE Trans Nanobioscience*, vol. 4, no. 2, pp. 180–195, 2005.

[30] A. Bianco, K. Kostarelos, C. D. Partidos, and M. Prato, "Biomedical applications of functionalised carbon nanotubes," *Chemical Communications*, no. 5, pp. 571–577, 2005.

[31] C. Biale, V. Mussi, U. Valbusa, S. Visentin, G. Viscardi, N. Barbero, N. Pedemonte, and L. Galietta, "Carbon nanotubes for targeted drug delivery," *2009 9th Ieee Conference on Nanotechnology*, pp. 644–646, 2009.

[32] B. Panchapakesan, B. Book-Newell, P. Sethu, M. Rao, and J. Irudayaraj, "Gold nanoprobes for theranostics.," *Nanomedicine (London, England)*, vol. 6, pp. 1787–811, Dec. 2011.

[33] Z. Zhang, J. Wang, and C. Chen, "Gold nanorods based platforms for light-mediated theranostics.," *Theranostics*, vol. 3, pp. 223–38, Jan. 2013.

[34] K. Morito, T. Hirose, J. Kinjo, T. Hirakawa, M. Okawa, T. Nohara, S. Ogawa, S. Inoue, M. Muramatsu, and Y. Masamune, "Interaction of phytoestrogens with estrogen receptors alpha and beta.," *Biological & pharmaceutical bulletin*, vol. 24, pp. 351–6, Apr. 2001.

[35] L.-H. Liu, H. Dietsch, P. Schurtenberger, and M. Yan, "Photoinitiated coupling of unmodified monosaccharides to iron oxide nanoparticles for sensing proteins and bacteria.," *Bioconjugate chemistry*, vol. 20, pp. 1349–55, July 2009.

[36] A. Bianco, K. Kostarelos, and M. Prato, "Applications of carbon nanotubes in drug delivery," *Current Opinion in Chemical Biology*, vol. 9, pp. 674–679, Dec. 2005.

[37] M. Foldvari and M. Bagonluri, "Carbon nanotubes as functional excipients for nanomedicines: II. Drug delivery and biocompatibility issues.," *Nanomedicine : nanotechnology, biology, and medicine*, vol. 4, pp. 183–200, Sept. 2008.

[38] M. Foldvari and M. Bagonluri, "Carbon nanotubes as functional excipients for nanomedicines: I. Pharmaceutical properties.," *Nanomedicine : nanotechnology, biology, and medicine*, vol. 4, pp. 173–82, Sept. 2008.

[39] R. Klingeler, S. Hampel, and B. Buchner, "Carbon nanotube based biomedical agents for heating, temperature sensoring and drug delivery," *International journal of hyperthermia*, vol. 24, no. 6, pp. 496–505., 2008.

[40] A. Bianco, J. Hoebeke, S. Godefroy, O. Chaloin, D. Pantarotto, J.-P. Briand, S. Muller, M. Prato, and C. D. Partidos, "Cationic carbon nanotubes bind to CpG oligodeoxynucleotides and enhance their immunostimulatory properties.," *Journal of the American Chemical Society*, vol. 127, pp. 58–9, Jan. 2005.

[41] H. Ali-Boucetta, K. T. Al-Jamal, D. McCarthy, M. Prato, A. Bianco, and K. Kostarelos, "Multiwalled carbon nanotube-doxorubicin supramolecular complexes for cancer therapeutics.," *Chemical communications*, pp. 459–61, Jan. 2008.

[42] E. Heister, V. Neves, C. Tîlmaciu, K. Lipert, V. S. Beltrán, H. M. Coley, S. R. P. Silva, and J. McFadden, "Triple functionalisation of single-walled carbon nanotubes with doxorubicin, a monoclonal antibody, and a fluorescent marker for targeted cancer therapy," *Carbon*, vol. 47, no. 9, pp. 2152–2160, 2009.

[43] W. Wu, S. Wieckowski, G. Pastorin, M. Benincasa, C. Klumpp, J. P. Briand, R. Gennaro, M. Prato, and A. Bianco, "Targeted delivery of amphotericin B to cells by using functionalized carbon nanotubes," *Angewandte Chemie-International Edition*, vol. 44, no. 39, pp. 6358–6362, 2005.

[44] L. Lacerda, A. Bianco, M. Prato, and K. Kostarelos, "Carbon nanotubes as nanomedicines: from toxicology to pharmacology," *Advanced Drug Delivery Reviews*, vol. 58, pp. 1460–1470, Dec. 2006.

[45] J. Robinson, K. Welsher, S. Tabakman, S. Sherlock, H. Wang, R. Luong, and H. Dai, "High performance in vivo near-IR imaging and photothermal cancer therapy with carbon nanotubes," *Nano Research*, vol. 3, pp. 779–793, 2010.

[46] K. Welsher, S. P. Sherlock, and H. Dai, "Deep-tissue anatomical imaging of mice using carbon nanotube fluorophores in the second near-infrared window.," *Proceedings of the National Academy of Sciences of the United States of America*, vol. 108, pp. 8943–8948,

2011.

[47] K. Bhattacharya, F. T. Andon, R. El-Sayed, and B. Fadeel, "Mechanisms of carbon nanotube-induced toxicity: Focus on pulmonary inflammation," *Advanced Drug Delivery Reviews*, vol. 65, no. 15, pp. 2087–209, 2013.

[48] S. Hussain, J. A. J. Vanoirbeek, and P. H. M. Hoet, "Interactions of nanomaterials with the immune system," *Wiley Interdisciplinary Reviews-Nanomedicine and Nanobiotechnology*, vol. 4, no. 2, pp. 169–183, 2012.

[49] B. S. Zolnik, A. Gonzalez-Fernandez, N. Sadrieh, and M. A. Dobrovolskaia, "Minireview: Nanoparticles and the Immune System," *Endocrinology*, vol. 151, no. 2, pp. 458–465, 2010.

[50] G. Dranoff, "Cytokines in cancer pathogenesis and cancer therapy.," *Nature reviews. Cancer*, vol. 4, pp. 11–22, 2004.

[51] J. Leleux and K. Roy, "Micro and nanoparticle-based delivery systems for vaccine immunotherapy: an immunological and materials perspective.," *Advanced healthcare materials*, vol. 2, pp. 72–94, Jan. 2013.

[52] A. Berger, "Th1 and Th2 responses: what are they?," *British medical journal*, vol. 321, p. 424, Aug. 2000.

Chapter 2

Interactions of the innate immune system with carbon nanotubes[1]

Abstract

The therapeutic application of nanoparticles requires that the nanoparticles are amenable to alteration in their intended target and fate in the body. The innate immune system is likely to be the first defence machinery that would recognise the nanoparticles as non-self. A number of studies have addressed the issue of how CNTs are dealt with by phagocytic cells, their surface receptors and intracellular processing. Recent establishment of their interaction with the complement system, the most potent and versatile innate immune mechanism, has shed interesting light on how complement activation can modulate phagocytosis and cytokine response to CNT challenge. The charge or altered molecular pattern on the surface of nanoparticles due to functionalization and derivatisation dictates the level of complement activation and subsequent handling and immune response by immune cells. Recent data appear to suggest that complement deposition may facilitate phagocytic uptake of CNTs and dampen pro-inflammatory response.

[1] The contents of this chapter are in preparation for publication as KM Pondman, M Sobik, RB Sim, U Kishore, "Interactions of the innate immune system with carbon nanotubes"

2.1 CNT characteristics and applications

Since lijima described their synthesis in 1991 [1], carbon nanotube (CNT)-based nanotechnology has rapidly emerged as a platform for a variety of uses, including many biomedical applications [2]. CNTs can be described as cylindrical tubes, composed of rolled graphene, with the carbon atoms hybridized in hexagonal sp2 arrangement. Depending on the number of concentric carbon tubes they can be divided into single-walled (SWNT), double-walled (DWNT) and multi-walled (MWNT) carbon nanotubes (figure 2.1). A principal characteristic is their high aspect ratio, resulting from their small diameter (1-3 nm for SWNT up to 2-100 nm for MWNTs) and extended length (up to 500 μm), which is a direct result from their method of synthesis. CNTs are grown on a substrate, either with or without (metallic) catalyst particles; the preparation methods include arc discharge, laser ablation and chemical vapour deposition (figure 2.2) [3].

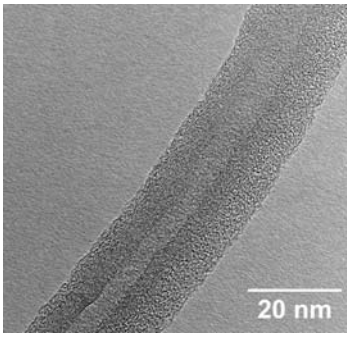

Figure 2.1: TEM micrograph of MWNTs, clearly showing the high number of concentric carbon sidewalls and a 5 nm inner tube diameter. The outer walls off the MWNT are undamaged.

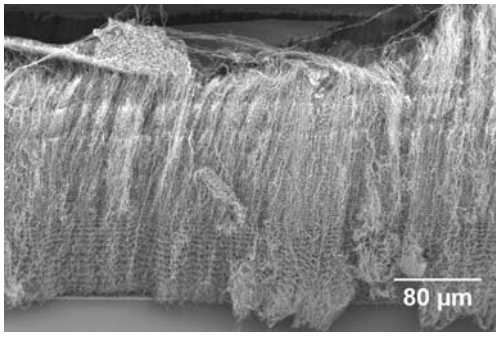

Figure 2.2: SEM micrograph of "as grown" MWNTs on a surface, also known as nanotube forest grown by chemical vapour deposition. These MWNTs are approximately 300 m in length and 50 nm in diameter. On the top a remainder of the catalyst layer can be seen.

Biomedical applications of CNTs include drug delivery [4–9], immunoassays [10], scaffolds [11, 12]. In combination with magnetic filling or particles CNTs can be used as MRI contrast agent [13–18], and in hyperthermia treatment [19, 20]. As their most promising application, CNTs in drug delivery have been reviewed extensively elsewhere [4, 21–24]. The large surface area of CNTs offers a substantially higher drug loading compared to other nanoparticles, while the dimensions of CNTs allow for entry in the smallest capillaries. Essential in targeted drug delivery is also the fact that CNTs are able to cross the cell and nuclear membrane [25–28]. Pharmaceuticals can be either entrapped inside the CNTs [29], or absorbed or attached on the surface [7, 8, 30]. Using these methods, CNTs have been shown to be versatile carriers for drugs [7–9, 21, 22, 30–35], genes [36], proteins [37] and peptides [26]. The drugs can, in principle, be intelligently delivered to specific targets (e.g. tumours) by attaching target-specific molecules (e.g. antibodies) [38, 39].

In order to be used for a variety of applications, CNTs have to be individually dispersed in physiological buffers. Owing to their hydrophobicity, strong $\pi - \pi$ interactions and length, CNTs are prone to rope and cluster formation, therefore, functionalizing or coating CNTs is essential [40]. Non-covalent modifications of the CNT surfaces include pre-coating with proteins [41], surfactants [42], polymers [43] and nucleic acids [44]. Covalent functionalization involves introducing new functional groups on the external walls, usually beginning with the oxidation of the walls creating defects and carboxyl groups [45]. The biocompatibility of CNTs can be significantly improved when their surfaces are functionalized [31, 46–49].

In all biomedical applications, contact between CNTs and blood or tissues is unavoidable, and, hence, an encounter with the immune system. These interactions may lead to severe inflammatory responses and tissue damage [50] and may interfere with the tissue targeting or intended application of the CNTs. It is, therefore, essential to study and understand the interactions between CNTs and all components of the immune response system. In this review, we focus on interactions of CNTs with the innate immune system, body's first line of defence, which is the first immune wing likely to have the largest influence on host-CNT interaction.

2.2 The innate immune system

The immune system is responsible for protection against micro-organisms (bacteria, fungi, viruses and parasites). In addition, altered or damaged cells and tissues are also cleared via the cellular and molecular immune components. Recognition of these altered self or non-self (e.g nanoparticles) is mediated by specific proteins, which bind to their targets and trigger downstream effector functions with the goal of eliminating the imminent danger to homeostasis. The human immune system consists of a complex conglomeration of inter-

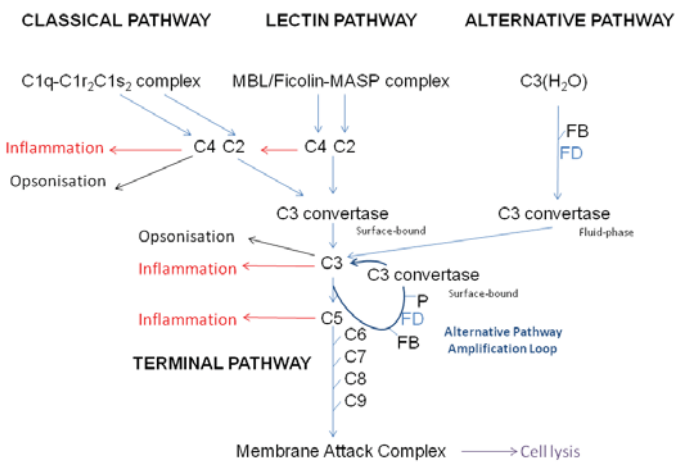

Figure 2.3: Pathways of the complement system. (Image reproduced from [50]) The three complement pathways: classical pathway, lectin pathway and alternative pathway, have different recognition strategies. The classical pathway starts with binding of C1q onto the target, the lectin pathway with analogous MBL and the alternative pathway with spontaneous lysis of C3. All pathways converge at the formation of C3 convertase and result in the formation of the membrane attack complex.

acting proteins, cells and various other components. In order to enhance short and long term efficiency of the clearance mechanisms, the immune system operates via two wings: innate immunity (rapid and broadly specific) and adaptive immunity (slow and narrowly specific). The innate immune system is governed by proteins, always present in the blood, body fluids and tissues, while in adaptive immunity new recognition proteins (e.g. antibodies) are generated specifically towards a newly presented threat.

The innate immune system response involves opsonisation of the pathogen by proteins of the complement system, migration and activation of phagocytic cells, mainly macrophages and immature dendritic cells (iDCs). The complement system consist of more than 40 soluble and cell surface proteins, working together via three activation pathways in order to recognise and opsonise foreign and altered-self components (figure 2.3) [51]. The recognition proteins of the complement system work through multiple low-affinity binding. A single binding between the recognition protein with its target, which can be a molecular motif such as a charge cluster, single neutral sugar, vicinal hydroxyl groups or a single acetyl group, is not strong enough to hold the target and protein together. Therefore, the recognition proteins have a multimeric structure with multiple contact/binding sites. The complement cascade is only activated when multiple bonds are formed allowing for a strong interaction.

The classical pathway is initiated by C1q (figure 2.4), a charge pattern recognition protein (460 kDa), consisting of 18 homologous polypeptide chains (6A, 6B and 6C chains) each consisting of a short N-terminal region, followed by a collagen like region with repeating

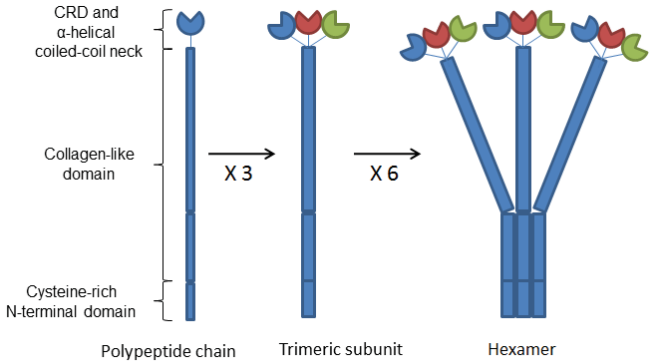

Figure 2.4: C1q is a charge pattern recognition protein (460 kDa), consisting of 18 homologous polypeptide chains (6A, 6B and 6C chains) with by a collagen like region (N terminal) with repeating Gly-X-Yaa triplets, and a globular head domain (C terminal), which bind to charge clusters or hydrophobic patches on targets. Each trimeric subunit has three globular head domains, called ghA, ghb, ghC. Image adapted from [50]

Gly-X-Yaa triplets, and a globular head domain (C terminal). The globular head domain binds to charge clusters or hydrophobic patches on targets [52]. In the lectin pathway, the recognition protein is mannose binding lectin (MBL), which mainly binds to vicinal diols on sugars, as mannose, fucose or glucosamine, or one of the three ficolins (L-,H- and M-ficolin) [50]. After binding of C1q to its targets, proteases C1r and C1s are activated (in case of MBL and ficolins, MASP-2 is activated), which in turn activate C4 and C2 forming C3 convertase (C4b2a), which cleaves C3 to form C3b, which then binds to the target particle. C3b interacts with C3b receptors on phagocytic cells but also is a binding site for C5, which is activated by the same protease which cleaves C3, and then forms a complex with C6, C7, C8 and C9 (C5-9), called membrane attack complex (MAC), which disrupts the lipid bilayer of cells [50].

The alternative pathway is involves a constant slow hydrolysis of C3 in solution, which forms C3(H2O), and alters the shape of the protein. This conformational chance allows the formation of a complex between factor B and C3(H2O), this complex allows factor D to cleave the bound factor B into Ba, which is removed and Bb, which remains bound. This leads to a coating of the particle with C3bBb, which can be further stabilized by properdin (factor P) to C3bBbP. This protein is an enzyme able to generate more C3b to bind, therefore the amplification mechanism needs to be balanced by down regulators: Factor H binds to C3b inhibiting C3 convertase formation, together with factor I it cleaves C3b to iC3b, which is unable to form C3bBb [50, 53, 54]. After the complement proteins have marked a particle (opsonisation), it is followed by interactions with cell bound receptors (e.g. red blood cells

through CR1/CR35) and phagocytosis (via CR3 and CR4). Once immature DCs ingest an antigen, they undergo a directed activation and maturation towards becoming a potent antigen presenting cell (APC), after which they migrate towards lymph nodes. This makes APCs the main link between the innate and adaptive immune system, as they provide signals for T-lymphocytes with the specific receptors for the presented epitope to become activated [55].

2.3 Interactions of CNTs with human plasma proteins

CNTs do not only interact with components of the immune system but also show highly specific interactions with other soluble plasma proteins. The bound proteins form a corona, which plays an important role in determining the effective size, surface charge, physico-chemical properties and aggregation state of the nanoparticles. In addition, it changes the recognition patterns, possibly presenting novel peptide motifs to the immune system and can, therefore, alter the nature of interaction with the complement system, cells and ultimately immune response and bio-distribution [56–58]. The composition of the protein corona changes with time depending on the binding affinities and stoichiometries of the particles and proteins. Affinities can be affected by surface properties such as available functional groups, but also the surface area and curvature. In general, a nanoparticle will be first covered by the most abundant plasma proteins (e.g. albumin and fibrinogen). These proteins are then replaced by proteins with higher affinity towards the particle surface (figure 2.5), a process called the "Vroman effect" [59–61]. The initial coating on the CNT can influence the binding of proteins, as some proteins have affinities towards e.g. charge, hydrophilicity, nucleic acids or carboxyl groups [61].

Oxidation of CNTs offers a more negatively charged surface and bind therefore more protein (figure 2.6) [63, 64]. Shannahan et al [64] performed an extensive proteomics study to identify the proteins in the corona of SWNTs (1 nm) and MWNTs (20-30 nm) unmodified, PVP (Polyvinylpyrrolidone) coated or oxidised. All CNT coronas contained 14 common proteins: serum albumin, titin, apolipoprotein-A-I, apolipoprotein A-II, α1-antiproteinase, α2-HS-glycoprotein, α-S1-casein and keratin. A much larger variety of proteins was found to bind only onto specific types of CNTs. A similar binding profile was found by Salvador-Morales et al, but they found more albumin bound to MWNTs and hypothesized that the plasma could enter the larger diameter MWNTs by capillary forces; these entrapped proteins are likely to be difficult to wash out [62, 65]. Cai et al showed larger diameter CNTs are able to bind a wide range of proteins on their surfaces, although increasing the diameter above 20 nm did not have any additional effect [66].

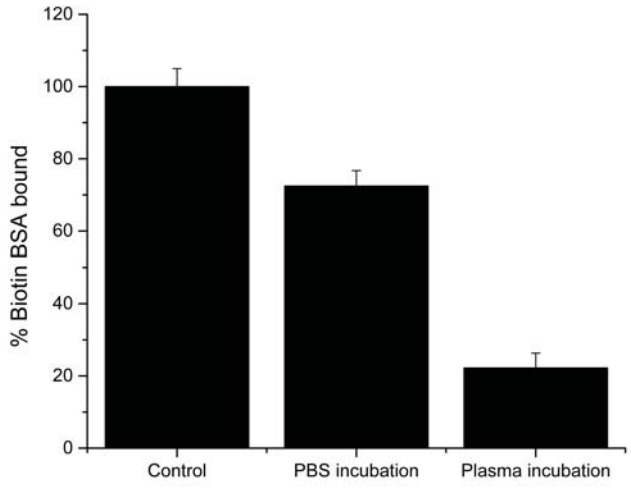

Figure 2.5: Biotinylated BSA was adsorbed onto DWNTs, which were subsequently dispersed in between sepharose beads. The DWNTs were washed extensively in PBS (Flow through OD280 $<$ 0.02) and amount of biotin was quantified. Thereafter biotin-BSA coated DWNTs in sepharose were incubated for 30 min in PBS or plasma followed by washing (flow through OD280 $<$ 0.02) and biotin was again quantified. Instability of the coating can be seen from a significant reduction in biotin in both PBS and especially plasma incubated samples. Experiments were performed in triplicates, error bars indicate $\pm$ standard deviation.

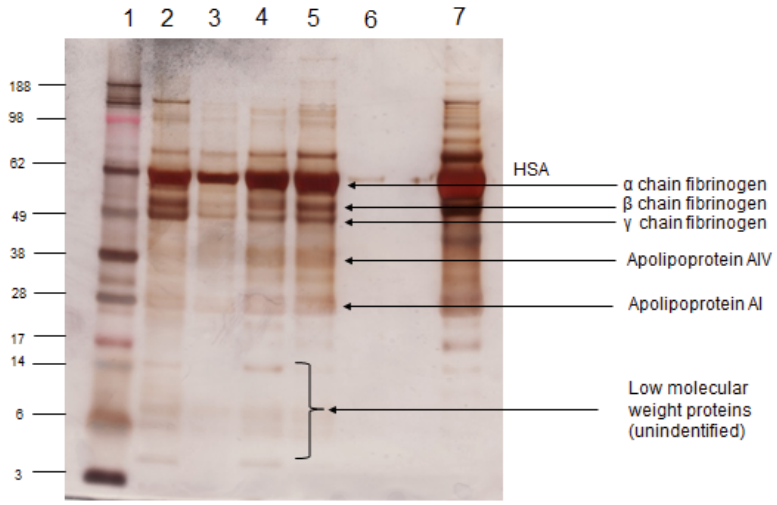

Figure 2.6: Human plasma proteins bind selectively to DWNTs. Samples of CNTs incubated with human plasma and washed were analyzed by SDS-PAGE in reduced conditions. Lane 1 Molecular weight marker, lane 2 human plasma proteins bound to highly oxidized DWNTs, lane 3 human plasma proteins bound to less oxidized DWNTs, lane 4 human plasma proteins bound to pristine DWNTs (1st batch), lane 5 human plasma proteins bound to pristine DWNTs (2nd batch), lane 6 control human plasma proteins bound to Sepharose, used as a carrier for DWNTs during incubation and washing, lane 7 human plasma. Protein bands were stained using a BioRad Silverstain Kit. The method used is described in [62] reproduced from [63]

2.4 Complement absorption and activation

As described above, certain components of the corona, opsonins, which include IgG, complement proteins and fibrinogen may enhance uptake of the material by macrophages and other cells of the reticulo-endothelial system [46]. The importance of complement activation by nanoparticles used in drug targeting was highlighted by a study on nanoliposome-encapsulated-doxirubicin. After hypersensitivity was reported in clinical application of these particles, it was shown that these side effects were caused by complement activation [67]. Complement proteins C1q, C3 and C3d were seen to bind to CNTs especially oxidised CNTs by SDS-PAGE and western blotting (figure 2.7). The complement proteins were concentrated on the CNTs indicating that the binding is specific. But specific binding does not necessary imply activation of the complement system.

Previous studies have shown that non-functionalized CNTs, when placed in contact with human serum, activate complement via the classical and (to a lesser extent) via the alternative pathway [62, 65]. Still the mode of binding of the recognition proteins to the CNTs has not fully been characterised and questions remain whether complement proteins bind directly to the CNTs or bind via other deposited (serum) proteins that can act as adaptors. Complement proteins C1q and MBL, as well as C-reactive protein, an acute phase protein and adaptor for C1q, are known to recognise repetitive structures or charge patterns, which are not found on pristine CNTs but commonly found on the surface of functionalized CNTs [68]. Ling et al [69] have recently shown that C1q "crystallizes" on pristine and functionalized CNTs, but is not bound in a way that allows it to activate the next step of the complement cascade. Other serum proteins thus have to form a stable layer on the CNTs, for indirect C1 binding and subsequent complement activation. Others [62, 65, 70], however, observed direct high affinity binding of C1q to CNTs by hydrophobic interactions, and concluded that direct binding of C1 would allow complement activation. Binding of C1q onto CNTs is not ionic or Calcium-ion-dependent and is of high affinity since denaturation of C1q is required to remove the C1q from the CNTs [71].

Recombinant forms of individual globular head regions of C1q A, B and C chains can be bound to pristine, oxidised and carboxymethyl cellulose coated MWNTs [70, 72], confirming that the binding is through the globular head regions, which is the ligand recognition domain of C1q [73]. Binding of C1 is followed by activation of C4 and C2, but activation may not go beyond that due to the lack of suitable covalent binding (OH, NH_2 or SH) sites for C4b or C3b [62]. However, it has been shown [70] that C3 and C5 turnover did occur with pristine and various protein coated CNTs and, therefore, it is likely that MAC is formed. This was confirmed by western blotting for binding of C3 and C4 (figure 2.7). These interactions are most likely via direct hydrophobic interactions with the surface of the CNTs [74]. Several

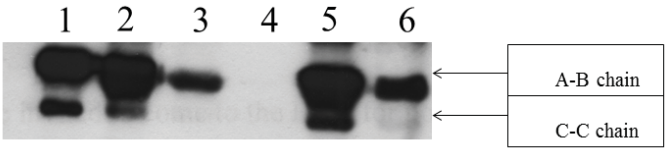

(a) C1q binding to CNTs. Samples of CNT incubated with plasma were analysed by SDS-PAGE in NON-REDUCED conditions and by Western blotting using anti-(human C1q). Track 1: standard C1q (250 ng); track 2: DWNT-1; track 3: DWNT-08; track 4: control experiment Sepharose carrier beads only; track 5: Ox-DWNT-2; track 6: Purified-DWNTs-2.

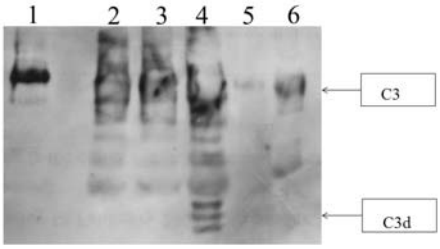

(b) C3 binding to CNTs. Samples of CNTs incubated with plasma were analysed by SDS-PAGE in NON-REDUCED conditions and by Western blotting using anti-(human C3 and C3d) antibodies. Track 1: C3 standard (250 ng). track 2: DWNTs-1; track 3: DWNTs-2: track 4: Ox-DWNTs, track 5: control experiment Sepharose only; tack 6 purified DWNTs-2. The C3 band is hard to distinguish because of the large amount of IgG on the blot, which co-runs with C3.

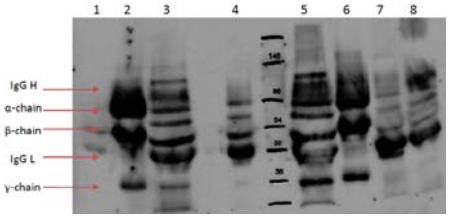

(c) C4 binding to CNTs. Samples of CNTs incubated with plasma were analysed by SDS-PAGE in REDUCED conditions and by Western blotting using anti-(human C4) antibodies. Track 1: Control experiment sepharose; Track 2: Purified C4 (unknown concentration); Track 3: Plasma sample; Track 4: DWNTs-1; Track 5: Ox-DWNTs; Track 6: Purified C4 (unknown concentration); Track 7: DWNTs-2; Track 8: Purified DWNTs-2.
IgG H and IgG L are detected by the anti-(human C4) antibody due to the purification method.

Figure 2.7: Western blot analysis of binding of complement proteins, C1q, C3 and C4 on pristine and oxidised CNTs.

studies have shown that functionalization, and therefore, altering of the surface properties of the CNTs, the extent of complement activation can be increased or decreased [47, 63, 65, 70–72, 75, 76]. Pre-coating CNTs will increase the dispersion state, making more surface area available for complement proteins to recognise and deposit themselves. RNA and BSA do not uniformly coat the CNT surface, therefore, binding sides on the CNT surface are made more available and complement activation might increase compared to clustered pristine CNTs. RNA itself can interact with C1q providing an additional binding site for complement [71]. Poly-ϵ-caprolactam (Nylon-6) and carboxymethyl cellulose (CMC) were shown to reduce the level of complement activation via the classical pathway most efficiently, but fail to eliminate opsonisation [65, 70].

Until a decade ago, PEGylation was considered to provide a shielding surface on nanoparticles, but in 2002, it was shown that PEGylated polystyrene microspheres could activate complement depending on the configuration of the PEG on the surface [77]. The effects of PEGylation on SWNTs as well as MWNTs have been extensively studied by the group of M.S. Moghimi [75, 78, 79]. They showed that although PEG can reduce complement activation via both classical and alternative pathway, levels of both C4d (cleavage product of C4) and MAC significantly increased. They concluded that complement activation was likely to occur through the lectin pathway. For MWNTs, complement activation was independent of the molecular mass of PEG chains and the effect was not caused by uncoated regions of the CNTs. The surface domains of the PEG derivatives may thus act as templates for the lectin pathway activating molecules (L-ficolin and MASP-2) [75, 78, 79].

Complement activation can be influenced by coating specific humoral factors onto the outer walls of CNTs. For instance binding of factor H, a downregulator of the alternative pathway, lowers the activation of the alternative pathway [65]. In contrast to full length C1q, the recombinant globular heads of C1q were shown to reduce complement activation (figure 3.6) [70]. This is likely to be caused by globular heads competing out the binding of whole C1q. Thereby diminishing complement activation. A similar technique to avoid recognition by the complement system is used by pathogenic bacteria, who have specific binding motifs on their surface to actively bind factor H, thus inhibiting alternative pathway activation [80].

2.5 Innate immune receptors, phagocytosis and immune response

The cells of the innate immune system, including macrophages and dendritic cells, have receptors that recognise and bind pathogens. These include toll-like receptors (TLRs), scavenger receptors, complement receptors, integrins, lectin-like receptors and Fc receptors, which

are capable of recognising nanoparticles. Once a particle is bound to a receptor, the particle will be attached to the cell and taken on its path, but can also be phagocytosed and ultimately, if possible, cleared from the system. The most important complement-activated opsonin is C3b, as it binds with multiple copies onto the surface of the nanoparticle. C3b interacts with complement receptor 1 (CR1 or CD35) which is abundant on red blood cells. Once C3b has bound, it is gradually broken down into iC3b, which has lower affinity towards CR1, but high affinity towards CR3 and CR4, which are commonly found on phagocytic cells. Therefore, the nanoparticles will be transferred from red blood cells towards phagocytic cells, especially during the passage of the red blood cells through the liver where macrophages are present in high numbers. The iC3b will be further broken down into C3d, which can interact with CR2 (CD21) on the surface of B-lymphocytes, and therefore, interact with the adaptive immune system. Opsonised CNTs absorb or bind onto the surface of red blood cells (Pondman et al, unpublished data), indicating that C3b is bound in a conformation that allows interaction with CR1. PEGylation, which downregulates complement activation, was shown to decrease uptake by monocytes, spleen and liver phagocytes, with increasing molecular weight and PEG coating density [81]. Phagocytosis of CNTs by macrophages (U937), monocytes and B-cells (Raji) is more efficient in the presence of serum; while complement inactivated (heat inactivated) serum does not enhance the phagocytosis, indicating an important additive effect of complement [70, 76]. Most interestingly, Jurkat T cells, which are known to express complement receptors feebly on their surface, were able to take up CNTs poorly and serum treatment did not increase uptake [76]. Complement adsorption on the surface of MWNTs was shown to reduce the expression of pro-inflammatory cytokines and increase expression of anti-inflammatory cytokines in monocytes and macrophages [70]. This indicates that complement might signal the cells to silently remove the CNTs by phagocytosis, but do not give out stress signals to their microenvironment. Even when only the initial complement proteins C1q, MBL are bound on the surface of the CNT, receptor interactions are possible with calreticulin working together with CD91 [82]. These bindings are less efficient as the density of deposited C1q and MBL is far lower than C3b and for adhesion hundreds of receptor-ligand pairs are needed. As was shown in [72], pre-coating the CNTs with the recombinant globular heads of human C1q and full length C1q can increase the phagocytosis by macrophages, while factor H is an inhibitor of phagocytosis.

2.6 Non complement dependent uptake

The method of entry of CNTs into cells is a highly debated subject in literature, complement dependent phagocytosis being one of the many possibilities. By changing or coating the walls of a CNT, its interaction with cells will change. This can be due to the chemical

nature of the coating; for example, macrophages are known to interact more strongly with positively charged particles due to the presence of sialic acid on their surface [83]. But altered uptake and interactions can also be a direct effect of the higher dispersability and, therefore, bioavailability of the functionalized CNTs. In general, hydrophilic or acidic polymer coated MWNTs are more internalized by macrophages than hydrophobic polymer coated MWNTs [84]. Direct penetration or needling through the plasma membrane is another described phenomenon [85, 86]. Others state that absorption of albumin or other serum proteins is essential to trigger scavenger receptor-mediated uptake [87]. Kam et al. found that for very short (50-200 nm) SWNTs, the nanoparticles enter cells (HeLa and H60 cell lines) through clathrin-depenent endocytosis [88]. However, Pantarotto et al [26]showed that slightly longer SWNTs (300-1000 nm) behave like cell penetrating peptides while entering human (3T6) and murine (3T3) fibroblasts.

After uptake by the cell, the CNTs can be found in the cytoplasm, endosomes, [9, 26, 86, 89], and in some cases, inside the nucleus [26, 85, 90].These variations can be due to different functionalizations [26, 85]. Exocytosis has not been reported often and the time course for the process varies between simultaneous with endocytosis [91] until after 5 h of the incubation [70, 76, 89].

2.7 Cytokine, inflammation and immune responses

In their bio-persistence as well as high aspect ratio, CNTs show similarities to asbestos, and therefore an incomplete uptake and frustrated phagocytosis with the related inflammation and glanuloma formation is a risk that has to be analysed [86, 92, 93]. Frustrated phagocytosis was analysed by Brown et al. with a variety of elongated carbon particles [94]. In their study, only individually dispersed long straight CNTs led to frustrated phagocytosis in PBMCs and THP-1 cells, which was correlated with superoxide anion and TNF-α release. The presence of CNTs interfered with the function of the macrophages as was shown by an inhibition of the ability of THP-1 cells to phagocytose E. coli. Clustered CNTs and nanofibres did not induce, apoptotic or necrotic effects [94]. Exposure to long (and not short) MWNTs resulted in a significant and dose-dependent release of IL-1β, TNF-α, IL-6 and IL-8 from THP-1, but not from mesothelial cells (Met5a) [92]. More interestingly, when cell medium from the THP-1 cells treated with long CNTs was added to Met5a cells, they too showed an increased cytokine production, indicating the essential role of macrophages in the immune response towards CNTs. Liu et al showed that immune response with pluronic F127 coated MWNTs in RAW (murine macrophages) and MCF-7 (breast cancer) was length-dependent [93]. RAW cells showed higher internalisation, resulting in higher toxicity due to CNTs than MCF-7. Long MWNTs (3-8 μm) were more toxic than short ($<$1.5 μm), but short

MWNTs gave more TNF-α release than long MWNTs, which could lead to a stronger inflammatory response. Besides cytokine response, indications of inflammasome formation by CNTs have been reported [86, 95, 96]. Many carbon nanomaterials (carbon black, short, long and tangled CNTs and long, needle like MWNTs, and asbestos) induced IL-1β secretion (indicator of inflammasome formation), but only long, needle like CNTs induced IL-1α secretion in LPS-primed macrophages [86]. DWNTs can synergize with TLR4 antagonists; when K^+ efflux is hindered, IL-1β secretion can be eliminated, indicating that phagocytosis is required for inflammasome activation. After phagocytosis, NF-kβ (nuclear factor kappa-light-chain-enhancer of activated B cells) and NLRP3 (nucleotide-binding oligomerization domain (NOD)-like receptors family, pyrin domain containing 3) inflammasomes are activated [95, 96].

Various carbon nanoparticles can modulate dendritic cell (DC) maturation [97]. Short, purified (oxidized) SWNTs, with no endotoxin content, induced no maturation of DC cultures and no secretion of IL-6,TNF-α, or IL-1β following their uptake. In comparison, incubation of DCs with LPS and CNTs induced IL-1β secretion, which was dose and NLRP3-dependent, indicating that LPS contamination causes this effect [98]. Dumortier et al. [48] showed that PEG_{1500}-SWNTs are taken up by B- and T-cells without affecting viability of the cells or causing damage, inhibiting or stimulating their function. Although they found no IL-2 and INF-α secretion (cytokines reflecting T-cell activation), PEGylated SWNTs did induce IL-6 and TNF-α secretion in macrophages (in vitro, peritoneal), which they attributed to the formation of CNT aggregates.

2.8 Lung innate immunity and CNTs

Most likely triggered by their asbestos like appearance [99], pulmonary toxicity of CNTs is one of the most discussed subjects in nanoparticles research. Disagreement started from the very first studies published by Lam [100] and Warheit [101] who independently concluded that CNTs were highly toxic and non-toxic to the lungs, respectively. First, they both showed that CNTs induced granulomas, but only Lam showed subsequent fibrogenesis. This effect can be explained by the fact that granuloma formation is mediated by the accumulation of alveolar macrophages at sites of particle deposition which become activated by the phagocytosis of the particles. The activated macrophages produce growth factors that stimulate the proliferation of fibroblasts, the collagen producing cells driving the fibrogenesis [102]. Whereas Lam found a dose- and time-dependent interstitial inflammation, Warheit did not see any inflammation and fibrosis; in addition, the granuloma formation was not dose-dependent. Warheit concluded that the toxicity of the CNTs was caused by aggregation of the CNTs due to the admission method (instillation), which even caused airway blocking. Shvedova

et al confirmed the results of Lam et al in mice and also showed dose-dependent functional respiratory deficiencies [103]. Subsequently, Mangum et al found no inflammation in SWNT exposed (oropharyngeal aspiration) rats, although they did find a few focal interstitial fibrotic lesions at locations with clusters of macrophages containing micron sized aggregates of SWNTs in the alveolar region. In addition, they reported, in bronchoalveolar lavage fluid (BALF), macrophages linked together with bridges of parallel bundles of SWNTs. They stated that this bridge formation is not similar to frustrated or incomplete phagocytosis seen in asbestos and other long fibers [102]. The origin in the variations of effects reported possibly owes it to a wide variation of nanoparticles (single, double or multi walled) with variable diameter and length, coating, aggregation states, contamination with other materials, administration method and route [104]. By comparing well-dispersed SWNTs with aggregated SWNTs, Shvedova et al found that poorly dispersed SWNTs formed clumps of 5 to 20 μm in the lungs, which triggered granuloma formation, whereas highly dispersed SWNTs that did not form any clumps and were found free in the tissue, gave rise to interstitial fibrosis but no granulomatous lesions [105–107]. This was confirmed by a study where well dispersed MWNTs were found in every cell and cell layer of the lung parenchyma, with signs of interstitial fibrosis of the alveolar wall but with very limited granuloma formation [108].

The lung innate immune defence is governed mainly by surfactant proteins A and D (SP-A and SP-D), together with lung leukocytes and the epithelial cells lining the alveolar surface. Like MBL, SP-A and SP-D are members of the collectin (collagenous lectins) family. SP-A and SP-D have a similar multimeric structure to C1q and MBL. Among other roles, SP-A and SP-D bind to invading particles (commonly onto vicinal diols) in a Ca^{2+} dependent manner and promote their binding to receptors on alveolar macrophages [109]. The concentrations of SP-A and SP-D are very low, therefore binding of pulmonary surfactant proteins to CNTs can cause significant depletion of the proteins and cause damage to the lung immune defence mechanisms [110].

Selective binding of SP-A and SP-D onto DWNTs from BALF in a Ca^{2+} dependent manner onto oxygen containing functional groups on the surface of CNTs, was confirmed in a study by Salvador-Morales by using acid treated (oxidized) MWNTs, which could be coated entirely with SP-A [111]. Oxidized DWNTs bound SP-A and SP-D more efficiently than non-oxidized DWNTs and purified DWNTs (figure 2.8). SP-A and IgG were detectable in all CNT samples. SP-A but also BSA coated MWNTs were able to enter the cytoplasm and the nucleus of alveolar macrophages in an in-vitro test. Interestingly, the high nitric oxide secretion evoked by pristine MWNTs and BSA-coated MWNTs was not observed after incubation with SP-A coated MWNTs, indicating a possible method to avoid an inflammatory response towards CNTs [111]. Allowing SWNTs to obtain a lung surfactant corona, consisting of SP-A, B and D enhanced the in vitro uptake of SWNT by RAW cells (murine macrophages)

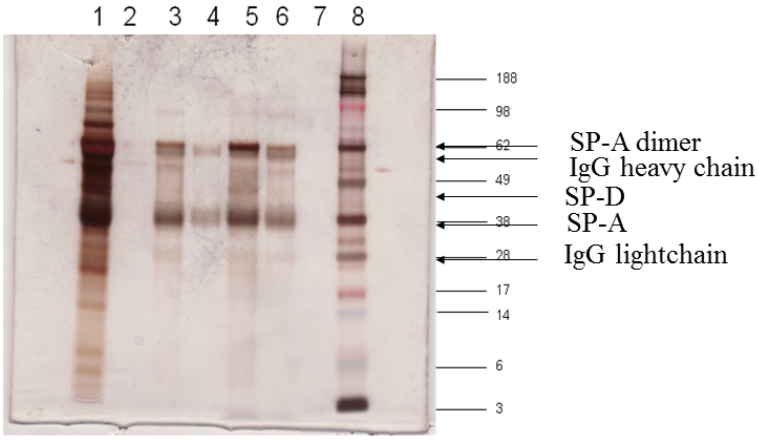

Figure 2.8: Selective binding of bronchoalveolar lavage fluid (BALF) proteins to different chemically modified CNT. 20 ml of undiluted BALF was passed through Sepharose and Sepharose-CNT columns. After exhaustive washing in the running buffer (10mM HEPES, 140 mM NaCl, 0.15 mM $CaCl_2$), samples of the resin were analysed by SDS-PAGE (reduced). Lane 1: BALF supernatant concentrated using StrataClean beads; Lane 2: Control experiment (BALF proteins bound to Sepharose); Lane3: BALF proteins bound to DWNTs-1; Lane 4 BALF proteins bound to DWNT-2; Lane 5: BALF proteins bound to Ox-DWNT-2; Lane 6: BALF proteins bound to Purified-DWNT-2; Lane 8: Molecular weightmarker. Protein bands were stained using BioRad Silverstain Kit image. Reproduced from [63].

[112]. Gasser et al [113] showed that pre-coating MWNTs (pristine, oxidised and aminated) with pulmonary surfactant induces clusters of coated MWNTs intracellulary, in monocyte derived macrophages, while they state more stable suspensions are obtained with coated MWNTs. They argue that both SP-A and phosphatidylserine might represent an "eat me" signal towards macrophages. A similar effect was seen by coating CNTs with SP-D [114]. Coating the MWNTs with surfactant slightly increased apoptosis while necrosis slightly decreased [113]. Interestingly, a decrease in TNF-α release was found, which might be attributed to the phosphatidylserine present in the surfactant. Coating of CMC-MWNTs and Ox-MWNTs with recombinant SP-D (rhSP-D) increased the phagocytosis by macrophages 2-fold, at the same time dampening the cytokine storm provoked by MWNTs without coating (reduction of IL-12, TGF-β, IL-1β, IL-6 and TNF-α production) [114] .

2.9 Conclusions

A number of studies have addressed how nanoparticles interact with the innate immune system including macro-phages and dendritic cells, cell surface pattern recognition receptors and soluble factors. The results obtained paint a varied and heterogeneous picture: primarily owing to the range of nanoparticles and model systems used. However, it is evident that in vitro experiments that earlier suggested pro-inflammatory response to nanoparticles need to be viewed in the context of complement. The recognition subcomponents of the three pathways of the complement system are fully capable of binding via pattern recognition presented as an array over the surface of pristine or modified nanoparticles. This recognition can lead to complement deposition, thus enhancing phagocytosis. Curiously and unexpectedly, complement deposition on the nanoparticles appear to skew the pro-inflammatory towards anti-inflammatory response, suggesting beneficial effects of complement. It is unclear how complement deposition enhances anti-inflammatory immune response although a link between heightened IL-10 levels and suppressed TNF-α and IL-1β is evident in recent studies. It is worth examining how altered pattern can affect CNT engagement with TLRs with or without complement deposition. Clearly, the ability of nanoparticles to induce pro-inflammatory and anti-inflammatory immune response in vivo is crucial for its long to medium term use as a therapeutic vehicle. Thus, their potency to deposit complement on the surface is going to acquire importance.

References

[1] K. Morito, T. Hirose, J. Kinjo, T. Hirakawa, M. Okawa, T. Nohara, S. Ogawa, S. Inoue, M. Muramatsu, and Y. Masamune, "Interaction of phytoestrogens with estrogen receptors alpha and beta.," *Biological & pharmaceutical bulletin*, vol. 24, pp. 351–6, Apr. 2001.

[2] F. Liang and B. Chen, "A review on biomedical applications of single-walled carbon nanotubes.," *Current medicinal chemistry*, vol. 17, pp. 10–24, 2010.

[3] J. Prasek, J. Drbohlavova, J. Chomoucka, J. Hubalek, O. Jasek, V. Adam, and R. Kizek, "Methods for carbon nanotubes synthesisreview," *Journal of Materials Chemistry*, vol. 21, no. 40, p. 15872, 2011.

[4] A. Bianco, J. Hoebeke, S. Godefroy, O. Chaloin, D. Pantarotto, J.-P. Briand, S. Muller, M. Prato, and C. D. Partidos, "Cationic carbon nanotubes bind to CpG oligodeoxynucleotides and enhance their immunostimulatory properties.," *Journal of the American Chemical Society*, vol. 127, pp. 58–9, Jan. 2005.

[5] C. Biale, V. Mussi, U. Valbusa, S. Visentin, G. Viscardi, N. Barbero, N. Pedemonte, and L. Galietta, "Carbon nanotubes for targeted drug delivery," *2009 9th Ieee Conference on Nanotechnology*, pp. 644–646, 2009.

[6] J. G. Li, W. X. Li, J. Y. Xu, X. Q. Cai, R. L. Liu, Y. J. Li, Q. F. Zhao, and Q. N. Li, "Comparative study of pathological lesions induced by multiwalled carbon nanotubes in lungs of mice by intratracheal instillation and inhalation," *Environmental Toxicology*, vol. 22, no. 4, pp. 415–421, 2007.

[7] H. Ali-Boucetta, K. T. Al-Jamal, D. McCarthy, M. Prato, A. Bianco, and K. Kostarelos, "Multiwalled carbon nanotube-doxorubicin supramolecular complexes for cancer therapeutics.," *Chemical communications*, pp. 459–61, Jan. 2008.

[8] E. Heister, V. Neves, C. Tîlmaciu, K. Lipert, V. S. Beltrán, H. M. Coley, S. R. P. Silva, and J. McFadden, "Triple functionalisation of single-walled carbon nanotubes with doxorubicin, a monoclonal antibody, and a fluorescent marker for targeted cancer therapy," *Carbon*, vol. 47, no. 9, pp. 2152–2160, 2009.

[9] W. Wu, S. Wieckowski, G. Pastorin, M. Benincasa, C. Klumpp, J. P. Briand, R. Gennaro, M. Prato, and A. Bianco, "Targeted delivery of amphotericin B to cells by using functionalized carbon nanotubes," *Angewandte Chemie-International Edition*, vol. 44, no. 39, pp. 6358–6362, 2005.

[10] A. Yang, W. Liu, Z. Li, L. Jiang, H. Xu, and X. Yang, "Influence of polyethyleneglycol modification on phagocytic uptake of polymeric nanoparticles mediated by immunoglobulin G and complement activation," *Journal of Nanoscience and Nanotechnology*,

vol. 10, no. 1, pp. 622–628, 2010.

[11] N. Aoki, T. Akasaka, F. Watari, and A. Yokoyama, "Carbon nanotubes as scaffolds for cell culture and effect on cellular functions," *Dental Materials Journal*, vol. 26, no. 2, pp. 178–185, 2007.

[12] X. F. Shi, B. Sitharaman, Q. P. Pham, F. Liang, K. Wu, W. E. Billups, L. J. Wilson, and A. G. Mikos, "Fabrication of porous ultra-short single-walled carbon nanotube nanocomposite scaffolds for bone tissue engineering," *Biomaterials*, vol. 28, no. 28, pp. 4078–4090, 2007.

[13] J. H. Choi, F. T. Nguyen, P. W. Barone, D. A. Heller, A. E. Moll, D. Patel, S. A. Boppart, and M. S. Strano, "Multimodal biomedical imaging with asymmetric single-walled carbon nanotube/iron oxide nanoparticle complexes," *Nano Letters*, vol. 7, no. 4, pp. 861–867, 2007.

[14] O. Vittorio, S. L. Duce, A. Pietrabissa, and A. Cuschieri, "Multiwall carbon nanotubes as MRI contrast agents for tracking stem cells," *Nanotechnology*, vol. 22, no. 9, 2011.

[15] P. K. Avti, Y. Talukdar, M. V. Sirotkin, K. R. Shroyer, and B. Sitharaman, "Toward single-walled carbon nanotube-gadolinium complex as advanced MRI contrast agents: Pharmacodynamics and global genomic response in small animals," *Journal of Biomedical Materials Research Part B-Applied Biomaterials*, vol. 101B, no. 6, pp. 1039–1049, 2013.

[16] E. Fidiani, P. M. F. J. Costa, A. U. B. Wolter, D. Maier, B. Buechner, and S. Hampel, "Magnetically Active and Coated Gadolinium-Filled Carbon Nanotubes," *Journal of Physical Chemistry C*, vol. 117, no. 32, pp. 16725–16733, 2013.

[17] X. J. Wang, R. Podila, J. H. Shannahan, A. M. Rao, and J. M. Brown, "Intravenously delivered graphene nanosheets and multiwalled carbon nanotubes induce site-specific Th2 inflammatory responses via the IL-33/ST2 axis," *International Journal of Nanomedicine*, vol. 8, pp. 1733–1748, 2013.

[18] B. D. Chen, H. Zhang, C. X. Zhai, N. Du, C. Sun, J. W. Xue, D. R. Yang, H. Huang, B. Zhang, Q. P. Xie, and Y. L. Wu, "Carbon nanotube-based magnetic-fluorescent nanohybrids as highly efficient contrast agents for multimodal cellular imaging," *Journal of Materials Chemistry*, vol. 20, no. 44, pp. 9895–9902, 2010.

[19] R. Klingeler, S. Hampel, and B. Buchner, "Carbon nanotube based biomedical agents for heating, temperature sensoring and drug delivery," *International journal of hyperthermia*, vol. 24, no. 6, pp. 496–505., 2008.

[20] I. Moench, A. Meye, and A. Leonhardt, "Ferromagnetic filled carbon nanotubes as novel and potential containers for anticancer treatment strategies," in *Nanomaterials*

for cancer therapy (C. Kumar, ed.), vol. 6, ch. 9, pp. 259–337, Weinheim: Wiley VCH Verlag, 2006.

[21] M. Foldvari and M. Bagonluri, "Carbon nanotubes as functional excipients for nanomedicines: II. Drug delivery and biocompatibility issues.," *Nanomedicine : nanotechnology, biology, and medicine*, vol. 4, pp. 183–200, Sept. 2008.

[22] M. Foldvari and M. Bagonluri, "Carbon nanotubes as functional excipients for nanomedicines: I. Pharmaceutical properties.," *Nanomedicine : nanotechnology, biology, and medicine*, vol. 4, pp. 173–82, Sept. 2008.

[23] L.-H. Liu, H. Dietsch, P. Schurtenberger, and M. Yan, "Photoinitiated coupling of unmodified monosaccharides to iron oxide nanoparticles for sensing proteins and bacteria.," *Bioconjugate chemistry*, vol. 20, pp. 1349–55, July 2009.

[24] A. M. A. Elhissi, W. Ahmed, I. U. Hassan, V. R. Dhanak, and A. D'Emanuele, "Carbon nanotubes in cancer therapy and drug delivery.," *Journal of drug delivery*, vol. 2012, p. 837327, Jan. 2012.

[25] M. VanHandel, D. Alizadeh, L. Zhang, B. Kateb, M. Bronikowski, H. Manohara, and B. Badie, "Selective uptake of multi-walled carbon nanotubes by tumor macrophages in a murine glioma model.," *Journal of neuroimmunology*, vol. 208, pp. 3–9, Mar. 2009.

[26] D. Pantarotto, J.-P. Briand, M. Prato, and A. Bianco, "Translocation of bioactive peptides across cell membranes by carbon nanotubes.," *Chemical communications*, pp. 16–7, Jan. 2004.

[27] N. A. Monteiro-Riviere, R. J. Nemanich, A. O. Inman, Y. Y. Wang, and J. E. Riviere, "Multi-walled carbon nanotube interactions with human epidermal keratinocytes.," *Toxicology letters*, vol. 155, pp. 377–84, Mar. 2005.

[28] A. E. Porter, M. Gass, K. Muller, J. N. Skepper, P. A. Midgley, and M. Welland, "Direct imaging of single-walled carbon nanotubes in cells.," *Nature nanotechnology*, vol. 2, pp. 713–7, Nov. 2007.

[29] S. Hampel, D. Kunze, D. Haase, K. Krämer, M. Rauschenbach, M. Ritschel, A. Leonhardt, J. Thomas, S. Oswald, V. Hoffmann, and B. Büchner, "Carbon nanotubes filled with a chemotherapeutic agent: a nanocarrier mediates inhibition of tumor cell growth.," *Nanomedicine (London, England)*, vol. 3, pp. 175–82, Apr. 2008.

[30] Z. Liu, X. M. Sun, N. Nakayama-Ratchford, and H. J. Dai, "Supramolecular chemistry on water-soluble carbon nanotubes for drug loading and delivery," *Acs Nano*, vol. 1, no. 1, pp. 50–56, 2007.

[31] A. Bianco, K. Kostarelos, and M. Prato, "Applications of carbon nanotubes in drug delivery," *Current Opinion in Chemical Biology*, vol. 9, pp. 674–679, Dec. 2005.

[32] W. Liu, X. Yang, Y. Zhu, H. Chen, and H. Xu, "Nanostructured lipid carriers as vehicles for transdermal iontophoretic drug delivery.," *Conference proceedings : ... Annual International Conference of the IEEE Engineering in Medicine and Biology Society. IEEE Engineering in Medicine and Biology Society. Conference*, vol. 2, pp. 1236–9, Jan. 2005.

[33] L. Lacerda, A. Bianco, M. Prato, and K. Kostarelos, "Carbon nanotubes as nanomedicines: from toxicology to pharmacology," *Advanced Drug Delivery Reviews*, vol. 58, pp. 1460–1470, Dec. 2006.

[34] N. Sinha and J. T. Yeow, "Carbon nanotubes for biomedical applications," *IEEE Trans Nanobioscience*, vol. 4, no. 2, pp. 180–195, 2005.

[35] T. L. Moore, S. W. Grimes, R. L. Lewis, and F. Alexis, "Multilayered polymer-coated carbon nanotubes to deliver dasatinib.," *Molecular pharmaceutics*, vol. 11, pp. 276–82, Jan. 2014.

[36] D. Pantarotto, R. Singh, D. McCarthy, M. Erhardt, J. P. Briand, M. Prato, K. Kostarelos, and A. Bianco, "Functionalized carbon nanotubes for plasmid DNA gene delivery," *Angewandte Chemie-International Edition*, vol. 43, no. 39, pp. 5242–5246, 2004.

[37] R. A. Graff, T. M. Swanson, and M. S. Strano, "Synthesis of nickel-nitrilotriacetic acid coupled single-walled carbon nanotubes for directed self-assembly with polyhistidine-tagged proteins," *Chemistry of Materials*, vol. 20, no. 5, pp. 1824–1829, 2008.

[38] S. K. Smart, A. I. Cassady, G. Q. Lu, and D. J. Martin, "The biocompatibility of carbon nanotubes," *Carbon*, vol. 44, pp. 1034–1047, 2005.

[39] M. R. McDevitt, D. Chattopadhyay, B. J. Kappel, J. S. Jaggi, S. R. Schiffman, C. Antczak, J. T. Njardarson, R. Brentjens, and D. A. Scheinberg, "Tumor targeting with antibody-functionalized, radiolabeled carbon nanotubes.," *Journal of nuclear medicine : official publication, Society of Nuclear Medicine*, vol. 48, pp. 1180–9, July 2007.

[40] R. Bandyopadhyaya, E. Nativ-Roth, O. Regev, and R. Yerushalmi-Rozen, "Stabilization of individual carbon nanotubes in aqueous solutions," *Nano Letters*, vol. 2, no. 1, pp. 25–28, 2002.

[41] C. Bertulli, H. J. Beeson, T. Hasan, and Y. Y. S. Huang, "Spectroscopic characterization of protein-wrapped single-wall carbon nanotubes and quantification of their cellular uptake in multiple cell generations," *Nanotechnology*, vol. 24, no. 26, p. 5102,

2013.

[42] M. F. Islam, E. Rojas, D. M. Bergey, A. T. Johnson, and A. G. Yodh, "High weight fraction surfactant solubilization of single-wall carbon nanotubes in water," *Nano Letters*, vol. 3, no. 2, pp. 269–273, 2003.

[43] N. Hadidi, F. Kobarfard, N. Nafissi-Varcheh, and R. Aboofazeli, "Optimization of single-walled carbon nanotube solubility by noncovalent PEGylation using experimental design methods," *International Journal of Nanomedicine*, vol. 6, pp. 737–746, 2011.

[44] M. Zheng, A. Jagota, E. D. Semke, B. A. Diner, R. S. Mclean, S. R. Lustig, R. E. Richardson, and N. G. Tassi, "DNA-assisted dispersion and separation of carbon nanotubes," *Nature Materials*, vol. 2, no. 5, pp. 338–342, 2003.

[45] Y. Li, X. Zhang, J. Luo, W. Huang, J. Cheng, Z. Luo, T. Li, F. Liu, G. Xu, X. Ke, L. Li, and H. J. Geise, "Purification of CVD synthesized single-wall carbon nanotubes by different acid oxidation treatments," *Nanotechnology*, vol. 15, pp. 1645–1649, 2004.

[46] K. Bhattacharya, F. T. Andon, R. El-Sayed, and B. Fadeel, "Mechanisms of carbon nanotube-induced toxicity: Focus on pulmonary inflammation," *Advanced Drug Delivery Reviews*, vol. 65, no. 15, pp. 2087–209, 2013.

[47] V. A. Basiuk, C. Salvador-Morales, E. V. Basiuk, R. M. J. Jacobs, M. Ward, B. T. Chu, R. B. Sim, and M. L. H. Green, "'Green' derivatization of carbon nanotubes with Nylon 6 and L-alanine," *Journal of Materials Chemistry*, vol. 16, no. 45, pp. 4420–4426, 2006.

[48] H. Dumortier, S. Lacotte, G. Pastorin, R. Marega, W. Wu, D. Bonifazi, J. P. Briand, M. Prato, S. Muller, and A. Bianco, "Functionalized carbon nanotubes are non-cytotoxic and preserve the functionality of primary immune cells," *Nano Letters*, vol. 6, no. 12, p. 3003, 2006.

[49] M. Shim, N. W. S. Kam, R. J. Chen, Y. M. Li, and H. J. Dai, "Functionalization of carbon nanotubes for biocompatibility and biomolecular recognition," *Nano Letters*, vol. 2, no. 4, pp. 285–288, 2002.

[50] M. V. Carroll and R. B. Sim, "Complement in health and disease," *Advanced Drug Delivery Reviews*, vol. 63, no. 12, pp. 965–975, 2011.

[51] E. Kang, K. Kim, and I. C. Kwon, "Multifunctional Nanoparticles for Molecular Imaging," *Journal of the Korean Medical Association*, vol. 52, no. 2, pp. 125–134, 2009.

[52] U. Kishore and K. B. Reid, "Modular organization of proteins containing C1q-like globular domain," *Immunopharmacology*, vol. 42, no. 1-3, pp. 15–21, 1999.

[53] U. Kishore and R. B. Sim, "Factor H as a regulator of the classical pathway activation.," *Immunobiology*, vol. 217, pp. 162–8, Feb. 2012.

[54] L. Kouser, M. Abdul-Aziz, A. Nayak, C. M. Stover, R. B. Sim, and U. Kishore, "Properdin and factor H: opposing players on the alternative complement pathway "see-saw"," *Frontiers in immunology*, vol. 4, p. 93, Jan. 2013.

[55] J. Leleux and K. Roy, "Micro and nanoparticle-based delivery systems for vaccine immunotherapy: an immunological and materials perspective.," *Advanced healthcare materials*, vol. 2, pp. 72–94, Jan. 2013.

[56] G. Maiorano, S. Sabella, B. Sorce, V. Brunetti, M. A. Malvindi, R. Cingolani, and P. P. Pompa, "Effects of Cell Culture Media on the Dynamic Formation of Protein-Nanoparticle Complexes and Influence on the Cellular Response," *ACS Nano*, vol. 4, no. 12, pp. 7481–7491, 2010.

[57] C. Sacchetti, K. Motamedchaboki, A. Magrini, G. Palmieri, M. Mattei, S. Bernardini, N. Rosato, N. Bottini, and M. Bottini, "Surface polyethylene glycol conformation influences the protein corona of polyethylene glycol-modified single-walled carbon nanotubes: potential implications on biological performance," *ACS Nano*, vol. 7, no. 3, pp. 1974–1989, 2013.

[58] A. Gustafsson, E. Lindstedt, L. S. Elfsmark, and A. Bucht, "Lung exposure of titanium dioxide nanoparticles induces innate immune activation and long-lasting lymphocyte response in the Dark Agouti rat," *Journal of Immunotoxicology*, vol. 8, no. 2, pp. 111–121, 2011.

[59] M. Rahman, S. Laurent, N. Tawil, L. Yahia, and M. Mahmoudi, "Nanoparticle and Protein Corona," *Protein-Nanoparticle interactions*, vol. 15, no. 2, pp. 21–44, 2013.

[60] M. Lundqvist, J. Stigler, G. Elia, I. Lynch, T. Cedervall, and K. A. Dawson, "Nanoparticle size and surface properties determine the protein corona with possible implications for biological impacts," *Proceedings of the National Academy of Sciences of the United States of America*, vol. 105, no. 38, pp. 14265–14270, 2008.

[61] P. Aggarwal, J. B. Hall, C. B. McLeland, M. A. Dobrovolskaia, and S. E. McNeil, "Nanoparticle interaction with plasma proteins as it relates to particle biodistribution, biocompatibility and therapeutic efficacy.," *Advanced drug delivery reviews*, vol. 61, pp. 428–37, June 2009.

[62] C. Salvador-Morales, E. Flahaut, E. Sim, J. Sloan, M. L. Green, and R. B. Sim, "Complement activation and protein adsorption by carbon nanotubes," *Molecular Immunology*, vol. 43, no. 3, pp. 193–201, 2006.

[63] M. Rybak-Smith, K. Pondman, E. Flahaut, C. Salvador-Morales, R. Sim, and ., "Recognition of Carbon Nanotubes by the Human Innate Immune System.," in *Carbon Nanotubes for Biomedical Applications* (R. Klingeler and R. B. Sim, eds.), pp. 183–210, Springer, 2011.

[64] J. H. Shannahan, J. M. Brown, R. Chen, P. C. Ke, X. Lai, S. Mitra, and F. A. Witzmann, "Comparison of nanotube-protein corona composition in cell culture media," *Small*, vol. 9, no. 12, pp. 2171–2181, 2013.

[65] C. Salvador-Morales, E. V. Basiuk, V. A. Basiuk, M. L. H. Green, and R. B. Sim, "Effects of covalent functionalisation on the biocompatibiltiy characteristics of multi-walled carbon nanotubes," *Journal of Nanoscience and Nanotechnology*, vol. 8, no. 5, pp. 2347–2356, 2007.

[66] X. Cai, R. Ramalingam, H. S. Wong, J. Cheng, P. Ajuh, S. H. Cheng, and Y. W. Lam, "Characterization of carbon nanotube protein corona by using quantitative proteomics.," *Nanomedicine : nanotechnology, biology, and medicine*, vol. 9, pp. 583–93, July 2013.

[67] A. Chanan-Khan, J. Szebeni, S. Savay, L. Liebes, N. M. Rafique, C. R. Alving, and F. M. Muggia, "Complement activation following first exposure to pegylated liposomal doxorubicin (Doxil): possible role in hypersensitivity reactions," *Annals of Oncology*, vol. 14, no. 9, pp. 1430–1437, 2003.

[68] S. M. Moghimi, A. J. Andersen, D. Ahmadvand, P. P. Wibroe, T. L. Andresen, and A. C. Hunter, "Material properties in complement activation," *Advanced Drug Delivery Reviews*, vol. 63, no. 12, pp. 1000–1007, 2011.

[69] W. L. Ling, A. Biro, I. Bally, P. Tacnet, A. Deniaud, E. Doris, P. Frachet, G. Schoehn, E. Pebay-Peyroula, and G. J. Arlaud, "Proteins of the Innate Immune System Crystallize on Carbon Nanotubes but Are Not Activated," *ACS Nano*, vol. 5, no. 2, pp. 730–737, 2011.

[70] K. M. Pondman, M. Sobik, A. Nayak, A. G. Tsolaki, A. Jäkel, E. Flahaut, S. Hampel, B. Ten Haken, R. B. Sim, and U. Kishore, "Complement activation by carbon nanotubes and its influence on the phagocytosis and cytokine response by macrophages.," *Nanomedicine : nanotechnology, biology, and medicine*, vol. 10, pp. 1287–1299, Mar. 2014.

[71] M. J. Rybak-Smith and R. B. Sim, "Complement activation by carbon nanotubes," *Advanced Drug Delivery Reviews*, vol. 63, no. 12, pp. 1031–1041, 2011.

[72] K. Pondman, A. Tsolaki, L. Pednekar, E. Dodagatta-Marri, L. Kouser, M. Sobik, T. B. Haken, R. B. Sim, and U. Kishore, "Innate immune humoral factors, C1q and factor H, with differential pattern recognition properties alter macrophage response to carbon

nanotubes.," *Small*, vol. submitted, 2014.

[73] U. Kishore, R. Ghai, T. J. Greenhough, A. K. Shrive, D. M. Bonifati, M. G. Gadjeva, P. Waters, M. S. Kojouharova, T. Chakraborty, and A. Agrawal, "Structural and functional anatomy of the globular domain of complement protein C1q.," *Immunology letters*, vol. 95, pp. 113–28, Sept. 2004.

[74] M. J. Rybak-Smith, C. Tripisciano, E. Borowiak-Palen, C. Lamprecht, and R. B. Sim, "Effect of Functionalization of Carbon Nanotubes with Psychosine on Complement Activation and Protein Adsorption," *Journal of Biomedical Nanotechnology*, vol. 7, pp. 830–839, Dec. 2011.

[75] O. A. Hamad, K. N. Ekdahl, P. H. Nilsson, J. Andersson, P. Magotti, J. D. Lambris, and B. Nilsson, "Complement activation triggered by chondroitin sulfate released by thrombin receptor-activated platelets," *Journal of Thrombosis and Haemostasis*, vol. 6, no. 8, pp. 1413–1421, 2008.

[76] K. Pondman, A. Tsolaki, A. Switzer, M. Shamji, B. ten Haken, R. Sim, and U. Kishore, "Complement deposition on nanoparticles can modulate immune responses by macrophage, B and T cells.," *Journal of Biomedical nanotechnology*, vol. Submitted, 2014.

[77] J. K. Gbadamosi, A. C. Hunter, and S. M. Moghimi, "PEGylation of microspheres generates a heterogeneous population of particles with differential surface characteristics and biological performance.," *FEBS letters*, vol. 532, pp. 338–44, Dec. 2002.

[78] A. J. Andersen, J. T. Robinson, H. J. Dai, A. C. Hunter, T. L. Andresen, and S. M. Moghimi, "Single-Walled Carbon Nanotube Surface Control of Complement Recognition and Activation," *ACS Nano*, vol. 7, no. 2, pp. 1108–1119, 2013.

[79] A. J. Andersen, B. Windschiegl, S. Ilbasmis-Tamer, I. T. Degim, A. C. Hunter, T. L. Andresen, and S. M. Moghimi, "Complement activation by PEG-functionalized multiwalled carbon nanotubes is independent of PEG molecular mass and surface density.," *Nanomedicine : nanotechnology, biology, and medicine*, vol. 9, pp. 469–73, May 2013.

[80] J. Hellwage, T. Meri, T. Heikkilä, A. Alitalo, J. Panelius, P. Lahdenne, I. J. Seppälä, and S. Meri, "The complement regulator factor H binds to the surface protein OspE of Borrelia burgdorferi.," *The Journal of biological chemistry*, vol. 276, pp. 8427–35, Mar. 2001.

[81] R. Gref, M. Lück, P. Quellec, M. Marchand, E. Dellacherie, S. Harnisch, T. Blunk, and R. Müller, "'Stealth' corona-core nanoparticles surface modified by polyethylene glycol (PEG): influences of the corona (PEG chain length and surface density) and of the core composition on phagocytic uptake and plasma protein adsorption.," *Colloids and surfaces. B, Biointerfaces*, vol. 18, pp. 301–313, Oct. 2000.

[82] C. A. Ogden, A. DeCathehneau, P. R. Hoffmann, D. Bratton, B. Ghebrehiwet, V. A. Fadok, and P. M. Henson, "C1q and mannose binding lectin engagement of cell surface calreticulin and CD91 initiates macropinocytosis and uptake of apoptotic cells," *Journal of Experimental Medicine*, vol. 194, no. 6, pp. 781–795, 2001.

[83] S. Hussain, J. A. J. Vanoirbeek, and P. H. M. Hoet, "Interactions of nanomaterials with the immune system," *Wiley Interdisciplinary Reviews-Nanomedicine and Nanobiotechnology*, vol. 4, no. 2, pp. 169–183, 2012.

[84] L. Tabet, C. Bussy, A. Setyan, A. Simon-Deckers, M. J. Rossi, J. Boczkowski, and S. Lanone, "Coating carbon nanotubes with a polystyrene-based polymer protects against pulmonary toxicity.," *Particle and fibre toxicology*, vol. 8, p. 3, Jan. 2011.

[85] K. Kostarelos, L. Lacerda, G. Pastorin, W. Wu, S. Wieckowski, J. Luangsivilay, S. Godefroy, D. Pantarotto, J. P. Briand, S. Muller, M. Prato, and A. Bianco, "Cellular uptake of functionalized carbon nanotubes is independent of functional group and cell type," *Nature nanotechnology*, vol. 2, no. 2, pp. 108–113, 2007.

[86] J. Palomaki, E. Valimaki, J. Sund, M. Vippola, P. A. Clausen, K. A. Jensen, K. Savolainen, S. Matikainen, and H. Alenius, "Long, needle-like carbon nanotubes and asbestos activate the NLRP3 inflammasome through a similar mechanism," *ACS Nano*, vol. 5, no. 9, pp. 6861–6870, 2011.

[87] G. Laverny, A. Casset, A. Purohit, E. Schaeffer, C. Spiegelhalter, F. de Blay, and F. Pons, "Immunomodulatory properties of multi-walled carbon nanotubes in peripheral blood mononuclear cells from healthy subjects and allergic patients.," *Toxicology letters*, vol. 217, pp. 91–101, Feb. 2013.

[88] N. W. S. Kam, Z. A. Liu, and H. J. Dai, "Carbon nanotubes as intracellular transporters for proteins and DNA: An investigation of the uptake mechanism and pathway," *Angewandte Chemie-International Edition*, vol. 45, no. 4, pp. 577–581, 2006.

[89] B. Kang, D.-C. Yu, S.-Q. Chang, D. Chen, Y.-D. Dai, and Y. Ding, "Intracellular uptake, trafficking and subcellular distribution of folate conjugated single walled carbon nanotubes within living cells.," *Nanotechnology*, vol. 19, p. 375103, Sept. 2008.

[90] Q. Mu, D. L. Broughton, and B. Yan, "Endosomal leakage and nuclear translocation of multiwalled carbon nanotubes: developing a model for cell uptake.," *Nano letters*, vol. 9, pp. 4370–5, Dec. 2009.

[91] H. Jin, D. a. Heller, and M. S. Strano, "Single-particle tracking of endocytosis and exocytosis of single-walled carbon nanotubes in NIH-3T3 cells.," *Nano letters*, vol. 8, pp. 1577–85, June 2008.

[92] F. A. Murphy, A. Schinwald, C. A. Poland, and K. Donaldson, "The mechanism of pleural inflammation by long carbon nanotubes: interaction of long fibres with macrophages stimulates them to amplify pro-inflammatory responses in mesothelial cells.," *Particle and fibre toxicology*, vol. 9, p. 8, Jan. 2012.

[93] D. Liu, L. Wang, Z. Wang, and A. Cuschieri, "Different cellular response mechanisms contribute to the length-dependent cytotoxicity of multi-walled carbon nanotubes," *Nanoscale research letters*, vol. 7, no. 1, p. 361, 2012.

[94] D. M. Brown, I. A. Kinloch, U. Bangert, A. H. Windle, D. M. Walter, G. S. Walker, C. A. Scotchford, K. Donaldson, and V. Stone, "An in vitro study of the potential of carbon nanotubes and nanofibres to induce inflammatory mediators and frustrated phagocytosis," *Carbon*, vol. 45, no. 9, pp. 1743–1756, 2007.

[95] C. P. Chio, S. C. Chen, K. C. Chiang, W. C. Chou, and C. M. Liao, "Oxidative stress risk analysis for exposure to diesel exhaust particle-induced reactive oxygen species," *Science of the Total Environment*, vol. 387, no. 1-3, pp. 113–127, 2007.

[96] E. Meunier, A. Coste, D. Olagnier, H. Authier, L. Lefevre, C. Dardenne, J. Bernad, M. Beraud, E. Flahaut, and B. Pipy, "Double-walled carbon nanotubes trigger IL-1 beta release in human monocytes through Nlrp3 inflammasome activation," *Nanomedicine-Nanotechnology Biology and Medicine*, vol. 8, no. 6, pp. 987–995, 2012.

[97] E. Koike, H. Takano, K. Inoue, R. Yanagisawa, and T. Kobayashi, "Carbon black nanoparticles promote the maturation and function of mouse bone marrow-derived dendritic cells," *Chemosphere*, vol. 73, no. 3, pp. 371–376, 2008.

[98] M. Yang, K. Flavin, I. Kopf, G. Radics, C. H. Hearnden, G. J. McManus, B. Moran, A. Villalta-Cerdas, L. A. Echegoyen, S. Giordani, and E. C. Lavelle, "Functionalization of Carbon Nanoparticles Modulates Inflammatory Cell Recruitment and NLRP3 Inflammasome Activation," *Small*, vol. 9, no. 24, pp. 4194–4206, 2013.

[99] J. H. Sánchez and C. Rinaldi, "Rotational Brownian dynamics simulations of non-interacting magnetized ellipsoidal particles in d.c. and a.c. magnetic fields," *Journal of Magnetism and Magnetic Materials*, vol. 321, pp. 2985–2991, Oct. 2009.

[100] C.-W. Lam, J. T. James, R. McCluskey, and R. L. Hunter, "Pulmonary toxicity of single-wall carbon nanotubes in mice 7 and 90 days after intratracheal instillation.," *Toxicological sciences : an official journal of the Society of Toxicology*, vol. 77, pp. 126–34, Jan. 2004.

[101] D. B. Warheit, B. R. Laurence, K. L. Reed, D. H. Roach, G. a. M. Reynolds, and T. R. Webb, "Comparative pulmonary toxicity assessment of single-wall carbon nanotubes in rats.," *Toxicological sciences : an official journal of the Society of Toxicology*,

vol. 77, pp. 117–25, Jan. 2004.

[102] J. B. Mangum, E. A. Turpin, A. Antao-Menezes, M. F. Cesta, E. Bermudez, and J. C. Bonner, "Single-walled carbon nanotube (SWCNT)-induced interstitial fibrosis in the lungs of rats is associated with increased levels of PDGF mRNA and the formation of unique intercellular carbon structures that bridge alveolar macrophages in situ.," *Particle and fibre toxicology*, vol. 3, p. 15, Jan. 2006.

[103] A. A. Shvedova, E. R. Kisin, R. Mercer, A. R. Murray, V. J. Johnson, A. I. Potapovich, Y. Y. Tyurina, O. Gorelik, S. Arepalli, D. Schwegler-Berry, A. F. Hubbs, J. Antonini, D. E. Evans, B. K. Ku, D. Ramsey, A. Maynard, V. E. Kagan, V. Castranova, and P. Baron, "Unusual inflammatory and fibrogenic pulmonary responses to single-walled carbon nanotubes in mice," *American Journal of Physiology-Lung Cellular and Molecular Physiology*, vol. 289, no. 5, pp. L698–L708, 2005.

[104] A. R. Murray, E. R. Kisin, A. V. Tkach, N. Yanamala, R. Mercer, S.-H. Young, B. Fadeel, V. E. Kagan, and A. A. Shvedova, "Factoring-in agglomeration of carbon nanotubes and nanofibers for better prediction of their toxicity versus asbestos.," *Particle and fibre toxicology*, vol. 9, p. 10, Jan. 2012.

[105] A. A. Shvedova, E. R. Kisin, A. R. Murray, C. Kommineni, V. Castranova, B. Fadeel, and V. E. Kagan, "Increased accumulation of neutrophils and decreased fibrosis in the lung of NADPH oxidase-deficient C57BL/6 mice exposed to carbon nanotubes," *Toxicology and Applied Pharmacology*, vol. 231, no. 2, pp. 235–240, 2008.

[106] A. A. Shvedova, E. Kisin, A. R. Murray, V. J. Johnson, O. Gorelik, S. Arepalli, A. F. Hubbs, R. R. Mercer, P. Keohavong, N. Sussman, J. Jin, J. Yin, S. Stone, B. T. Chen, G. Deye, A. Maynard, V. Castranova, P. A. Baron, and V. E. Kagan, "Inhalation vs. aspiration of single-walled carbon nanotubes in C57BL/6 mice: inflammation, fibrosis, oxidative stress, and mutagenesis," *American Journal of Physiology-Lung Cellular and Molecular Physiology*, vol. 295, no. 4, pp. L552–L565, 2008.

[107] A. A. Shvedova, J. P. Fabisiak, E. R. Kisin, A. R. Murray, J. R. Roberts, Y. Y. Tyurina, J. M. Antonini, W. H. Feng, C. Kommineni, J. Reynolds, A. Barchowsky, V. Castranova, and V. E. Kagan, "Sequential exposure to carbon nanotubes and bacteria enhances pulmonary inflammation and infectivity," *American Journal of Respiratory Cell and Molecular Biology*, vol. 38, no. 5, pp. 579–590, 2008.

[108] D. W. Porter, A. F. Hubbs, R. R. Mercer, N. Wu, M. G. Wolfarth, K. Sriram, S. Leonard, L. Battelli, D. Schwegler-Berry, S. Friend, M. Andrew, B. T. Chen, S. Tsuruoka, M. Endo, and V. Castranova, "Mouse pulmonary dose- and time course-responses induced by exposure to multi-walled carbon nanotubes.," *Toxicology*, vol. 269, pp. 136–47, Mar. 2010.

[109] U. Kishore, T. J. Greenhough, P. Waters, A. K. Shrive, R. Ghai, M. F. Kamran, A. L. Bernal, K. B. M. Reid, T. Madan, and T. Chakraborty, "Surfactant proteins SP-A and SP-D: Structure, function and receptors," *Molecular Immunology*, vol. 43, no. 9, pp. 1293–1315, 2006.

[110] C. Salvador-Morales, P. Townsend, E. Flahaut, C. Venien-Bryan, A. Vlandas, M. L. H. Green, and R. B. Sim, "Binding of pulmonary surfactant proteins to carbon nanotubes; potential for damage to lung immune defense mechanisms," *Carbon*, vol. 45, no. 3, pp. 607–617, 2007.

[111] C. Salvador-Morales, Z. Khan, J. Zamory, V. Tran, A. Cadeno, J. Umanzor-Alvarez, U. Kishore, and R. B. Sim, "Acid-treated multi-walled carbon nanotubes coated with lung Surfactant Protein SP-A do not induce a lung inflammatory response," *Journal of advanced microscopy research*, vol. 8, pp. 93–99, 2013.

[112] A. A. Kapralov, W. H. Feng, A. A. Amoscato, N. Yanamala, K. Balasubramanian, D. E. Winnica, E. R. Kisin, G. P. Kotchey, P. Gou, L. J. Sparvero, P. Ray, R. K. Mallampalli, J. Klein-Seetharaman, B. Fadeel, A. Star, A. A. Shvedova, and V. E. Kagan, "Adsorption of surfactant lipids by single-walled carbon nanotubes in mouse lung upon pharyngeal aspiration," *ACS Nano*, vol. 6, no. 5, pp. 4147–4156, 2012.

[113] M. Gasser, P. Wick, M. J. D. Clift, F. Blank, L. Diener, B. Yan, P. Gehr, H. F. Krug, and B. Rothen-Rutishauser, "Pulmonary surfactant coating of multi-walled carbon nanotubes (MWCNTs) influences their oxidative and pro-inflammatory potential in vitro.," *Particle and fibre toxicology*, vol. 9, p. 17, Jan. 2012.

[114] K. Pondman, E. Dodagatta-Marri, A. Tsolaki, M. Sobik, B. ten Haken, R. Sim, and U. Kishore, "Pulmonary surfactant protein SP-D opsonises carbon nanotubes and modulates immune response by macrophage and alveolar epithelial cells.," *Nanotoxicology*.

Chapter 3

Complement activation by carbon nanotubes and its influence on the phagocytosis and cytokine response by macrophages[1]

Abstract

Carbon nanotubes (CNTs) have promised a range of applications in biomedicine. Although influenced by the dispersants used, CNTs are recognized by the innate immune system, predominantly by the classical pathway of the complement system. Here, we confirm that complement activation by the CNTs used continues up to C3 and C5, indicating that the entire complement system is activated including the formation of membrane-attack complexes. Using recombinant forms of the globular regions of human C1q (gC1q) as inhibitors of CNT-mediated classical pathway activation, we show that C1q, the first recognition subcomponent of the classical pathway, binds CNTs via the gC1q domain. Complement opsonisation of CNTs significantly enhances their uptake by U937 cells, with concomitant downregulation of pro-inflammatory cytokines and upregulation of anti-inflammatory cytokines in both U937 cells and human monocytes. We propose that CNT-mediated complement activation may cause recruitment of cellular infiltration, followed by phagocytosis without inducing a pro-inflammatory immune response.

[1]The contents of this chapter have been published as: K.M. Pondman, M. Sobik, A. Nayak, A.G. Tsolaki, A. Jäkel, E. Flahaut, S. Hampel, B. ten Haken, R.B. Sim, U. Kishore, "Complement activation by carbon nanotubes and its influence on the phagocytosis and cytokine response by macrophages", *Nanomedicine: Nanotechnology, Biology, and Medicine*, vol. 10, no 6, p 1287-1299, august 2014

3.1 Introduction

The unique physical and chemical properties of carbon nanotubes (CNTs) make them very desirable materials in a range of biomedical applications [1, 2]. CNT mediated drug delivery has generated special interest [1, 3–11]. By functionalising the outer walls of the nanotubes via attaching target-specific molecules (e.g. antibodies), drugs can be delivered to specific targets. Iron filled CNTs (Fe-MWNTs), filled with a ferromagnetic material, promise magnetic drug delivery and hyperthermia therapy [3, 12, 13].

Due to their hydrophobicity and length, making stable dispersions of CNTs in physiological buffers, essential for drug delivery, is a common obstacle. Thus, non-covalent and covalent modifications of the CNT surfaces that include pre-coating with proteins, surfactants, nucleic acids, or introducing new functional groups on the external walls, are used. The biocompatibility of CNTs can be significantly improved when their surface is functionalized [1, 14–16].

Understanding the interactions between nanoparticles and immune system would facilitate their strategic and specific in vivo delivery [17]. The innate immune system plays a key role in protection against microorganisms and synthetic particles including CNTs [18–21]. Activation of the complement system, a major component of innate immunity [22], can influence therapeutic activity and effectiveness of CNTs, as it can in principle cause nanoparticles to adhere to immune cells. In addition, activation of complement releases the bioactive peptides C3a, C4a, C5a, which contribute to inflammation [19–22].

The complement system is composed of a group of > 40 plasma and cell surface proteins [22], which recognises and clears non-self (microorganisms), and altered self (apoptotic and necrotic cells, aggregated proteins). It can be activated via three pathways: classical, alternative or lectin, which converge on the formation of a C3 convertase, a protease which activates C3 that gets cleaved into C3b [23]. The target-bound C3b and a degradation product, iC3b are powerful opsonins, i.e. they mediate binding of the target to phagocytic cells. In the classical pathway, C1q binds to charged or hydrophobic clusters on targets [23], via its globular (gC1q) domain, followed by activation of two protease proenzymes, C1r and C1s, which, with C1q, form the C1 complex. This is followed by cleavage of C4 and C2, to form C4b2a, the C3 convertase. In the lectin pathway, Mannose-Binding Lectin (MBL) and Ficolins recognise neutral sugar and other uncharged features [24], and form C4b2a via the MASPs. The alternative pathway involves a constant but slow hydrolysis of C3 in solution, which forms C3(H2O). It forms a complex with Factor B, activated by Factor D (FD) to form C3(H2O)Bb (a C3 convertase) [25]. C3b, which binds randomly and covalently to any nearby surface or particle, is stabilised by properdin, an upregulator of the alternative pathway. This stage is followed by generation of C5 convertase to cleave C5 to form C5a and C5b. C5b

binds to C6, C7, C8 and C9 to form the C5b-9 complex, or membrane attack complex (MAC), which can insert into the lipid bilayer of the target and cause cell lysis [25]. The small fragments, C3a, C4a and C5a, promote inflammation as anaphylotoxic or chemotactic factors. Once C3b is deposited on a complement-activating particle, it is processed to form the products iC3b and C3dg/C3d. These fragments are recognised by different receptors on various cell types, and the receptor-ligand interaction can cause the particle to adhere to the cell [22]. The receptors involved include Complement Receptor 1 (CR1) which binds C3b and C4b, CR2 which binds C3dg/C3d, CR3 and CR4 which bind iC3b, and CRIg (C3b and iC3b) [26].

Non-functionalized SWNTs (single-walled) and DWNTs (double-walled), when placed in contact with human serum, activate complement via the classical and (to a lesser extent) the alternative pathway [19]. SWNTs stabilised with several poly(ethylene glycol) (PEG) derivatives show no alternative pathway activation but C4 cleavage, suggesting complement activation via the lectin pathway [27]. Functionalization (altering the surface properties of the CNTs) can increase or decrease the extent of complement activation [15, 18, 27, 28], while differing surface modifications can switch complement activation from one pathway to another. The mode of binding of the recognition subcomponents of the three pathways to CNTs, and whether they bind directly or via other deposited (serum)adaptor proteins, remains unclear. According to Ling et al [29], C1q "crystallizes" on CNTs, but is not bound in a way that allows activation of the next step of the complement cascade. Thus, other serum proteins may form a stable layer on the CNTs, triggering indirect C1 binding and complement activation. Salvador-Morales et al [18, 21], however, observed direct binding of C1q to CNTs, suggesting direct binding of C1 and subsequent complement activation.

In this study, we show several types of pristine and non-covalently functionalized CNTs activate the complement system predominantly via the classical pathway, which continues up to activation of C3 and C5, confirming the findings of Andersen et al [28] that the entire complement system is activated, leading to the formation of MAC. The interaction of C1q with these CNTs appears to occur via the gC1q domain since the recombinant forms of the gC1q regions of A, B and C chains bind CNTs stably. The binding of globular heads takes place in an orientation that inhibits the binding of serum C1q, thus suppressing C1-mediated classical pathway activation. We also report that complement activation and deposition on the surface of these CNTs enhance their uptake by macrophages (U937 cell line) in a time-dependent manner. Complement opsonisation of CNTs also leads to modulation of pro-inflammatory and anti-inflammatory cytokine production by U937 cells and human monocytes.

3.2 Material and methods

3.2.1 Carbon nanotube dispersions

Purified catalytic vapour deposition DWNTs and Fe-MWNTs were made as described earlier [30, 31]. To remove the iron filling (MWNTs), the samples were annealed under Argon at 2500°C [32]. SWNTs were purchased from Nanocyl (Sambreville, Belgium) and dispersed using non covalent functionalization via 2 min ultrasonication in PBS containing various dispersants with 5 mM EDTA, pH 7.4. Proteins used for dispersion were 4% w/v human fibrinogen (FBG) (Calbiochem), 4% w/v bovine serum albumin (BSA) (Sigma), and 4% (w/v) human serum albumin (HSA) (Sigma). Other dispersants used were 1% v/v Tween20 (Sigma), 2% w/v Carboxymethyl cellulose (CMC) (Sigma), 2% w/v phospholipid polyethylene glycol amine (PL-PEG-NH2) (Avanti Polar Lipids) and 1% w/v bakers yeast RNA (Sigma). After sonication, the samples were centrifuged at 8000 g for 5 min to remove aggregates and the supernatants were washed by vacuum filtering using a 0.2 μm polycarbonate filter (Whatman) with PBS - 5 mM EDTA, to remove excess of surfactants. Functionalized CNTs were re-suspended in PBS-EDTA and analysed using a Zeiss HR-LEO 1550 FEG Scanning Electron Microscope (SEM), figure 3.1. Length and diameter distributions of the MWNTs were determined from TEM images (data not shown) length 2.3 $\pm$ 1.9 μm (n=562) diameter 23 $\pm$ 11 nm (n=275).

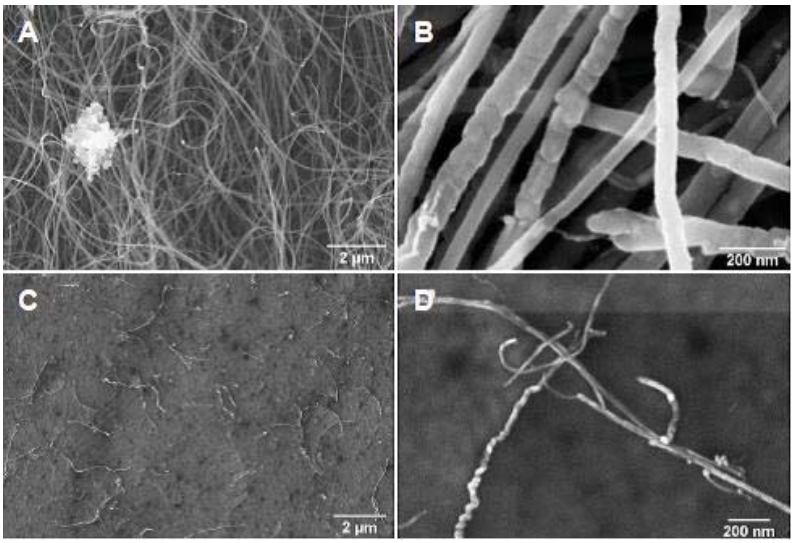

Figure 3.1: Scanning electron microscopy images of pristine (A and B) and CMC-coated (C and D) Fe-MWNTs showing high purity of the pristine samples and high dispersion of the functionalized samples. The dispersions are all very stable (non-sedimenting).

Concentrations and extinction coefficients at 730 nm of RNA-functionalized CNTs were determined in triplicate using a gravimetric method [33]. Briefly, CNTs were functionalized using RNA as described above, and after washing, absorption at 730 and 808 nm was measured for a series of dilutions. The solution was incubated with RNAse (1 mg/ml) (Sigma) at 37°C for 3 h. After extensive washing, CNTs were dried on a Whatman 0.2 μm filter. The extinction coefficients found were used to determine the concentrations of the other functionalized CNT samples.

3.2.2 Coating of CNTs with C1q, ghA, ghB and ghC proteins

C1q was purified from human plasma using affinity chromatography on IgG-Sepharose [34]. The C-terminal globular regions of human C1q A, B and C chains, designated ghA, ghB and ghC, were expressed as maltose-binding-protein fusion proteins in E. coli [35]. CMC-MWNTs were incubated with C1q, ghA, ghB or ghC,separately or mixed together, at 1:2 w/w ratios in 50 mM Tris, 100 mM NaCl, 5 mM $CaCl_2$, overnight at 4°C. Excess proteins were removed by washing three times in the same buffer. Protein binding was analysed by SDS-PAGE.

3.2.3 Complement Activation and Consumption Assay for the classical pathway

To investigate whether CNTs activated (consumed) complement in human serum [19], CNTs were incubated with normal human serum (SeraLab) for 1 h at 37°C, removed by centrifugation, and then the capacity of the incubated serum to lyse antibody-sensitised sheep erythrocytes (EA) was tested. EA were prepared [19] using sheep erythrocytes from TCS Biosciences and stored in dextrose gelatin veronal buffer ($DGVB^{++}$: 2.5 mM sodium barbital, 71 mM NaCl, 0.15 mM $CaCl_2$, 0.5mM $MgCl_2$, 2.5% w/v glucose, 0.1% w/v gelatin, pH 7.4) at 10^9 cells/ml.

CNT suspensions (100 μl of 0.1 mg/ml) in PBS were added to 100 μl of 1:1 diluted human serum in $DGVB^{++}$. Zymosan (0.2 mg in 100 μl PBS; Sigma) served as a positive control. Samples were incubated with occasional shaking at 37°C for 1 h followed by centrifugation (13000 g, 10 min). The supernatants of each sample were serially double-diluted (1/10 to 1/5120 in $DGVB^{++}$) and placed in microtitre wells. 100 μl of each dilution was incubated with 100 μl of EA (10^8 cells/ml in $DGVB^{++}$ in U-shaped wells (Fisher Scientific) for 1h at 37°C. Next, cells were spun down (700 g, 10 min, RT), and released haemoglobin in the supernatant was read at 405 nm. Total haemolysis (100%) was measured by lysing EA with water. Background spontaneous haemolysis (0%) was determined by incubating EA with buffer only. CH50 values, which correspond to the dilution factor of the serum that results in 50% cell lysis were calculated and compared.

To investigate whether coating CNTs with C1q or ghA, ghB and ghC modifies the activation of complement in human serum induced by CNTs, complement consumption assay was performed similarly [19]. Samples of pre-coated and uncoated CMC-MWNTs at 100 µg/ml in 50 mM Tris, 150 mM NaCl, and 5 mM $CaCl_2$ buffer were incubated at 37°C for 1 h with equal volumes of serum to give a total volume of 50 µl followed by centrifugation (13000 g, 10 min), supernatants were collected and assayed.

3.2.4 Complement Activation and Consumption Assay by the alternative pathway

EAIgG cells were made by treating SRBCs with the IgG fraction of rabbit anti-SRBC antibodies (GE Healthcare). EAIgG cells were diluted to 10^9 cells/ml in DGVB-Mg-EGTA (2.5 mM sodium barbital, 71 mM NaCl, 7 mM $MgCl_2$, 10 mM EGTA, 2.5% w/v glucose, 0.1% w/v gelatin, pH 7.4). Nanotube suspensions (100 µl of 0.1 mg/ml) were added to 100 µl undiluted human serum. Zymosan served as a positive control. The supernatants of each sample were serially diluted (1/5 to 1/320 in DGVB-Mg-EGTA) and placed in microtitre wells. 100 µl of each dilution was incubated with 100 µl of EAIgG (10^9 cells/ml in DGVB-Mg-EGTA) for 1 h at 37°C. Further steps were performed as above.

3.2.5 C3 and C5 consumption assay

To analyse whether the complement activation by CNTs continues to the activation of C3 and C5, an adapted haemolytic assay was performed. 20 µl of serum diluted 1/20 in $DGVB^{++}$ was incubated for 1 h at 37°C with or without nanotubes, the nanotubes removed by centrifugation, then the supernatant added to 20 µl 1/20 diluted C3-depleted serum (Sigma) or C5- depleted serum (Quidel) and 100 µl EA cells at 10^8 cells/ml in $DGVB^{++}$ for 1 h at 37°C. Further procedures and the calculation of the activity (titre) of C3 or C5 were done as described above.

3.2.6 Phagocytosis assay

To obtain biotinylated carbon nanotubes, MWNTs functionalized with CMC were washed thoroughly to remove excess CMC. CMC-CNTs were dialysed into 0.1 M MES buffer (2-(N-morpholino) ethanesulfonic acid, pH 5) and made to 0.2 mg/ml. Pentylamine biotin (Pierce) (10 mg) was added to 10 ml of the CMC-CNTs at 0.2 mg/ml and 100 µl of a 20 mg/ml solution of EDC (1-Ethyl-3-(3-dimethylaminopropyl) carbodiimide) (Pierce) in 0.1 M MES buffer pH 5 was added. The reaction (figure 3.2), was allowed to take place for 2h at RT with stirring, and was stopped by adding 100 µl of 0.1 M ethanolamine, pH 8.2. The resulting biotin-CMC-CNTs were dialysed into PBS (pH 7.4) to remove remaining reactants and MES.

U937 cells (a monocytic cell line derived from histiocytic lymphoma) were cultured in complete RPMI containing 10% fetal calf serum (FCS), 2 mM L-glutamine, 100 U/ml penicillin, 100 µg/ml streptomycin and 1 mM sodium pyruvate, and passaged before use.

In each well of a 24 well plate, 5×10^5 cells were incubated in complete or AIM-V AlbuMAX serum free medium (GIBCO) with above-mentioned supplements. 20 µg of biotin-CMC-CNTs in PBS were added to each well and incubated for 15, 30, 45, 60, 120 or 360 min. Cells were harvested and washed five times in PBS using centrifugation at 300 g and stored at -80°C until further use. A test with the same washing and Sepharose beads (in place of cells) with biotin-CMC-CNT dispersion showed that suspended nanotubes remained in dispersion and were washed away by this method. The supernatants were removed and 25 µl lysis buffer (10 mM HEPES, 20 mM NaCl, 0.5 mM EDTA, 1% w/v Triton X 100) was added to the cells. After lysing the cells, 25 µl of 0.1 mg/ml horse IgG in PBS was added to the dispersion to use in the quantification assay. The IgG was added as a blocking agent to minimise non-specific binding reactions.

An ELISA type assay was developed to quantify the amount of CNTs taken up by cells (figure 3.3). Microtitre wells (NUNC, polysorb) were coated with 100 µl Avidin (Pierce) at 50 µg/ml in 0.1 M Na_2CO_3, pH 9 for 1 h at RT, followed by blocking with 1 mg/ml horse IgG in PBS for 1 h at RT. Next, 50 µl of a solution or cell lysate containing biotin-CMC-CNTs and 50 µl of 0.1 mg/mL horse IgG was incubated for 1h in each well. The plate was washed 7 times with 0.1 mg/ml IgG to remove excess CNTs and incubated with 1:2000 Streptavidin-HRP (Horseradish peroxidase) (Sigma) for 1h at RT. Following washing again, O-Phenylenediamine dihydrochloride (OPD) (Sigma) was used as a substrate for the HRP and the yellow 2, 3-Diaminophenazine product was read at 450 nm.

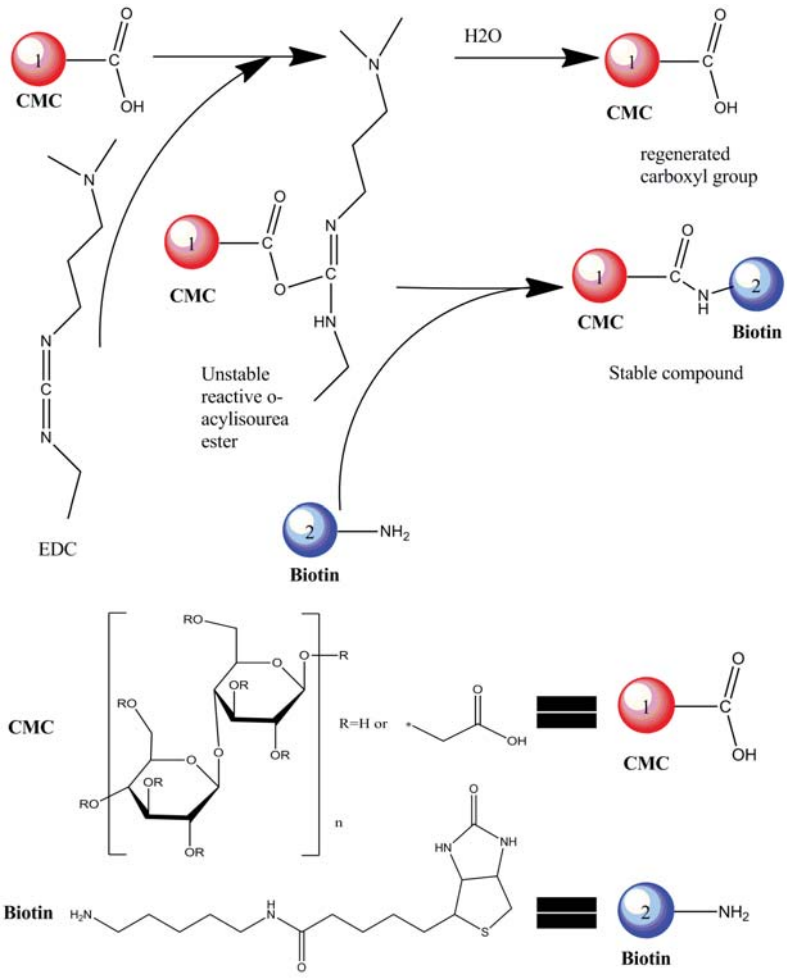

Figure 3.2: Biotinylation of CMC-MWNTs CMC-CNTs were dialysed into 0.1 M MES buffer (2-(N-morpholino)ethanesulfonic acid, pH 5) and made to 0.2 mg/ml. Pentylamine biotin (Pierce, Thermo Fisher Scientific) (10 mg) was added to 10 ml of the CMC-CNTs at 0.2 mg/ml and 100 µl of a 20 mg/ml solution of EDC (1-Ethyl-3-(3-dimethylaminopropyl)carbodiimide) was added. The reaction was allowed to take place for 2 h at RT with stirring, and was stopped by adding 100 µl of 0.1 M ethanolamine (Sigma). The resulting biotinylated-CMC-CNTs were dialysed into PBS (pH 7.4) to remove remaining reactants and MES.

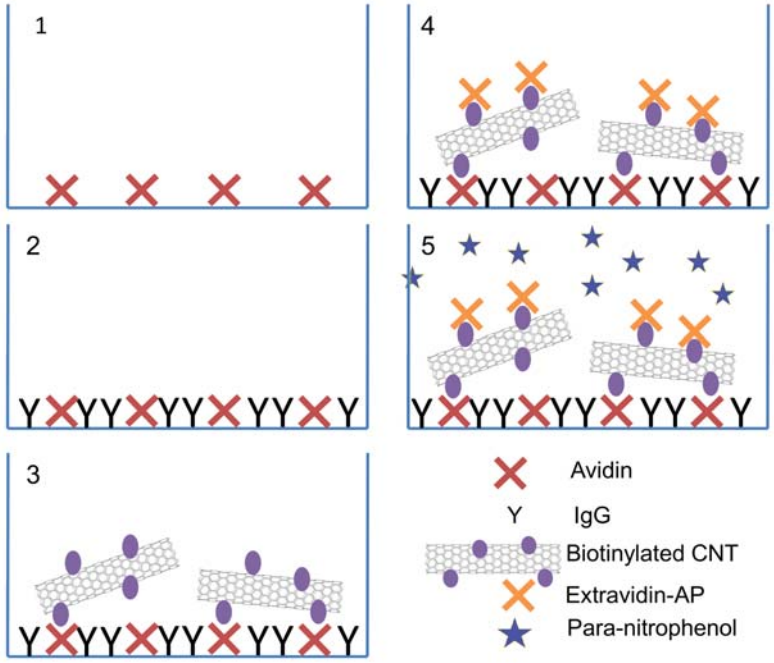

Figure 3.3: Steps in the quantification assay.
1. The plate is coated with Avidin in PBS at 50 µg/ml for 1 h.
2. The 96 well plate is blocked with IgG in PBS at 1 mg/ml for 1 h.
3. The sample containing biotinylated nanotubes is incubated on the plate for 1 h after which the plate is washed 7 times with 0.1 mg/ml IgG in PBS.
4. Streptavidin-HRP at 1:2000 in 0.1 mg/ml IgG in PBS is incubated for 1 h after which the plate is washed again 7 times with 0.1 mg/ml igG in PBS.
5. O-Phenylendiamine dihydrochloride is used as a substrate to form
2,3-Diaminophenazine. The yellow colour is measured at 450 nm using a plate reader.

3.2.7 Measurement of cytokine expression using quantitative PCR analysis

In a 24 well cell culture plate, 20 µg of CMC-MWNTs or RNA-MWNTs in 20 µl PBS were added to each well containing $5 \cdot 10^5$ U937 cells and incubated for 15, 30, 45, 60, 120 or 360 min; control samples were incubated with PBS only for 30 min. Cells were harvested and spun down (3000 g, 5 min) and stored at -80°C. Total RNA was extracted from frozen cell pellets using the GenElute Mammalian Total RNA Purification Kit (Sigma-Aldrich). Samples were treated with DNase I to remove any contaminating DNA. To inactivate both DNase I and RNase, samples were heated at 70°C for 10 min, and subsequently chilled on ice. The amount of total RNA was determined at 260 nm using the NanoDrop 2000/2000c (Thermo-Fisher Scientific), and the purity using the ratio of absorbance at 260 nm and 280 nm. cDNA was synthesized using High Capacity RNA to cDNA Kit (Applied Biosystems) from a quantity of 2 µg of total RNA extract.

Primer sequences were designed and analysed for specificity using the nucleotide BLAST and Primer-BLAST (http://blast.ncbi.nlm.nih.gov/Blast.cgi). The following primers were used:

18S forward (5-ATGGCCGTTCTTAGTTGGTG-3), 18S reverse (5-CGCTGAGCCA GTCAGTGTAG-3), IL-1β forward (5-GGACAAGCTGAGGAAGATGC-3), IL-1β reverse (5-TCGTTATCCCATGTGTCGAA-3), IL-6 forward (5-GAAAGCAGCAAAGAG GCACT-3), IL-6 reverse (5-TTTCACCAGGCAAGTCTCCT-3), IL-10 forward (5-TTACC TGGAGGAGGTGATGC-3), IL-10 reverse (5-GGCCTTGCTCTTGTTTTCAC-3), IL-12 forward (5-AACTTGCAGCTGAAGCCATT-3), IL-12 reverse (5-GACCTGAACGCAGA ATGTCA-3), TGF-β forward (5-GTACCTGAACCCGTGTTGCT-3), TGF-β reverse (5-GTATCGCCAGGAATTGTTGC-3), TNF-α forward (5-AGCCCATGTTGTAGCAAACC-3) and TNF-α reverse (5-TGAGGTACAGGCCCTCTGAT-3).

The qPCR reaction consisted of 5 µl Power SYBR Green MasterMix (Applied Biosystems), 75 nM of forward and reverse primer and 500 ng template cDNA in a 10 µl final reaction volume. PCR was performed in a 7900HT Fast Real-Time PCR System (Applied Biosystems). The initiation steps involved 2 min at 50°C followed by 10 min at 95°C. The template was then amplified for 40 cycles, each cycle comprised of 15 sec at 95°C and 1 min at 60°C. Samples were normalized using the expression of human 18S rRNA. Data was analyzed using the RQ Manager Version 1.2.1 (Applied Biosystems). Ct (cycle threshold) values for each cytokine target gene were calculated and the relative expression of each cytokine target gene was calculated using the Relative Quantification (RQ) value, using the equation:

$$RQ = 2^{-\Delta\Delta Ct} \tag{3.1}$$

for each cytokine target gene, and comparing relative expression with that of the 18SRNA constitutive gene product. Assays were conducted in triplicate.

3.2.8 Complement dependent interactions of CNTs with human monocytes and measurement of cytokine expression

Human monocytes were isolated from fresh blood from a healthy consenting individual using a Ficol-Paque plus (GE Healthcare) gradient according to the manufacturer's instructions. Lymphocytes and monocytes (PBMCs) obtained from the interface of plasma and Ficol-Paque were washed twice in RPMI 1640 and suspended in RPMI 1640. $2.5 \cdot 10^6$ PBMCs were plated out in each well of a 12 well plate (SPL Life Sciences), pre-coated with human serum overnight. After 2 h of incubation at 37°C in 5% CO_2, the non-adherent PBMC were gently removed from adherent monocytes. Medium was replaced by complete RPMI 1640 containing 10% human serum, or complete RPMI 1640 containing 10% heat inactivated human serum (30 min 56°C) or AIM-V AlbuMAX serum free medium (GIBCO) with 2 mM L-glutamine, 100 U/ml penicillin, 100 µg/ml streptomycin and 1mM sodium pyruvate. 10 µg CMC-MWNTs in PBS were added to each well and incubated for 15, 30, 45 or 60 min, control samples were incubated with PBS only for 30 min. Cells were harvested and spun down (3000 g, 5 min) and stored at -80°C. Further treatment and preparations were similar to those described above.

3.2.9 Statistical Analysis

Statistical analysis was performed using GraphPad Prism version 6.0 (GraphPad Software). For the experiments with U937 cells an unpaired 2-side t-test was used to compare the means of the cytokine targets with and without serum for any significant difference in expression. P values were computed and graphs compiled and analysed. A 2-way ANOVA was performed on the data obtained from the monocyte experiments and significant differences in expression at a given time point between serum and no serum-treated samples; and serum and heat-inactivated serum treated samples were determined.

3.3 Results

3.3.1 Complement (classical and alternative) is activated by various forms of CNTs

The activation of the classical and alternative pathway by Fe-MWNTs coated with CMC, RNA and PL-PEG-NH2 is shown in figure 3.4. All the CNT samples tested activated complement through both pathways, but predominantly through the classical pathway. C3 and

C5 consumption analysis showed that complement activation continued up to C5, indicating formation of MAC (figure 3.5). Differences in complement activation might be caused by degree of coating of the CNTs, as well as by the chemical nature of the coating substance.

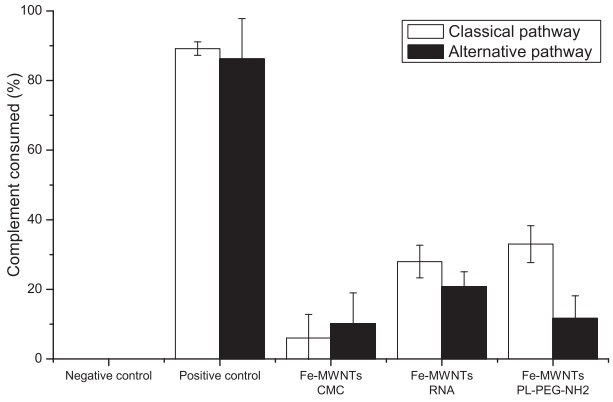

Figure 3.4: Complement activation via both the classical and alternative pathway for various coated Fe-MWNTs. Samples were incubated with human serum for 1 h. Zymosan was used as the positive control. Zero complement consumption was based on a negative control: Serum incubated without CNTs. Percentage complement consumption was calculated as (C-Ci)/C x 100%, where C represents the total complement activity in CH50 units of the negative control, Ci is the amount of activity remaining in the supernatant of the sample tested. All experiments were done in triplicate; error bars represent $\pm$ standard deviation.

3.3.2 C1q binds to CNTs via its gC1q domain

The binding of C1q was analysed by incubating CMC-MWNTs with individual C1q globular heads. All globular heads were shown to bind to the CNTs (figure 3.6a and 3.6b), indicating the orientation of C1q on the CNTs with the head regions onto the CNTs. This binding is most likely through charge pattern recognition. In this orientation binding of C1r and C1rs is possible and therefore complement activation via the classical pathway is initiated. Coating MWNTs with globular heads showed very effective inhibition of complement activation by these MWNTs (figure 3.6c). This opens up a way to reduce the recognition of the particles by the innate immune system.

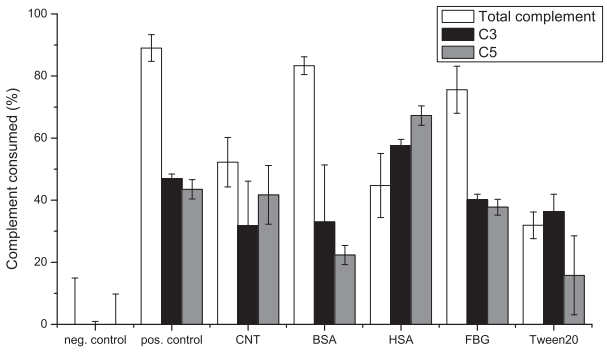

Figure 3.5: Complement consumption for total complement (classical pathway assay) and C3 and C5 consumption for DWNTs both pristine and coated with various plasma proteins (BSA, HSA, FBG) or Tween 20. Samples were pre-coated as described in Methods and incubated with human serum for 1 h. Zymosan samples were used as the positive control. Zero complement consumption was based on a negative control: Serum incubated without CNTs. Percentage of complement consumption was calculated as (C-Ci)/C x 100%, where C represents the total complement activity in CH50 units of the negative control, Ci is the amount of activity remaining in the supernatant of the sample tested. All experiments were done in triplicate; error bars represent $\pm$ standard deviation.

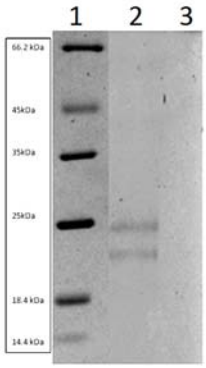

(a) Binding of C1q onto CMC-CNTs. Samples of CMC-MWNTs incubated with purified C1q and washed extensively were analysed by SDS-PAGE (8%) in reduced conditions. Lane 1. Molecular weight marker; lane 2 C1q coated CMC-MWNTs; lane 3 CMC-MWNTs. The bands visible are C1q A and B chains (25 kDa) running above the C chain (22 kDa).

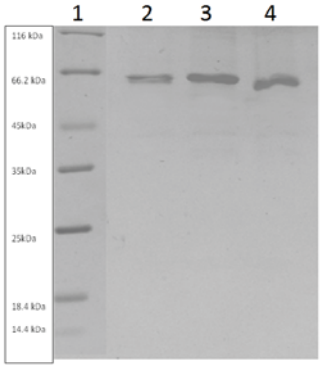

(b) Binding of ghA, ghB and ghC onto CMC-CNTs. Samples of CMC-MWNTs incubated with recombinant ghA, ghB or ghC and washed extensively were analysed by SDS-PAGE (12%) in reduced conditions. Lane 1: Molecular weight marker; lane 2: ghA coated CMC-MWNTs; lane 3: ghB coated CMC-MWNTs; lane 4: ghC coated CMC-MWNTs. The bands seen at about 65 kDa are fusion proteins formed from C1q globular heads a, b, or c, and maltose binding protein.

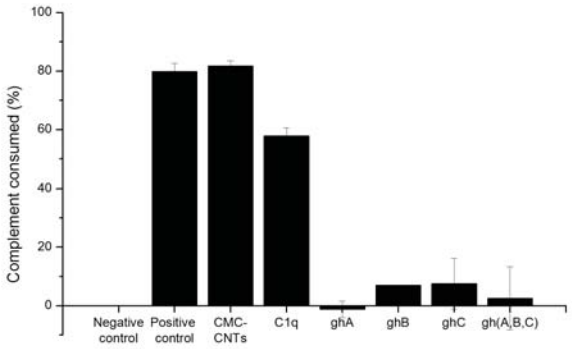

(c) Complement inhibition assay. Pre-coating of CNTs with ghA, ghB, ghC or an equimolar mixture of all three inhibits complement activation. CNTs were coated with the proteins in a ratio of 1:2 w/w, by incubating the CNTs with proteins overnight followed by extensive washing. Samples were incubated with human serum for 1 h. Zero complement consumption was based on a negative control: Serum incubated without CNTs. Percentage of complement consumption was calculated as (C-Ci)/C x 100%, where C represents the total complement activity in CH50 units of the negative control, Ci is the amount of activity remaining in the supernatant of the sample tested. Zymoszan was used as positive control. All experiments were done in duplicates; error bars represent $\pm$ standard deviation.

Figure 3.6: Individual globular heads of C1q, ghA, ghB and ghC bind to CNTs and inhibit complement activation.

3.3.3 Complement dependent interactions of CNTs with U937 cells and monocytes, phagocytosis and cytokine expression

CNTs were incubated with U937 cells in the presence and absence of serum, either allowing complement activation to occur or not and monitored for phagocytosis through a newly developed assay for up to 6 h. The efficiency of phagocytosis of CNTs by U937 cells is enhanced by the presence of serum strongly suggesting that complement proteins may be involved in this process (Figure 3.7). In order to examine the pro- and anti-inflammatory responses during this interaction, 6 key cytokines were analyzed for their expression during the course of phagocytosis (Figure 3.8). The data show that all cytokine responses studied are dampened in the presence of serum. The immune responses also showed similar expression patterns when compared between two types of CNTs. For the RNA-CNT without serum, cytokine responses have a biphasic pattern with a sharp upregulation in the first 15 min of phagocytosis, which diminishes and then peaks again at 45 min (Figure 3.9). IL-10 is also downregulated in the early stages of phagocytosis, but is slowly upregulated between 60 min and 360 min. A similar pattern is also observed in IL-12, IL-6 and IL-1β, although the effect seems more subtle in nature. For the CMC-CNT, similar patterns of cytokine expression to those seen with RNA-CNT were observed, although it does not appear to be biphasic in nature (Figure 3.8 and 3.10). The initial upregulation appears to be longer in duration (during the first 30 min), but then seems to diminish and plateau and be slightly downregulated.

In all six cytokines studied for the RNA-CNTs, there is on average a log two-fold difference in expression between serum-treated versus untreated during the first 15 min of phagocytosis. In the presence of serum, cytokine expression is always downregulated, and this is particularly notable in IL-12 where a log two-fold down regulation is observed. The differences in cytokine expression observed for CMC-CNTs is similar, although the average fold difference between expression in serum treated versus no serum during the first 15 min of phagocytosis was less, at about log one-fold difference. IL-10 is down-regulated in the presence of serum quite markedly during the early stages of phagocytosis with a log two-fold difference between serum and no serum. To further validate the results obtained using CNTs and U937 cells, freshly isolated monocytes were incubated with CMC-CNTs with and without normal human serum, as well as heat-inactivated serum. Heat inactivated serum yielded results comparable with serum free conditions, suggesting that downregulation of pro-inflammatory cytokines by serum results from complement proteins. This effect was most evident for TNF-α and IL-1β, and also for TGF-β, IL-12 and IL-6 in the late phase.

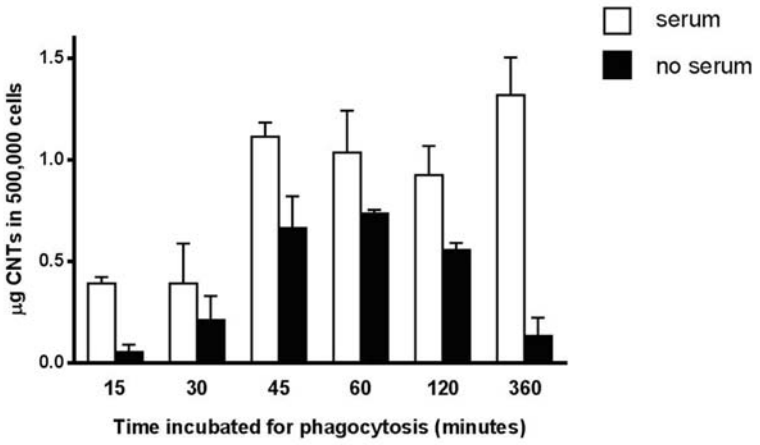

Figure 3.7: Uptake of CNTs by U937 cells in the presence and absence of serum. U937 cells were incubated with biotinylated CMC-MWNTs for 15, 30, 45, 60, 120 and 360 min. Excess CNTs were washed away and cells were lysed. The amount of CNTs in the lysate was quantified using a newly developed assay. A standard curve with known concentrations of biotin-CNTs was performed in the same assay to calculate the mass of the CNTs in the cell samples. All experiments were done in triplicate; error bars represent $\pm$ standard deviation.

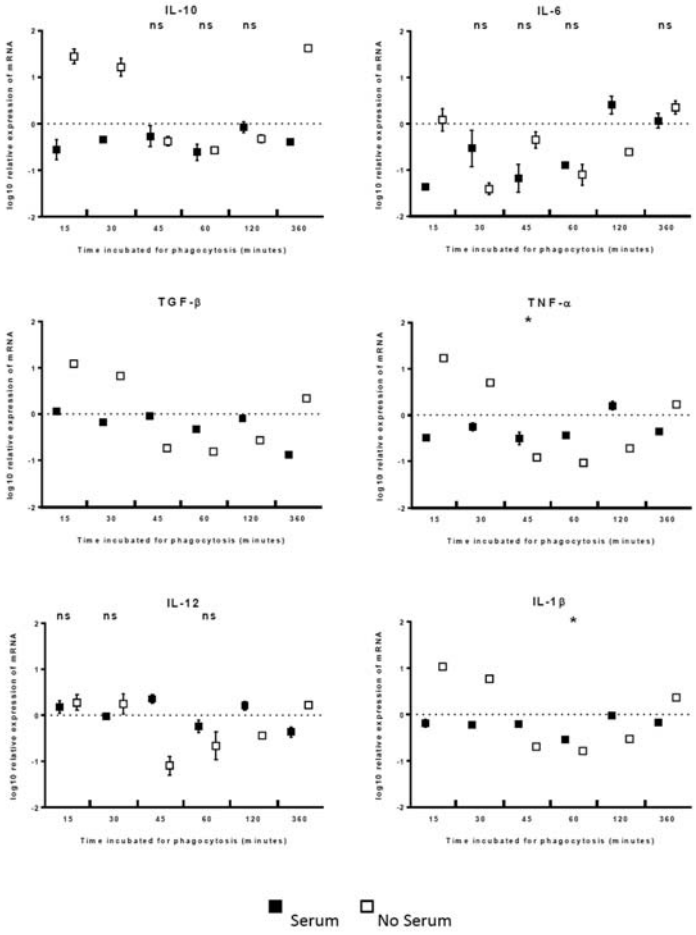

Figure 3.8: In vitro expression of cytokines by U937 incubated with CMC-CNTs. U937 cells were incubated with CMC-MWNTs in the presence or absence of serum for 15, 30, 45, 60, 120 and 360 min. The expression of cytokines was measured using real time qPCR and the data normalised to 18S rRNA gene expression as a control. Relative expression (RQ) was calculated by using the comparative Ct method with cells incubated with PBS for 30 min as the calibrator (data not shown). The RQ value was calculated using the formula: RQ = $2^{-\Delta\Delta^{Ct}}$. Assays were conducted in triplicate. Error bars represent $\pm$ standard error of the mean. A two-side t-test was performed on the data and significant differences in expression at a given time point between serum and no serum-treated samples are shown as follows: All time points showed significant differences in expression, $p < 0.01$, except where shown significant, $* : 0.01 < p < 0.05$, and ns: not significant.

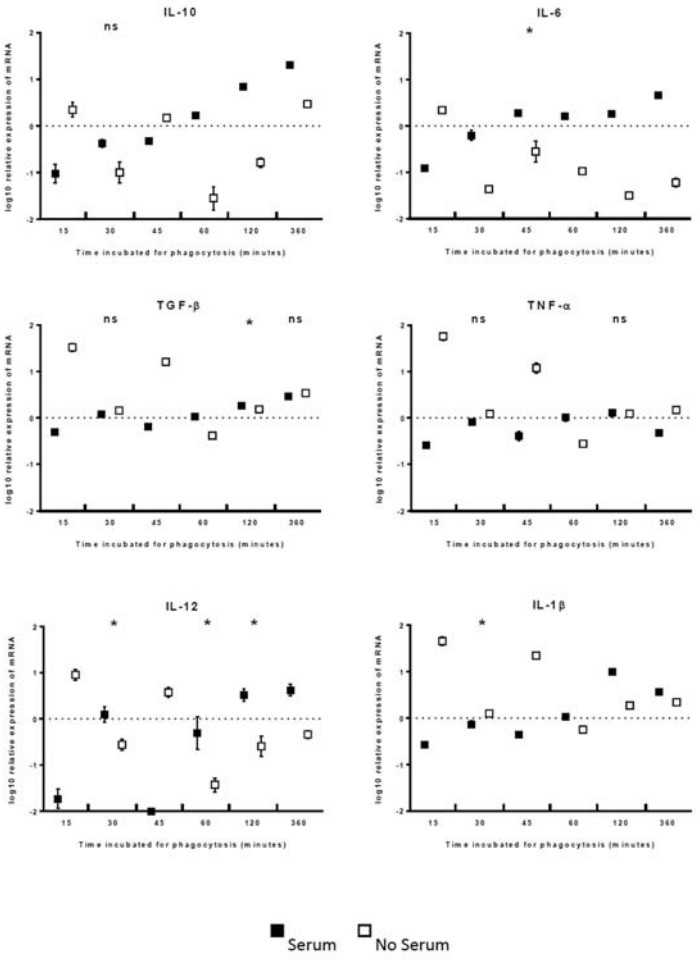

Figure 3.9: In vitro expression of cytokines by U937 incubated with RNA-MWNTs. U937 cells were incubated with RNA-MWNTs in the presence or absence of serum for 15, 30, 45, 60, 120 and 360 min. The expression of cytokines was measured using real time qPCR and the data normalised to 18S rRNA gene expression as a control. Relative expression (RQ) was calculated by using the comparative Ct method with cells incubated with PBS for 30 min as the calibrator (data not shown). The RQ value was calculated using the formula: RQ = $2^{-\Delta\Delta^{Ct}}$. Assays were conducted in triplicate. Error bars represent $\pm$ standard error of the mean. For U937 cells, a two-side t-test was performed on the data and significant differences in expression at a given time point between serum and no serum-treated samples are shown as follows: All time points showed significant differences in expression, $p < 0.01$, except where shown significant, $*$: $0.01 < p < 0.05$, and ns: not significant.

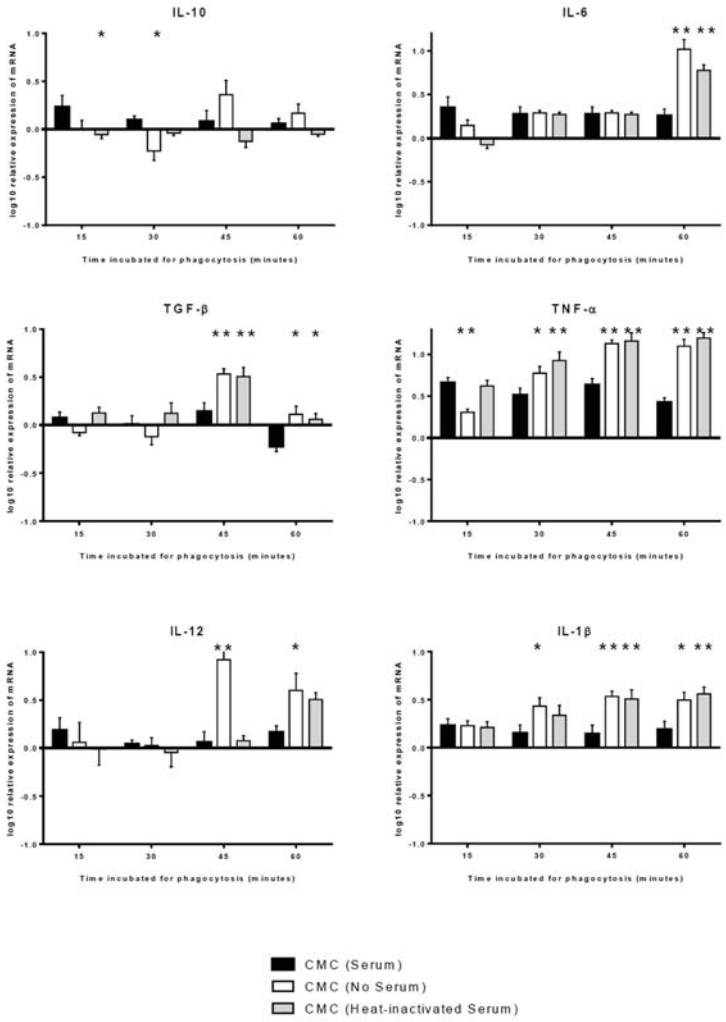

Figure 3.10: In vitro expression of cytokines by adherent monocytes incubated with CMC-CNTs. Monocytes were incubated with CMC-MWNTs for 15, 30, 45, 60 min in the presence of serum, heat inactivated serum, or without serum present. The expression of cytokines was measured using real time qPCR and the data normalised to 18S rRNA gene expression as a control. Relative expression (RQ) was calculated by using the comparative Ct method with cells incubated with PBS for 30 min as the calibrator (data not shown). The RQ value was calculated using the formula: RQ = $2^{-\Delta\Delta^{Ct}}$. Assays were conducted in triplicate. Error bars represent $\pm$ standard error of the mean. A 2-way ANOVA was performed on the data and significant differences in expression at a given time point between serum and no serum-treated samples and serum and heat-inactivated serum are shown as follows: All time points showed non-significant differences in expression, $p < 0.01$, except where shown significant, $* : 0.01 < p < 0.05$, and **:p> 0.01.

3.4 Discussion

The precise inflammatory properties of CNTs are still being examined, but various studies suffer from inconsistent findings. The type of functionalization on the surface of CNTs appears to be one of the key factors in modulating these inflammatory properties [36]. Host serum proteins can also enhance and/or mask the physiochemical characteristics of these CNTs. CNT interactions with complement proteins clearly play a key role in inflammation. The rationale for the predominant classical pathway activation remains an area of investigation. It is established that C1q binds to CNTs [19] but a recent study has reported that CNT-bound C1q fails to activate complement due to lack of C1 assembly [29]. C1q binds generally by ionic interactions with rearrangement to stronger hydrophobic interaction [37]. C1q is a charge pattern recognition molecule [38, 39]. It is likely that derivatisation of CNTs creates diverse C1q-recognisable patterns. Thus, in the case of CMC-CNTs, C1q binds via the gC1q domain in an orientation that supports complement activation. It is possible that under certain circumstances, C1q adaptor molecules such as IgG, IgM, CRP, SAP and PTX3 can first bind to CNTs, thus, allowing C1q to dock and then trigger classical pathway activation. However, the classical pathway complement inhibition caused by direct coating of CNTs with recombinant ghA, ghB and ghC appears to suggest a direct interaction between C1q and the CNTs.

C1q binding alone does not guarantee that the whole complement system is activated, or that the nanotube becomes coated with C3b. In order to activate the whole complement system, pristine or surface-modified CNTs need surface features which allow binding of C4 and C3. If, for example, a surface binds and activates C1, then C4 is activated, but if there is no site to which C4b can bind, C4b2a will not form efficiently and there will be very limited turnover of C3 [40]. If C4b2a forms on the surface, either by hydrophobic absorption or by covalent attachment of C4b to OH, NH_2 or SH groups, C3 will be activated (consumed). The C5 convertase C4b2a3b will be formed, if C4b2a is accessible on the surface to bind C3b. If C3b can bind appropriately, C5 will be activated (consumed). Each complement pathway ends in the formation of the C5-9 complex or MAC. A rise in MAC levels after interaction between PEGylated SWNTs and human serum has been reported,indicating that complement activation proceeds through the entire complement cascade [27], and further work by Andersen et al. [28] shows clearly that for a variety of derivatised CNTs, that the complete complement cascade is activated. This is important in understanding the capacity of nanomaterials to generate anaphylatoxins such as complement fragments C4a, C3a and C5a. In our study, we confirm that complement is activated until the consumption of C3 and C5 for both pristine and derivatised CNTs. Consumption of C5 is a clear indicator of formation of MAC. Since C3 and C5 consumption is substantial, C3 and C5 convertases must form on the

CNT surface. This, in turn, means that there are binding sites for C4b and C3b. Formation of complement fragments C3a, C4a and C5a promote inflammation, and depending on dose and route of administration, may cause problems when CNTs are used as drug delivery agents [41]. As noted above, C3b and C4b can bind covalently to surface nucleophilic groups, such as OH, NH_2. These will be of very low abundance on the pristine CNT surface, but possibly adsorbed dispersant, protein or HDL provide such sites. SDS-PAGE and Western blotting analysis of C3 fragments bound to CNTs (data not included) suggested that C3b does not form covalent adducts with higher molecular weight species (proteins) when bound to the CNT. It may bind covalently to molecules such as unesterified cholesterol (in adsorbed HDL) [19, 42], or it may bind by hydrophobic interactions possibly directly to the CNT surface.

An important role of protein adsorbed on the CNT surface in uptake by phagocytic cells has been noted [43]. CNTs have been shown to be engulfed by phagocytic cells via a range of phagocytic and endocytic mechanisms [44]. The phagocytosis data here is consistent with the known role complement plays in facilitating microbial uptake by macrophages. Thus, serum opsonisation or complement deposition enhanced uptake of labelled CNTs almost by two-fold at the time points tested. Curiously, the quantity of intracellular serum treated CNTs continued to increase post 60 min whereas the level of non-opsonised CNTs started to diminish. It will be interesting to track the intracellular route of opsonised and non-opsonised CNTs in order to understand their fate following uptake.

Complement or serum protein deposition likely renders CNTs resistant to phagolysosomal degradation of their coating, with possible loss of biotin label. Alternatively, untreated CNTs could potentially be transcytosed by the cells being recognised as biologically irrelevant debris. Studies to delineate various aspects of cytoplasmic trafficking of CNTs are under way. Reports suggest that CNTs stay in the cytoplasm either free or in endosomes [8, 45], while others state that the CNTs also entered the cell nucleus [46–48]. Exocytosis has not been reported often and the time course for the process varies between simultaneous with endocytosis [49] until after 5 h of incubation [45].

MWCNTs have been shown to stimulate pro-inflammatory cytokines such as IL-1β, TNF-α, IL-8 and IL-6 [50, 51]. CNTs induce an acute and robust inflammatory response in mice [52] as well as by human monocytes in vitro [53]. Here, we report that CMC-CNTs alone induced upregulation of IL-10, TNF-α and IL-1β within 30 min of the exposure to U937 cells; most of these responses were dampened in the presence of serum/complement deposition. In the case of RNA-CNTs, IL-10 was weakly upregulated by the opsonisation, which may raise the antigen threshold for an adaptive immune response. The biphasic TNF-α and IL-1β response induced by RNA-CNTs was seriously dampened by serum treatment. Serum also appears to have dampened IL-12 production by U937 cells. It appears that complement deposition may sequester CNT-mediated pro-inflammatory response towards an

anti-inflammatory environment. Further studies are required to understand role of specific complement proteins in modulating phagocytic and immune properties of macrophages. It also indicates that complement may facilitate the dampening of inflammation during this phagocytic process, resulting in more efficient cell recruitment. The importance of complement activation and deposition was further analysed by heat inactivation of the serum in the experiments with monocytes. Under these conditions cytokine profiles were similar for heat inactivated and serum free conditions. These observations have particular importance in targeted tissues and cells, where the use of CNTs in therapy may lead to tissue damage as a result of inflammation. The presence of complement proteins as opsonins for CNTs or the coating of tissues by these proteins will facilitate a reduction in any possible tissue damage as a result of an exaggerated inflammatory response to the CNTs. It is therefore important to further elucidate the precise immunological signature of these functionalized CNTs, not only to predict their use as a therapeutic vehicle, but also to gain insights into any unwanted pathologies or toxicity particulary on targeted tissues and cells. The data and assays presented here, may serve as important screens for new functionalized CNTs before they are tested in in vivo studies.

CNTs are not biodegradable and are unlikely to be used for muliple-dose administration, but they could be used in protheses, or in single dose treatments and with the increase of use of CNTs the risk of accidental exposure increases. Studies on complement activation by CNTs are useful as models for other (carbon based) nanomaterials and also for toxicology.

References

[1] A. Bianco, K. Kostarelos, C. D. Partidos, and M. Prato, "Biomedical applications of functionalised carbon nanotubes," *Chemical Communications*, no. 5, pp. 571–577, 2005.

[2] N. Sinha and J. T. Yeow, "Carbon nanotubes for biomedical applications," *IEEE Trans Nanobioscience*, vol. 4, no. 2, pp. 180–195, 2005.

[3] R. Klingeler, S. Hampel, and B. Buchner, "Carbon nanotube based biomedical agents for heating, temperature sensoring and drug delivery," *International journal of hyperthermia*, vol. 24, no. 6, pp. 496–505., 2008.

[4] A. Bianco, K. Kostarelos, and M. Prato, "Applications of carbon nanotubes in drug delivery," *Current Opinion in Chemical Biology*, vol. 9, pp. 674–679, Dec. 2005.

[5] C. Biale, V. Mussi, U. Valbusa, S. Visentin, G. Viscardi, N. Barbero, N. Pedemonte, and L. Galietta, "Carbon nanotubes for targeted drug delivery," *2009 9th Ieee Conference on Nanotechnology*, pp. 644–646, 2009.

[6] H. Ali-Boucetta, K. T. Al-Jamal, D. McCarthy, M. Prato, A. Bianco, and K. Kostarelos, "Multiwalled carbon nanotube-doxorubicin supramolecular complexes for cancer therapeutics.," *Chemical communications*, pp. 459–61, Jan. 2008.

[7] E. Heister, V. Neves, C. Tîlmaciu, K. Lipert, V. S. Beltrán, H. M. Coley, S. R. P. Silva, and J. McFadden, "Triple functionalisation of single-walled carbon nanotubes with doxorubicin, a monoclonal antibody, and a fluorescent marker for targeted cancer therapy," *Carbon*, vol. 47, no. 9, pp. 2152–2160, 2009.

[8] W. Wu, S. Wieckowski, G. Pastorin, M. Benincasa, C. Klumpp, J. P. Briand, R. Gennaro, M. Prato, and A. Bianco, "Targeted delivery of amphotericin B to cells by using functionalized carbon nanotubes," *Angewandte Chemie-International Edition*, vol. 44, no. 39, pp. 6358–6362, 2005.

[9] M. Foldvari and M. Bagonluri, "Carbon nanotubes as functional excipients for nanomedicines: I. Pharmaceutical properties.," *Nanomedicine : nanotechnology, biology, and medicine*, vol. 4, pp. 173–82, Sept. 2008.

[10] M. Foldvari and M. Bagonluri, "Carbon nanotubes as functional excipients for nanomedicines: II. Drug delivery and biocompatibility issues.," *Nanomedicine : nanotechnology, biology, and medicine*, vol. 4, pp. 183–200, Sept. 2008.

[11] L. Lacerda, A. Bianco, M. Prato, and K. Kostarelos, "Carbon nanotubes as nanomedicines: from toxicology to pharmacology," *Advanced Drug Delivery Reviews*, vol. 58, pp. 1460–1470, Dec. 2006.

[12] A. Taylor, K. Kraemer, S. Hampel, S. Fuessel, R. Klingeler, M. Ritschel, B. Buechner, M. O. Grimm, and M. P. Wirth, "Carbon coated nanomagnets as potential hyperthermia agents," *Journal of Urology*, vol. 179, no. 4, pp. 392–393, 2008.

[13] Y. Krupskaya, C. Mahn, A. Parameswaran, A. Taylor, K. Kramer, S. Hampel, A. Leonhardt, M. Ritschel, B. Buchner, and R. Klingeler, "Magnetic study of iron-containing carbon nanotubes: Feasibility for magnetic hyperthermia," *Journal of Magnetism and Magnetic Materials*, vol. 321, no. 24, pp. 4067–4071, 2009.

[14] B. S. Bhattacharya, "Implementing the cellular mechanisms of synaptic transmission in a neural mass model of the thalamo-cortical circuitry.," *Frontiers in computational neuroscience*, vol. 7, p. 81, Jan. 2013.

[15] V. A. Basiuk, C. Salvador-Morales, E. V. Basiuk, R. M. J. Jacobs, M. Ward, B. T. Chu, R. B. Sim, and M. L. H. Green, "'Green' derivatization of carbon nanotubes with Nylon 6 and L-alanine," *Journal of Materials Chemistry*, vol. 16, no. 45, pp. 4420–4426, 2006.

[16] H. Dumortier, S. Lacotte, G. Pastorin, R. Marega, W. Wu, D. Bonifazi, J. P. Briand, M. Prato, S. Muller, and A. Bianco, "Functionalized carbon nanotubes are non-cytotoxic and preserve the functionality of primary immune cells," *Nano Letters*, vol. 6, no. 12, p. 3003, 2006.

[17] B. S. Zolnik, A. Gonzalez-Fernandez, N. Sadrieh, and M. A. Dobrovolskaia, "Minireview: Nanoparticles and the Immune System," *Endocrinology*, vol. 151, no. 2, pp. 458–465, 2010.

[18] C. Salvador-Morales, E. V. Basiuk, V. A. Basiuk, M. L. H. Green, and R. B. Sim, "Effects of covalent functionalisation on the biocompatibiltiy characteristics of multi-walled carbon nanotubes," *Journal of Nanoscience and Nanotechnology*, vol. 8, no. 5, pp. 2347–2356, 2007.

[19] C. Salvador-Morales, E. Flahaut, E. Sim, J. Sloan, M. L. Green, and R. B. Sim, "Complement activation and protein adsorption by carbon nanotubes," *Molecular Immunology*, vol. 43, no. 3, pp. 193–201, 2006.

[20] C. Salvador-Morales, M. L. H. Green, and R. B. Sim, "Interaction between carbon nanotubes and biomolecules.," in *Chemistry of carbon nanotubes* (E. V. Basiuk and V. A. Basiuk, eds.), ch. 27, American Scientific Publishers, 2007.

[21] M. Rybak-Smith, K. Pondman, E. Flahaut, C. Salvador-Morales, R. Sim, and ., "Recognition of Carbon Nanotubes by the Human Innate Immune System.," in *Carbon Nanotubes for Biomedical Applications* (R. Klingeler and R. B. Sim, eds.), pp. 183–210, Springer, 2011.

[22] M. V. Carroll and R. B. Sim, "Complement in health and disease," *Advanced Drug Delivery Reviews*, vol. 63, no. 12, pp. 965–975, 2011.

[23] Y.-H. Kang, L. A. Tan, M. V. Carroll, M. E. Gentle, and R. B. Sim, "Target pattern recognition by complement proteins of the classical and alternative pathways.," *Advances in experimental medicine and biology*, vol. 653, pp. 117–128, 2009.

[24] K. Ikeda, T. Sannoh, N. Kawasaki, T. Kawasaki, and I. Yamashina, "Serum lectin with known structure activates complement through the classical pathway.," *Journal of biological chemistry*, vol. 262, pp. 7451–7454, 1987.

[25] S. Bhakdi and J. Tranum-Jensen, "Complement lysis: a hole is a hole.," *Immunology today*, vol. 12, pp. 318–20; discussion 321, Sept. 1991.

[26] M. C. Carroll, "The role of complement and complement receptors in induction and regulation of immunity.," *Annual review of immunology*, vol. 16, pp. 545–568, 1998.

[27] I. Hamad, A. C. Hunter, K. J. Rutt, Z. Liu, H. Dai, and S. M. Moghimi, "Complement activation by PEGylated single-walled carbon nanotubes is independent of C1q and alternative pathway turnover," *Molecular Immunology*, vol. 45, no. 14, pp. 3797–3803, 2008.

[28] A. J. Andersen, J. T. Robinson, H. J. Dai, A. C. Hunter, T. L. Andresen, and S. M. Moghimi, "Single-Walled Carbon Nanotube Surface Control of Complement Recognition and Activation," *ACS Nano*, vol. 7, no. 2, pp. 1108–1119, 2013.

[29] W. L. Ling, A. Biro, I. Bally, P. Tacnet, A. Deniaud, E. Doris, P. Frachet, G. Schoehn, E. Pebay-Peyroula, and G. J. Arlaud, "Proteins of the Innate Immune System Crystallize on Carbon Nanotubes but Are Not Activated," *ACS Nano*, vol. 5, no. 2, pp. 730–737, 2011.

[30] E. Flahaut, R. Bacsa, A. Peigney, and C. Laurent, "Gram-scale CCVD synthesis of double-walled carbon nanotubes," *Chemical Communications*, no. 12, pp. 1442–1443, 2003.

[31] C. Muller, S. Hampel, D. Elefant, K. Biedermann, A. Leonhardt, M. Ritschel, and B. Buchner, "Iron filled carbon nanotubes grown on substrates with thin metal layers and their magnetic properties," *Carbon*, vol. 44, no. 9, pp. 1746–1753, 2006.

[32] K. Lipert, F. Kretzschmar, M. Ritschel, A. Leonhardt, R. Klingeler, and B. Buchner, "Nonmagnetic carbon nanotubes," *Journal of Applied Physics*, vol. 105, no. 6, pp. 063906–063910, 2009.

[33] J. C. G. Jeynes, E. Mendoza, D. C. S. D. Chow, P. C. R. P. Watts, J. Mcfadden, S. R. P. Silva, and B. J. C. G. Jeynes, "Generation of chemically unmodified pure single-walled carbon nanotubes by solubilizing with RNA and treatment with ribonuclease A,"

Advanced Materials, vol. 18, pp. 1598–1602, June 2006.

[34] L. A. Tan, B. Yu, F. C. J. Sim, U. Kishore, and R. B. Sim, "Complement activation by phospholipids: the interplay of factor H and C1q.," *Protein & cell*, vol. 1, pp. 1033–49, Nov. 2010.

[35] U. Kishore, S. K. Gupta, M. V. Perdikoulis, M. S. Kojouharova, B. C. Urban, and K. B. M. Reid, "Modular organization of the carboxyl-terminal, globular head region of human C1q A, B, and C chains.," *Journal of immunology*, vol. 171, pp. 812–20, July 2003.

[36] M. Yang, K. Flavin, I. Kopf, G. Radics, C. H. Hearnden, G. J. McManus, B. Moran, A. Villalta-Cerdas, L. A. Echegoyen, S. Giordani, and E. C. Lavelle, "Functionalization of Carbon Nanoparticles Modulates Inflammatory Cell Recruitment and NLRP3 Inflammasome Activation," *Small*, vol. 9, no. 24, pp. 4194–4206, 2013.

[37] L. Roumenina, S. Bureeva, A. Kantardjiev, D. Karlinsky, J. E. Andia-Pravdivy, R. Sim, A. Kaplun, M. Popov, U. Kishore, and B. Atanasov, "Complement C1q-target proteins recognition is inhibited by electric moment effectors," *Journal of Molecular Recognition*, vol. 20, no. 5, pp. 405–415, 2007.

[38] R. Ghai, P. Waters, L. T. Roumenina, M. Gadjeva, M. S. Kojouharova, K. B. M. Reid, R. B. Sim, and U. Kishore, "C1q and its growing family," *Immunobiology*, vol. 212, no. 4-5, pp. 253–266, 2007.

[39] U. Kishore, C. Gaboriaud, P. Waters, A. K. Shrive, T. J. Greenhough, K. B. M. Reid, R. B. Sim, and G. J. Arlaud, "C1q and tumor necrosis factor superfamily: modularity and versatility.," *Trends in immunology*, vol. 25, pp. 551–61, Oct. 2004.

[40] A. W. Dodds and R. R. Porter, "Activation of Complement Components by Aggregates of Antibodies and Their Fragments," *Molecular Immunology*, vol. 16, no. 12, pp. 1059–1062, 1979.

[41] J. Szebeni, P. Bedocs, D. Csukas, L. Rosivall, R. Bunger, and R. Urbanics, "A porcine model of complement-mediated infusion reactions to drug carrier nanosystems and other medicines," *Advanced Drug Delivery Reviews*, vol. 64, no. 15, pp. 1706–1716, 2012.

[42] W. Vogt, I. von Zabern, B. Damerau, D. Hesse, B. Luhmann, and R. Nolte, "Mechanisms of complement activation by crystalline cholesterol," *Molecular Immunology*, vol. 22, no. 2, pp. 101–106, 1985.

[43] D. Dutta, S. K. Sundaram, J. G. Teeguarden, B. J. Riley, L. S. Fifield, J. M. Jacobs, S. R. Addleman, G. A. Kaysen, B. M. Moudgil, and T. J. Weber, "Adsorbed proteins influence the biological activity and molecular targeting of nanomaterials.,"

Toxicological sciences : an official journal of the Society of Toxicology, vol. 100, pp. 303–15, Nov. 2007.

[44] K. Bhattacharya, F. T. Andon, R. El-Sayed, and B. Fadeel, "Mechanisms of carbon nanotube-induced toxicity: Focus on pulmonary inflammation," *Advanced Drug Delivery Reviews*, vol. 65, no. 15, pp. 2087–209, 2013.

[45] B. Kang, D.-C. Yu, S.-Q. Chang, D. Chen, Y.-D. Dai, and Y. Ding, "Intracellular uptake, trafficking and subcellular distribution of folate conjugated single walled carbon nanotubes within living cells.," *Nanotechnology*, vol. 19, p. 375103, Sept. 2008.

[46] K. Kostarelos, L. Lacerda, G. Pastorin, W. Wu, S. Wieckowski, J. Luangsivilay, S. Godefroy, D. Pantarotto, J. P. Briand, S. Muller, M. Prato, and A. Bianco, "Cellular uptake of functionalized carbon nanotubes is independent of functional group and cell type," *Nature nanotechnology*, vol. 2, no. 2, pp. 108–113, 2007.

[47] D. Pantarotto, J.-P. Briand, M. Prato, and A. Bianco, "Translocation of bioactive peptides across cell membranes by carbon nanotubes.," *Chemical communications*, pp. 16–7, Jan. 2004.

[48] Q. Mu, D. L. Broughton, and B. Yan, "Endosomal leakage and nuclear translocation of multiwalled carbon nanotubes: developing a model for cell uptake.," *Nano letters*, vol. 9, pp. 4370–5, Dec. 2009.

[49] H. Jin, D. a. Heller, and M. S. Strano, "Single-particle tracking of endocytosis and exocytosis of single-walled carbon nanotubes in NIH-3T3 cells.," *Nano letters*, vol. 8, pp. 1577–85, June 2008.

[50] F. A. Murphy, A. Schinwald, C. A. Poland, and K. Donaldson, "The mechanism of pleural inflammation by long carbon nanotubes: interaction of long fibres with macrophages stimulates them to amplify pro-inflammatory responses in mesothelial cells.," *Particle and fibre toxicology*, vol. 9, p. 8, Jan. 2012.

[51] A. J. Andersen, P. P. Wibroe, and S. M. Moghimi, "Perspectives on carbon nanotube-mediated adverse immune effects," *Advanced Drug Delivery Reviews*, vol. 64, no. 15, pp. 1700–1705, 2012.

[52] A. A. Shvedova, E. R. Kisin, A. R. Murray, C. Kommineni, V. Castranova, B. Fadeel, and V. E. Kagan, "Increased accumulation of neutrophils and decreased fibrosis in the lung of NADPH oxidase-deficient C57BL/6 mice exposed to carbon nanotubes," *Toxicology and Applied Pharmacology*, vol. 231, no. 2, pp. 235–240, 2008.

[53] E. Meunier, A. Coste, D. Olagnier, H. Authier, L. Lefevre, C. Dardenne, J. Bernad, M. Beraud, E. Flahaut, and B. Pipy, "Double-walled carbon nanotubes trigger IL-1 beta release in human monocytes through Nlrp3 inflammasome activation," *Nanomedicine-*

Nanotechnology Biology and Medicine, vol. 8, no. 6, pp. 987–995, 2012.

Chapter 4

Au coated Ni nanowires with tuneable dimensions for biomedical applications[1]

Abstract

Due to their shape anisotropy, high aspect ratio magnetic nanoparticles offer many advantages in biomedical applications. For biocompatibility, it is essential to have full control over the dimensions and surface chemistry of the particles. The aim of this study was to make biocompatible nanowires with tuneable dimensions. This was achieved by electrodeposition of Ni in polycarbonate membranes. To assure biocompatibility, a continuous gold coating was deposited onto the Ni wires by a newly developed electroless deposition method. The coating was analysed using electron microscopy and X-ray diffraction. Magnetic properties, anisotropy and Au film thickness were studied using vibrating sample magnetometry. After biofunctionalization, no significant cytotoxic effects were found in studies involving a diverse range of primary and tumour cells exposed to increasing concentrations of nanowires for up to 7 days. These nanowires may thus be used for in-vivo applications such as magnetic drug delivery.

[1] The contents of this chapter have been published as: K.M. Pondman, A.W. Maijenburg, F.B. Celikkol, A.A. Pathan, U. Kishore, B. ten Haken and J.E. ten Elshof, "Au coated Ni nanowires with tuneable dimensions for biomedical applications", *Journal of Materials Chemistry B*, vol. 1, p. 6129-6136, 2013

4.1 Introduction

Magnetic nanoparticles offer attractive possibilities in biomedicine, e.g. in magnetic separation, therapeutic drug, gene and radionuclide delivery, hyperthermia, and as contrast agents in magnetic resonance imaging [1]. To date, the majority of magnetic nanoparticles used are spherical, consisting of one or multiple magnetic cores with a biocompatible coating and active ligands. Within biomedicine, magnetic nanowires are receiving growing attention [2–6]. Due to their elongated shape and anisotropic physical properties, these particles interact very differently with tissues, cells and bio-molecules [3, 7–9]. Due to their increased surface to volume ratio, more drugs and ligands can be bound for drug delivery or immunoassays. While the small diameter of nanowires makes it possible for the particle to pass through the narrow capillaries, the large remnant magnetization increases the range and effectiveness of magnetic interactions at a distance from external magnets. This allows not only magnetic drug targeting at locations deeper inside the body [4] and cell guidance [10], but also increases the effectiveness of cell separation significantly [6, 9, 11, 12]. Nanowires, with lengths matching the cell diameter, have previously been shown to outperform magnetic beads for cell separation, highlighting the importance of the dimension of the nanowires [9, 11]. Whereas spherical particles only respond to magnetic flux gradients, high aspect ratio particles allow the application of torque with a relatively weak external field to perform dynamic targeted cell therapy [13]. The torque can also be used to align the nanowires, and after their uptake by cells, it allows for the spatial organization of cells [3, 12]. Most research on elongated nanoparticles was performed with carbon nanotubes. This research showed that elongated particles are capable of entering cells by penetration, allowing for direct access to the cytosol without the need of endosome escape strategies [7, 14, 15]. Several chemical methods to make elongated nanoparticles can be found in literature (Figure 4.1).

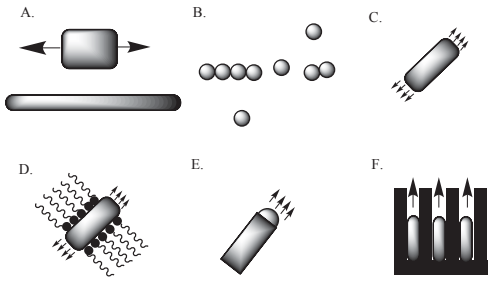

Figure 4.1: (A) Size reduction of a 1D-microstructure; (B) (Self)assembly of spherical nanostructures; (C) Spontaneous synthesis by dictation by the anisotropic crystallographic structure of a solid; (D) Kinetic control by a capping reagent; (E)Confinement by a liquid droplet in a vaporliquidsolid procedure; (F) Direction through the use of a template [16].

Templated electrodeposition has several advantages in this application, including ease of fabrication, reproducibility, and low cost. Nanowires made by this method are always continuous since any breakage would halt the growth of the nanowires. Depending on the template and deposition time used, nanowires can be made with nanometer to micrometer dimensions, spanning several relevant biological length scales. Various magnetic metals such as iron (Fe), cobalt (Co), nickel (Ni), and their alloys have been used to form nanowires inside the pores of silica, anodized alumina, or polycarbonate membranes [17–20].

Having full control over the dimensions of nanowires is essential for biomedical applications. Earlier research on asbestos and carbon nanotubes has suggested that cytotoxicity is highly dependent on aspect ratio. Long nanowires have been associated with inflammation, fibrosis and malignant mesothelioma and are likely to generate reactive oxygen species that can cause DNA damage and cell death [21]. Unfortunately, most proposed nanowires [8, 9, 22] are larger than cells, leaving the wires to protrude from the cells, thereby reducing the viability of the cells. Particles longer than 5 μm cannot be considered as "safe"in terms of uptake and clearance by macrophages and possibly induce inflammation and carcinogenic effects [23]. A length below 5 μm will also make it possible for the nanowires to flow through the curvy capillaries allowing for local drug delivery. In addition to dimensional restrictions, the materials and surface chemistry of the particle should be biocompatible and stable during use. Fe is often considered the most advantageous option, but due to the ease of oxidation of Fe, Ni is often preferred as magnetic phase for nanowires. Although Ni is a naturally occurring transition material and an essential nutrient [24] there are indications that Ni may be a carcinogen and induce apoptosis [25–27]. Studies on toxicity of Ni wires are divided; some studies indicate no toxicity of Ni nanowires at low concentrations, and the need of long term exposure to act as carcinogens [4, 28]. But at higher concentration, even short incubation times have been shown to be lethal to cells [8]. Some authors indicate the benefits of induced apoptosis by Ni nanowires, e.g. reactive oxygen species mediated apoptosis caused by Ni nanowires in human pancreatic adenocarcinoma cells [29]. Unfortunately, these apoptotic effects are not specific to carcinoma cells and would therefore also occur in other bystander healthy cells. Shielding of the potentially toxic Ni from contact with the body was therefore considered essential in this study. The coating is also important to protect the Ni from oxidation. For this purpose, various polymers, proteins and phospholipids have been proposed [22, 30, 31]. These coatings are biocompatible but cannot shield the particles from oxygen. Therefore, a solid Au shell is considered most advantageous as Au is known for its excellent biocompatibility and it cannot be removed by factors within the body [32]. Furthermore, Au provides a platform for functionalization, such as conjugation of biomolecules, targeting moieties and drugs [33, 34]. This work aims at the development of a magnetic nanowire for application in magnetic drug delivery and similar biomedical

applications. The proposed electrodeposited Ni nanowire has a tuneable length below 5 µm with narrow size distribution. To increase the biocompatibility, the nanowires were coated with an Au shell. To limit toxic effects, use of cyanide, which is commonly used in Au coatings [32], was avoided. Therefore, a new coating procedure was developed, inspired by a method to make Au nanotubes by electroless deposition [35]. The nanowires were characterized using a variety of techniques in order to determine their dimensions, magnetic properties, crystallographic structure and biocompatibility.

4.2 Materials and methods

4.2.1 Materials

Commercially available polycarbonate track-etched membranes (PCTE, Whatman, UK) with nominal (quoted by the supplier) pore size of 50 nm, were used as template membranes. Nickel(II)sulfate hexahydrate ($NiSO_4 \cdot 6\,H_2O$), boric acid (H_3BO_3), ammonia NH_4OH, 37%, and glutathione (GSH) were obtained from Sigma-Aldrich and were used without further purification. Thiolated polyethylene glycol (mPEG-SH, 2 kDa) was purchased from Rapp Polymere (Tübingen, Germany). Dichloromethane (CH_2Cl_2) was used as obtained from Thermo Fisher Scientific (Waltham, USA). Trifluoroacetic acid, 11-aminoundecanoic acid, sodium sulfite (Na_2SO_3), sodiumcarbonate ($NaHCO_3$), silver nitrate ($AgNO_3$), and formaldehyde were purchased at Acros (Geel, Belgium). Tin(II)chloride ($SnCl_2$) was purchased from Alfa Aesar (Ward Hill, USA). Oromerse-B was purchased from Technic Inc. (Cranston, RI, USA). Materials for cell culture: Dubecco's modified Eagle medium (DMEM) and fetal bovine serum (heat inactivated) were purchased from PAA laboratories (Pasching, Austria), Penicillin-Streptomycin, Trypan Blue and phosphate buffered saline (PBS) from Invitrogen (Carlsbad, CA, USA), and CellTiter-Blue (CTB) from Promega Corp (Madison, WI, USA).

4.2.2 Nanowire synthesis

Ni nanowires were synthesized by templated electrodeposition in a conventional three-electrode setup. First, an Au layer was sputtered onto a PCTE membrane with a pore size of 50 nm using a Perkin-Elmer 2400 sputtering system under Ar. The Au layer (also called back electrode) was used as working electrode in the electrochemical deposition process. Prior to deposition, the backside of the back electrode was isolated using a glass plate. A small Pt mesh was used as counter electrode and Ag/AgCl in 3 M KCl (Metrohm Autolab) was used as the reference electrode. All reported potentials are with respect to the reference electrode. The electrodes were connected to a potentiostat (Autolab PGSTAT 128N from Metrohm Autolab, Netherlands). For electrodeposition of nanowires, the electrodes were

placed inside a plating solution containing $NiSO_4 \cdot 6\,H_2O$ (1.4 M) and H_3BO_3(0.73 M), and a voltage of -1.0 V versus reference was applied for 6 min. After deposition, the membranes were dissolved in dichloromethane and washed at least 3 times in dichloromethane and 3 times in milliQ water by centrifugation.

4.2.3 Electroless Au coating of Ni nanowires

Au coating was achieved using 5 subsequent steps adapted from ref [30] as depicted schematically in figure 4.2. Clean Ni nanowires were dispersed by sonication in an aqueous solution of 10 mM 11-aminoundecanoic acid for 2 h, to form an aminated monolayer (step 1 in figure 4.2). The nanowires were then washed at least 3 times in H_2O. A fresh aqueous solution containing 54 mM $SnCl_2$ and 70 mM trifluoroacetic acid was added to the nanowires for 45 min. Sn(II) ions interacted with the electronegative amine groups forming a layer of electrostatically bound Sn^{2+} on the surface (step 2 in figure 4.2). After incubation, the nanowires were washed repeatedly in H_2O. Sn^{2+} was oxidized by Ag^+ via $Sn^{2+} + 2\,Ag^+ \longrightarrow Sn^{4+} + 2\,Ag^0$, by adding an aqueous solution containing 29 mM $AgNO_3$ and 100 mM NH_4OH (Step 3 in figure 4.2). After repeated washing in H_2O, the Ag phase can be replaced by Au. A solution of 1 g Na_2SO_3, 0.6 g $NaHCO_3$, 6 ml $Na_3Au(SO_3)_2$ (Oromerse B) and 480 ml H_2O was prepared. The nanowires were placed in 10 ml aliquots of this solution and sonicated at 3.6°C for 30 min. To allow for the formation of a closed layer of Au on the Ni nanowires, 25 µl/ml formaldehyde was added to the solution. This destabilized the Au^+-sulfite complex, and induced the galvanic replacement reaction $Ag_0 + Au^+ \longrightarrow Ag^+ + Au_0$ (steps 4 and 5 in figure 4.2), and further electroless growth of the Au layer. The nanowires were sonicated for 12 h at 3.6°C, and washed at least 5 times in H_2O to remove free ions. Nanowires made using this method are named Au-Ni nanowires.

4.2.4 Biofunctionalization

The biofunctionalization of the Au-Ni nanowires was accomplished by incubating 100 µg/ml Ni or Au-Ni nanowires with 9 mM glutathione and 1 mM mPEG-SH in PBS for 24 h at 4°C. Excess surfactant was removed by washing in PBS. The functionalization was analysed by Fourier transform infrared spectroscopy (FTIR, Thermo Scientific smart orbit Nicolet 6700 ATR-IR spectrometer) on KBr pellets with 0.5% dried and crushed Au-Ni nanowires.

4.2.5 Characterization

Analysis of the nanowires was performed with a Zeiss HR-LEO 1550 FEG Scanning Electron Microscope (SEM) operating at 2.0 kV. X-ray diffraction (XRD) was performed on samples randomly deposited on a glass plate with a Bruker D2 Phaser with a Cu Kα X-ray source and

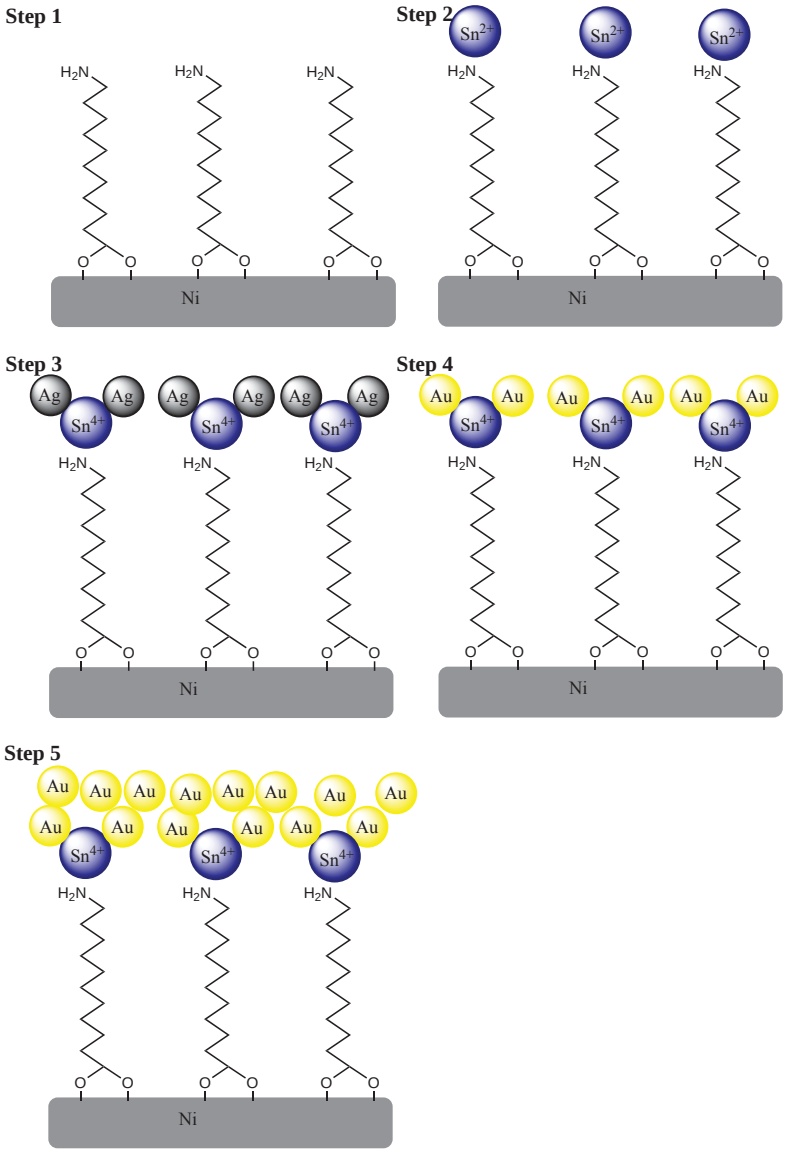

Figure 4.2: Scheme showing stepwise Au coating on Ni nanowires. 1. Amination. 2. Sn^{2+} deposition.3. Ag deposition. 4. Replacement of Ag by Au. 5. Growth of Au layer.

a wavelength of 1.54 Å. Magnetic characterization was performed using a vibrating sample magnetometer (VSM) (Model 10 Mark II VSM, Microsense). Samples were dried in a glass container before measurement; a blank measurement was subtracted from the sample data. Dispersed samples were measured in a glass container closed with Parafilm, and a blank containing the liquid in which the dispersion was made was subtracted from the data.

4.2.6 Cell culture

A number of tumour as well as non-tumour cell lines were used to assess the effect of nanoparticles on cell viability. These included: THP-1 (a monocytic cell line derived from acute monocytic leukemia); Jurkat cell line (a T cell line derived from acute T cell leukemia); U937 (a monocytic cell line derived from histiocytic lymphoma); Raji (a B cell line derived from Burkitts lymphoma); GBM (a primary cell line derived from glioblastoma multiforme); HeLa (a human cervical carninoma epithelial cell line); A431 (an epithelial cell line derived from epidermoid carcinoma), RAW264.7 (a murine macrophage cell line) and A549 (an epithelial cell line derived from lung carcinoma). The non- adherent cell lines THP-1, Jurkat, U937, Raji cell lines were grown in complete RPMI containing 10% heat inactivated FCS, 2 mM L-glutamine, 100 U/ml of penicillin and 100 µg/ml of streptomycin and 1 mM of sodium pyruvate, whereas adherent cell lines A431, A549 and GBM, RAW264.7 and HeLa were grown in complete DMEM containing above mentioned supplements. Human monocytes and lymphocytes, PBMC were isolated from blood samples from 2 healthy subjects using Ficol-Paque plus (GE Healthcare) gradient according to manufacturers instruction. PBMC obtained from the interface of plasma and Ficol-Paque were washed twice in RPMI and suspended in complete RPMI. $5 \cdot 10^6$ PBMC in complete RPMI were plated out in each well of a 6 well plate (SPL Life Sciences), pre-coated with human AB serum overnight. After 2 h of incubation at 37°C in 5% CO_2, the non-adherent PBMC (containing T, B and NK cells) were gently removed from adherent cells (monocytes).

4.2.7 Confocal imaging

A Zeiss (Göttingen, Germany) LSM 510 confocal laser scanning microscope (CLSM) was used to image uptake of Au-Ni nanowires by cells in bright field. 10^4 cells/well were incubated in a 96-well plate. Cells were allowed to adhere for 2 h after which Au-Ni nanowires were added with a nanowire concentration of approximately 10 nanowires per cell. This concentration was estimated by assuming the nanowires have the density of bulk Ni and Au and average dimensions as estimated from SEM images. Control samples contained no nanowires. Images were obtained after 24 h incubation at 37°C in 5% CO_2 atmosphere.

4.2.8 Concentration dependent short term cell viability tests on phagocytotic and non phagocytotic cells

Adherent cells, RAW264.7 and HeLa, were seeded on 96-well culture plates at $5{\cdot}10^3$ cells/well in 100 µl of cell medium. Cells were allowed to adhere to the plate for 24 h at 37°C in 5% CO_2 atmosphere. Incubation of Ni and Au-Ni nanowires was done by adding 100 µl of Au-Ni nanowire dispersion in cell medium to the cells on the 96-well culture plates, for 48 h at 37°C in 5% CO_2 atmosphere. The final concentrations of the Au-Ni nanowires were 0, 1, 10, 100 and 1000 nanowires/cell. All experiments were performed in triplicates. After 48 h the cell medium was carefully removed and the cells were washed with PBS, thereafter 100 µl of cell medium was added with 10 µl of CellTiter Blue and incubated for 4 h. The fluorescence was measured on a spectrophotometer (Victor, Perkin Elmer) with an excitation wavelength of 560 nm and an emission wavelength of 590 nm. The fluorescence values were normalized by the controls and expressed as percent viability. Validity of the assay was assessed by cell counting and visual inspection of the cells.

4.2.9 Long term cell viability following exposure to Au-Ni nanowires

The long term cytotoxicity of Au-Ni nanowires was investigated by measuring viable and dead cells. Non adherent cells were seeded at 10^5 cells/well in a 24 well plate and $2 \cdot 10^4$ cells/well and were allowed to adhere for 2 h at 37°C in 5% CO_2. Au-Ni nanowires in 50 µl of PBS were added to duplicate wells at a concentration of 100 nanowires/cell. Duplicate control wells were treated with equal volume PBS. The cells were then incubated at 37°C in 5% CO_2 for 12 h, 1, 2, 5 and 7 days. At each time point, the cells were suspended (using trypsin-EDTA to detach adherent cells). 20 µl of the cell suspensions were then mixed with equal volume trypan blue (0.4%). At least 100 cells from each duplicate culture were observed for morphology and staining of cells using a haemocytometer and inverted microscope (Leica). Blue stained cells were considered dead. Adherent and non-adherent PBMC were cultured at $5 \cdot 10^5$ cells/well, the ratio of cell to nanowire was similar to other cell lines. Approximately 200 cells from each culture were observed under the microscope using trypan blue at each time points as mentioned above.

4.3 Results and Discussion

4.3.1 Synthesis and characterisation

Ni nanowires with an average diameter of 150 nm and a length of 2.6± 0.3 µm (SEM n=100) were obtained by electrodeposition of Ni in the pores of a PCTE membrane for 6 min at -1.0 V versus Ag/AgCl reference electrode. The nanowires were released into suspension by dissolving the membrane and several washings in dichloromethane and water. An Au coating was deposited by electroless deposition onto the Ni nanowires and the morphology of the Au-coated Ni nanowires was investigated by HR-SEM as shown in figure 4.3. Employing only the Au deposition reaction with Oromerse B (step 4 and 5 in figure 4.2) did not result in Au nucleation on the Ni nanowire surface as can be seen in figure 4.3b. Therefore, an activation step was introduced in which Sn nuclei were deposited, followed by galvanic replacement by Ag, and finally growth of Au on the Ag nuclei. Unfortunately, the Au coating was still discontinuous (figure 4.3 c), most likely due to an insufficient concentration of Sn nuclei on the Ni surface. An amination step, using 11-aminoundecanoic acid, was introduced to provide more homogenous Sn deposition, allowing a continuous Au coating to form over the entire nanowire surface (figure 4.3d), with an approximate thickness of 40 nm as estimated from SEM. Longer Au deposition will result in the formation of a thicker Au layer.

The phase and grain size of the Ni nanowires and Au coating were investigated by XRD (figure 4.4). Ni nanowires showed diffraction peaks corresponding to the (111) and (200) planes of cubic Ni. The peak at $2\theta = 38°$ can be assigned to the Au (111) plane of the back electrode. After the complete Au coating procedure diffraction peaks were detected, which can be assigned to Au(110), (111), (200), (220) and (311). The Ni(111) and Au(200) peaks overlap, therefore it is not possible to distinguish between them. The broader peaks in the Au spectrum compared to the Ni spectrum indicate a smaller crystallite size for the Au layer. Using the Debye-Scherrer equation

$$\tau = \frac{K\lambda}{\beta \cos\theta} \tag{4.1}$$

where $\tau$is the mean size of the crystalline domain, K the shape factor, β the full width at half maximum, θ the Bragg angle and λ the x-ray wave length. The estimated crystallite sizes are 54 nm for Ni and 20 nm for Au. By comparing the crystallite sizes from XRD with SEM imaging, we can conclude that the crystalline domain size in the central Ni nanowire is about 1/3 of its diameter, and it is surrounded by an Au layer with an equivalent thickness of about 2 grains.

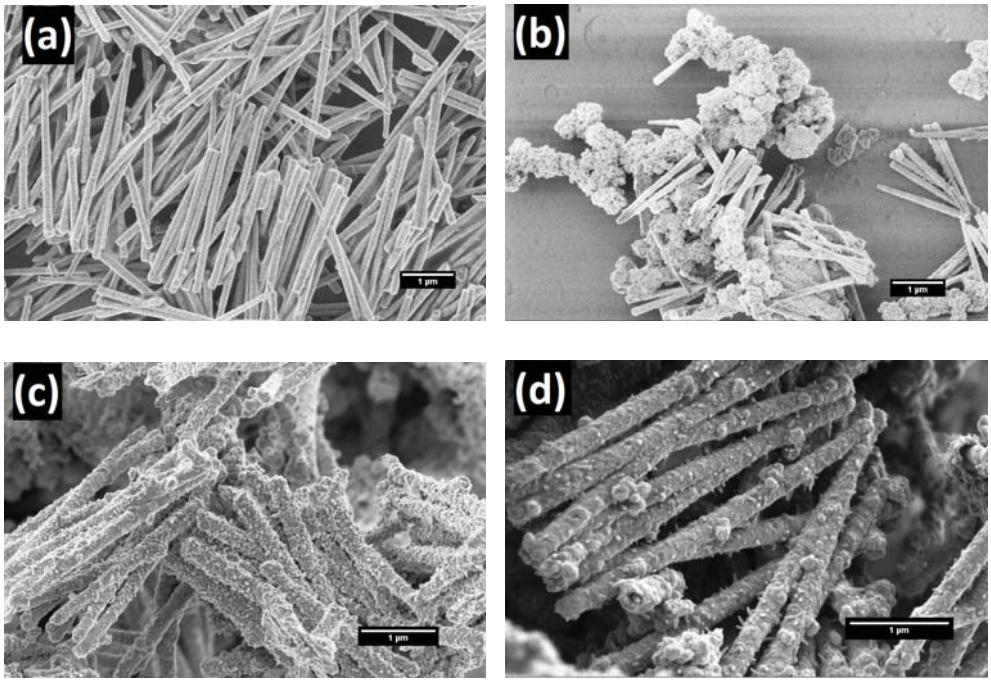

Figure 4.3: HR-SEM images of Ni nanowires and Au-Ni nanowires. (a) Original Ni nanowires. (b) Oromerse-B Ni nanowires. (c) Sn-Ag-Au Ni nanowires. (d) 11-aminoundecanoic acid-Sn-Ag-Au nanowires, hereafter indicated as Au-Ni nanowires.

4.3.2 Dispersion and magnetic properties

Figure 4.5, shows the room temperature magnetization curves for uncoated Ni nanowires inside the template with magnetic field (H) applied in two directions, i.e. parallel and perpendicular to the wire direction. The squareness ratio Mr/Ms and coercivity are known to increase significantly with aspect ratio [36]. The obtained hysteresis loops show magnetic anisotropy where the magnetic easy direction is along the axis, as can be seen from the squareness ratio Mr/Ms = 0.48 in parallel direction. From VSM measurements on randomly orientated nanowires as depicted in figure 4.6, the saturation magnetization of the Ni nanowires was found to be 34 emu/g, which is significantly less than the value for bulk Ni (55.4 emu/g). This can be explained by the surface anisotropy which is significant for a wire with small diameter. After Au coating of the Ni nanowires the saturation magnetization decreased to 10 emu/g. From this value, the diameter and length of the Ni nanowire and the densities of Ni ($8.9 \cdot 10^6$ g/m^3) and Au ($19.3 \cdot 10^6$ g/m^3), the shell thickness can be calculated. Neglecting the influence of the other coating layers the Au layer thickness is approximately 34 nm, which is in good agreement with the thickness estimated from HR-SEM images.

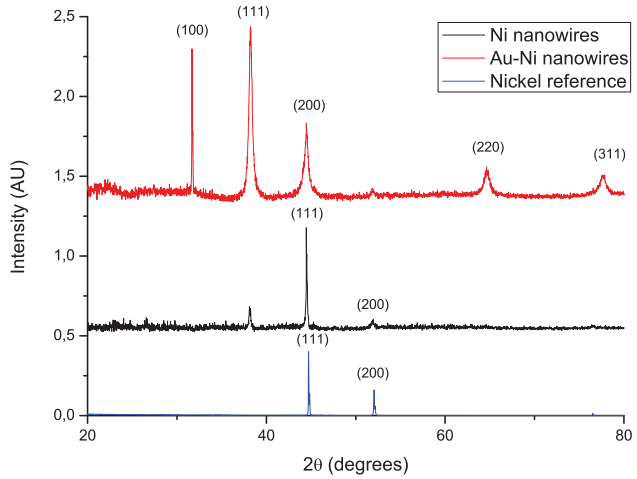

Figure 4.4: XRD patterns of randomly oriented Ni nanowires and Au-Ni nanowires and a pure Ni reference sample.

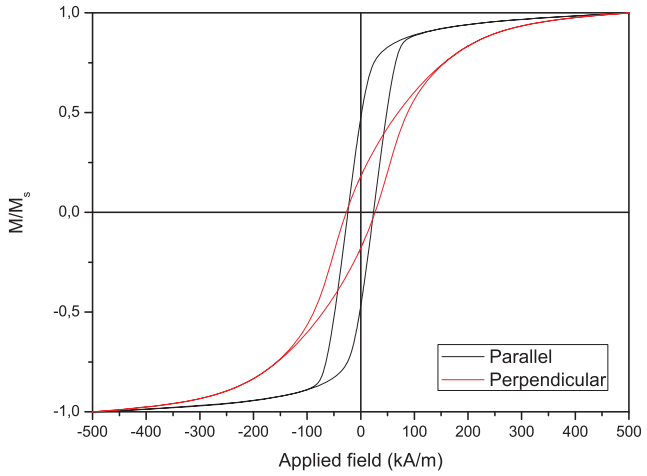

Figure 4.5: Magnetic hysteresis curves of Ni nanowires measured inside the membrane under external field parallel and perpendicular to the nanowire long axis. Parallel coercivity value of 302 Oe and Mr/Ms=0.48, perpendicular coercivity of 378 Oe and Mr/Ms=0.17.

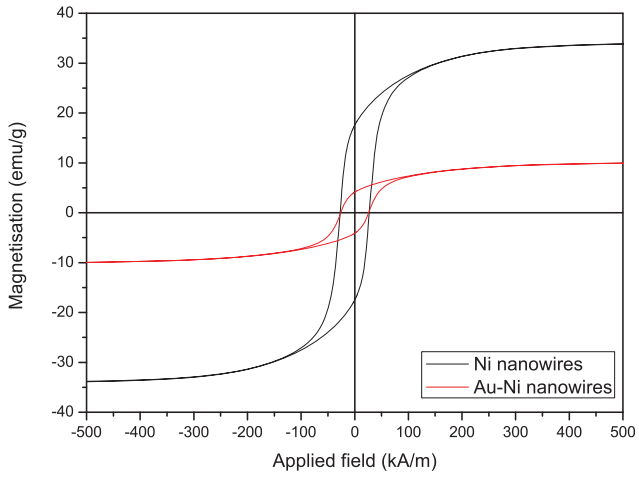

Figure 4.6: Hysteresis curves measured of Ni nanowires and Au-Ni nanowires in random orientation under external field. Ms=34 emu/g for uncoated and Ms=10 emu/g for Au coated Ni nanowires, suggesting a coating thickness of 34 nm on a 2.6 µm long Ni nanowire with 150 nm diameter.

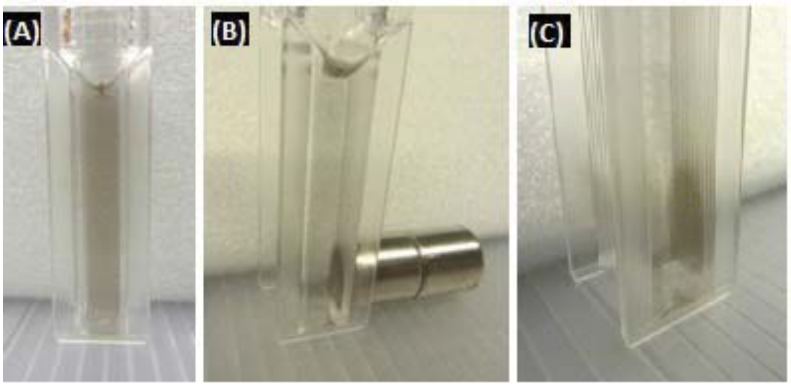

Figure 4.7: (a) Suspension of Au-Ni nanowires stabilised with GSH and mPEG-SH. (b,c) The Au-Ni nanowires can be collected using a permanent magnet

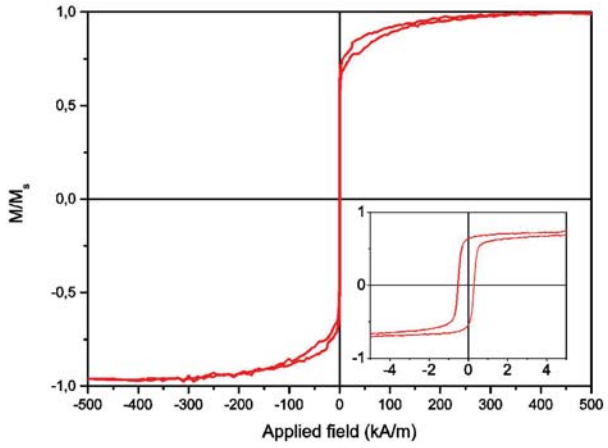

Figure 4.8: Magnetisation loop M vs applied field H for suspended Au-Ni nanowires showing superparamagnetic behaviour. Insert shows that the coercivity of the Au-Ni nanowires is approximately 1 kA/m for dispersed samples.

After biofunctionalization using SH-PEG and glutathione, a suspension of Au-Ni nanowires was obtained (figure 4.7). The nanowires could be easily collected using a permanent magnet and dispersed by vortexing. Due to the possibility to move freely in the liquid, the magnetization curves of suspended nanowires showed superpara-magnetic behaviour, with no remnant magnetisation (figure 4.8). Attachment of GSH and mPEG-SH was examined by FTIR spectroscopy (figure 4.9). GSH attachment can be identified by two bands around 1600 cm^{-1} for both cysteine and glutamic acid-carbonyl. The anchoring is via the thiol group as the band at 2500 cm^{-1} for SH stretching is not visible on the Au-Ni nanowires. Binding of mPEG-SH can be seen by a strong band at 1380 cm^{-1} showing C-H stretching, and the band at 1080 cm^{-1}shows C-O-C stretching from mPEG-SH.

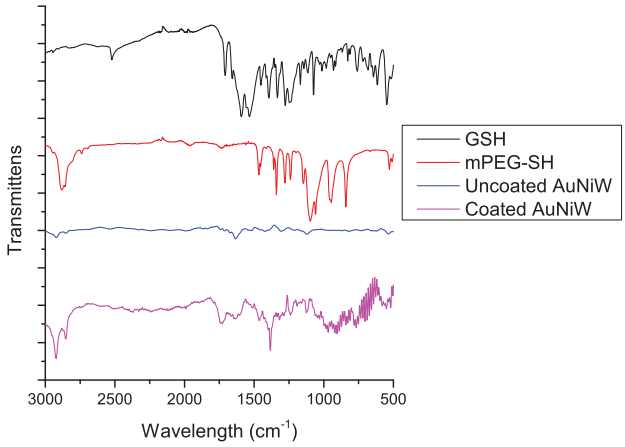

Figure 4.9: FTIR spectra of GSH, mPEG-SH, uncoated Au-Ni nanowires, and the attachment of GSH and mPEG-SH to the Au-Ni nanowires.

4.3.3 Biocompatiblity

The uptake of Au-Ni nanowires was studied by confocal microscopy (figure 4.10). 3D imaging not shown here ascertained that the particles were inside the cells and not simply adhered to the membrane. After 24 h of incubation, RAW-264.7 cells had taken up many nanowires and clusters of nanowires. As these cells are macrophages, the uptake pathway is most likely phagocytosis. Confocal microscopy analysis showed that the nanowires were completely taken up by these cells without signs of frustrated phagocytosis. This indicates that macrophages will be able to remove the particles from the bloodstream. Jurkat cells are not capable of phagocytosis and only take up particles by receptor mediated endocytosis. As expected, these cells did not take up any nanowires, and appeared as healthy as control untreated cells.

The effects of Au-Ni nanowires on cell viability were evaluated using a CTB assay. Au-Ni nanowires did not show a decrease in cell viability of both HeLa and RAW cells over 48 h (figure 4.11). In a study between phagocytic and non-phagocytic cells, a slightly higher cytotoxicity was observed for phagocytic (RAW 264.7) cells compared to non-phagocytic (HeLa) cells, which might indicate the importance of uptake on cytotoxicity. It should be noted that the high concentration of 1000 nanowires per cell is much higher than targeted in potential applications in biomedicine, and is only used here to investigate the biocompatibility of the nanowires. In RAW cells Ni nanowires showed increased cytotoxicity compared to the

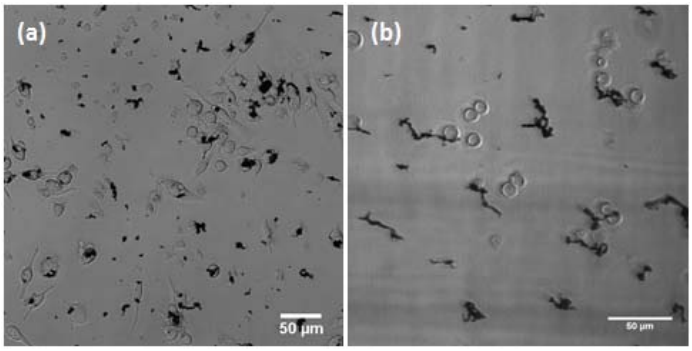

Figure 4.10: Interaction of Au-Ni nanowires with (a) RAW 264.7 cells and (b) Jurkat cells

Au coated Ni nanowires, indicating the necessity of the Au coating. The used concentration of nanowires is much higher than the lethal concentration of Ni nanowires with a length of 20 µm found by Byrne et al [8], which indicates and illustrates the high biocompatibility of the much shorter Ni and Au-Ni nanowires.

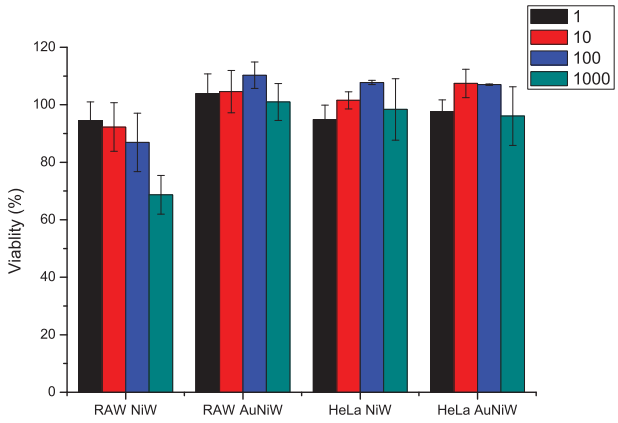

Figure 4.11: Short term viability compared to untreated control of RAW and HeLa cells assessed by CTB assay after 48 h incubation with Ni and Au-Ni nanowires. Bars indicate standard deviation.

A range of cells-primary and cancerous, phagocytic and non-phagocytic, adherent and non-adherent-were used in order to systematically investigate cytotoxicity over long term (Table 4.1). All 9 different cell types used in this study did not show significant cytotoxicity of the Au-Ni nanowires for periods up to 7 days. Images of the cells taken at day 5 are depicted in figure 4.12

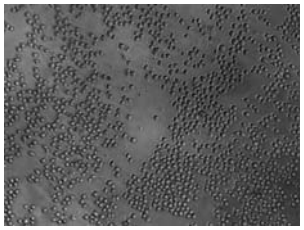

(a) U937 control

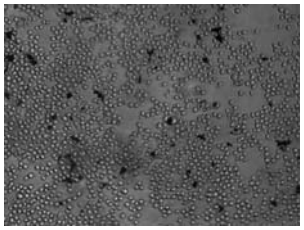

(b) U937 Au-Ni wires

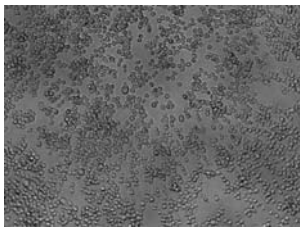

(c) THP1 control

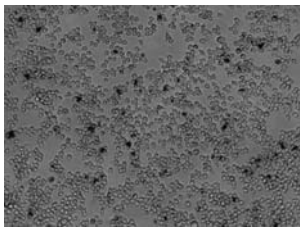

(d) THP1 Au-Ni wires

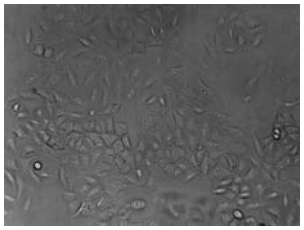

(e) A549 control

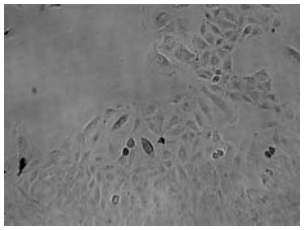

(f) A549 Au-Ni wires

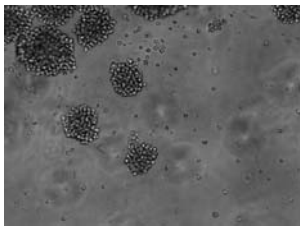

(g) Raji control

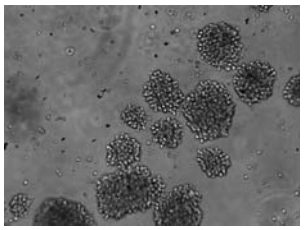

(h) Raji Au-Ni wires

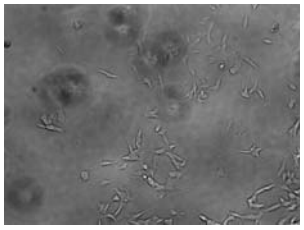

(i) GBM control

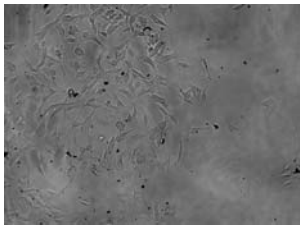

(j) GBM Au-Ni wires

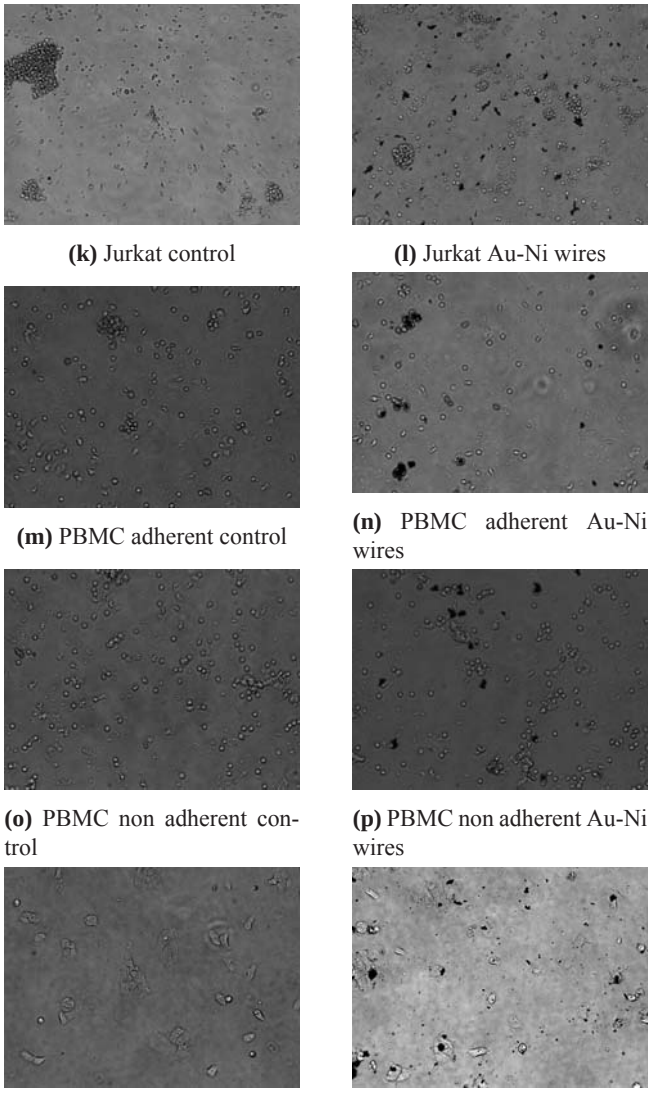

(k) Jurkat control

(l) Jurkat Au-Ni wires

(m) PBMC adherent control

(n) PBMC adherent Au-Ni wires

(o) PBMC non adherent control

(p) PBMC non adherent Au-Ni wires

(q) A431 control

(r) A431 Au-Ni wires

Figure 4.12: Microscopy images of 9 different cell lines after 5 days of culture without (control) or with Au-Ni wires. All cells behave similarly to control cells.

Table 4.1: Long term viability of 9 different cell lines showed no significant cytotoxicity

cell type		12 h	24 h	48 h	5 d	7 d
U937 (non-adherent)	Control	97.6 ± 1.0	96.3 ± 0.6	96.9 ± 0.4	98.1 ± 0.4	97.2 ± 0.1
	Au-Ni wires	96.5 ± 0.7	96.5 ± 0.7	96.7 ± 0.6	98.7 ± 1.4	98.2 ± 1.2
THP1 (non-adherent)	Control	99.7 ± 0.5	95.7 ± 0.1	98.0 ± 1.5	99.0 ± 0.3	98.5 ± 0.4
	Au-Ni wires	98.5 ± 0.5	93.7 ± 0.1	95.5 ± 1.8	99.0 ± 0.4	99.3 ± 0.3
A549 (adherent)	Control	95.3 ± 1.4	98.1 ± 0.6	92.9 ± 0.3	98.5 ± 1.4	97.0 ± 0.9
	Au-Ni wires	98.8 ± 0.6	98.6 ± 0.2	94.2 ± 1.4	98.5 ± 1.3	96.6 ± 0.7
Raji (non-adherent)	Control	97.7 ± 0.3	98.2 ± 0.4	98.7 ± 0.1	99.5 ± 0.1	96.6 ± 0.6
	Au-Ni wires	97.9 ± 0.1	97.7 ± 0.4	98.6 ± 0.7	98.4 ± 0.4	95.4 ± 2.9
GBM (adherent)	Control	98.7 ± 0.1	97.8 ± 3.1	99.1 ± 0.5	96.0 ± 0.7	96.3 ± 2.5
	Au-Ni wires	98.9 ± 0.2	98.4 ± 0.0	98.7 ± 0.7	96.1 ± 0.7	97.1 ± 0.9
Jurkat (non-adherent)	Control	98.4 ± 0.3	96.9 ± 0.6	97.8 ± 0.7	94.6 ± 0.8	93.6 ± 1.7
	Au-Ni wires	97.8 ± 0.5	97.9 ± 0.2	98.1 ± 1.0	94.6 ± 0.1	92.0 ± 1.0
PBMC (adherent)	Control	99.5 ± 0.2	98.4 ± 0.6	99.5 ± 0.4	98.4 ± 1.0	98.4 ± 0.5
	Au-Ni wires	99.8 ± 0.2	99.3 ± 0.5	99.5 ± 0.4	98.4 ± 0.9	98.5 ± 0.4
PBMC (non-adherent)	Control	99.5 ± 0.4	97.8 ± 0.9	99.8 ± 0.3	96.3 ± 1.3	98.2 ± 0.9
	Au-Ni wires	99.6 ± 0.4	98.5 ± 0.8	99.7 ± 0.2	96.1 ± 1.4	97.7 ± 0.6
A431 (adherent)	Control	98.7 ± 0.1	98.6 ± 0.1	96.2 ± 1.9	96.1 ± 3.8	96.1 ± 3.8
	Au-Ni wires	98.9 ± 0.2	98.2 ± 1.1	95.6 ± 0.2	95.2 ± 1.7	95.2 ± 1.7

4.4 Conclusions

Biocompatible nanowires with tuneable dimensions were made by templated electrodeposition of Ni in PCTE membranes. The dimensions of the nanowires can be fully tuned by adapting the deposition time and template dimensions. An Au coating procedure was developed to assure biocompatibility by complete shielding of the Ni phase from the biological environment. The newly developed procedure involves amination of the Ni surface, activation by Sn and Ag, followed by electroless Au deposition. A coating thickness of approximately 40 nm was achieved by 12 h electroless Au deposition. SEM imaging shows a smooth and continuous layer of Au on the Ni nanowires. Elemental analysis confirmed the formation of Au on Ni. Magnetic measurements were used to reveal the shape anisotropy and ferromagnetic properties of the Au-Ni nanowires. Stable suspensions of nanowires were obtained by biofunctionalization using GSH and mPEG-SH. Cell studies indicate that the nanowires can be completely engulfed by cells without signs of frustrated phagocytosis. No significant cytotoxic effects and morphological alterations were found when nanowires were exposed to a variety of cell lines, arguing the potential use of the nanowires in biomedical applications, such as magnetic drug delivery.

References

[1] Q. a. Pankhurst, J. Connolly, S. K. Jones, and J. Dobson, "Applications of magnetic nanoparticles in biomedicine," *Journal of Physics D: Applied Physics*, vol. 36, pp. R167–R181, July 2003.

[2] Q. I. N. Hu, Y. Q. I. LIU, N. Li, C. Cheng, S. G. Xu, N. Wang, W. E. I. Qin, and B. Z. E. N. Z. TANG, "Ni-NTA-Coated nanowire materials for protein enrichment and the application in a medical device used for blood glucose degradation," *Nano*, vol. 8, no. 3, p. 1350029, 2013.

[3] A. Hultgren, M. Tanase, C. S. Chen, G. J. Meyer, D. H. Reich, and L. A. Bauer, "Cell manipulation using magnetic nanowires," *Journal of Applied Physics*, vol. 93, no. 10, pp. 7275–7280, 2003.

[4] A. Prina-Mello, Z. Diao, and J. M. D. Coey, "Internalization of ferromagnetic nanowires by different living cells.," *Journal of nanobiotechnology*, vol. 4, p. 9, Jan. 2006.

[5] H. T. Huang, T. R. Ger, Y. H. Lin, and Z. H. Wei, "Single cell detection using a magnetic zigzag nanowire biosensor," *Lab on a Chip*, vol. 13, no. 15, pp. 3098–3104, 2013.

[6] A. Sharma, Y. C. Zhu, S. Thor, F. Zhou, B. Stadler, and A. Hubel, "Magnetic Barcode Nanowires for Osteosarcoma Cell Control, Detection and Separation," *Ieee Transactions on Magnetics*, vol. 49, no. 1, pp. 453–456, 2013.

[7] M. Safi, M. H. Yan, M.-A. A. Guedeau-Boudeville, H. Conjeaud, V. Garnier-Thibaud, N. Boggetto, A. Baeza-Squiban, F. Niedergang, D. Averbeck, and J.-F. F. Berret, "Interactions between magnetic nanowires and living cells: uptake, toxicity, and degradation.," *ACS Nano*, vol. 5, pp. 5354–64, July 2011.

[8] F. Byrne, A. Prina-Mello, A. Whelan, B. M. Mohamed, A. Davies, Y. K. Gun'ko, J. M. D. Coey, and Y. Volkov, "High content analysis of the biocompatibility of nickel nanowires," *Journal of Magnetism and Magnetic Materials*, vol. 321, no. 10, pp. 1341–1345, 2009.

[9] A. Hultgren, M. Tanase, C. S. Chen, and D. H. Reich, "High-yield cell separations using magnetic nanowires," *Ieee Transactions on Magnetics*, vol. 40, no. 4, pp. 2988–2990, 2004.

[10] F. Johansson, M. Jonsson, K. Alm, and M. Kanje, "Cell guidance by magnetic nanowires," *Experimental Cell Research*, vol. 316, no. 5, pp. 688–694, 2010.

[11] A. Hultgren, M. Tanase, E. J. Felton, K. Bhadriraju, A. K. Salem, C. S. Chen, and D. H. Reich, "Optimization of yield in magnetic cell separations using nickel nanowires of different lengths.," *Biotechnology progress*, vol. 21, no. 2, pp. 509–15, 2005.

[12] M. Tanase, E. J. Felton, D. S. Gray, A. Hultgren, C. S. Chen, and D. H. Reich, "Assembly of multicellular constructs and microarrays of cells using magnetic nanowires," *Lab on a Chip*, vol. 5, no. 6, pp. 598–605, 2005.

[13] A. O. Fung, V. Kapadia, E. Pierstorff, D. Ho, and Y. Chen, "Induction of cell death by magnetic actuation of nickel nanowires internalized by fibroblasts," *Journal of Physical Chemistry C*, vol. 112, no. 39, pp. 15085–15088, 2008.

[14] M. M. Song, W. J. Song, H. Bi, J. Wang, W. L. Wu, J. Sun, and M. Yu, "Cytotoxicity and cellular uptake of iron nanowires," *Biomaterials*, vol. 31, no. 7, pp. 1509–1517, 2010.

[15] X. H. Shi, A. von dem Bussche, R. H. Hurt, A. B. Kane, and H. J. Gao, "Cell entry of one-dimensional nanomaterials occurs by tip recognition and rotation," *Nature Nanotechnology*, vol. 6, no. 11, pp. 714–719, 2011.

[16] Y. N. Xia, P. D. Yang, Y. G. Sun, Y. Y. Wu, B. Mayers, B. Gates, Y. D. Yin, F. Kim, and Y. Q. Yan, "One-dimensional nanostructures: Synthesis, characterization, and applications," *Advanced Materials*, vol. 15, no. 5, pp. 353–389, 2003.

[17] H. Schlorb, V. Haehnel, M. S. Khatri, A. Srivastav, A. Kumar, L. Schultz, and S. Fahler, "Magnetic nanowires by electrodeposition within templates," *Physica Status Solidi B-Basic Solid State Physics*, vol. 247, no. 10, pp. 2364–2379, 2010.

[18] M. G. Maas, E. J. B. Rodijk, A. W. Maijenburg, D. H. A. Blank, and J. E. ten Elshof, "Microstructure development in zinc oxide nanowires and iron oxohydroxide nanotubes by cathodic electrodeposition in nanopores," *Journal of Materials Research*, vol. 26, no. 17, pp. 2261–2267, 2011.

[19] A. George, A. W. Maijenburg, M. G. Maas, D. H. A. Blank, and J. E. ten Elshof, "Electrodeposition in Capillaries: Bottom-up Micro- and Nanopatterning of Functional Materials on Conductive Substrates," *Acs Applied Materials & Interfaces*, vol. 3, no. 9, pp. 3666–3672, 2011.

[20] A. W. Maijenburg, E. J. B. Rodijk, M. G. Maas, M. Enculescu, D. H. A. Blank, and J. E. ten Elshof, "Hydrogen Generation from Photocatalytic Silver vertical bar Zinc Oxide Nanowires: Towards Multifunctional Multisegmented Nanowire Devices," *Small*, vol. 7, no. 19, pp. 2709–2713, 2011.

[21] J. H. Sánchez and C. Rinaldi, "Rotational Brownian dynamics simulations of non-interacting magnetized ellipsoidal particles in d.c. and a.c. magnetic fields," *Journal of Magnetism and Magnetic Materials*, vol. 321, pp. 2985–2991, Oct. 2009.

[22] L. A. Bauer, D. H. Reich, and G. J. Meyer, "Selective functionalization of two-component magnetic nanowires," *Langmuir*, vol. 19, no. 17, pp. 7043–7048, 2003.

[23] P. H. Hoet, I. Bruske-Hohlfeld, O. V. Salata, and I. Brüske-Hohlfeld, "Nanoparticles - known and unknown health risks," *Journal of Nanobiotechnology*, vol. 2, p. 12, Dec. 2004.

[24] F. H. Nielsen, "Is nickel nutritionally important?," *Nutrition today*, vol. 28, no. 1, pp. 14–19, 1993.

[25] J. J. Pan, Q. S. Chang, X. Wang, Y. Son, Z. Zhang, G. Chen, J. Luo, Y. Y. Bi, F. Chen, and X. L. Shi, "Reactive Oxygen Species-Activated Akt/ASK1/p38 Signaling Pathway in Nickel Compound-Induced Apoptosis in BEAS 2B Cells," *Chemical Research in Toxicology*, vol. 23, no. 3, pp. 568–577, 2010.

[26] J. Zhao, L. Bowman, X. Zhang, X. Shi, B. Jiang, V. Castranova, and M. Ding, "Metallic nickel nano- and fine particles induce JB6 cell apoptosis through a caspase-8/AIF mediated cytochrome c-independent pathway," *Journal of Nanobiotechnology*, vol. 7, p. 2, 2009.

[27] M. Costa, "Molecular biology of nickel carcinogenesis," *Fresenius Journal of Analytical Chemistry*, vol. 361, no. 4, pp. 381–385, 1998.

[28] N. Gao, H. J. Wang, and E. H. Yang, "An experimental study on ferromagnetic nickel nanowires functionalized with antibodies for cell separation," *Nanotechnology*, vol. 21, no. 10, p. 105107, 2010.

[29] M. Z. Hossain and M. G. Kleve, "Nickel nanowires induced and reactive oxygen species mediated apoptosis in human pancreatic adenocarcinoma cells," *International Journal of Nanomedicine*, vol. 6, pp. 1475–1485, 2011.

[30] N. S. Birenbaum, B. T. Lai, C. S. Chen, D. H. Reich, and G. J. Meyer, "Selective non-covalent adsorption of protein to bifunctional metallic nanowire surfaces," *Langmuir*, vol. 19, no. 23, pp. 9580–9582, 2003.

[31] D. Magnin, V. Callegari, S. Matefi-Tempfli, M. Matefi-Tempfli, K. Glinel, A. M. Jonas, and S. Demoustier-Champagne, "Functionalization of magnetic nanowires by charged biopolymers," *Biomacromolecules*, vol. 9, no. 9, pp. 2517–2522, 2008.

[32] I. T. Jeon, M. K. Cho, J. W. Cho, B. H. An, J. H. Wu, R. Kringel, D. S. Choi, and Y. K. Kim, "Ni-Au core-shell nanowires: synthesis, microstructures, biofunctionalization, and the toxicological effects on pancreatic cancer cells," *Journal of Materials Chemistry*, vol. 21, no. 32, pp. 12089–12095, 2011.

[33] G. Han, P. Ghosh, and V. M. Rotello, "Functionalized gold nanoparticles for drug delivery," *Nanomedicine*, vol. 2, no. 1, pp. 113–123, 2007.

[34] R. Venkatesan, A. Pichaimani, K. Hari, P. K. Balasubramanian, J. Kulandaivel, and K. Premkumar, "Doxorubicin conjugated gold nanorods: a sustained drug delivery

carrier for improved anticancer therapy," *Journal of Materials Chemistry B*, vol. 1, no. 7, pp. 1010–1018, 2013.

[35] P. Kohli, J. E. Wharton, O. Braide, and C. R. Martin, "Template synthesis of gold nanotubes in an anodic alumina membrane," *Journal of Nanoscience and Nanotechnology*, vol. 4, no. 6, pp. 605–610, 2004.

[36] B. Das, K. Mandal, and P. Sen, "Preparation and characterization of cobalt nanowires with high aspect ratio," *Magnetic Materials*, vol. 1003, pp. 46–48, 2008.

Chapter 5

Complement deposition on nanoparticles determines inflammatory response by immune cells[1]

Abstract

Nanoparticles are attractive drug delivery vehicles for targeted organ-specific as well as systemic therapy. However, their interaction with the immune system offers an intriguing challenge. Recently, we showed that pristine and derivatised carbon nanotubes (CNT) can activate complement mainly via the classical pathway, leading to enhanced uptake by phagocytic cells and transcriptional downregulation of pro-inflammatory cytokines. Here, we examined interaction of complement-activating CMC-CNT and RNA-CNT, and non-complement-activating gold-nickel (Au-Ni) nanowires with cell lines representing macrophage, B and T cells. Complement deposition considerably enhanced uptake of CNTs by immune cells known to overexpress complement receptors. qPCR and multiplex array analyses showed serum-dependent downregulation of TNF-α and IL-1β and upregulation of IL-12 by CMC- and RNA-CNTs, revealing IL-10 as a crucial regulator during nanoparticle-immune cell interaction. Nanoparticles offer diverse molecular patterns to the complement system and subsequent handling and immune response by antigen capturing and presenting cells, which can shape innate and adaptive immune axis.

[1]The contents of this chapter have been submitted as: Kirsten M. Pondman, Anthony G. Tsolaki, Mohamed H.Shamji, Amy Switzer, Suhair M. Abozaid, Bennie ten Haken, Robert B. Sim, Uday Kishore, Complement deposition on nanoparticles can modulate immune responses by macrophage, B and T cells, *Journal of biomedical nanotechnology*

5.1 Introduction

Nanoparticles are attractive drug delivery vehicles being considered for a number of biomedical applications [1]. Due to their advantageous properties, CNTs have been extensively explored for biological and biomedical applications [2–5] including drug delivery [2–4, 6–11], and diagnostics via in vivo imaging [12, 13]. The effectiveness of nanoparticles as intravenous drug delivery platforms is dictated by its rapid elimination by the immune cells, which can otherwise lead to potentially hazardous inflammatory responses. Therefore, understanding the interactions between nanoparticles and immune system is essential for their strategic and specific use for in vivo delivery [14, 15]. The innate immune system plays a key role in the clearance of pathogens and synthetic particles including nanoparticles [15–20].

Activation of the complement system, a major humoral component of the innate immunity [21], can influence therapeutic effectiveness of nanoparticles, as it coats the surface of the particles with opsonic fragments (mainly C3b and iC3b), labelling them for recognition, adherence and clearance by phagocytic cells. Of the three complement pathways, the classical pathway starts by binding of C1q to targets including CNTs [16] (charge pattern) either directly, or via adaptor proteins (antibodies and pentraxins) [22]. Binding of C1q causes activation of C1r and C1s, which catalyzes cleavage of C2 and C4, leading to the formation of C4bC2a, a surface bound C3 convertase. The lectin pathway recognizes a different range of target motifs, via the proteins Mannose-binding lectin (MBL), the ficolins, or Collectin 11, which activates the MBL-associated serine proteases (MASP), which activate C2 and C4, forming C4bC2a. The alternative pathway starts with the spontaneous cleavage of C3 into C3a and C3b, which binds directly onto surfaces e.g. microbes and modified (non-pristine) CNTs [20, 23, 24]. Surface-bound C3b binds factor B, which is cleaved by factor D, forming C3bBb complexes, a C3 convertase, and activate more C3b, which can bind to the same surface. Binding of C3b to the convertases, forming C4b2a3b and C3b2Bb, which now cleaves C5 to C5b, forms a complex with C6, C7, C8 and C9, known as the membrane attack complex (MAC) [21]. The MAC can form pores in the membrane of cellular targets. The formation of MAC on the surface of CNTs may potentially cause damage to tissue in the direct environment [16]. In addition, the smaller cleaved products C3a, C4a and C5a generated during the complement activation are potent anaphylatoxins for infiltrating immune cells contributing to inflammation [16, 19–21].

Non-functionalized, and thus, highly hydrophobic CNTs activate complement via the classical and (to a lesser extent) the alternative pathway [16]. Functionalization of CNTs to increase their dispersability and biocompatibility [2, 25–27] can affect both the extent and the pathway of complement activation [17, 23, 25]. For instance, PEGylation, commonly used to limit protein interactions with the particles, increase biocompatibility, and prolong

the circulation time in blood [28], can activate lectin pathway [23, 29]. CNTs, in general, are widely considered to activate complement [16, 18, 20, 29–36].

As elongated nanoparticles with an aspect ratio similar to asbestos, CNTs are often considered more hazardous than other types of nanoparticles, longer CNTs elicit more profound cytotoxic responses [37–41]). Brown et al. [42], while analyzing phagocytosis of a range of carbon-based nanoparticles in PBMCs and the THP-1 cells, found frustrated phagocytosis when straight and individually dispersed CNTs were used; the effect correlated with superoxide anion and TNF-α release. Palomaki et al. [40] showed that all carbon particles induced IL-1β secretion, indicating NLRP3 inflammasome formation, but only long CNTs induced IL-1α secretion [43, 44]. Interestingly, when phagocytosis was hindered by blocking K+ efflux, IL-1β secretion was consequently eliminated, indicating that phagocytosis is required for inflammasome activation [43].

Phagocytosis is the most likely mechanism of entry of CNTs into cells, but CNTs have also been localized in many non-phagocytic cells possibly via direct penetration or needling [40, 45]. CNT-endocytosis can be scavenger receptor-meditated and requires absorption of albumin or other serum proteins [46]. The immune cells can also respond to the presence of nanoparticles by producing pro- and anti-inflammatory cytokines, which can potentiate and regulate innate and adaptive immune responses. MWCNTs have been shown to stimulate secretion of pro-inflammatory cytokines such as IL-1β, TNF-α, IL-8 and IL-6 [36, 38, 40]. Both in mice [47] as well as in human monocytes [43], aerosolized pristine SWNTs induced an acute and robust inflammatory response.

Recently, we showed that several types of pristine and non-covalently functionalized CNTs activate the complement system up to activation of C3 and C5, confirming that the entire complement system is activated [24]. Complement activation and deposition on the surface of these CNTs enhanced their uptake by macrophages (U937 cell line) and human monocytes in a time-dependent manner. Complement opsonisation of CNTs also led to modulation (mostly downregulation) of pro-inflammatory and anti-inflammatory cytokine production by U937 cells and human monocytes.

In this study, three different nanoparticles are examined: two functionalized CNTs and a gold coated nickel (Au-Ni) nanowire with similar dimension to the CNTs. Although gold nanoparticles are even more fashionable in nanomedicine than CNTs [48, 49], very little is known about their interactions with the immune system. Several gold nanoparticles have been suggested to be invisible to the immune system and do not induce any complement activation [50, 51]. Dobrovolskaia [50] showed that C3 is able to bind to gold nanoparticles, but there was no induction of complement activation [49]. Most gold nanoparticles are spherical or rod-like, but here, we use wire-like particles to assure shape induced responses are similar for the gold and carbon based particles.

We also examined whether complement deposition or lack of it can disrupt innate-adaptive axis via modulation of regulatory cytokines. Thus, CMC-CNT, RNA-CNT, and Au-Ni nanowires were challenged against U937 (macrophage cell line), Raji (B cell line) and Jurkat (T cell line) cells with and without complement deposition. Our results suggest that complement deposition on CNTs determines the balance between pro-inflammatory and anti-inflammatory immune responses. Au-Ni nanowires were poor inducers of complement activation, and on their own, were not pro-inflammatory. However, lack of complement deposition shifted that balance towards inflammatory response when treated with serum. Complement deposition can sequester CNTs towards a non-inflammatory uptake by immune cells that express complement receptors on their surfaces, such as macrophages and B lymphocytes. Complement deposition also altered IL-10 and IL-12 cytokine profile, which is likely to raise the threshold of adaptive immune response. In addition, massive upregulation of IL-10 is a likely mechanism for the downregulation of proinflammaory cytokines by complement-opsonized nanoparticles. These results have implications in the consideration of systemic and direct-to-organ/tissue delivery of the nanoparticles.

5.2 Materials and methods

5.2.1 Nanoparticles

MWNTs, prepared and described in ref [52] were dispersed using noncovalent functionalization, by 2 min ultrasonication in PBS containing 1% carboxymethyl cellulose (CMC, Sigma, # 21901) or 1% (w/v) ribonucleic acid from bakers yeast (RNA) (Sigma, #R6750). PBS is 2.7 mM KCl, 1.5 mM KH_2PO_4, 136.9 mM NaCl, 8.9 mM Na_2HPO_4, pH 7.4. Excess surfactant was removed by washing with PBS. Au-Ni nanowires were prepared by electrodeposition and fully characterized and described in [53] and coated with 9 mM glutathione and 1 mM mPEG-SH (Rapp Polymere, Germany) in PBS for 24 h at 4°C. Excess surfactant was removed by washing by centrifugation in PBS. Analysis of the nanoparticles was performed with a Zeiss HR-LEO 1550 FEG Scanning Electron Microscope (SEM) (figure 5.1).

5.2.2 Complement Activation and Consumption Assay for the classical and alternative pathways

To investigate whether the nanoparticles activate (consume) complement in human serum, a complement activation/consumption assay was performed as described by Salvador-Morales et al [16]. Briefly, nanoparticle suspensions (100 µl of 100 µg/ml) in PBS were added to 100 µl of fresh human serum diluted 1:1 in $DGVB^{++}$. $DGVB^{++}$ is 2.5 mM sodium barbital, 71 mM NaCl, 0.15 mM $CaCl_2$, 0.5 mM $MgCl_2$, 2.5% w/v glucose, 0.1% w/v gelatin, pH

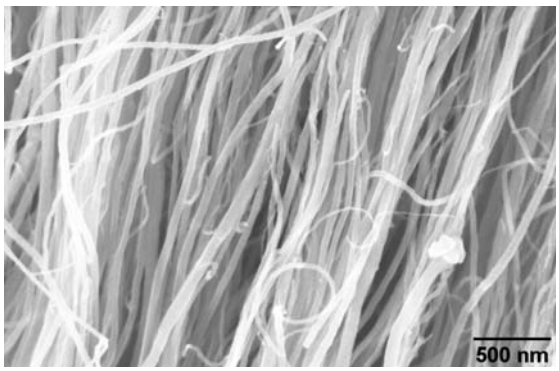

(a) SEM image of pristine MWNTs

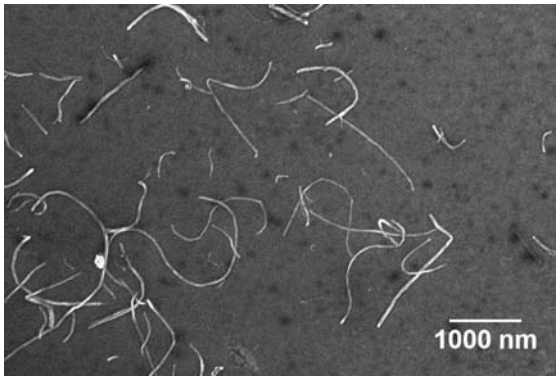

(b) SEM image of CMC coated and dispersed MWNTs.

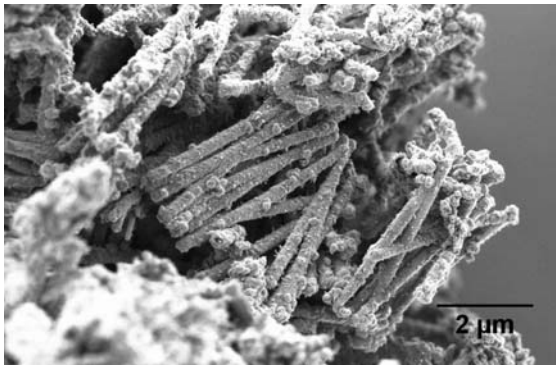

(c) SEM image of Au coated Ni nanowires.

Figure 5.1: Scanning electron microscopy (SEM) images of the used nanoparticles

7.4. Zymosan (0.2 mg in 100 µl PBS; Sigma) served as a positive control. To avoid possible interference of the nanoparticles with the assay, the samples were centrifuged (13000 g, 10 min) after 1 h incubation at 37°C, removing all particles from the sera. The supernatants of each sample were serially diluted 2-fold (1/10-1/5120 in $DGVB^{++}$) using a 96 well plate. 100 µl of each dilution was incubated with 100 µl of antibody-sensitized sheep erythrocytes (EA) (TCS, Buckingham, UK) as described [16] (10^8 cells/ml in $DGVB^{++}$) for 1 h at 37 °C. After incubation, cells were spun down (700 g, 10 min, RT), and hemoglobin was measured at 541 nm in the supernatant. Total hemolysis (100%) was measured by lysing EA with water. Background spontaneous hemolysis (0%) was determined by incubating EA with buffer only. CH50 values, serum dilution required for 50% cell lysis, were calculated and compared.

For the alternative pathway assay, [16] nanoparticle suspensions (100 µl of 0.1 mg/ml) in PBS were added to 100 µl undiluted human serum (Zymosan as a positive control). After 1 hr of incubation at 37 °C, the nanoparticles were removed by centrifugation (13000 g, 10 min). The supernatants of each sample were serially diluted 2-fold (1/5-1/320 in DGVB-Mg-EGTA to inhibit activation through the classical and lectin pathways in the absence of Ca^{2+}) and placed in 96 well plates. 100 µl of each dilution was incubated with 100 µl of antibody sensitized rabbit erythrocytes (10^9 cells/ml in DGVB-Mg-EGTA) for 1 h at 37 °C. Although the nanoparticles were removed from the sera, control experiments were performed incubating the CNTs with rabbit and sheep red blood cells for 2 h at 37 °C no hemolysis could be found in these experiments.

5.2.3 Phagocytosis assay

CMC-CNTs were dialysed into 0.1 M MES buffer and to 0.2 mg/ml. Pentylamine biotin (Pierce) (10 mg) was added to 10 ml of CMC-CNT and 100 µl of a solution of EDC (20 mg/ml Pierce) was added. After 2 h reaction at RT with stirring, the reaction was stopped by adding 100 µl of 0.1 M ethanolamine, and dialysed extensively against PBS. Stability of the biotin was analysed by incubating the CNTs in various media, followed by removing the CNTs by centrifugation and performing the assay described below to detect biotin in the supernatant.

U937 (a monocytic cell line derived from histiocytic lymphoma), Raji (a B cell line derived from Burkitts lymphoma) and Jurkat cell line (a T cell line derived from acute T cell leukemia) cells were cultured in complete RPMI containing 10% fetal calf serum (FCS), 2 mM L-glutamine, 100 U/ml of penicillin and 100 µg/ml of streptomycin and 1mM of sodium pyruvate. All cells were passaged before use. In a 24 well plate $5 \cdot 10^5$ cells per well, were incubated in complete RPMI with above supplements or AIM-V AlbuMAX serum free medium (GIBCO) with 2 mM L-glutamine, 100 U/ml penicillin and 100 g/ml streptomycin

and 1mM of sodium pyruvate. 20 μg biotinylated-CMC-CNTs were added to each well and incubated for 15, 30, 45, 60, 120 or 360 min. Control experiments were performed with cells and PBS only. Cells were harvested and washed five times in PBS pH 7.4 using centrifugation at 300 g and stored at -80°C until further use. A test with Sepharose beads instead of cells showed that suspended nanotubes remained in dispersion and were washed away by this method. The supernatants were removed and 25 μl lysis buffer (10 mM HEPES, 20 mM NaCl, 0.5 mM EDTA, 1% w/v Triton X100) was added to the cells. After lysing the cells, 25 μl of 0.1 mg/ml horse IgG (MRC Immunochemistry Unit, Oxford, UK) in PBS was added to the dispersion to use in the quantification assay. The IgG was added as a blocking agent to minimise non-specific binding reactions.

An ELISA type assay described in detail in [24] was used to quantify the amount of CNTs taken up by cells. Briefly microtitre wells (NUNC, polysorb) were coated with 100 μl Avidin [Pierce, Thermo Fisher Scientific] at 50 μg/ml in 0.1 M Na_2CO_3, pH 9 overnight at 4°C, followed by blocking with 1 mg/ml horse IgG in PBS (pH 7.4) for 1 h at RT. Next, 50 μl of a solution or cell lysate containing biotinylated-CMC-CNTs and 50 μl of 0.1 mg/mL horse IgG in PBS was incubated for 1 h in each well. The plate was washed 7 times with 0.1 mg/ml IgG in PBS to remove excess CNTs and incubated with 1:2000 Streptavidin-HRP (horseradish peroxidise) (Sigma) for 1 h at RT. Then the wells were washed 7 times with 0.1 mg/ml IgG in PBS. O-Phenylenediamine dihydrochloride (OPD) (Sigma, buffered tablets) was used as a substrate for the HRP and the yellow 2,3-Diaminophenazine product was measured at 450 nm.

5.2.4 Measurement of cytokine expression using quantitative PCR analysis

To a 24 well cell culture plate, containing $5 \cdot 10^5$ U937, Raji or Jurkat cells, 20 μg of CMC-MWNTs or RNA-MWNTs or PEG-Au-Ni nanowires in PBS were added and incubated for 15, 30, 45, 60, 120 or 360 min, control samples were incubated with PBS only for 30 min. Cells were harvested and spun down (3000 g, 5 min) and stored at -80°C. Total RNA was extracted from frozen cell pellets using the GenElute Mammalian Total RNA Purification Kit (Sigma-Aldrich). Samples were treated with DNase I to remove any contaminating DNA. To inactivate both DNase I and RNase, samples were heated at 70°C for 10 min, and subsequently chilled on ice. The amount of total RNA was determined at 260 nm using the NanoDrop 2000/2000c (Thermo-Fisher Scientific), and the purity using the ratio of absorbance at 260 nm and 280 nm. cDNA was synthesized using High Capacity RNA to cDNA Kit (Applied Biosystems) from a quantity of 2 μg of total RNA extract. Primer sequences were designed and analysed for specificity using the nucleotide BLAST and Primer-BLAST (http://blast.ncbi.nlm.nih.gov/Blast.cgi). The following primers were used:

18S forward (5-ATGGCCGTTCTTAGTTGGTG-3), 18S reverse (5-CGCTGAGCCA GTCAGTGTAG-3), IL-1β forward (5-GGACAAGCTGAGGAAGATGC-3), IL-1β reverse (5-TCGTTATCCCATGTGTCGAA-3), IL-6 forward (5-GAAAGCAGCAAAGAG GCACT-3), IL-6 reverse (5-TTTCACCAGGCAAGTCTCCT-3), IL-10 forward (5-TTACC TGGAGGAGGTGATGC-3), IL-10 reverse (5-GGCCTTGCTCTTGTTTTCAC-3), IL-12 forward (5-AACTTGCAGCTGAAGCCATT-3), IL-12 reverse (5-GACCTGAACGCAGA ATGTCA-3), TGF-β forward (5-GTACCTGAACCCGTGTTGCT-3), TGF-β reverse (5-GTATCGCCAGGAATTGTTGC-3), TNF-α forward (5-AGCCCATGTTGTAGCAAACC-3) and TNF-α reverse (5-TGAGGTACAGGCCCTCTGAT-3). The qPCR reaction consisted of 5 µl Power SYBR Green MasterMix (Applied Biosystems), 75 nM of forward and reverse primer and 500 ng template cDNA in a 10 µl final reaction volume. PCR was performed in a 7900HT Fast Real-Time PCR System (Applied Biosystems). The initiation steps involved 2 min at 50°C followed by 10 min at 95°C. The template was then amplified for 40 cycles, each cycle comprised of 15 sec at 95°C and 1 min at 60°C. Samples were normalized using the expression of human 18S rRNA. Data was analyzed using the RQ Manager Version 1.2.1 (Applied Biosystems). Ct (cycle threshold) values for each cytokine target gene were calculated and the relative expression of each cytokine target gene was calculated using the Relative Quantification (RQ) value, using the equation:

$$RQ = 2^{-\Delta\Delta Ct} \tag{5.1}$$

for each cytokine target gene, and comparing relative expression with that of the 18S rRNA constitutive gene product. Assays were conducted in triplicate.

5.2.5 Multiplex cytokine array analysis

Cytokines (IL-1α, IL-1β, IL-6, IL-8, IL-10, TNF-α) and chemokines/growth factor (MCP-1, VEGF, GM-CSF and GRO) concentrations were measured by using a commercially available MagPix Milliplex kit (EMD Millipore). Briefly, 25 µl of assay buffer was added to each well of a 96-well plate. This was followed by addition of 25 µl of Standard, controls or supernatants of cells treated with CMC-CNTs, RNA-CNTs or Au-Ni nanowires as described above, to appropriate wells. 25 µl of magnetic beads coupled to analytes of interest were added in each well. Plates were then incubated on a shaker for 18 h at 4°C. The 96-well plate was washed with assay buffer and 25 µl of detection antibodies were incubated with the beads for 1 h at RT. 25 µl of Streptavidin-Phycoerythrin was then added and incubated for 30 min. Following a washing step, 150 µl of sheath fluid was added to each well and the plate was read on the Luminex Magpix instrument.

5.3 Results

5.3.1 Au-Ni nanowires very weakly activate the classical and the alternative complement pathways compared to the CMC- and RNA-MWNTs

The full characterization of all the nanoparticle samples has been reported earlier [52, 53], the batch consistency, in terms of size, purity, absence of debris and contaminations (e.g. catalyst particles) was tested by extensive SEM imaging. Representive images in figure 1 show no indications of impurities. After coating with RNA or CMC, CNTs were well-dispersed and relatively monodisperse for CNTs (length 2.8 $\pm$ 0.5 μm, diameter 42 $\pm$ 8 nm). The excess dispersants were well removed (analysed by OD260 measurements for RNA and no present carbon film visable on SEM and TEM images (not presented)). Au-Ni nanowires are well coated with Au and have a smooth surface, without any impurities or other particles present, and are highly monodisperse (length 2.6 $\pm$ 0.3 μm, diameter 150 nm), the particles can be well dispersed in cell media (analysed by microscopy).

The activation of the classical and alternative pathway by MWNTs coated with CMC and RNA and by Au-Ni nanowires (coated for dispersability with glutathione and PEG-SH) is shown in figure 5.2. All CNT samples tested activated complement through the classical pathway and negligibly by the alternative pathway. Au-Ni nanowires showed negligible complement activation. Differences in the complement activation might be caused by degree of coating of the CNTs, as well as by the chemical nature of the coating substance. Au-Ni particles are known to show little complement activation in general [50]. Commonly small (3-100 nm) Au particles are used in biomedical applications, but increasing their dimensions seems to have no effect on their interactions with complement proteins.

5.3.2 Cell lines expressing complement receptors (U937 and Raji cells) show enhanced uptake of CNTs in the presence of serum

Phagocytosis of moderately complement-activating nanoparticles, CMC-CNTs, was studied in three different cell lines by an ELISA type assay. Their uptake, primarily seen in macrophages (U937) and B (Raji) cells and, to a lesser extent, in Jurkat T cells, was time-dependent and occurred mainly over the first 45 min (figure 5.3).

The highest level of phagocytosis of CNTs in the presence of complement-sufficient serum by Raji cells is an indicator of the involvement of complement receptors in the phagocytic process. B cells are known to present high numbers of CD21 and CD35 (CR2 and CR1), receptors for iC3b, C3d and C4b, on their cell surface. U937 cells express CR1 as well as the iC3b receptors, CR3 and CR4 (CD11b, CD18; Cd11c, CD18). T cells such as Jurkat cell lines have very low level of CD35 and CD11b/CD18 [54], which explains varying levels

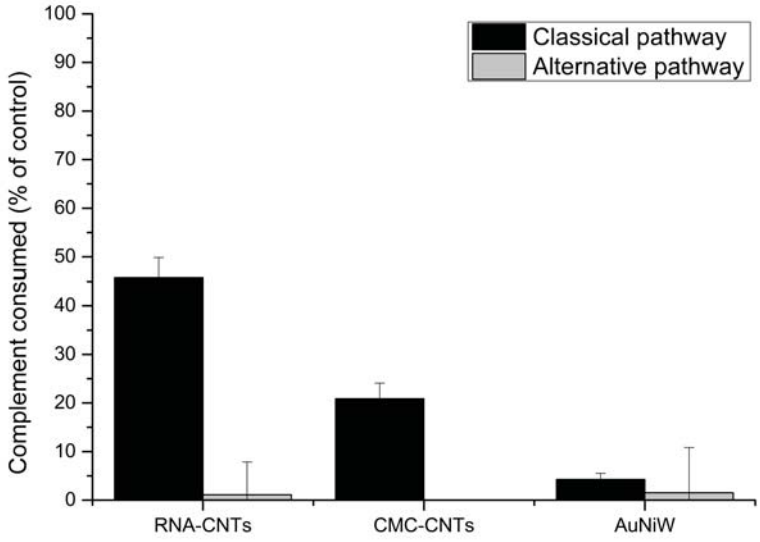

Figure 5.2: Complement activation via the classical and alternative pathway for RNA-CNTs, CMC-CNTs and PEG-Au-Ni nanowires. Indicating the significantly lower complement activation by CMC coating compared to RNA coating and near absence of complement activation by the PEG-Au-Ni nanowires.

of CNT uptake by U937, Raji and Jurkat cells. In all cell types, uptake of CMC-CNTs was enhanced in the presence of serum, indicating the importance of complement deposition on the uptake of CNTs.

5.3.3 Complement deposition on CMC- and RNA-CNTs prime U937 cells for suppression of pro-inflammatory response

CMC-CNT induced considerable expression of TGF-β, IL-12, TNF-α and IL-1β within 1 h of the challenge to U937 cells, compared to the control samples (Figure 5.4). Serum-treated CMC-CNTs significantly down- regulated IL-6, IL-10, TNF-α, TGF-β and IL-1β mRNA expression by U937 cells, while suppressing IL-12 slightly in a biphasic manner. Levels of IL-1β, IL-6, MCP-1, TNF-a and VEGF in U937 cells were lower in serum-treated CMC-CNTs when compared to CMC-CNTs without serum (figure 5.7. In contrast, IL-10 was higher with CMC-CNT in the presence of serum when compared to the absence of serum.

In the case of RNA-CNT, the expression of IL-10, IL-6, TGF-β, TNF-α and IL-1β was up regulated without serum but down-regulated in the presence of serum (Figure 5.5). Levels of MCP-1, TNF-α and VEGF were lower for RNA-CNTs in the presence of serum compared to no serum present (figure 5.7).

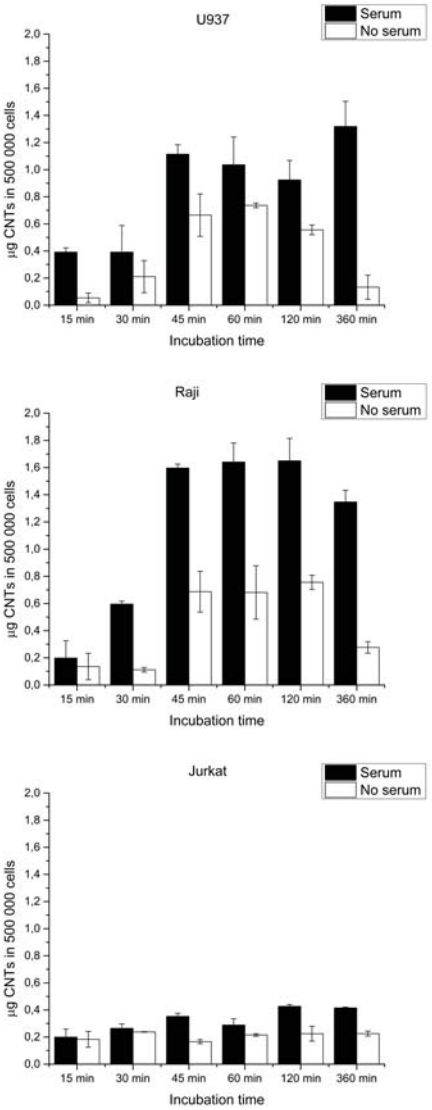

Figure 5.3: Uptake of CMC-CNTs by Raji, U937 and Jurkat cells with and without serum present. In the absence of serum uptake is significantly reduced. As expected T-cells (Jurkat) show little uptake of particles whereas macrophages (U937) and B-cells (Raji) show much greater take up of CMC-CNTs.

5.3.4 Complement-deposited CNTs downregulate pro-inflammatory cytokine mRNA synthesis but enhance IL-12 transcripts by the B cell (Raji) line

Challenging Raji cells with CMC-CNT with serum led to downregulation of IL-6, IL-10, TNF-α, TGF-β and IL-1β (figure 5.4). Curiously, IL-12 levels were considerably upregulated by serum treatment, suggesting likely enhancement of antigen presentation and Th1 activation leading to IFN-α. In the case of RNA-CNT, IL-10 was consistently upregulated in the presence of serum, while TGF-β and IL-12 were dramatically upregulated within 30 min of complement-activated RNA-CNTs exposure to Raji cells (Figure 5.5). Consistent with the observations in U937 cells, IL-1β and TNF-α were downregulated.

5.3.5 Jurkat T cells appear to respond feebly in terms of cytokine production when challenged with CNTs with or without serum

Consistent with poor uptake of CNTs, Jurkat T cells were weak responders to immune challenge in terms of cytokine mRNA synthesis (Figure 5.4 and 5.5). In the case of CMC-CNT, Jurkat cells produced very little cytokine expression, which was further suppressed by the presence of serum. With RNA-CNTs, most cytokine responses were down.

5.3.6 Lack of complement activation by PEG-Au-Ni nanowires exaggerates pro-inflammatory cytokine production

PEG-Au-Ni nanowires in general produced feeble effects on their own, except IL-6 production by Jurkat cells and IL-1β by U937 cell line (Figure 5.6). However, serum-treated PEG-Au-Ni nanowires significantly upregulated IL-10, TNF-α and IL-1β expression (Figure 5.6). More interestingly, the expression of IL-10, TGF-β, IL-12, IL-6, TNF-α, and IL-1β were dramatically upregulated when serum-treated PEG-Au-Ni nanowires were challenged against Raji cells.

5.3.7 Multiplex cytokine array analysis reveals differential ability of CNTs and nanowires to trigger regulatory cytokines by the U937 cells in a complement-dependent manner

To assess the cytokine biosynthesis and secretion over a period of 48 hours, a multiplex cytokine array was used. CMC-CNT induced massive upregulation of GM-CSF in U937 cell lines by 24 h, which declined by 48 h. However, RNA-CNT and Au-Ni induced poor GM-CSF response. In the case of CMC-CNT, complement deposition up-regulated GRO, IL-1β, IL-8 and IL-10 while GM-CSF, MCP-1, TNF-α and VEGF were down-regulated (Figure 5.7). Complement-deposited RNA-CNT up-regulated GM-CSF, GRO, IL-1β, IL-6 and IL-8

while down-regulating IL-10, MCP-1, TNF-α and VEGF. Au-Ni nanowires, which are poor activators of complement, on its own without serum treatment up regulated IL-2α, IL-10 and MCP-1 while being a poor inducer of TNF-α. Serum-treated Au-Ni nanowires up-regulated GM-CSF, GRO, IL-1β, IL-6 and IL-8 while down-regulating IL-2α (figure 5.7). Thus, on its own, Au-Ni nanowires were good inducers of IL-10 and poor inducers of TNF-α and IL-1β.

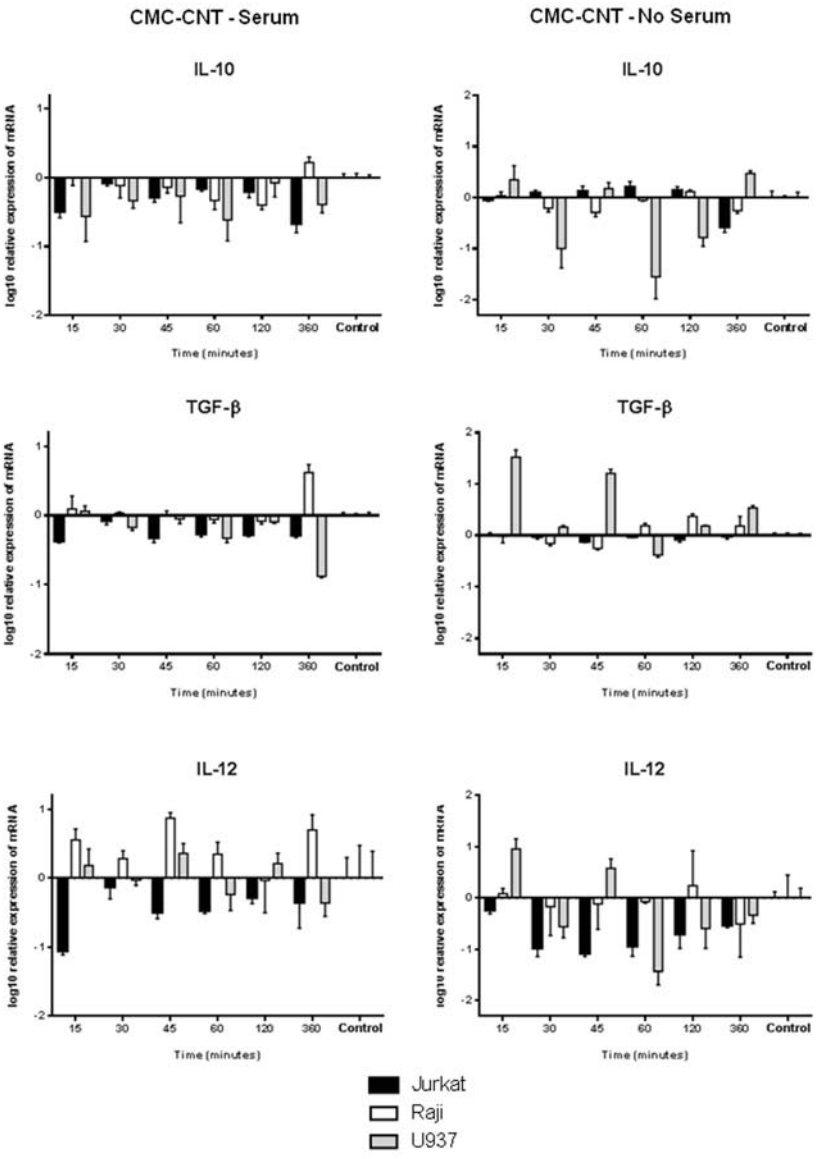
CMC-CNT - Serum
CMC-CNT - No Serum
IL-10
IL-10
TGF-β
TGF-β
IL-12
IL-12
log10 relative expression of mRNA
Time (minutes)
15
30
45
60
120
360
Control
Jurkat
Raji
U937

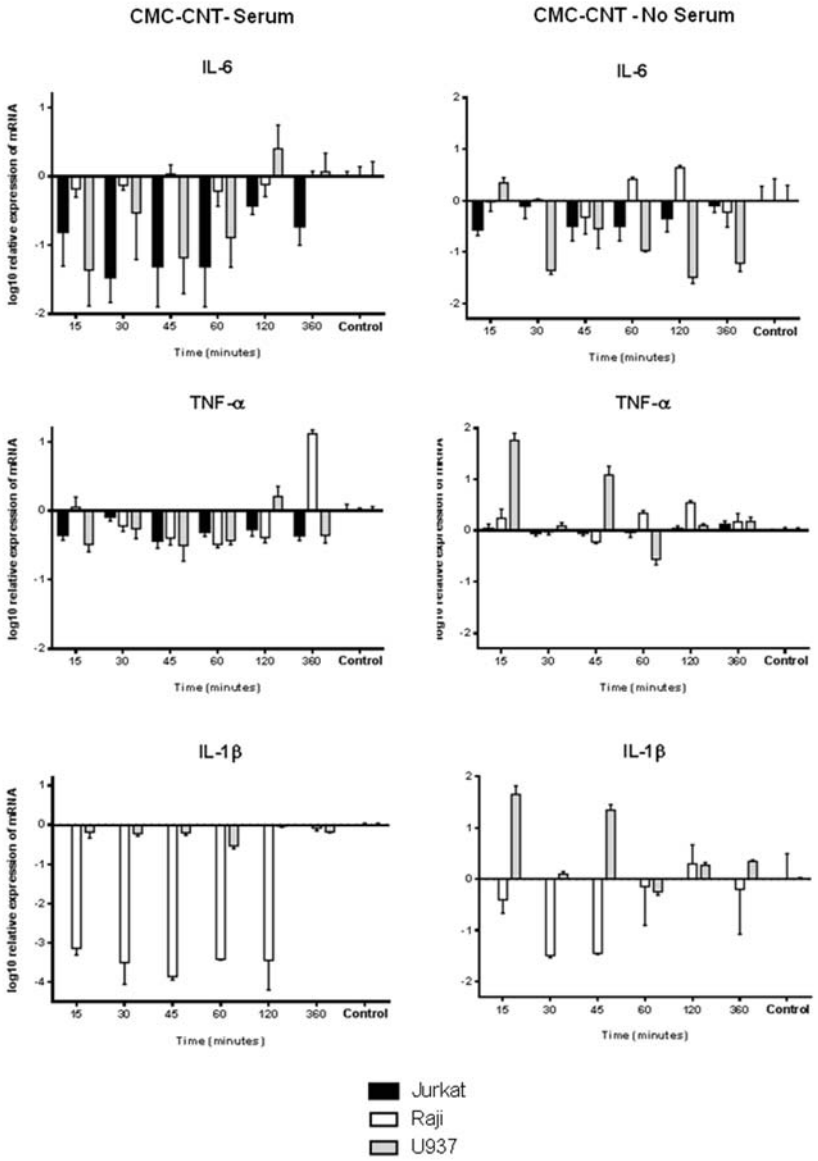

Figure 5.4: Expression of cytokines by U937, Raji and Jurkat cells in vitro during incubation with CMC-CNTs. (a) Anti-inflammatory cytokines: Cells incubated with CMC-CNTs with serum and without serum. (b) Pro-inflammatory cytokines: Cells incubated with CMC-CNTs with serum and without serum. Cells were incubated with CNTs for 15, 30, 45, 60, 120 and 360 min. The expression of cytokines was measured using real time qPCR and the data normalized to 18S rRNA gene expression as a control. Relative expression (RQ) was calculated by using the comparative Ct method with cells incubated with PBS for 30 mins as the calibrator. The RQ value was calculated using the formula: RQ = $2^{-\Delta\Delta Ct}$. Assays were conducted in triplicate. Error bars represent $\pm$ standard error of the mean.

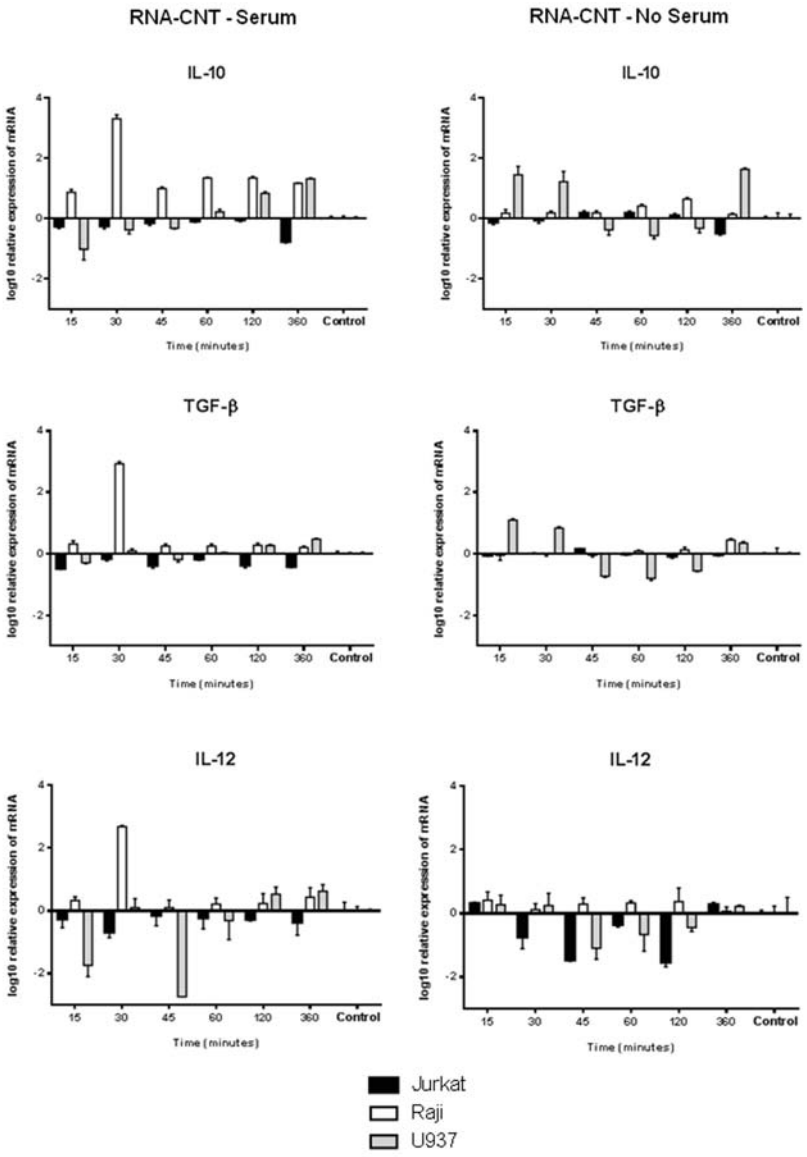
RNA-CNT - Serum
RNA-CNT - No Serum
IL-10
IL-10
TGF-β
TGF-β
IL-12
IL-12
log10 relative expression of mRNA
Time (minutes)
15
30
45
60
120
360
Control
Jurkat
Raji
U937

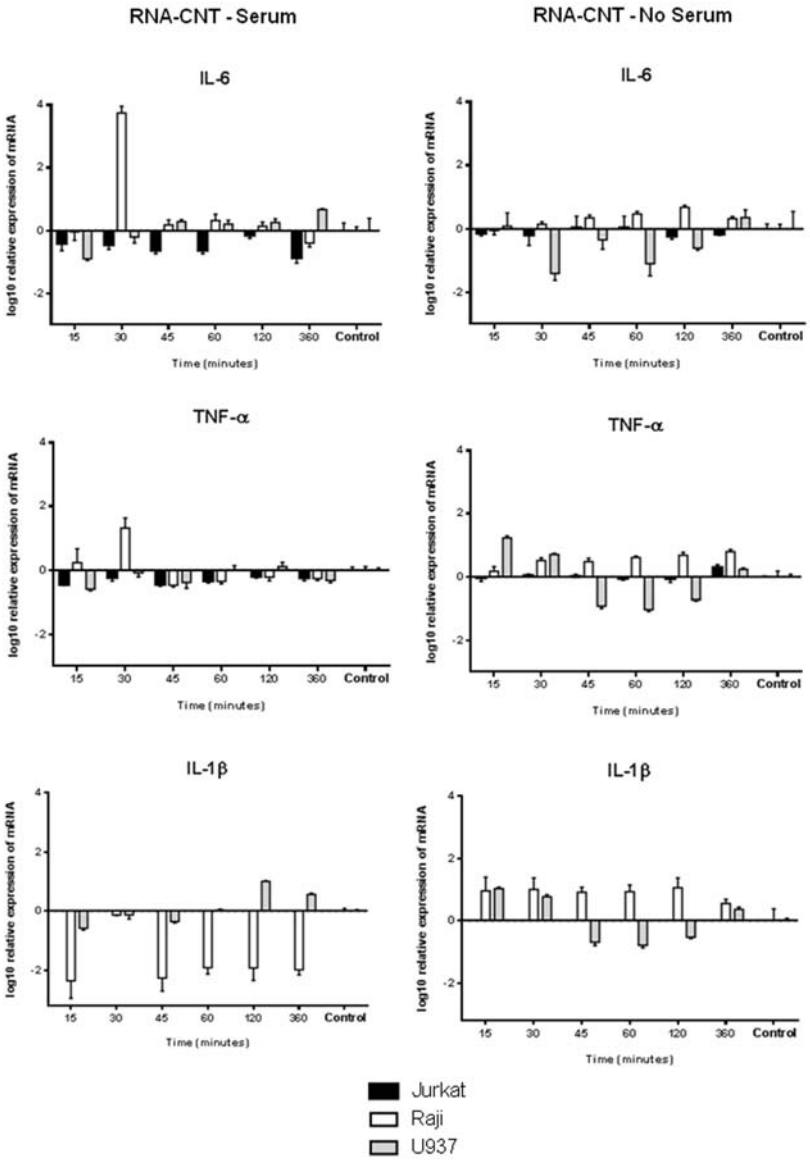

Figure 5.5: Expression of cytokines by U937, Raji and Jurkat cells in vitro during incubation with RNA-CNTs. (a) Anti-inflammatory cytokines: Cells incubated with RNA-CNTs with serum and without serum. (b) Pro-inflammatory cytokines: Cells incubated with CMC-CNTs with serum and without serum. Cells were incubated with CNTs for 15, 30, 45, 60, 120 and 360 min. The expression of cytokines was measured using real time qPCR and the data normalized to 18S rRNA gene expression as a control. Relative expression (RQ) was calculated by using the comparative Ct method with cells incubated with PBS for 30 mins as the calibrator. The RQ value was calculated using the formula: RQ = $2^{-\Delta\Delta Ct}$. Assays were conducted in triplicate. Error bars represent $\pm$ standard error of the mean.

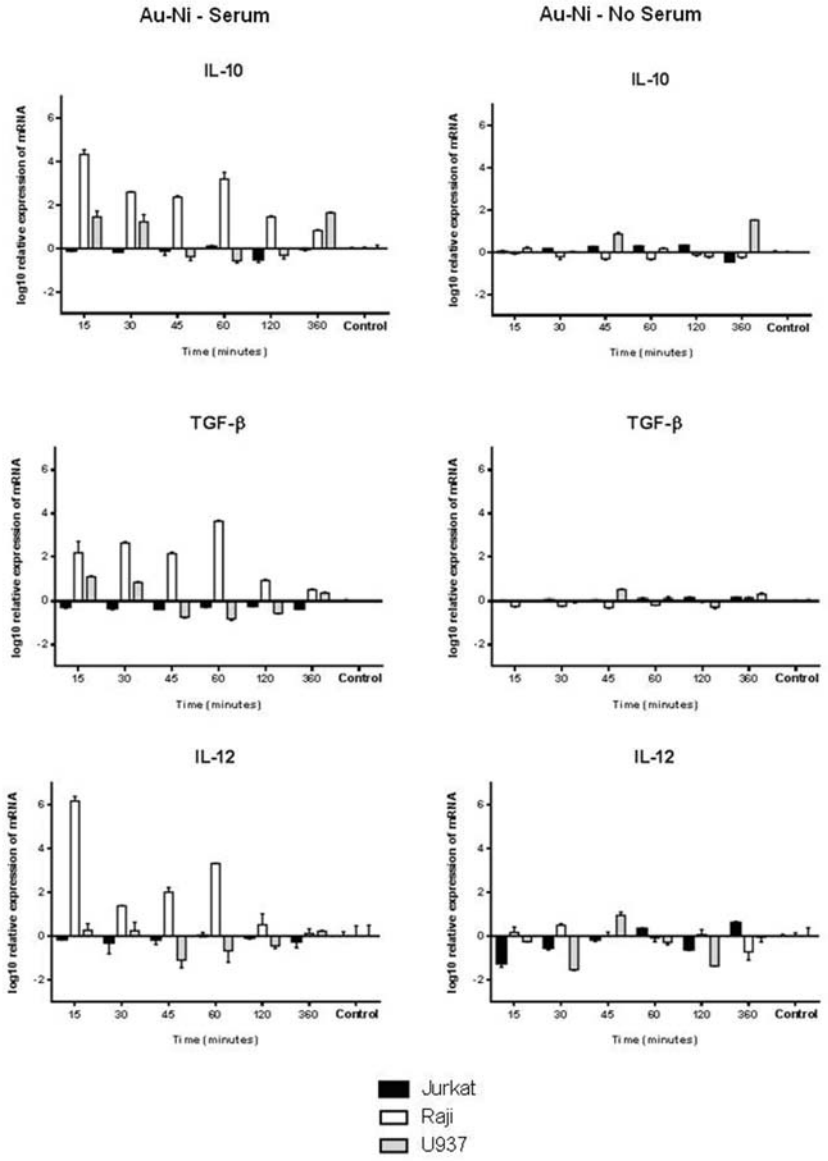
Au-Ni - Serum
Au-Ni - No Serum
IL-10
IL-10
TGF-β
TGF-β
IL-12
IL-12
log10 relative expression of mRNA
Time (minutes)
15
30
45
60
120
360
Control
Jurkat
Raji
U937

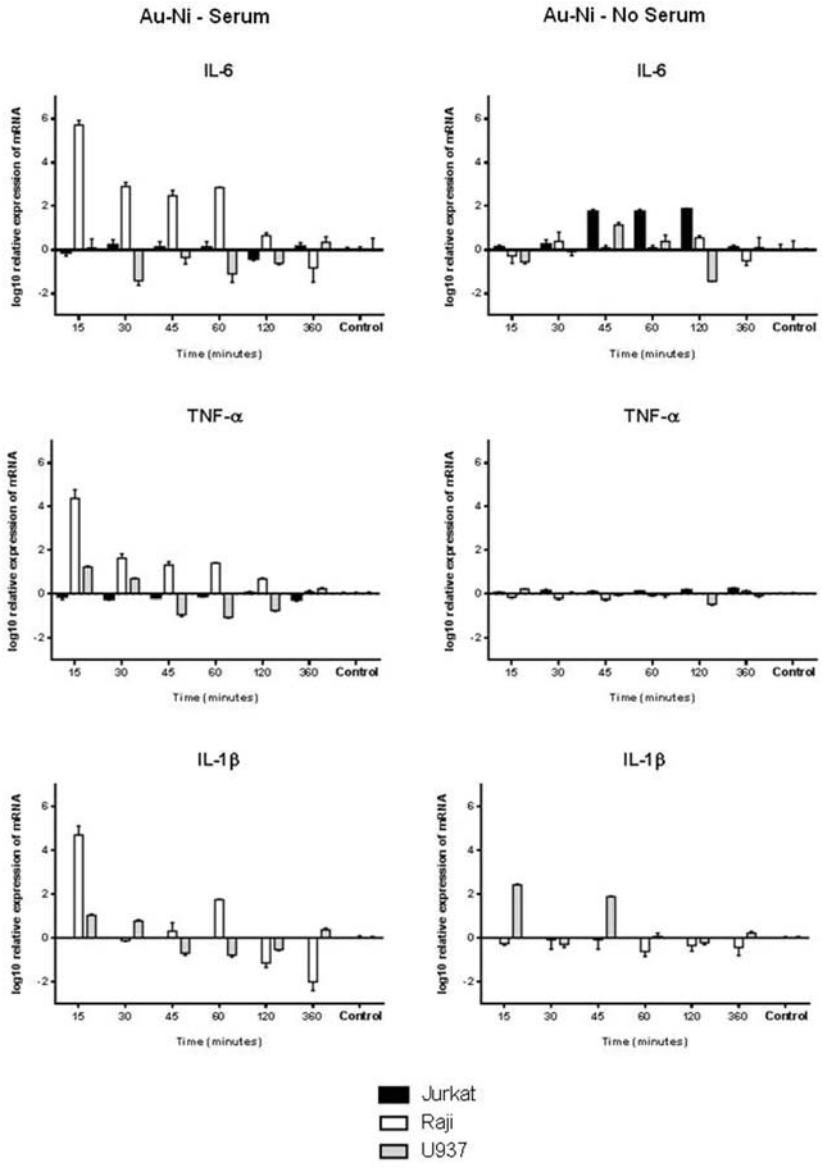

Figure 5.6: Expression of cytokines by U937, Raji and Jurkat cells in vitro during incubation with Au-Ni nanowires. (a) Anti-inflammatory cytokines: Cells incubated with Au-Ni nanowires with serum and without serum. (b) Pro-inflammatory cytokines: Cells incubated with CMC-CNTs with serum and without serum. Cells were incubated with CNTs for 15, 30, 45, 60, 120 and 360 min. The expression of cytokines was measured using real time qPCR and the data normalized to 18S rRNA gene expression as a control. Relative expression (RQ) was calculated by using the comparative Ct method with cells incubated with PBS for 30 mins as the calibrator. The RQ value was calculated using the formula: RQ = $2^{-\Delta\Delta Ct}$. Assays were conducted in triplicate. Error bars represent $\pm$ standard error of the mean.

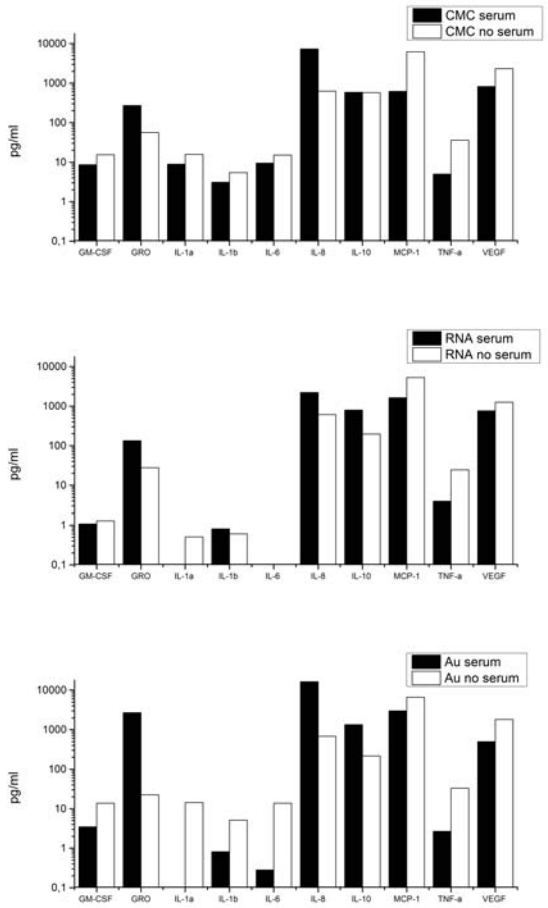

Figure 5.7: Multiplex cytokine array analysis of supernatants of U937 cells treated with CMC-CNTs, RNA-CNTs or Au-Ni nanowires. Cytokines (IL-1α, IL-1β, IL-6, IL-8, IL-10, TNF-α) and chemokines/growth factors (MCP-1, VEGF, GM-CSF and GRO, concentrations were measured by using a commercially available MagPix Milliplex kit (EMD Millipore) and the plate was read on the Luminex Magpix instrument.

5.4 Discussion

Recently, we have shown that several types of pristine and non-covalently functionalized CNTs activate the complement system predominantly via the classical pathway until MAC formation. The interaction of C1q with these CNTs takes place via its ligand-binding globular head (gC1q) domain [24], which could inhibit the binding of serum C1q, thus suppressing classical pathway activation. Complement deposition on the surface of these CNTs enhanced their uptake by U937 cell line and human monocytes. A significant dampening of pro-inflammatory cytokine response by U937 cells was observed with serum.

The cytokine signatures of the innate immune response can shape and orient the adaptive immunity. Thus, we wished to examine if complement deposition can influence the handling of nanoparticles by macrophages (U937) and B (Raji) cells, both expressing abundant complement receptors and are capable of antigen presentation, and on Jurkat T cells that are not phagocytic, express very little complement receptors, and are amenable to modulation by cytokines secreted by macrophages and B cells. In addition to using CMC-CNTs and RNA-CNTs that are complement-activating, Au-Ni nanowires were also examined since gold 'nanoparticles' are not known to activate complement [50]. We show here, for the first time, that gold-coated 'nanowires' do not activate complement significantly through the classical and alternative pathway. Due to the notable difference in complement activation by these similarly sized and shaped particles, these particles were considered ideal candidates for clarifying the relationship between complement activation and cytokine expression for elongated nanoparticles by various immune cells.

The phagocytosis of CMC-CNTs by U937 and Raji cells, both known to over-express complement receptors, was considerably enhanced by serum/complement deposition (Figure 5.3). Jurkat cells, which are known to express complement receptors feebly on their surface, were able to uptake the two CNTs poorly. Serum treatment of the CNTs did not alter the extent of their uptake by Jurkat cells. The maximum intracellular CMC-CNTs were detected at 360 and 60 minutes for U937 and Raji cells, respectively, suggesting very rapid turn-over and processing of CNTs by Raji cells. Curiously, CNTs that were not serum-treated were less detectable by the 360 minute time-point, suggesting that immune cells are either degrading the (coating of) non-opsonized CNTs, or discarding them via transcytosis; this is currently being investigated. Complement-coated CNTs continued to be detectable inside the cells at least until 360 min, suggesting that complement deposition may render the intracellular stay of CNTs longer. It is possible that intracellular PRRs such as TLR7 and TLR9 are also able to recognize non-opsonized CNTs, leading up to pro-inflammatory response.

On its own, CMC-CNT and RNA-CNT induced very early transcriptional upregulation of pro-inflammatory cytokines TNF-α and IL-1β by U937 cells that was significantly down-

regulated by complement deposition. Serum treatment also induced higher IL-10 transcription by CMC-CNT. Raji cells showed reduced mRNA expression of TNF-α and IL-1β by CMC-CNT. Up-regulated expression of IL-12 following complement deposition is likely to cause enhancement of antigen presentation and Th1 activation leading to IFN-γ. For complement-deposited RNA-CNT, IL-10 was consistently up-regulated, TGF-β and IL-12 dramatically up-regulated, while IL-1β and TNF-α were down-regulated. However, Jurkat T cells were weak responders, and whatever little cytokine mRNA expression these cells had was further suppressed by complement deposition. It appears that T cells are more likely to be modulated indirectly by soluble factors produced following nanoparticle interaction with antigen capturing and presenting cells such as macrophages and dendritic cells. Complement deposition may be involved in counterbalancing pro-inflammatory signals arising due to immune cell-nanoparticle interaction. In contrast, Au-Ni nanowires, which are poor complement activators, enticed a weak transcriptional synthesis of cytokines tested via qPCR analysis. Serum-treated Au-Ni nanowires significantly up-regulated mRNA synthesis of TNF-α and IL-1β by U937 cells, in addition to dramatic up-regulation of IL-10, TGFβ, IL-12, IL-6, TNF-α, and IL-1β transcripts by Raji cells, suggesting that some of the serum proteins, other than complement components, which are known to bind to gold nanoparticles can alter or exaggerate the immune response. A lack of complement coating on the nanowires probably makes room for interactions with other serum factors.

Transcriptional analysis via qPCR experiments yields early mRNA synthesis within few minutes and hours of cell response. In order to gauge cytokine secretion over a period up to 48 hours, a multiplex cytokine array was carried out using supernatants from nanoparticle-challenged immune cells. CMC-CNT induced massive upregulation of pro-inflammatory GM-CSF by all three cell lines by 24h, which declined by 48h. However, RNA-CNT and Au-Ni induced poor GM-CSF response. GM-CSF is known to be a potent chemotactic factor for neutrophil recruitment. Complement deposition up-regulated GRO, IL-1, IL-8 and IL-10 while GM-CSF, MCP-1, TNF-α and VEGF were down-regulated by CMC-CNT. Complement-opsonized RNA-CNTs up-regulated GM-CSF, GRO, IL-1β IL-6 and IL-8, while down-regulating IL-10, MCP-1, TNF-α and VEGF. Au-Ni nanowires, on its own, up-regulated IL-2α, IL-10 and MCP-1 while being a poor inducer of TNF-α. Serum-treated Au-Ni nanowires up-regulated GM-CSF, GRO, IL-1β, IL-6 and IL-8 while down-regulating IL-2α Thus, on its own, Au-Ni nanowires were good inducers of IL-10 and poor inducers of TNF-α and IL-1β. This emphasizes the issue that complement deposition in general can sequester phagocytic and cytokine response and make it more complement-receptor-dependent, leading to suppressive anti-inflammatory milieu. A lack of complement deposition, most likely due to the absence of charge pattern that can be recognized by complement recognition subcomponents, can render nanoparticles open to be coated by other serum proteins and

factors [50] that can neutralize the advantages offered by complement opsonization (as is the case here with Au-Ni nanowires).

The suppression of pro-inflammatory cytokines is most likely due to the immunomodulatory effects of IL-10, which has pleiotropic properties on various cell types and influences innate and adaptive immune responses. IL-10 has been shown to down-regulates antigen presentation via MHC class II molecules, pro-inflammatory chemokine and cytokine secretion through an autocrine negative-feedback loop [55]. IL-10 released by macrophages can down-regulate iNOS, ROI , T cell cytokine release, and MHC expression. IL-10 is also linked with anergy induction and regulatory T cell (Treg) cell maturation in addition to dampening DC activation and subsequent cytokine release. Being an anti-inflammatory cytokine, IL-10 may have an important role in limiting the immune response to nanoparticles that may cause injury and inflammation. Activation of TLRs or NOD2 signalling can lead to high levels of IL-10 production which can be regulated by NF-κB [56]. Further work is required to understand the partnership of PRR and signalling pathways leading to diverse transcriptional activation that leads to nanoparticle-induced IL-10 production and its enhancement by complement deposition.

Another issue that is central to immune response to CNT-complement deposition is an upregulation of IL-12, an obligate requirement for Th1 cell proliferation and maturation that can cause T cell cytotoxicity, in addition to being involved in B cell activation. IL-12, in the presence of IL-18, promotes Th1 phenotypic development, characterized ultimately by IFN-γ producing T helper type 1 (Th1) effector cells. IFN-γ drives macrophage priming and activation and adhesion molecule expression. IFN-γ ultimately may retard tissue destruction, perhaps by suppressing osteoclast activation. IL-12 and IL-10-mediated effects due to complement deposition may be limiting the acute danger signals while phagocytosing the nanoparticles and subsequent cytokine storm.

This study thus highlights a careful consideration of the ability of nanoparticles to activate complement and immune cells of innate and adaptive wings. An altered charge or chemical pattern can lead to an entirely different set of immune response by antigen capturing and presenting cells, B and T cells, which can modify the intended outcome of their applications. Thus, nanoparticles need to be examined carefully for their surface molecular patterns, ability to activate complement, and generate cytokine storm by immune cells.

References

[1] L. Y. Rizzo, B. Theek, G. Storm, F. Kiessling, and T. Lammers, "Recent progress in nanomedicine: therapeutic, diagnostic and theranostic applications.," *Current opinion in biotechnology*, vol. 24, pp. 1159–66, Dec. 2013.

[2] A. Bianco, K. Kostarelos, C. D. Partidos, and M. Prato, "Biomedical applications of functionalised carbon nanotubes," *Chemical Communications*, no. 5, pp. 571–577, 2005.

[3] M. Foldvari and M. Bagonluri, "Carbon nanotubes as functional excipients for nanomedicines: II. Drug delivery and biocompatibility issues.," *Nanomedicine : nanotechnology, biology, and medicine*, vol. 4, pp. 183–200, Sept. 2008.

[4] M. Foldvari and M. Bagonluri, "Carbon nanotubes as functional excipients for nanomedicines: I. Pharmaceutical properties.," *Nanomedicine : nanotechnology, biology, and medicine*, vol. 4, pp. 173–82, Sept. 2008.

[5] Z. Liu, S. Tabakman, K. Welsher, and H. Dai, "Carbon Nanotubes in Biology and Medicine: In vitro and in vivo Detection, Imaging and Drug Delivery," *Nano Research*, vol. 2, pp. 85–120, 2009.

[6] W. Wu, S. Wieckowski, G. Pastorin, M. Benincasa, C. Klumpp, J. P. Briand, R. Gennaro, M. Prato, and A. Bianco, "Targeted delivery of amphotericin B to cells by using functionalized carbon nanotubes," *Angewandte Chemie-International Edition*, vol. 44, no. 39, pp. 6358–6362, 2005.

[7] L. Lacerda, A. Bianco, M. Prato, and K. Kostarelos, "Carbon nanotubes as nanomedicines: from toxicology to pharmacology," *Advanced Drug Delivery Reviews*, vol. 58, pp. 1460–1470, Dec. 2006.

[8] H. Ali-Boucetta, K. T. Al-Jamal, D. McCarthy, M. Prato, A. Bianco, and K. Kostarelos, "Multiwalled carbon nanotube-doxorubicin supramolecular complexes for cancer therapeutics.," *Chemical communications*, pp. 459–61, Jan. 2008.

[9] R. Klingeler, S. Hampel, and B. Buchner, "Carbon nanotube based biomedical agents for heating, temperature sensoring and drug delivery," *International journal of hyperthermia*, vol. 24, no. 6, pp. 496–505., 2008.

[10] C. Biale, V. Mussi, U. Valbusa, S. Visentin, G. Viscardi, N. Barbero, N. Pedemonte, and L. Galietta, "Carbon nanotubes for targeted drug delivery," *2009 9th Ieee Conference on Nanotechnology*, pp. 644–646, 2009.

[11] E. Heister, V. Neves, C. Tîlmaciu, K. Lipert, V. S. Beltrán, H. M. Coley, S. R. P. Silva, and J. McFadden, "Triple functionalisation of single-walled carbon nanotubes with doxorubicin, a monoclonal antibody, and a fluorescent marker for targeted cancer

therapy," *Carbon*, vol. 47, no. 9, pp. 2152–2160, 2009.

[12] J. Robinson, K. Welsher, S. Tabakman, S. Sherlock, H. Wang, R. Luong, and H. Dai, "High performance in vivo near-IR imaging and photothermal cancer therapy with carbon nanotubes," *Nano Research*, vol. 3, pp. 779–793, 2010.

[13] K. Welsher, S. P. Sherlock, and H. Dai, "Deep-tissue anatomical imaging of mice using carbon nanotube fluorophores in the second near-infrared window.," *Proceedings of the National Academy of Sciences of the United States of America*, vol. 108, pp. 8943–8948, 2011.

[14] B. S. Zolnik, A. Gonzalez-Fernandez, N. Sadrieh, and M. A. Dobrovolskaia, "Minireview: Nanoparticles and the Immune System," *Endocrinology*, vol. 151, no. 2, pp. 458–465, 2010.

[15] S. Hussain, J. A. J. Vanoirbeek, and P. H. M. Hoet, "Interactions of nanomaterials with the immune system," *Wiley Interdisciplinary Reviews-Nanomedicine and Nanobiotechnology*, vol. 4, no. 2, pp. 169–183, 2012.

[16] C. Salvador-Morales, E. Flahaut, E. Sim, J. Sloan, M. L. Green, and R. B. Sim, "Complement activation and protein adsorption by carbon nanotubes," *Molecular Immunology*, vol. 43, no. 3, pp. 193–201, 2006.

[17] C. Salvador-Morales, E. V. Basiuk, V. A. Basiuk, M. L. H. Green, and R. B. Sim, "Effects of covalent functionalization on the biocompatibility characteristics of multiwalled carbon nanotubes," *Journal of Nanoscience and Nanotechnology*, vol. 8, no. 5, pp. 2347–2356, 2008.

[18] C. Salvador-Morales, E. V. Basiuk, V. A. Basiuk, M. L. H. Green, and R. B. Sim, "Effects of covalent functionalisation on the biocompatibiltiy characteristics of multiwalled carbon nanotubes," *Journal of Nanoscience and Nanotechnology*, vol. 8, no. 5, pp. 2347–2356, 2007.

[19] C. Salvador-Morales, M. L. H. Green, and R. B. Sim, "Interaction between carbon nanotubes and biomolecules.," in *Chemistry of carbon nanotubes* (E. V. Basiuk and V. A. Basiuk, eds.), ch. 27, American Scientific Publishers, 2007.

[20] M. Rybak-Smith, K. Pondman, E. Flahaut, C. Salvador-Morales, R. Sim, and ., "Recognition of Carbon Nanotubes by the Human Innate Immune System.," in *Carbon Nanotubes for Biomedical Applications* (R. Klingeler and R. B. Sim, eds.), pp. 183–210, Springer, 2011.

[21] M. V. Carroll and R. B. Sim, "Complement in health and disease," *Advanced Drug Delivery Reviews*, vol. 63, no. 12, pp. 965–975, 2011.

[22] R. Ghai, P. Waters, L. T. Roumenina, M. Gadjeva, M. S. Kojouharova, K. B. M. Reid, R. B. Sim, and U. Kishore, "C1q and its growing family," *Immunobiology*, vol. 212, no. 4-5, pp. 253–266, 2007.

[23] O. A. Hamad, K. N. Ekdahl, P. H. Nilsson, J. Andersson, P. Magotti, J. D. Lambris, and B. Nilsson, "Complement activation triggered by chondroitin sulfate released by thrombin receptor-activated platelets," *Journal of Thrombosis and Haemostasis*, vol. 6, no. 8, pp. 1413–1421, 2008.

[24] K. M. Pondman, M. Sobik, A. Nayak, A. G. Tsolaki, A. Jäkel, E. Flahaut, S. Hampel, B. Ten Haken, R. B. Sim, and U. Kishore, "Complement activation by carbon nanotubes and its influence on the phagocytosis and cytokine response by macrophages.," *Nanomedicine : nanotechnology, biology, and medicine*, vol. 10, pp. 1287–1299, Mar. 2014.

[25] V. A. Basiuk, C. Salvador-Morales, E. V. Basiuk, R. M. J. Jacobs, M. Ward, B. T. Chu, R. B. Sim, and M. L. H. Green, "'Green' derivatization of carbon nanotubes with Nylon 6 and L-alanine," *Journal of Materials Chemistry*, vol. 16, no. 45, pp. 4420–4426, 2006.

[26] H. Dumortier, S. Lacotte, G. Pastorin, R. Marega, W. Wu, D. Bonifazi, J. P. Briand, M. Prato, S. Muller, and A. Bianco, "Functionalized carbon nanotubes are non-cytotoxic and preserve the functionality of primary immune cells," *Nano Letters*, vol. 6, no. 12, p. 3003, 2006.

[27] K. Bhattacharya, F. T. Andon, R. El-Sayed, and B. Fadeel, "Mechanisms of carbon nanotube-induced toxicity: Focus on pulmonary inflammation," *Advanced Drug Delivery Reviews*, vol. 65, no. 15, pp. 2087–209, 2013.

[28] M. Bottini, N. Rosato, and N. Bottini, "PEG-Modified Carbon Nanotubes in Biomedicine: Current Status and Challenges Ahead," *Biomacromolecules*, vol. 12, no. 10, pp. 3381–3393, 2011.

[29] A. J. Andersen, J. T. Robinson, H. J. Dai, A. C. Hunter, T. L. Andresen, and S. M. Moghimi, "Single-Walled Carbon Nanotube Surface Control of Complement Recognition and Activation," *ACS Nano*, vol. 7, no. 2, pp. 1108–1119, 2013.

[30] C. Salvador-Morales, P. Townsend, E. Flahaut, C. Venien-Bryan, A. Vlandas, M. L. H. Green, and R. B. Sim, "Binding of pulmonary surfactant proteins to carbon nanotubes; potential for damage to lung immune defense mechanisms," *Carbon*, vol. 45, no. 3, pp. 607–617, 2007.

[31] I. Hamad, A. C. Hunter, K. J. Rutt, Z. Liu, H. Dai, and S. M. Moghimi, "Complement activation by PEGylated single-walled carbon nanotubes is independent of C1q and alternative pathway turnover," *Molecular Immunology*, vol. 45, no. 14, pp. 3797–3803, 2008.

[32] S. M. Moghimi, a. J. Andersen, S. H. Hashemi, B. Lettiero, D. Ahmadvand, a. C. Hunter, T. L. Andresen, I. Hamad, and J. Szebeni, "Complement activation cascade triggered by PEG-PL engineered nanomedicines and carbon nanotubes: the challenges ahead.," *Journal of controlled release*, vol. 146, pp. 175–81, Sept. 2010.

[33] W. L. Ling, A. Biro, I. Bally, P. Tacnet, A. Deniaud, E. Doris, P. Frachet, G. Schoehn, E. Pebay-Peyroula, and G. J. Arlaud, "Proteins of the Innate Immune System Crystallize on Carbon Nanotubes but Are Not Activated," *ACS Nano*, vol. 5, no. 2, pp. 730–737, 2011.

[34] M. J. Rybak-Smith, C. Tripisciano, E. Borowiak-Palen, C. Lamprecht, and R. B. Sim, "Effect of Functionalization of Carbon Nanotubes with Psychosine on Complement Activation and Protein Adsorption," *Journal of Biomedical Nanotechnology*, vol. 7, pp. 830–839, Dec. 2011.

[35] M. J. Rybak-Smith and R. B. Sim, "Complement activation by carbon nanotubes," *Advanced Drug Delivery Reviews*, vol. 63, no. 12, pp. 1031–1041, 2011.

[36] A. J. Andersen, P. P. Wibroe, and S. M. Moghimi, "Perspectives on carbon nanotube-mediated adverse immune effects," *Advanced Drug Delivery Reviews*, vol. 64, no. 15, pp. 1700–1705, 2012.

[37] F. A. Murphy, C. A. Poland, R. Duffin, K. T. Al-Jamal, H. Ali-Boucetta, A. Nunes, F. Byrne, A. Prina-Mello, Y. Volkov, S. Li, S. J. Mather, A. Bianco, M. Prato, W. Macnee, W. A. Wallace, K. Kostarelos, and K. Donaldson, "Length-dependent retention of carbon nanotubes in the pleural space of mice initiates sustained inflammation and progressive fibrosis on the parietal pleura.," *The American journal of pathology*, vol. 178, pp. 2587–600, June 2011.

[38] F. A. Murphy, A. Schinwald, C. A. Poland, and K. Donaldson, "The mechanism of pleural inflammation by long carbon nanotubes: interaction of long fibres with macrophages stimulates them to amplify pro-inflammatory responses in mesothelial cells.," *Particle and fibre toxicology*, vol. 9, p. 8, Jan. 2012.

[39] F. A. Murphy, C. A. Poland, R. Duffin, and K. Donaldson, "Length-dependent pleural inflammation and parietal pleural responses after deposition of carbon nanotubes in the pulmonary airspaces of mice," *Nanotoxicology*, vol. 7, pp. 1157–1167, 2013.

[40] J. Palomaki, E. Valimaki, J. Sund, M. Vippola, P. A. Clausen, K. A. Jensen, K. Savolainen, S. Matikainen, and H. Alenius, "Long, needle-like carbon nanotubes and asbestos activate the NLRP3 inflammasome through a similar mechanism," *ACS Nano*, vol. 5, no. 9, pp. 6861–6870, 2011.

[41] D. Liu, L. Wang, Z. Wang, and A. Cuschieri, "Different cellular response mechanisms contribute to the length-dependent cytotoxicity of multi-walled carbon nanotubes,"

Nanoscale research letters, vol. 7, no. 1, p. 361, 2012.

[42] D. M. Brown, I. A. Kinloch, U. Bangert, A. H. Windle, D. M. Walter, G. S. Walker, C. A. Scotchford, K. Donaldson, and V. Stone, "An in vitro study of the potential of carbon nanotubes and nanofibres to induce inflammatory mediators and frustrated phagocytosis," *Carbon*, vol. 45, no. 9, pp. 1743–1756, 2007.

[43] E. Meunier, A. Coste, D. Olagnier, H. Authier, L. Lefevre, C. Dardenne, J. Bernad, M. Beraud, E. Flahaut, and B. Pipy, "Double-walled carbon nanotubes trigger IL-1 beta release in human monocytes through Nlrp3 inflammasome activation," *Nanomedicine-Nanotechnology Biology and Medicine*, vol. 8, no. 6, pp. 987–995, 2012.

[44] M. Yang, K. Flavin, I. Kopf, G. Radics, C. H. Hearnden, G. J. McManus, B. Moran, A. Villalta-Cerdas, L. A. Echegoyen, S. Giordani, and E. C. Lavelle, "Functionalization of Carbon Nanoparticles Modulates Inflammatory Cell Recruitment and NLRP3 Inflammasome Activation," *Small*, vol. 9, no. 24, pp. 4194–4206, 2013.

[45] K. Kostarelos, L. Lacerda, G. Pastorin, W. Wu, S. Wieckowski, J. Luangsivilay, S. Godefroy, D. Pantarotto, J. P. Briand, S. Muller, M. Prato, and A. Bianco, "Cellular uptake of functionalized carbon nanotubes is independent of functional group and cell type," *Nature nanotechnology*, vol. 2, no. 2, pp. 108–113, 2007.

[46] G. Laverny, A. Casset, A. Purohit, E. Schaeffer, C. Spiegelhalter, F. de Blay, and F. Pons, "Immunomodulatory properties of multi-walled carbon nanotubes in peripheral blood mononuclear cells from healthy subjects and allergic patients.," *Toxicology letters*, vol. 217, pp. 91–101, Feb. 2013.

[47] A. A. Shvedova, E. R. Kisin, A. R. Murray, C. Kommineni, V. Castranova, B. Fadeel, and V. E. Kagan, "Increased accumulation of neutrophils and decreased fibrosis in the lung of NADPH oxidase-deficient C57BL/6 mice exposed to carbon nanotubes," *Toxicology and Applied Pharmacology*, vol. 231, no. 2, pp. 235–240, 2008.

[48] D. A. Giljohann, D. S. Seferos, W. L. Daniel, M. D. Massich, P. C. Patel, and C. A. Mirkin, "Gold nanoparticles for biology and medicine," *Angewandte Chemie-International Edition*, vol. 49, no. 19, pp. 3280–3294, 2010.

[49] L. Dykman and N. Khlebtsov, "Gold nanoparticles in biomedical applications: recent advances and perspectives.," *Chemical Society reviews*, vol. 41, pp. 2256–82, Mar. 2012.

[50] M. A. Dobrovolskaia, A. K. Patri, J. Zheng, J. D. Clogston, N. Ayub, P. Aggarwal, B. W. Neun, J. B. Hall, and S. E. McNeil, "Interaction of colloidal gold nanoparticles with human blood: effects on particle size and analysis of plasma protein binding profiles.," *Nanomedicine : nanotechnology, biology, and medicine*, vol. 5, pp. 106–17, June 2009.

[51] K. P. Kumar, W. Paul, and C. P. Sharma, "Green synthesis of gold nanoparticles with Zingiber officinale extract: Characterization and blood compatibility," *Process Biochemistry*, vol. 46, no. 10, pp. 2007–2013, 2011.

[52] K. Lipert, F. Kretzschmar, M. Ritschel, A. Leonhardt, R. Klingeler, and B. Buchner, "Nonmagnetic carbon nanotubes," *Journal of Applied Physics*, vol. 105, no. 6, pp. 063906–063910, 2009.

[53] K. M. Pondman, A. W. Maijenburg, F. B. Celikkol, A. A. Pathan, U. Kishore, B. ten Haken, and J. E. ten Elshof, "Au coated Ni nanowires with tuneable dimensions for biomedical applications.," *Journal of Materials Chemistry B*, vol. 1, pp. 6129–6136, 2013.

[54] C. Wagner, C. Ochmann, M. Schoels, T. Giese, S. Stegmaier, R. Richter, F. Hug, and G. M. Hansch, "The complement receptor 1, CR1 (CD35), mediates inhibitory signals in human T-lymphocytes," *Molecular Immunology*, vol. 43, no. 6, pp. 643–651, 2006.

[55] S. Pestka, C. D. Krause, D. Sarkar, M. R. Walter, Y. Shi, and P. B. Fisher, "Interleukin-10 and related cytokines and receptors.," *Annual review of immunology*, vol. 22, pp. 929–979, 2004.

[56] M. Saraiva and A. O'Garra, "The regulation of IL-10 production by immune cells.," *Nature reviews. Immunology*, vol. 10, pp. 170–81, Mar. 2010.

Chapter 6

Innate immune humoral factors with differential pattern recognition properties alter macrophage response to carbon nanotubes [1]

Abstract

The effectiveness of carbon nanotubes (CNTs) in biomedical applications, especially in drug targeting, is strongly influenced by its interactions with the innate immune system, including the complement system. We have recently shown that pristine and derivatised CNTs can activate complement system primarily via the classical pathway. Complement opsonisation led to enhanced uptake of CNTs and downregulated production of pro-inflammatory cytokines by a macrophage cell line and human monocytes. Here, we show that CMC-MWNT and Ox-MWNT are viewed as a charge pattern non-self by C1q, the recognition subcomponent of the classical pathway, which is known to be involved in the clearance of non-self (pathogens) and altered/transformed self (apoptotic, necrotic and cancer cells) as revealed by mutational studies. Factor H, which is a negative regulator of the alternative pathway, is also known to inhibit classical pathway for certain C1q ligands. Factor H was partly able to inhibit C1q-mediated classical pathway activation by CNTs. C1q and the recombinant globular head modules, but not factor H, enhanced uptake of CNTs by U937 macrophage-like cell line. Binding of C1q

[1] The contents of this chapter have been submitted as: K.M. Pondman, A.G. Tsolaki, E. Dodagatta-Marri, L. Pednekar, L. Kouser, A. Nayak, M. Sobik, B. ten Haken, R.B. Sim, U Kishore, "Innate immune humoral factors, C1q and factor H, with differential pattern recognition properties alter macrophage response to carbon nanotubes", *Small*

and its globular head modules to CNTs was able to downregulate pro-inflammatory cytokines and transcriptional factor, NF-κB, and NLRP3 inflammasome. However, the effects of factor H on CNT-induced cytokine storm were not significant. Thus, the recombinant C1q globular heads can be an attractive candidate for coating CNTs due to their ability to (1) dampen the classical pathway activation; (2) enhance their clearance by phagocytes; and (3) downregulate pro-inflammatory cytokine production. We also conclude that pattern recognising soluble complement factors can interact differentially with CNTs, exerting overlapping effects in a complement-independent manner. These results have implications on regulating complement activation prior to designing therapeutic strategies based on nanoparticles.

6.1 Introduction

Over the last decade, carbon nanotubes (CNTs) have been actively explored as drug delivery vehicles for targeted organ-specific as well as systemic therapy [1–5]. The effectiveness of nanoparticles as intravenous drug delivery platforms is strongly influenced by interactions with immune cells, because rapid elimination of the particles from the systemic circulation prevents the drug from reaching the target tissue [6]. Furthermore, the activation of the innate and adaptive immune system can lead to severe inflammatory reactions. Therefore, understanding the interactions of nanoparticles with cellular and humoral components of the immune system is essential for their strategic and specific use for in vivo delivery [6–10].

CNTs are hydrophobic, and therefore, surface modifications are essential to disperse them in aqueous media. Dispersing CNTs can be achieved either covalently or non-covalently. Non-covalent methods use adsorption of dispersants such as proteins, polymers and nucleases onto the surface of CNTs without altering the structure of CNTs. Covalent functionalization of the CNTs alters their walls by making small defects, commonly by oxidation using concentrated acids at high temperature, leading to carboxyl groups on the surface [11]. It is likely that oxidized CNTs interact differently with the innate immune system, an aspect that has not been extensively studied. In this study, we functionalized a type of pristine multi-walled CNTs (MWNTs), either covalently by oxidation (Ox-MWNT), or non-covalently with carboxymethyl-cellulose (CMC-MWNT) and compared different functionalization methods while assuring the functional groups on the CNTs have equal (carboxyl) differences, therefore, should be a result of decreased length and lower impurities in the oxidized samples.

The innate immune system plays a key role in protection against pathogens and synthetic particles including nanoparticles and carbon nanotubes (CNTs) [6, 10, 12–14]. The complement system, consisting of a complex system of interacting soluble and membrane bound proteins, is one of the key innate immune humoral defence mechanisms and gets activated through three distinctive pathways. The classical pathway is initiated by C1q, a charge pattern

recognition protein (460 kDa), consisting of 18 polypeptide chains (6A, 6B and 6C chains) followed by a collagen like region (N terminal) and a globular head domain (C terminal) of A, B and C chains (ghA, ghB or ghC). It most notably binds to IgG and IgM though the globular head regions, but can also bind to charge clusters of C1q proteases C1r and C1s are activated and in turn activate C4 and C2 forming protease C4b2a (C3 convertase) causing C3b to bind to the target. C3b interacts with C3b receptors on phagocytic cells but also causes activation of C5 and ultimately formation of C5-9 or the membrane attack complex (MAC), which forms a channel in membranes lysing cells [15]. In the lectin pathway the recognition protein are mannose binding lectin (MBL) or ficolins, which mainly bind to vicinal diols on sugars, activating MASP-2 which in turn activates C4 and C2 where the pathway is similar to the classical pathway [15]. The alternative pathway is triggered by a conformational change in C3, causing its cleavage to C3a and C3b [16]. As in the classical and lectin pathways, C3b binds covalently to surfaces where it can be stabilized by factor B forming C3bB complex, factor D is able to cleave C3Ba bound factor B into Ba and Bb fragments. The Bb fraction remains bound to C3b leading to C3bBb which can be stabilized by properdin to C3bBbP, a protease able to generate more C3b to bind to the target. The route of the rest of the pathway towards MAC formation is similar to the other pathways. Factor H and factor I are the down-regulators of the alternative pathway. Factor H binds to C3b inhibiting formation of C3bB, and together with factor I, it cleaves C3b to iC3b, which is unable to form C3bBb [15, 17, 18].

Pristine and functionalized CNTs are widely recognized to activate complement, principally through the classical pathway, and to a minor extent through the alternative pathway [8, 10, 14, 19–23] and the lectin pathway [8, 24, 25]. Activation of the complement system by CNTs offers an intriguing challenge since C3b-opsonised CNTs can be cleared quickly via complement receptors by phagocytes prior to reaching the intended target tissue for drug delivery. The breakdown products of the complement cascade (C3a, C4a and C5a), which are potent anaphylatoxins, can induce inflammation and hypersensitivity reactions [10, 12, 14, 15]. Furthermore formation of MAC can cause damage to cells and tissues in the direct surroundings of the CNT [12]. We have recently shown that CNTs, which were able to activate complement mostly via the classical pathway, get internalized more efficiently by macrophages, leading to down regulation of pro-inflammatory cytokine mRNA expression [26]. However, similarly dimensionalised Au-Ni nanowires activate complement very poorly, which impacts upon phagocytosis and cytokine/chemokine production by U937 (a macrophage cell line), Raji (a B cell line) and Jurkat (a T cell line) cells [27]. It appears that complement deposition sequesters CNTs away from classical pathogen-associated molecular patterns (PAMP)-pattern recognition receptors (PRR) interaction, and, therefore, dampens the cytokine storm, likely via dramatic upregulation of anti-inflammatory IL-10. In the absence of complement deposition, CNTs can acquire other serum proteins which can give rise to

a robust pro-inflammatory immune response by macrophages and B cells, leading to tissue injury [27]. Given that CNTs (pristine or functionalised) offer repetitive recognition patterns of polarity and hydrophobicity, we wished to examine the nature of interaction of C1q, the first recognition subcomponent of the classical pathway, with Ox-MWNT and CMC-MWNT. In recent studies, factor H, in addition to being an opsonin, has been shown to be a competitive inhibitor of C1q for certain ligands [17]. Both C1q and factor H, which can be locally synthesised during immune cell activation, have also been shown to have a range of complement-independent functions [28]. Here, we show that interaction of C1q via its gC1q domain and factor H with CNTs involves charge pattern recognition, which can impact upon complement activation, phagocytosis, and immune response. Thus, the recombinant globular head modules can be an excellent inhibitor to be coated on CNTs prior to therapeutic applications by virtue of their ability to down-regulate classical pathway and pro-inflammatory cytokine response, in addition to enhancing the CNT clearance by phagocytic cells.

6.2 Methods

6.2.1 Dispersion of MWNTs: non-covalent and covalent functionalization

MWNTs were purchased from Arrynano (Frechen Knigsdorf, Germany) having outer diameter 10-20 nm, length 5-20 μm. Non-covalent functionalization was achieved by sonication in 2:1 mass ratio with carboxymethyl cellulose (CMC), in PBS followed by centrifugation at 8000 g to remove clusters and subsequent washing of excess CMC using a 0.2 μm pore size polycarbonate track-etched membrane filter (Whatman). For covalent functionalization, a modified procedure described by Li [11] was used to oxidise the MWNTs. 100 mg of pristine MWNTs were added to a 50 ml mixture of sulfuric acid (H_2SO_4, 10 M) and nitric acid (HNO_3, 10 M) using a 3:1 volume ratio. The mixture was sonicated in a bath at RT for 1 h and probe sonicated for 30 effective min (50%ON, 50%OFF) on ice, in order to exfoliate the MWNTs and homogenize the dispersion of CNTs. Finally, the acidic mixture with the MWNTs was refluxed at 120°C for 48 hours. The resulting mixture of ox-MWNTs, after being cooled down and diluted with distilled water, was centrifuged at 11000 g for 30 min. Distilled water was added to the pellets to re-suspend the ox-MWNT pellets and centrifugation was repeated three times. The amorphous carbon due to the partial oxidation of the outer structure was removed by stirring the Ox-MWNTs in 10 mM NaOH overnight [29]. The dispersion was then filtered through a membrane filter (0.1 μm pore size polycarbonate track-etched membrane filter Whatman) followed by extensive washings in H_2O in order to remove NaOH. Finally, the ox-MWNTs were dialyzed against distilled water.

6.2.2 Purification of human C1q and factor H from human plasma

C1q was purified from human plasma using affinity chromatography on IgG-Sepharose as described by Tan et al. [30]. Briefly, freshly-thawed plasma was made 5 mM EDTA and centrifuged to remove lipids. The plasma was then incubated with non-immune IgG coupled to CNBr-activated Sepharose (GE Healthcare, UK) for 1 h at 4°C. The C1q-bound sepharose was washed extensively with 10 mM HEPES, 140 mM NaCl, 0.5 mM EDTA pH 7.0 and C1q was eluted with 100 mM CAPS, 1 M NaCl, 0.5 mM EDTA, pH 11.0. IgG contaminants were removed by passing C1q through a HiTrap ProteinG column (PierceNet, USA) and dialyses against the washing buffer. Fractions were analyzed for purity by SDS-PAGE (results not shown).

Factor H was purified as described in [30] from human plasma using an antibody against factor H (MRCOX23) coupled to CNBr-activated sepharose. Freshy thawed plasma was made 5 mM EDTA and dialysed overnight against 25 mM Tris-HCl, 140 mM NaCl, 0.5 mM EDTA, pH 7.5 and passed through the MRCOX23-Sepharose column. After extensive washing using the same buffer, factor H was eluted using 3 M $MgCl_2$ pH 6.9. The eluted fractions were neutralized using 1M Tris pH 7.5 and dialysed against H_2O, followed by 10 mM K_2HPO_4, 140 mM NaCl, 0.5 mM EDTA pH 7.5. The samples were analysed for purity by SDS-PAGE (results not shown).

6.2.3 Recombinant forms of human C1q globular head regions of A (ghA), B (ghB) and C (ghC) chains

The recombinant forms of globular head modules (ghA, ghB and ghC) and their substitution mutants were expressed in E. coli BL21 strain, as described previously [31–33]. Bacterial cells were grown in 200 ml LB (luria broth) medium containing ampicillin (100 µg/ml) at 37°C. Once grown to an OD_{600} of 0.6, the bacterial cells were induced with IPTG (Isopropyl β-D-1-thiogalactopyranoside) for 3 h and centrifuged (4500 rpm for 15 min). The cell pellet was suspended in 25 ml of lysis buffer (20 mM Tris pH 8.0, 0.5 M NaCl, 1 mM EDTA, 0.2% v/v Tween 20, 5% glycerol, 0.1 mM PMSF (phenylmethanesulfonylfluoride) and 0.1 g lysozyme) and incubated at 4°C for 1 h. The cells were then probe sonicated for 30 sec with 2 min intervals for 10 cycles. After centrifugation (13 000 rpm for 15 min) the supernatant was diluted 5-fold in buffer I (20 mM Tris pH 8.0, 100 mM NaCl, 0.2% Tween 20, 1 mM EDTA and 5% glycerol) and passed through an amylose resin column, and then washed with 3 bed volumes of buffer I, followed by buffer II (250 ml of buffer I without Tween 20). The protein was then eluted in 1 ml fractions with 10 mM maltose in 100 ml of buffer II and frozen at -20°C.

5 ml of Polymyxin B agarose gel (Sigma) was packed in a 20 ml column and washed with 50 ml of 1% sodium deoxycholate and then further rinsed with 50 ml of autoclaved distilled water to completely remove 1% sodium deoxycholate. After rinsing the column, the proteins ghA, ghB and ghC were loaded onto three different columns, and left to incubate at room temperature for half an hour for the protein to bind completely. After the incubation period the protein was eluted and collected in 1.0 mL fractions. The LPS free ghA, ghB and ghC proteins were then checked for purity by running it on 15% SDS gel to ensure the removal of LPS. The endotoxin level was examined by QCL-1000 Limulus amebocyte lysate system (BioWhittaker, Walkersville, MD, USA) and was found to be ˜4 pg μg^{-1} for ghA and ghB and of ˜5 pg μg^{-1}. The proteins were further quantified by measuring the absorbance at 280 nm of the eluted samples and the concentration of the sample was determined via NanoDrop.

6.2.4 Coating of CNTS with C1q, ghA, ghB, ghC and factor H

Human C1q, ghA, ghB, ghC, substitution mutants and factor H were incubated overnight at a 2:1 mass ratio with CMC-MWNT or Ox-MWNT in 50 mM Tris-HCl, pH 7.5, 150 mM NaCl, 5 mM $CaCl_2$. Excess proteins were washed by repeated centrifugation at 17000 g for 10 min and redispersed. Protein binding was analysed by SDS-PAGE. A range of protein: CNT ratio was analysed (1:2, 1:1, 2:1, 4:1 and 8:1). No increase in binding was found above a 2:1 ratio, therefore, this ratio was chosen for subsequent experiments.

6.2.5 Complement consumption assay for the classical pathway

To investigate whether coating CNTs with complement proteins could potentially modulate the activation of the classical pathway, a complement consumption assay was performed similar as previously described [12]. Samples of coated and uncoated CMC-MWNT and Ox-MWNT at 100 µg/ml in buffer containing 50 mM Tris-HCl, 150 mM NaCl, 5 mM $CaCl_2$, pH 7.5 were incubated with occasional shaking at 37°C for 1 h with an equal volume of human serum in dextrose gelatin veronal buffer $DGVB^{++}$ (2.5mM sodium barbital, 71 mM NaCl, 0.15 mM CaCl2, 0.5 mM $MgCl_2$, 2.5% w/v glucose, 0.1% w/v gelatin, pH 7.4) (1:1) to give a total volume of 50 µl. This was followed by centrifugation (13000 g, 10 min), and the collected supernatants were tested for its complement activity by measuring its capacity to lyse antibody-sensitised sheep erythrocytes (EA) (TCS, Biosciences, Buckingham, UK). 100 µl of EA cells ($1 \cdot 10^8$ cells/ml) were added to each sample of the supernatant and incubated for 1h at 37C. Following centrifugation for 5 min at 5000 rpm, 100 µl of the supernatant was collected and released haemoglobin was measured at 541 nm. Total haemolysis (100%) was measured by lysing EA with water. Background spontaneous haemolysis (0%) was determined by incubating EA with buffer only.

6.2.6 Biotinylation of CNTs

CMC-MWNTs and Ox-MWNTs were dialysed into 0.1 M MES buffer (2-(N-morph-olino)-ethanesulfonic acid, pH 5) and their concentration adjusted to 0.2 mg/ml. Pentylamine biotin (Pierce, Thermo Fisher Scientific) (2 mg) was added to 2 ml of CMC-MWNT or Ox-MWNT at 0.2 mg/ml and 20 µl of a 20 mg/ml solution of EDC [1-Ethyl-3-(3-dimethylaminopropyl) carbodiimide] was added. The reaction was allowed to take place at RT for 2 h with stirring, and then stopped by adding 100 µl of 0.1 M ethanolamine (Sigma). The resulting biotin-CMC-MWNT and biotin-Ox-MWNT were dialyzed extensively against PBS (pH 7.4) in order to remove residual reactants and MES.

6.2.7 Phagocytosis

U937 cells (a monocytic cell line derived from histiocytic lymphoma) were cultured in complete RPMI containing 10% fetal calf serum (FCS), 2mM L-glutamine, 100 U/ml penicillin, 100 µg/ml streptomycin and 1mM sodium pyruvate, and passaged and washed in serum free medium before use. In each well of a 24 well plate, $5 \cdot 10^5$ cells were seeded in AIM-V AlbuMAX serum free medium (GIBCO) with above-mentioned supplements (no FCS). 20 µg of biotin-CMC-CNT or biotin-Ox-MWNTs coated with complement proteins were added to each well and incubated for 6 h. Cells were harvested and washed five times in PBS using centrifugation at 300 g and stored at -80°C until further use. All experiments were performed in duplicate. Quantification was performed as described earlier [27]. Briefly, 25 µl lysis buffer (10 mM HEPES, 20 mM NaCl, 0.5 mM EDTA, 1% w/v Triton X100) was added to the cells. After cell lysis, 25 µl of 0.1 mg/ml horse IgG in PBS (as a blocking agent) was added to the dispersion for use. Microtitre wells (NUNC, polysorb) were coated with 100 µl Avidin (Pierce) at 50 µg/ml in 0.1 M Na_2CO_3, pH 9.0 for 1 h at RT, followed by blocking with 1 mg/ml horse IgG in PBS for 1 h at RT. Next, 50 µl of a solution or cell lysate containing biotin-CMC-MWNT or biotin-Ox-MWNT and 50 µl of 0.1 mg/ml horse IgG was incubated for 1 h in each well. The plate was washed 7 times with 0.1 mg/ml IgG to remove excess CNTs and incubated with 1:2000 Streptavidin-HRP (Sigma) for 1h at RT. 3,3',5,5'-Tetramethylbenzidine (TMB) (Biolegend, London, UK) was used as a substrate for the HRP and the yellow product, obtained after stopping the reaction with 2N H_2SO_4 was read at 450 nm.

6.2.8 Measurement of cytokine expression using quantitative PCR analysis

In a 24 well cell culture plate, 10 µg of protein-coated CMC-MWNTs or ox-MWNTs in PBS were added to each well containing $5 \cdot 10^5$ U937 cells and incubated for 15, 30, 45, 60, 120 or 360 min inside a CO_2 (5% v/v) incubator at 37°C. Control samples were incubated with PBS only for 30 min. Cells were harvested and spun down (3000 g, 5 min) and stored at -80°C. Total RNA was extracted from frozen cell pellets using the GenElute Mammalian Total RNA Purification Kit (Sigma-Aldrich). Samples were treated with DNase I to remove any contaminating DNA. To inactivate both DNase I and RNase, samples were heated at 70°C for 10 min, and subsequently chilled on ice. The amount of total RNA was determined at 260 nm using the NanoDrop 2000/2000c (Thermo-Fisher Scientific), and the purity using the ratio of absorbance at 260 nm and 280 nm. The cDNA was synthesized using High Capacity RNA to cDNA Kit (Applied Biosystems) from a quantity of 2 µg of total RNA extract. Primer sequences were designed and analyzed for specificity using the nucleotide BLAST and Primer-BLAST (http://blast.ncbi.nlm.nih.gov/Blast.cgi). The following primers were used: 18S forward (5-ATGGCCGTTCTTAGTTGGTG-3), 18S reverse (5-CGCTGAGCCAGTCAGTGTAG-3), IL-1β forward (5-GGACAAGCTGAGGAAGATGC-3), IL-1β reverse (5-TCGTTATCCCATGTGTCGAA-3), IL-6 forward (5-GAAAGCAGCAAAGAGGCACT-3), IL-6 reverse (5-TTTCACCAGGCAAGTCTCCT-3), IL-10 forward (5-TTACCTGGAGGAGGTGATGC-3), IL-10 reverse (5-GGCCTTGCTCTTGTTTTCAC-3), IL-12 forward (5-AACTTGCAGCTGAAGCCATT-3), IL-12 reverse (5-GACCTGAACGCAGAATGTCA-3), TGF-β forward (5-GTACCTGAACCCGTGTTGCT-3), TGF-β reverse (5-GTATCGCCAGGAATTGTTGC-3), TNF-α forward (5-AGCCCATGTTGTAGCAAACC-3) and TNF-α reverse (5-TGAGGTACAGGCCCTCTGAT-3). The qPCR reaction consisted of 5 µl Power SYBR Green MasterMix (Applied Biosystems), 75nM of forward and reverse primer and 500ng template cDNA in a 10 µl final reaction volume. PCR was performed in a StepOne PCR System (Applied Biosystems). The initiation steps involved 2 min at 50°C followed by 10 min at 95°C. The template was then amplified for 40 cycles, each cycle comprised of 15 sec at 95°C and 1 min at 60°C. Samples were normalized using the expression of human 18S rRNA. Data was analyzed using ExpressionSuite software v1.0.3 (Applied Biosystems). Ct (cycle threshold) values for each cytokine target gene were calculated and the relative expression of each cytokine target gene was calculated using the Relative Quantification (RQ) value, using the equation: RQ $=2^{-\Delta\Delta Ct}$ for each cytokine target gene, and comparing relative expression with that of the 18S rRNA constitutive gene product. Assays were conducted in triplicate.

6.2.9 Multiplex cytokine array analysis

Cytokines (IL-6, IL-8, IL-10, IL12p40, IL12p70, IL-23, IL-27, IL-1α and IL-1β) and chemokines/growth factors (MIG, I-TAC, MCP-1, G-CSF and M-CSF) concentrations were measured by MagPix Milliplex kit (EMD Millipore). Briefly, 25 µl of assay buffer was added to each well of a 96-well plate. This was followed by addition of 25 µl of Standard, controls or supernatants of cells treated with CMC-CNTs, RNA-CNTs or Au-Ni nanowires, to appropriate wells. 25 µl of magnetic beads coupled to analytes of interest were added in each well, followed by incubation for 18h at 4°C. The 96-well plate was washed with assay buffer and 25 µl of detection antibodies were incubated with the beads for 1h at RT. 25 µl of Streptavidin-Phycoerythrin was then added and incubated for 30 minutes. Following a washing step, 150 µl of sheath fluid was added to each well and the plate was read using the Luminex Magpix instrument.

6.3 Results

6.3.1 Binding of CNTs with wild type and substitution mutants of individual C1q globular domains suggests a charge-charge interaction

Pristine MWNTs of 5-20 µm length and diameter 10-20 nm (Figure 6.1a) were well-dispersed by non-covalent coating with CMC. The samples were highly dispersed and stable for months. Oxidation was achieved by treatment with concentrated acids (Figure 6.1d). By TEM imaging defects could be seen on the surface of the MWNTs (Figure 6.1b) which was not found on pristine MWNTs (Figure 6.1a) and the nanotubes were significantly shortened (length 100-500nm; Figure 6.1c). The NaOH treatment removed all amorphous carbon from the surface of the nanotubes.

Recombinant gC1q proteins ghA, ghB, ghC and their substitution mutants, ArgA162-Ala/Glu, ArgB114Gln/Glu, HisB117Asp, ArgB129Ala/Glu, LysB136Glu, ArgB163Ala/Glu, TyrB175Leu, HisC101Ala, ArgC156Glu, and LysC170Glu were generated as described [31–33] (Figure 6.3). These substitution mutations were engineered based on earlier data showing their involvement in C1q binding to a range of ligands including IgG, IgM, CRP and PTX3 [31–33]. While C1q and factor H bound CNTs normally (Figure 6.2a and 6.2b), a differential binding can be seen in figure 6.4, using the same concentration of all mutants. For ghA, the Arg162 residue is important in binding as evident from a strong decrease in binding for ArgA162Ala, while both wild type and ArgA162Glu bound similarly. Wild type ghB binds less efficiently than ghA, substitution of Lys136 to Glu (LysB136Glu) abolished binding completely. Furthermore, the substitution of the Arg129 residue of the ghB module had an effect. When this was substituted for Ala, a decrease in binding was observed, while substitution for

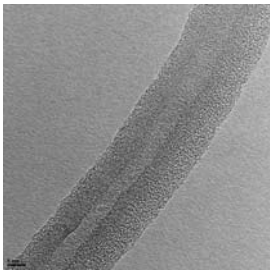

(a) High resolution TEM image of pristine MWNT. The MWNTs consist of a high number of parallel carbon walls, which are undamaged. The external diameter is approximately 22 nm while the inner diameter of the CNT is only 5 nm.

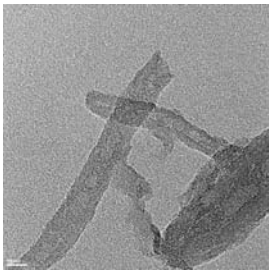

(b) High resolution TEM image of Ox-MWNT; After acid treatment at high temperature, the outer walls of the CNTs show a high number of defects a clear indication of the formation of carboxyl groups on the surface of the MWNT.

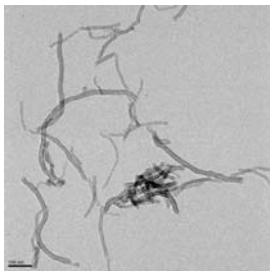

(c) During the oxidation process the MWNTs are shortened and the outer walls functionalised with carboxyl groups, the overall structure of the MWNTs is still intact. Amorphous carbon is effectively removed by washing in NaOH.

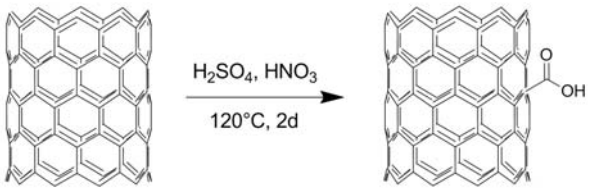

(d) Cartoon depicting the oxidation process. After sonication to exfoliate and homogenize the MWNTs. To form carboxyl groups on the surface of the MWNTs they are refluxed in a 3:1 mixture of concentrated sulfuric acid and nitric acid for 48 hrs at 120°C. Followed by washings in distilled water and NaOH to remove amorphous carbon.

Figure 6.1: The oxidation procedure creates carboxyl groups on the surface of the MWNTs, as can be seen in the TEM images.

Glu did not have an effect. No other substitutions in ghB tested had a significant influence on binding. The wild type ghC bound more efficiently than ghB; substitution of His101 and Lys170 did not have an effect on binding, but an increase in binding efficiently was observed for ArgC156Glu. In addition, we observed clustering in ghA, ghB, ArgA162Ala and ArgA162Glu but not in other mutant samples (Figure 6.5), an indication of differential and multivalent binding that could cause aggregation of CNTs. These results appear to suggest a charge-charge interaction between C1q and CNTs involving hydrophobic clusters of the gC1q domain and side chains of the modules. Residues central to C1q binding to IgG appear also appear to be involved in the gC1q interaction with both forms of the CNTs.

6.3.2 Opsonisation of CNTs with innate immune humoral fact and effect on the classical pathway complement activation

Both CMC-MWNT and Ox-MWNT were efficiently coated with all three globular heads, C1q, and factor H (Figure 6.2a and 6.2b). When C1q was pre-coated on Ox-MWNT and CMC-MWNT, complement consumption was inhibited by 40% for Ox-MWNTs, suggesting that the interaction of C1q with Ox-MWNT is in a conformation that may or may not necessarily activate the classical pathway via binding to C1r and C1s, while this is not the case with CMC-MWNT (Figure 6.6). We have previously shown that ghA, ghB and ghC can inhibit the classical pathway activation by serum considerably [24]. However, both CNTs when pre-coated with factor H were able to consume 40% less complement than the uncoated ones. Thus, factor H and C1q may be recognising charge patterns that are overlapping, and that factor H may be acting as an inhibitor of the CNT-induced classical pathway activation. This is consistent with the emerging evidence that for certain C1q ligands, factor H can be an inhibitor of the classical pathway [30, 34].

6.3.3 Effect of CNT opsonisation with C1q, ghA, ghB, ghC and factor H on phagocytosis by U937 cells

Binding of innate immune proteins onto the surface of CNTs had an impact on the phagocytosis of the CNTs by U937 cells and the effects were differential for Ox-MWNT and CMC-MWNT. For CMC-MWNT, phagocytosis was increased by C1q (3.5 fold), ghA (4 fold), and ghC (6 fold). For Ox-MWNT, no significant effect was seen for any of the globular head domains, but phagocytosis was slightly more efficient for C1q (1.3 fold). For factor H, a 2.6 fold reduction of uptake was seen (Figure 6.7). The dramatic enhancement of CMC-MWNT phagocytosis by ghC is quite curious, probably suggesting a role for this C1q module in an interaction via a possible receptor on the cell surface of macrophages.

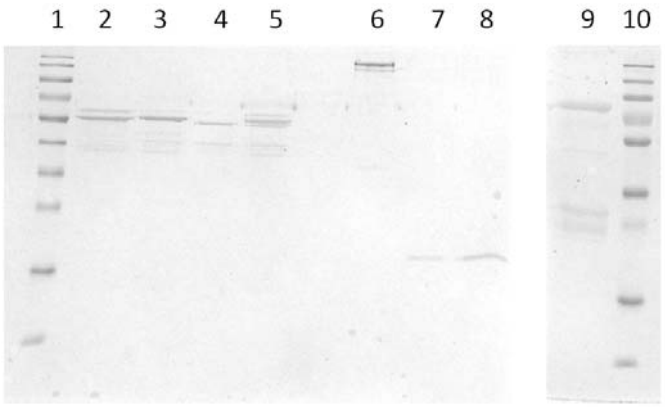

(a) SDS-PAGE of Ox-CNTs coated with innate immune humoral factors. CNTs were coated with the proteins in a ratio of 1:2 w/w, by incubating the CNTs with proteins for 2 h and washed extensively. Lane 1: molecular weight marker; Lane 2: ghA; Lane 3: ghB; Lane 4: ghC; Lane 5: equimolar ghA, ghB and ghC; Lane 6: factor H; Lane 7: SP-A; Lane 8: SP-D; Lane 9: C1q.

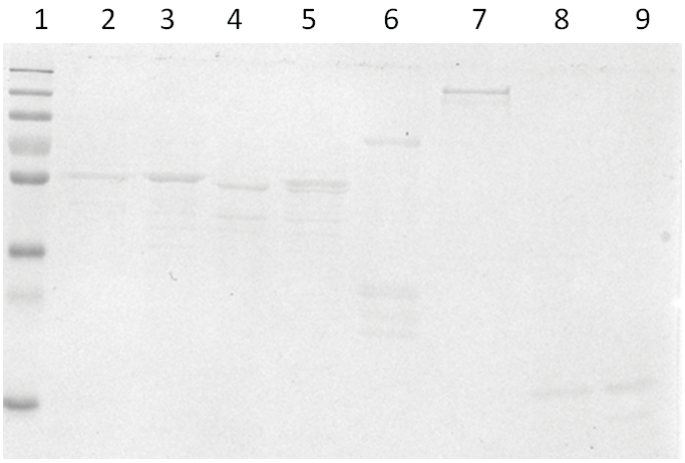

(b) SDS-PAGE of CMC-CNTs coated with innate immune humoral factors. CNTs were coated with the proteins in a ratio of 1:2 w/w, by incubating the CNTs with proteins for 2 h and washed extensively. Lane 1: molecular weight marker; Lane 2: ghA; Lane 3: ghB; Lane 4: ghC; Lane 5: equimolar ghA, ghB and ghC; Lane 6: C1q; Lane 7: factor H; Lane 8: SP-A; Lane 9: SP-D;

Figure 6.2: The binding of innate immune humoral factors onto CNTs is selective and differential

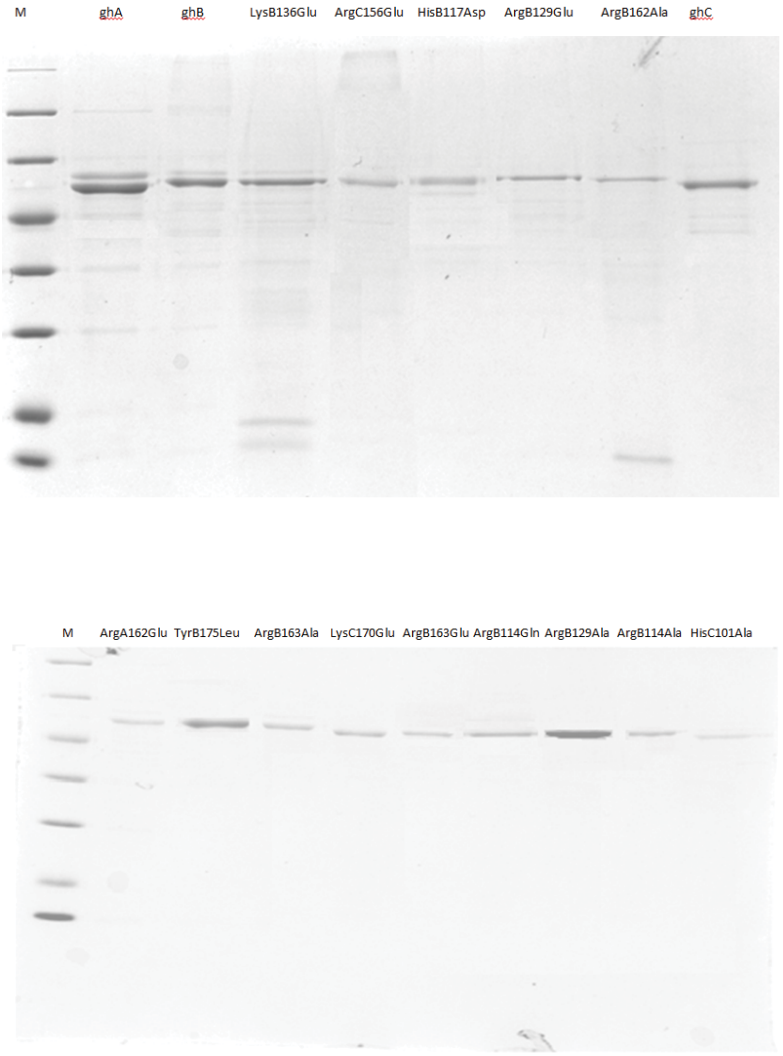

Figure 6.3: SDS-PAGE analysis of the mutants of globular heads of C1q. In all lanes 5 µg of the indicated mutant of globular heads were loaded. All mutants have equal size.

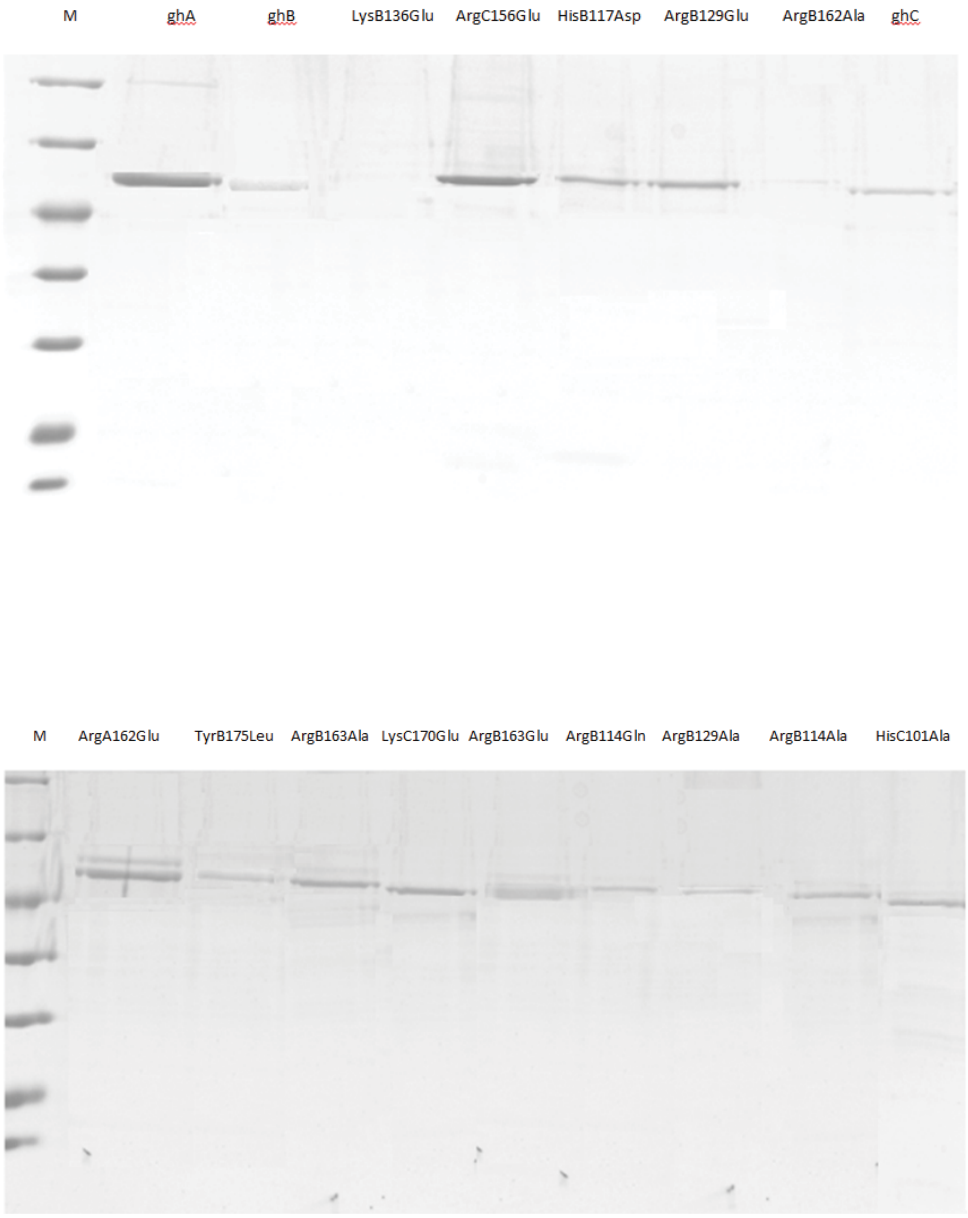

Figure 6.4: SDS-PAGE of differential binding of mutants of the globular heads of C1q onto Ox-MWNTs. CNTs were coated with the proteins in a ratio of 1:2 w/w, by incubating the CNTs with proteins for 2 h and washed extensively. Several mutant forms of globular heads show higher affinity for the Ox-MWNTs surface.

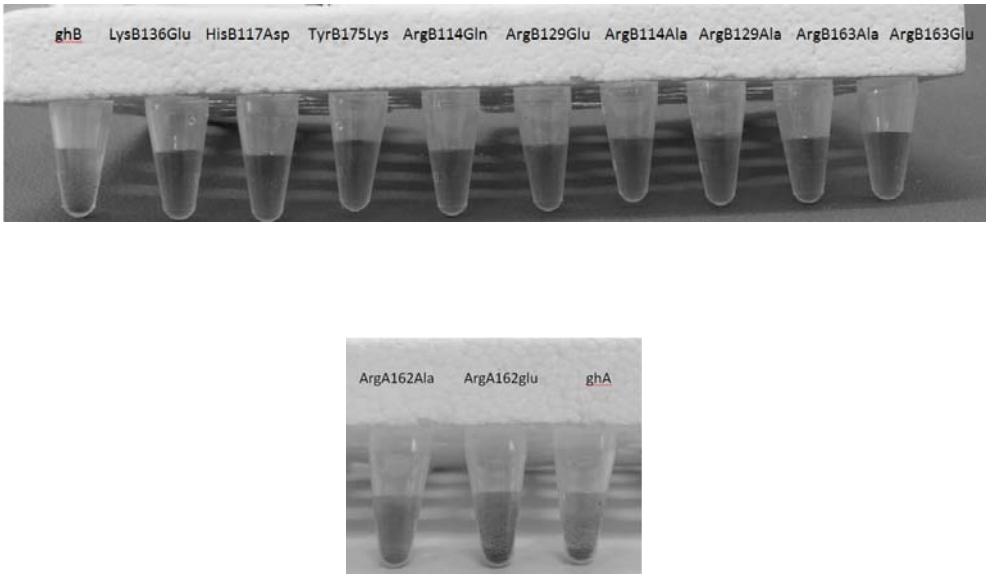

Figure 6.5: Images of the incubation of mutants of the globular heads of C1q with Ox-MWNTs. Showing differential aggregation for different mutants after 1 h of incubation with the Ox-MWNTs, indicating variations in binding.

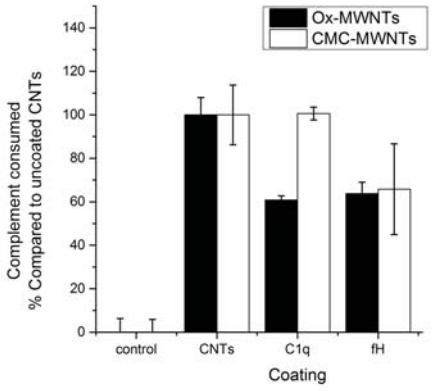

Figure 6.6: Complement inhibition assay to show that pre-coating of CNTs with C1q, factor H and SP-D influences complement activation. CNTs were coated with the proteins in a ratio of 1:4 w/w, by incubating the CNTs with proteins overnight and washed. Samples were incubated with human serum for 1 h. Zero complement consumption was based on a negative control: Serum incubated without CNTs. Percentage of complement consumption was calculated as (C-Ci)/C x 100%, where C represents the total complement activity in CH50 units of the negative control, Ci is the amount of activity remaining in the supernatant of the sample tested. All experiments were done in triplicate; error bars represent $\pm$ standard deviation.

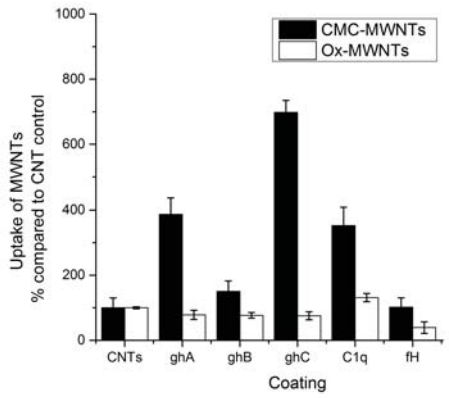

Figure 6.7: Differential uptake of opsonised CNTs by U937 cells in the absence of serum. CMC coated or oxidised CNTs were biotinylised. And incubated with indicated opsonins in 1:2 w/w ratio (CNT:protein). 500 000 U937 cells were incubated with 20 µg of CNTs for 6 hrs. Followed by extensive washing in PBS. The cells were lysed and the amount of CNTs quantified by an ELISA type assay. A standard curve with known concentrations of biotin-CMC-CNTs or biotin-Ox-CNTs was performed in the same assay to calculate the mass of the CNTs in the cell samples. All experiments were done in triplicate; error bars represent ± standard deviation.

6.3.4 Modulation of cytokine and transcription factors mRNA expression by Ox-MWNTs and CMC-MWNTs with and without opsonisation with C1q, ghA, ghB, ghC or factor H

The mRNA expression for both pro- and anti-inflammatory cytokines by U937 cells following challenge with Ox-MWNT and CMC-MWNT and the effect of pre-coating with innate immune soluble factors was analysed by qPCR at early time-points (figure 6.8 and 6.9. Transcriptional expression of IL-10 by U937 cells was strongly upregulated by Ox-MWNT up to a 300-fold after 6h; for CMC-MWNT, the upregulation was seen only after 2h. For Ox-MWNT, pre-coating with C1q and ghC dampened the IL-10 expression compared to uncoated Ox-MWNTs. For CMC-MWNTs, all immune proteins tested here except factor H had a slight inhibitory effect on the mRNA expression of IL-10. IL-12 transcription was similarly upregulated for Ox-MWNTs but the effect was dampened slightly by factor H. The mRNA expression of IL-12 was very different when U937 cells were challenged with CMC-MWNT; there is not much effect for most samples. Curiously, ghC opsonisation of CMC-MWNTs appeared to enhance IL-12 transcription (Figure 6.8). The expression of TGF-β by U937 cells was not altered significantly by either type of MWNT, for Ox-MWNT all samples were slightly down-regulated until 1h. Only factor H coated Ox-MWNT yielded an

upregulated expression, suggesting an immunosuppressive effect of factor H (figure 6.9). For CMC-MWNT, the upregulation was slightly later at 2h, no effect was seen by the protein coating. IL-1β was upregulated for all Ox-MWNT; the transcription level was dampened by C1q and ghC. In the case of CMC-MWNT, there was a downregulation of IL-1β within 2h. With these CNTs, coating with ghA caused the upregulation to occur earlier at 60 minutes. TNF-α transcription was upregulated by Ox-MWNTs, whereas CMC-MWNTs caused an initial downregulation. However, after 1 h, the TNF-α mRNA expression was upregulated. The ghB and ghC modules caused the upregulation to occur already at 15 min. In order to examine the activation of transcription factors, NF-κB, and inflammasome marker NLRP3, RNA samples from U937 cells challenged with CNTs, with and without coating, were used in qPCR analysis (figure 6.10). For CMC-MWNT, factor H was able to significantly suppress NF-κB expression initially for up to 2h, while C1q caused slight inhibition. Contrary to this suppressive effect by full length C1q (and factor H), the globular head modules were unable to inhibit mRNA synthesis. However, the inhibitory effect of immune proteins was more pronounced for Ox-MWNTs, even with ghA, ghB, and ghC. C1q, ghC and factor H down-regulated NLRP3 expression, consistent with their ability to suppress CNT-mediated IL-1β secretion (figure 6.10).

6.3.5 Opsonisation of CNTs by complement proteins had modulatory effects on the cytokine/chemokine secretion by U937 cells

In order to assess the effect of opsonins on the CNT-mediated cytokine and chemokine secretion by U937 cells, we performed multiplex cytokine array analysis using supernatants from the experiments at 12, 24 and 48 h time points (figure 6.11). In general, C1q and factor H suppressed MCP-1, IL-8 and TNF-α (factor H being more pronounced for Ox-MWNT), IL-10, IL-1α and IL-1β. For G-CSF and IL-12p40, C1q enhanced whereas factor H suppressed the cytokine production. All the globular head modules had suppressive effect on IL-8 and MCP-1, while TNF-α was slightly suppressed by ghB and ghC. The effect on IL-10 secretion was slightly enhanced whereas ghB considerably suppressed IL-1α and IL-1β for CMC-MWNT. The recombinant globular head modules enhanced G-CSF production whereas only ghA was able to enhance IL-12 secretion. The effect of globular head modules on MIG and I-TAC was not significant.

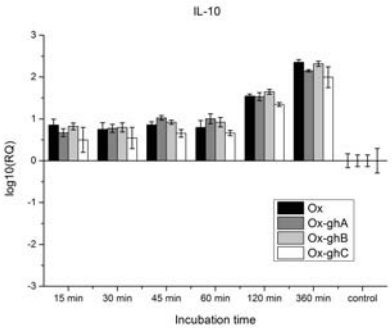
IL-10
log10(RQ)
Incubation time
15 min
30 min
45 min
60 min
120 min
360 min
control
Ox
Ox-ghA
Ox-ghB
Ox-ghC

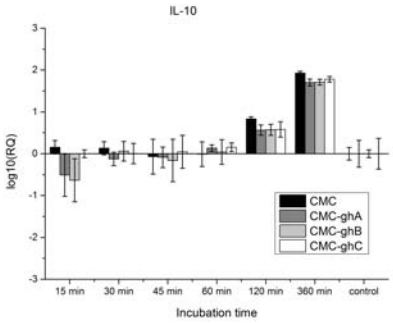
IL-10
log10(RQ)
Incubation time
15 min
30 min
45 min
60 min
120 min
360 min
control
CMC
CMC-ghA
CMC-ghB
CMC-ghC

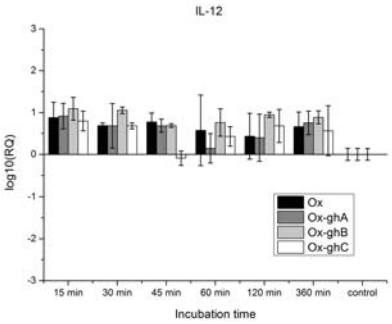
IL-12
log10(RQ)
Incubation time
15 min
30 min
45 min
60 min
120 min
360 min
control
Ox
Ox-ghA
Ox-ghB
Ox-ghC

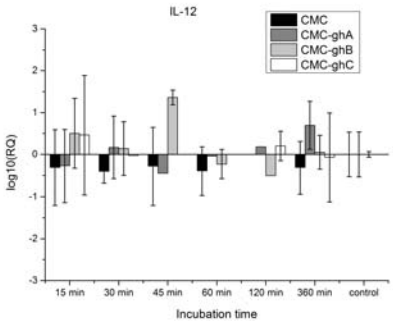
IL-12
log10(RQ)
Incubation time
15 min
30 min
45 min
60 min
120 min
360 min
control
CMC
CMC-ghA
CMC-ghB
CMC-ghC

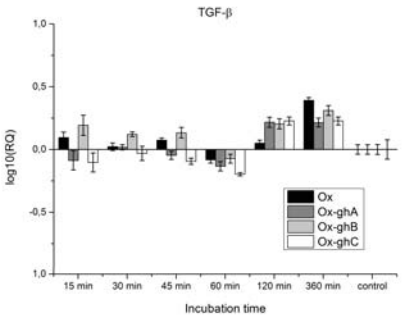
TGF-β
log10(RQ)
Incubation time
15 min
30 min
45 min
60 min
120 min
360 min
control
Ox
Ox-ghA
Ox-ghB
Ox-ghC

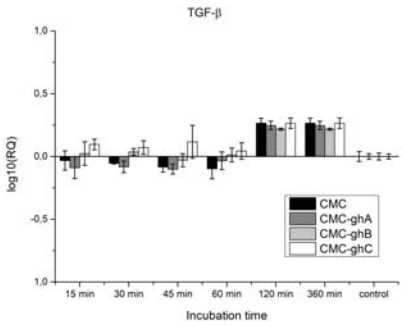
TGF-β
log10(RQ)
Incubation time
15 min
30 min
45 min
60 min
120 min
360 min
control
CMC
CMC-ghA
CMC-ghB
CMC-ghC

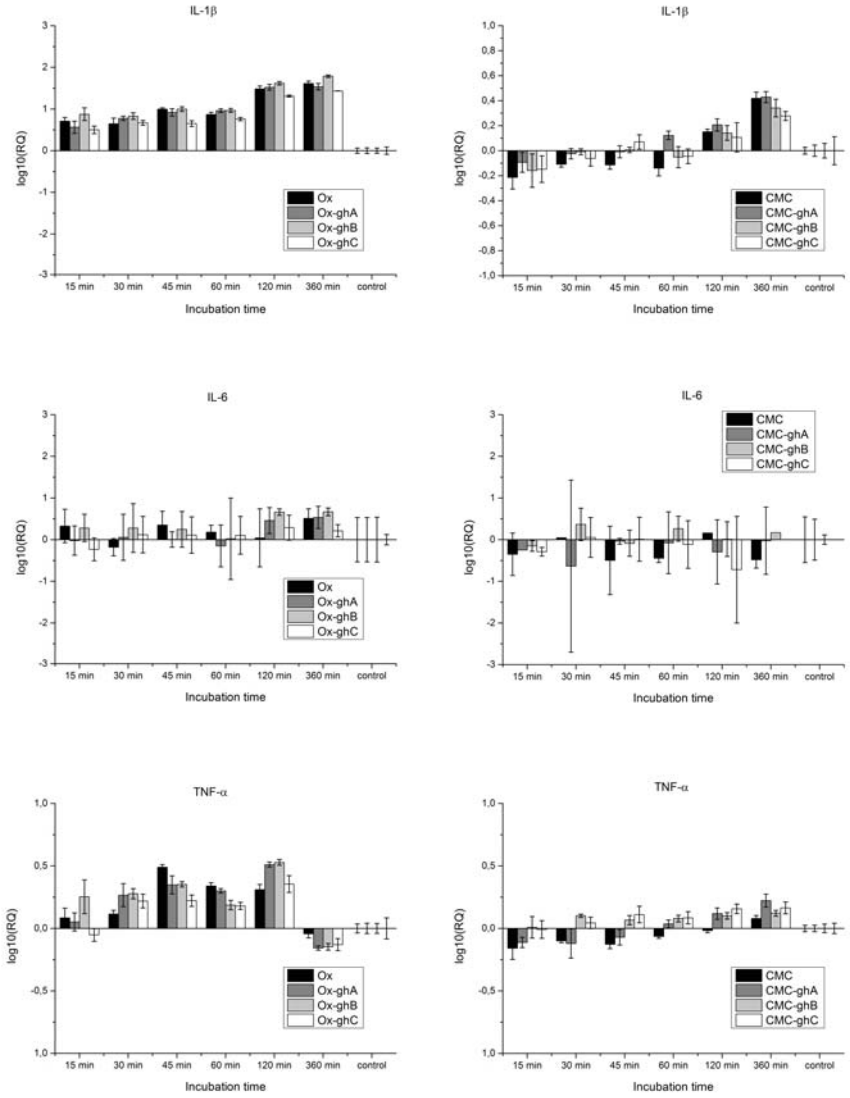

Figure 6.8: Expression of cytokines by U937 cells in vitro during incubation with Ox-MWNTs and CMC-MWNTs coated with recombinant globular heads of C1q. Cells were incubated with coated Ox-MWNTs or CMC-MWNTs for 15, 30, 45, 60, 120 and 360 min. The expression of cytokines was measured using real time qPCR and the data normalized to 18S rRNA gene expression as a control. Relative expression (RQ) was calculated by using the comparative Ct method with cells incubated with PBS for 30 mins as the calibrator. The RQ value was calculated using the formula: RQ $=2^{-\Delta\Delta Ct}$. Assays were conducted in triplicate. Error bars represent $\pm$ standard error of the mean.

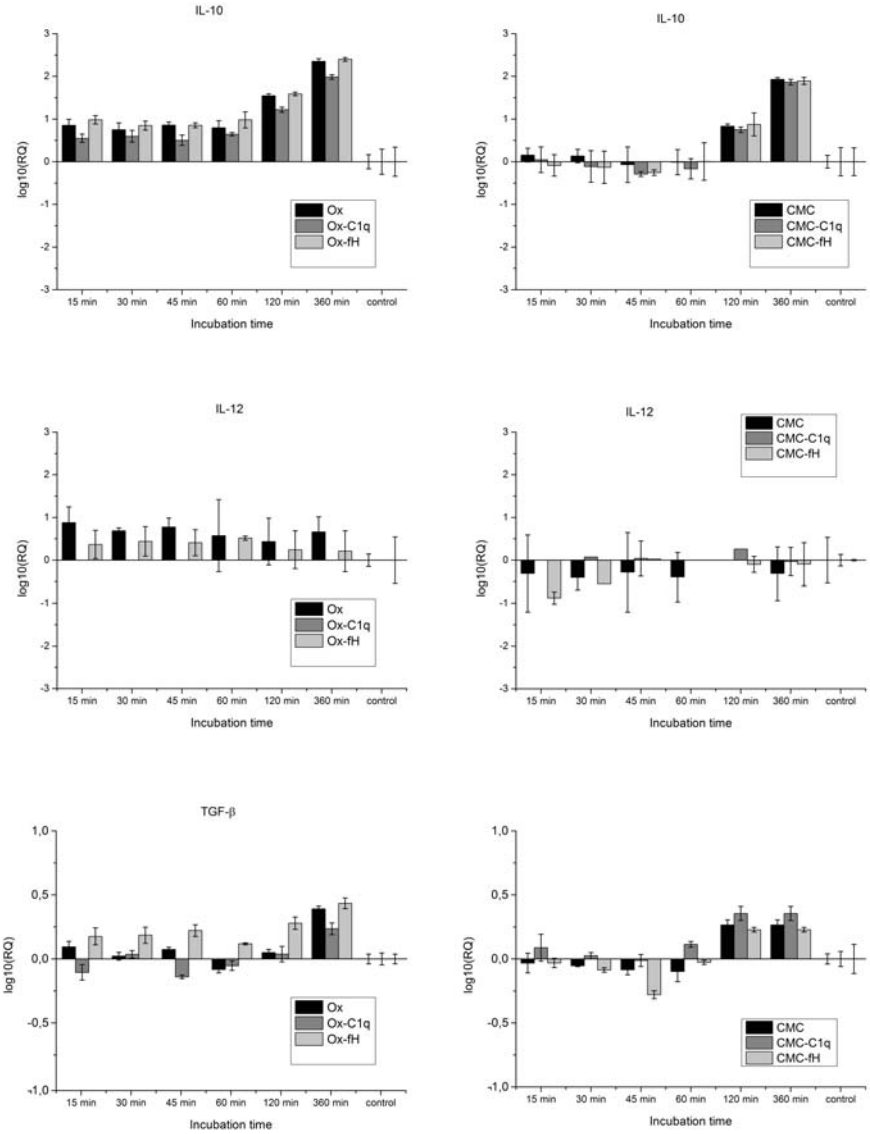
IL-10
log10(RQ)
Ox
Ox-C1q
Ox-fH
15 min
30 min
45 min
60 min
120 min
360 min
control
Incubation time
IL-10
log10(RQ)
CMC
CMC-C1q
CMC-fH
Incubation time
IL-12
log10(RQ)
Ox
Ox-C1q
Ox-fH
Incubation time
IL-12
log10(RQ)
CMC
CMC-C1q
CMC-fH
Incubation time
TGF-β
log10(RQ)
Ox
Ox-C1q
Ox-fH
Incubation time
log10(RQ)
CMC
CMC-C1q
CMC-fH
Incubation time

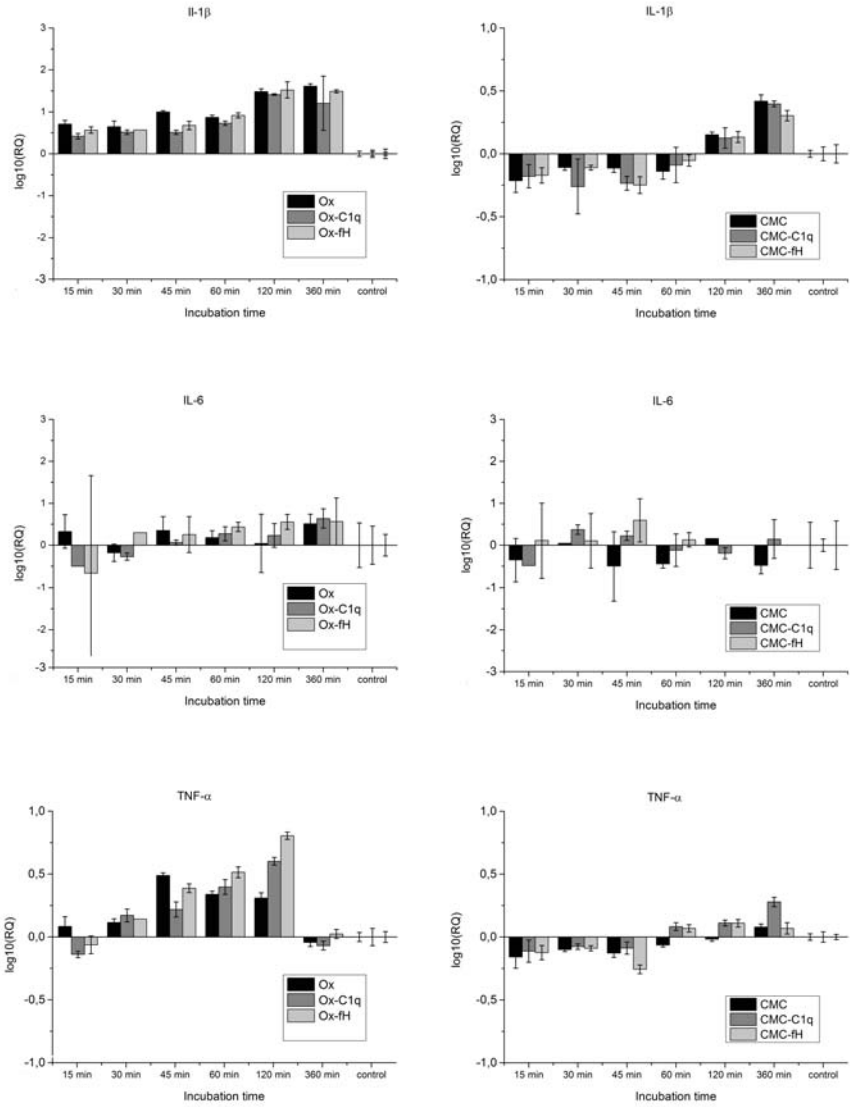

Figure 6.9: Expression of cytokines by U937 cells in vitro during incubation with Ox-MWNTs and CMC-MWNTs coated with C1q or Factor H. Cells were incubated with coated Ox-MWNTs or CMC-MWNTs for 15, 30, 45, 60, 120 and 360 min. The expression of cytokines was measured using real time qPCR and the data normalized to 18S rRNA gene expression as a control. Relative expression (RQ) was calculated by using the comparative Ct method with cells incubated with PBS for 30 mins as the calibrator. The RQ value was calculated using the formula: RQ $=2^{-\Delta\Delta Ct}$. Assays were conducted in triplicate. Error bars represent $\pm$ standard error of the mean.

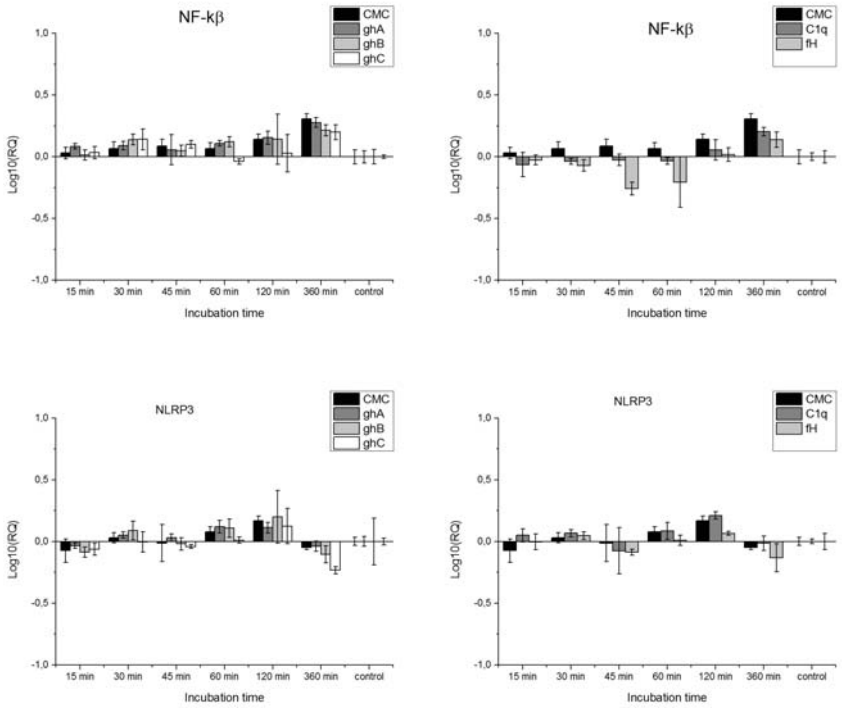
NF-kβ
CMC
ghA
ghB
ghC
Log10(RQ)
1,0
0,5
0,0
-0,5
-1,0
15 min
30 min
45 min
60 min
120 min
360 min
control
Incubation time
NF-kβ
CMC
C1q
fH
Log10(RQ)
Incubation time
NLRP3
CMC
ghA
ghB
ghC
Log10(RQ)
Incubation time
NLRP3
CMC
C1q
fH
Log10(RQ)
Incubation time

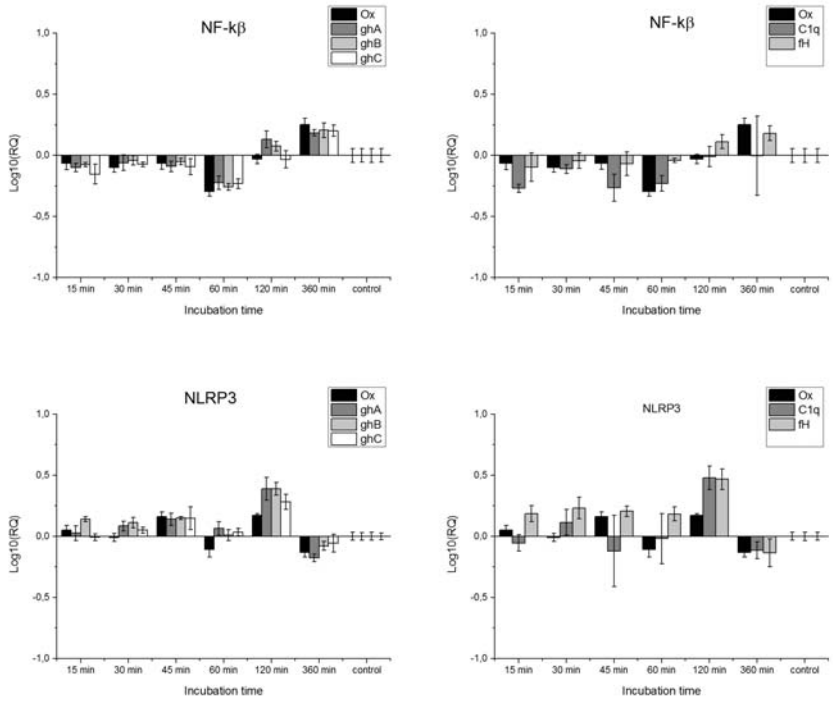

Figure 6.10: Expression of NF-κB and NLRP3 by U937 cells in vitro during incubation with Ox-MWNTs and CMC-MWNTs coated with C1q or Factor H. Cells were incubated with coated Ox-MWNTs or CMC-MWNTs for 15, 30, 45, 60, 120 and 360 min. The expression was measured using real time qPCR and the data normalized to 18S rRNA gene expression as a control. Relative expression (RQ) was calculated by using the comparative Ct method with cells incubated with PBS for 30 mins as the calibrator. The RQ value was calculated using the formula: RQ =$2^{-\Delta\Delta Ct}$. Assays were conducted in triplicate. Error bars represent $\pm$ standard error of the mean.

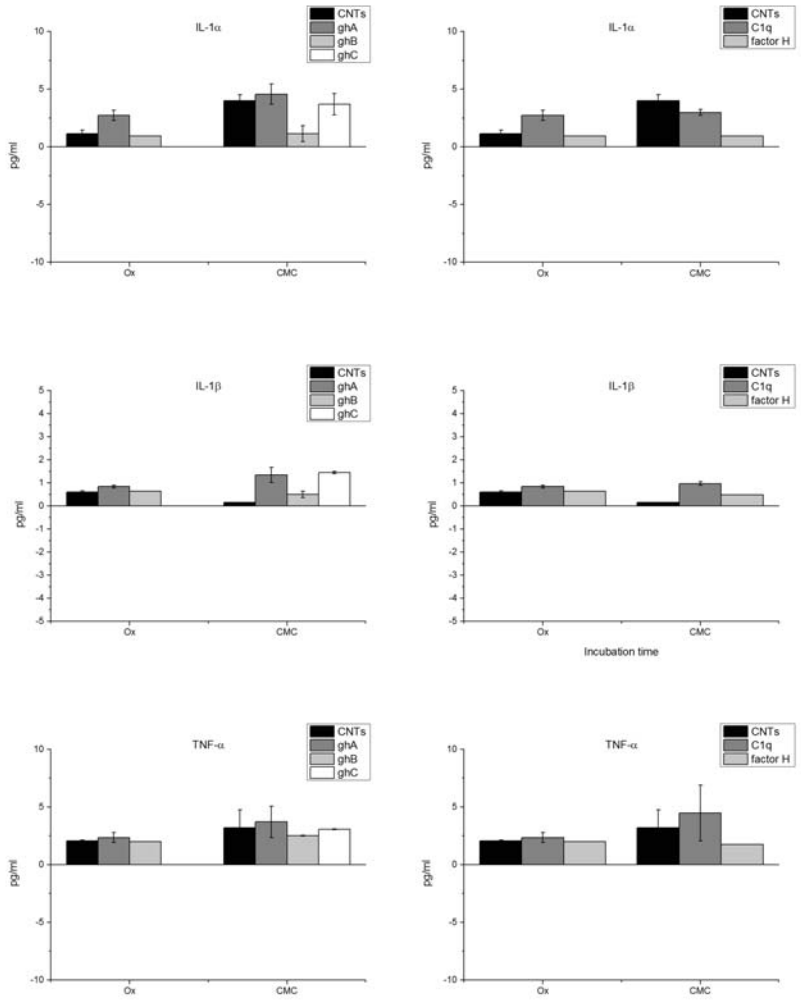
IL-1α
CNTs
ghA
ghB
ghC
pg/ml
Ox
CMC
IL-1α
CNTs
C1q
factor H
pg/ml
Ox
CMC
IL-1β
CNTs
ghA
ghB
ghC
pg/ml
Ox
CMC
IL-1β
CNTs
C1q
factor H
pg/ml
Ox
CMC
Incubation time
TNF-α
CNTs
ghA
ghB
ghC
pg/ml
Ox
CMC
TNF-α
CNTs
C1q
factor H
pg/ml
Ox
CMC

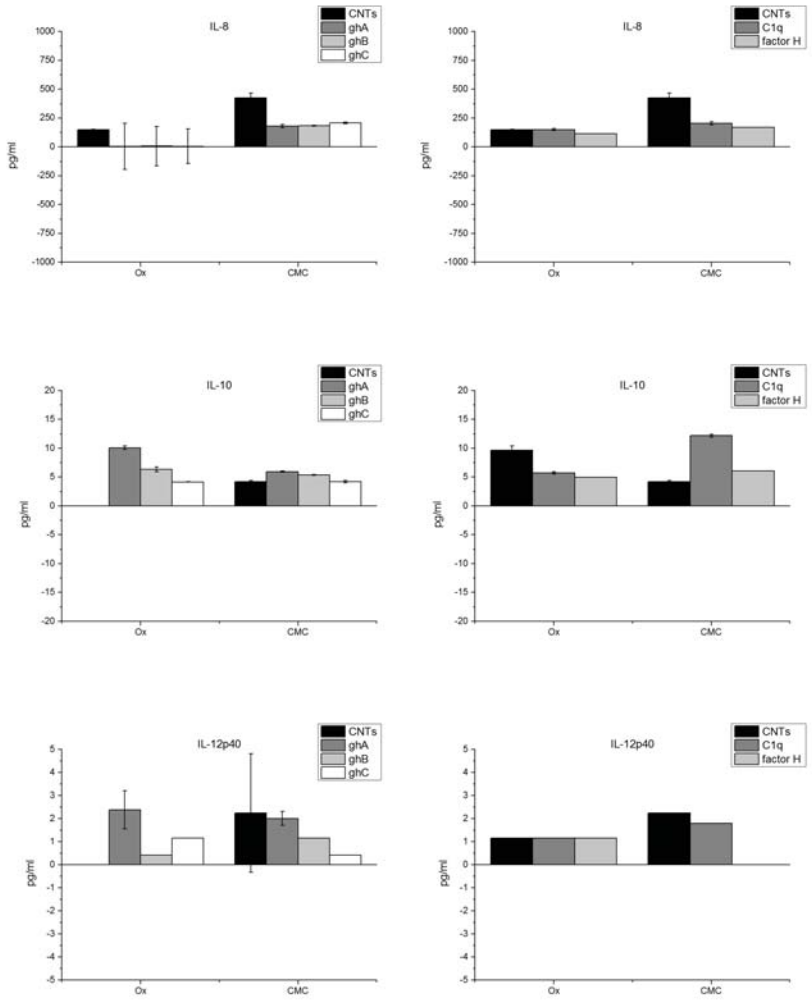
IL-8
CNTs
ghA
ghB
ghC
pg/ml
1000
750
500
250
0
-250
-500
-750
-1000
Ox
CMC
IL-8
CNTs
C1q
factor H
pg/ml
Ox
CMC
IL-10
CNTs
ghA
ghB
ghC
pg/ml
20
15
10
5
0
-5
-10
-15
-20
Ox
CMC
IL-10
CNTs
C1q
factor H
pg/ml
Ox
CMC
IL-12p40
CNTs
ghA
ghB
ghC
pg/ml
5
4
3
2
1
0
-1
-2
-3
-4
-5
Ox
CMC
IL-12p40
CNTs
C1q
factor H
pg/ml
Ox
CMC

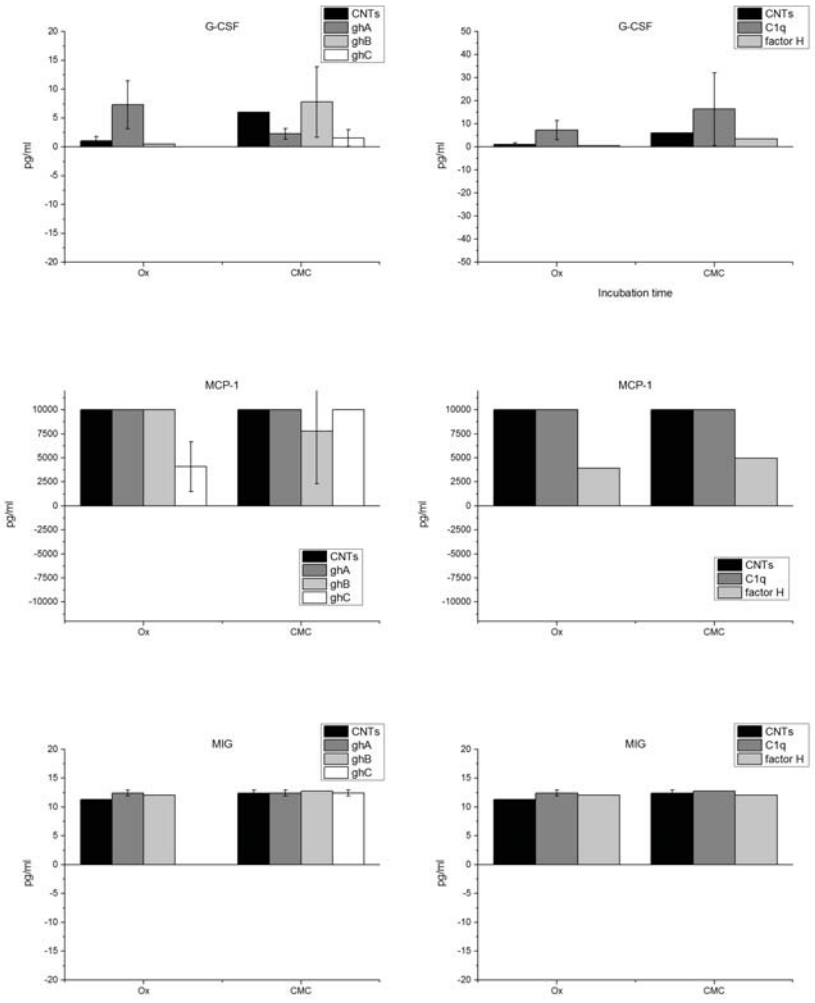
G-CSF
CNTs
ghA
ghB
ghC
pg/ml
Ox
CMC
G-CSF
CNTs
C1q
factor H
pg/ml
Ox
CMC
Incubation time
MCP-1
CNTs
ghA
ghB
ghC
pg/ml
Ox
CMC
MCP-1
CNTs
C1q
factor H
pg/ml
Ox
CMC
MIG
CNTs
ghA
ghB
ghC
pg/ml
Ox
CMC
MIG
CNTs
C1q
factor H
pg/ml
Ox
CMC

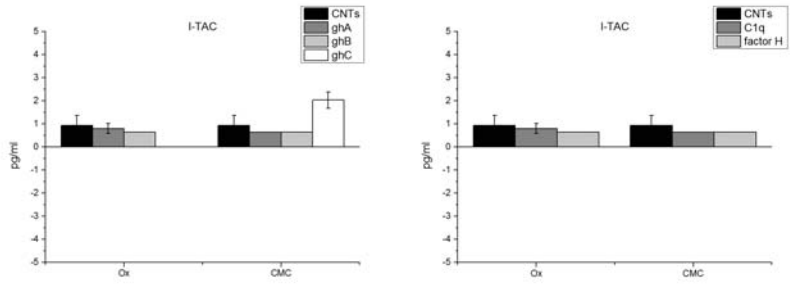

Figure 6.11: Multiplex cytokine array analysis of supernatants of U937 cells treated with Ox-MWNT and CMC-CNT for 24 h. Cytokines, chemokines and growth factors (IL-6, IL-8, IL-10, IL12p40, IL12p70, IL-23, IL-27, IL-1α and IL-1β, MIG, I-TAC, MCP-1, G-CSF and M-CSF) concentrations were measured by using a commercially available MagPix Milliplex kit (EMD Millipore).

6.4 Discussion

Due to a variety of advantages associated with CNTs that are determined by their structural and functional attributes, CNTs have wide ranging applications including translational medicine [2, 35–42]. There are a number of therapeutic strategies involving the applications of CNTs in vaccination, drug delivery, antibody-mediated tissue targeting, and enhancement of immunity [2, 35, 36, 38, 40, 41, 43, 44], which are dependent on systemic administration of the CNTs. This invariably leads to CNTs coming in contact with blood, and hence serum and complement. Complement system is the most important humoral factor in the blood that is involved in the clearance of pathogens, debris and synthetic particles [15, 22]. Any surface that offers a molecular pattern as a signature of non-self and altered self is amenable to complement recognition and activation. Thus, CNTs have been shown to activate complement, predominantly via the classical pathway and to a lesser extent by alternative and lectin pathways [10, 12, 22, 26]. We have recently shown that complement deposition on pristine as well as derivatised CNTs enhance their clarance via phagocytic cells in addition to the down-regulation of pro-inflammatory cytokines [26]. The enhancement of complement deposition mediated uptake was pronounced in complement receptor bearing antigen capturing and presenting cells such as macrophages and B cells, but not in T cells. We also found that the dampening of the pro-inflammatory cytokine production by complement-opsonised CNTs was being mediated by upregulation of IL-10, an anti-inflammatory cytokine [27]. What was curious that gold-nickel nanowires [27, 45], which were poor complement activators, were potent inducers of pro-inflammatory cytokines following serum treatment,

suggesting that a lack of complement deposition by nanoparticles may lead to recruitment of other serum proteins that can have pro-inflammatory consequences [27]. The ability of a number of CNTs, pristine and functionally derivatised, to activate complement via the classical pathway brought the focus of this study on the nature of the interaction between C1q, the first recognition subcomponent of the classical complement pathway [46], and CNTs. Earlier, we reported the binding of human native C1q, the recognition subcomponent of the classical pathway, as well as its individual globular head regions onto CMC-MWNTs [26]. All three recombinant forms of the globular head regions derived from human C1q A, B and C chains were able to bind onto the surface indicating the binding of C1q onto CNTs is through charge pattern recognition through the head region of C1q, enabling binding of C1r and C1s and further complement activation. In addition, we showed coating the globular heads lead to very effective inhibition of complement activation [26]. Here, we have also expressed and purified single residue substitute mutations of ghA, ghB and ghC to enable us to identify which residues on the C-terminal globular regions are implicated in the CNT-C1q interaction. Additionally, we set out to analyse the effect of binding of intact native C1q and recombinant globular head modules, but also factor H (as down-regulator of the alternative pathway) onto CNTs on phagocytosis and cytokine expression. Salvador-Morales et al [47] showed previously that factor H reduces complement activation by CNTs through the alternative pathway. For a number of C1q ligands, factor H acts an inhibitor of C1q, and thus dampens or modifies the classical pathway [17, 34]. In addition to being the recognition subcomponent of the classical pathway, C1q is a versatile and potent pattern recognition innate immune molecule. C1q recognises an array of self, non-self and altered-self ligands. The broad-spectrum ligand-binding potential of C1q is facilitated by the modular organisation of the heterotrimeric globular head region, its ability to change its conformation in a very subtle way, and the manner in which this ancient molecule appears to have evolved to deal with the different types of ligands. Its versatility of being able to bind a number of self and non-self ligands and modulate various biological and cellular responses is conferred due to the modular organisation of the individual globular heads (A, B and C) [48], where each module can have independence of structure and function [33]. The individual globular heads of C1q, ghA, ghB and ghC are known to be functionally independent modules which bind ligands specifically and preferentially [33, 46, 48]. These variations in binding are attributed to differences in electrostatic surface potentials of the different modules [49]. In the present study not only recombinant forms of ghA, ghB and ghC were used, but also a mutational analyses was performed by a large number of single-residue mutants of ghA, ghB and ghC (ArgA162Ala/Glu, ArgB114Gln/Glu, HisB117Asp, ArgB129Ala/Glu, LysB136Glu, ArgB163Ala/Glu, TyrB175Leu, HisC101Ala, ArgC156Glu, and LysC170Glu). These mutants were designed based on structure-function studies and ConSurf [50]. where

most variable residues were considered most likely to be central to C1q-ligand interaction. From this analysis, we found that the Arg162 residue in ghA is important in binding of this globular head. For ghB residues 136 and 129 were identified as essential in interaction. Previously the Arg114 and Arg129 of the B chain were identified as essential in the C1q-IgG interaction [31], but in this analysis a mutation at the 114th residue did not give altered interactions. Interestingly, an increase of binding was found for substitution of the Arg in the 156 residue of ghC for Glu. These results appear to suggest involvement of side chains and hydrophobic patches within the C1q globular heads in their interaction with CNTs. Binding of macromolecules on CNTs is not fully explored, which may involve charge transfer, hydrophobic interaction, etc. [51, 52]. Thus, molecular patterns offered by CNTs are likely to act as a nucleation centre for an ordered binding of C1q and factor H. The multivalency of interaction with CNTs was evident from the ability of a few recombinant globular head modules to aggregate CNTs in solution. These molecular patterns may impact upon the level of C1q binding to CNTs, their clearance by phagocytic cells, and cellular toxicity. Several studies reported that oxidized CNTs are less toxic than pristine CNTs [53–57], although there is also some evidence for the opposite effect [58, 59]. These effects, and the disagreements can be attributed to possible reduction of impurities (catalyst) in the samples, a decrease in length of the nanotubes, an increase of functional groups and higher dispersability leading to higher bioavailability [60, 61]. Biopersistence was identified as an important parameter in nanoparticle in-vivo toxicity. In contrast to pristine CNTs, highly carboxylated CNTs were shown to be rapidly (within 3 h) cleared out from the systematic circulation through the renal excretion route [53]. Recently, there have been some reports on enzymatic degradation of CNTs, for example with horseradish peroxidase [57, 62] and myeloperoxidase (which is expressed in neutrophils) [63], oxidation of the CNTs reduces the time necessary for degradation significantly [57, 64]. The dissection of C1q interaction with CNTs is insightful given that C1q is capable of binding charge clusters, polar regions, or small hydrophobic patches [48]. Since CNTs, pristine or derivatised, offer repetitive patterns of polarity and hydrophobicity, C1q is best suited to bind them, activate the classical pathway, and also enhance their phagocytic uptake directly, even without complement deposition. Here, we report that opsonising CNTs with recombinant globular heads can inhibit the classical pathway activation, enhance uptake of CNTs by phagocytic cells, and at the same time down-regulate pro-inflammatory cytokine storm. Thus, dissecting C1q-CNT interaction is likely to be a great facilitator in designing and characterising CNTs for in vivo applications. This becomes more pertinent in view of planned trials using CNTs coated with therapeutic antibodies [41, 44, 65–67] which are likely to offer an array of closely spaced Fc regions for C1q to bind.

References

[1] S. Alidori, B. M. Zeglis, D. A. Scheinberg, J. S. Lewis, and M. R. McDevitt, "Carbon nanotubes constructs as drug delivery systems for tumor targeting and imaging," *Journal of Labelled Compounds & Radiopharmaceuticals*, vol. 54, pp. S61–S61, 2011.

[2] C. Biale, V. Mussi, U. Valbusa, S. Visentin, G. Viscardi, N. Barbero, N. Pedemonte, and L. Galietta, "Carbon nanotubes for targeted drug delivery," *2009 9th Ieee Conference on Nanotechnology*, pp. 644–646, 2009.

[3] A. M. A. Elhissi, W. Ahmed, I. U. Hassan, V. R. Dhanak, and A. D'Emanuele, "Carbon nanotubes in cancer therapy and drug delivery.," *Journal of drug delivery*, vol. 2012, p. 837327, Jan. 2012.

[4] R. Klingeler, S. Hampel, and B. Buchner, "Carbon nanotube based biomedical agents for heating, temperature sensoring and drug delivery," *International journal of hyperthermia*, vol. 24, no. 6, pp. 496–505., 2008.

[5] L.-H. Liu, H. Dietsch, P. Schurtenberger, and M. Yan, "Photoinitiated coupling of unmodified monosaccharides to iron oxide nanoparticles for sensing proteins and bacteria.," *Bioconjugate chemistry*, vol. 20, pp. 1349–55, July 2009.

[6] S. Hussain, J. A. J. Vanoirbeek, and P. H. M. Hoet, "Interactions of nanomaterials with the immune system," *Wiley Interdisciplinary Reviews-Nanomedicine and Nanobiotechnology*, vol. 4, no. 2, pp. 169–183, 2012.

[7] B. S. Zolnik, A. Gonzalez-Fernandez, N. Sadrieh, and M. A. Dobrovolskaia, "Minireview: Nanoparticles and the Immune System," *Endocrinology*, vol. 151, no. 2, pp. 458–465, 2010.

[8] A. J. Andersen, P. P. Wibroe, and S. M. Moghimi, "Perspectives on carbon nanotube-mediated adverse immune effects," *Advanced Drug Delivery Reviews*, vol. 64, no. 15, pp. 1700–1705, 2012.

[9] H. Dumortier, "When carbon nanotubes encounter the immune system: Desirable and undesirable effects," *Advanced Drug Delivery Reviews*, vol. 65, no. 15, pp. 2120–2126, 2013.

[10] M. Rybak-Smith, K. Pondman, E. Flahaut, C. Salvador-Morales, R. Sim, and ., "Recognition of Carbon Nanotubes by the Human Innate Immune System.," in *Carbon Nanotubes for Biomedical Applications* (R. Klingeler and R. B. Sim, eds.), pp. 183–210, Springer, 2011.

[11] Y. Li, X. Zhang, J. Luo, W. Huang, J. Cheng, Z. Luo, T. Li, F. Liu, G. Xu, X. Ke, L. Li, and H. J. Geise, "Purification of CVD synthesized single-wall carbon nanotubes by different acid oxidation treatments," *Nanotechnology*, vol. 15, pp. 1645–1649, 2004.

[12] C. Salvador-Morales, E. Flahaut, E. Sim, J. Sloan, M. L. Green, and R. B. Sim, "Complement activation and protein adsorption by carbon nanotubes," *Molecular Immunology*, vol. 43, no. 3, pp. 193–201, 2006.

[13] C. Salvador-Morales, M. L. H. Green, and R. B. Sim, "Interaction between carbon nanotubes and biomolecules.," in *Chemistry of carbon nanotubes* (E. V. Basiuk and V. A. Basiuk, eds.), ch. 27, American Scientific Publishers, 2007.

[14] C. Salvador-Morales, E. V. Basiuk, V. A. Basiuk, M. L. H. Green, and R. B. Sim, "Effects of covalent functionalization on the biocompatibility characteristics of multi-walled carbon nanotubes," *Journal of Nanoscience and Nanotechnology*, vol. 8, no. 5, pp. 2347–2356, 2008.

[15] M. V. Carroll and R. B. Sim, "Complement in health and disease," *Advanced Drug Delivery Reviews*, vol. 63, no. 12, pp. 965–975, 2011.

[16] W. Xu, S. P. Berger, L. A. Trouw, H. C. de Boer, N. Schlagwein, C. Mutsaers, M. R. Daha, and C. van Kooten, "Properdin binds to late apoptotic and necrotic cells independently of C3b and regulates alternative pathway complement activation.," *Journal of immunology*, vol. 180, pp. 7613–21, June 2008.

[17] U. Kishore and R. B. Sim, "Factor H as a regulator of the classical pathway activation.," *Immunobiology*, vol. 217, pp. 162–8, Feb. 2012.

[18] L. Kouser, M. Abdul-Aziz, A. Nayak, C. M. Stover, R. B. Sim, and U. Kishore, "Properdin and factor H: opposing players on the alternative complement pathway "see-saw"," *Frontiers in immunology*, vol. 4, p. 93, Jan. 2013.

[19] I. Hamad, A. C. Hunter, K. J. Rutt, Z. Liu, H. Dai, and S. M. Moghimi, "Complement activation by PEGylated single-walled carbon nanotubes is independent of C1q and alternative pathway turnover," *Molecular Immunology*, vol. 45, no. 14, pp. 3797–3803, 2008.

[20] W. L. Ling, A. Biro, I. Bally, P. Tacnet, A. Deniaud, E. Doris, P. Frachet, G. Schoehn, E. Pebay-Peyroula, and G. J. Arlaud, "Proteins of the Innate Immune System Crystallize on Carbon Nanotubes but Are Not Activated," *ACS Nano*, vol. 5, no. 2, pp. 730–737, 2011.

[21] S. M. Moghimi, a. J. Andersen, S. H. Hashemi, B. Lettiero, D. Ahmadvand, a. C. Hunter, T. L. Andresen, I. Hamad, and J. Szebeni, "Complement activation cascade triggered by PEG-PL engineered nanomedicines and carbon nanotubes: the challenges ahead.," *Journal of controlled release*, vol. 146, pp. 175–81, Sept. 2010.

[22] M. J. Rybak-Smith and R. B. Sim, "Complement activation by carbon nanotubes," *Advanced Drug Delivery Reviews*, vol. 63, no. 12, pp. 1031–1041, 2011.

[23] M. J. Rybak-Smith, C. Tripisciano, E. Borowiak-Palen, C. Lamprecht, and R. B. Sim, "Effect of Functionalization of Carbon Nanotubes with Psychosine on Complement Activation and Protein Adsorption," *Journal of Biomedical Nanotechnology*, vol. 7, pp. 830–839, Dec. 2011.

[24] A. J. Andersen, J. T. Robinson, H. J. Dai, A. C. Hunter, T. L. Andresen, and S. M. Moghimi, "Single-Walled Carbon Nanotube Surface Control of Complement Recognition and Activation," *ACS Nano*, vol. 7, no. 2, pp. 1108–1119, 2013.

[25] A. J. Andersen, B. Windschiegl, S. Ilbasmis-Tamer, I. T. Degim, A. C. Hunter, T. L. Andresen, and S. M. Moghimi, "Complement activation by PEG-functionalized multi-walled carbon nanotubes is independent of PEG molecular mass and surface density.," *Nanomedicine : nanotechnology, biology, and medicine*, vol. 9, pp. 469–73, May 2013.

[26] K. M. Pondman, M. Sobik, A. Nayak, A. G. Tsolaki, A. Jäkel, E. Flahaut, S. Hampel, B. Ten Haken, R. B. Sim, and U. Kishore, "Complement activation by carbon nanotubes and its influence on the phagocytosis and cytokine response by macrophages.," *Nanomedicine : nanotechnology, biology, and medicine*, vol. 10, pp. 1287–1299, Mar. 2014.

[27] K. Pondman, A. Tsolaki, A. Switzer, M. Shamji, B. ten Haken, R. Sim, and U. Kishore, "Complement deposition on nanoparticles can modulate immune responses by macrophage, B and T cells.," *Journal of Biomedical nanotechnology*, vol. Submitted, 2014.

[28] A. Nayak, E. Dodagatta-Marri, A. G. Tsolaki, and U. Kishore, "An Insight into the Diverse Roles of Surfactant Proteins, SP-A and SP-D in Innate and Adaptive Immunity.," *Frontiers in immunology*, vol. 3, p. 131, Jan. 2012.

[29] R. Verdejo, S. Lamoriniere, B. Cottam, A. Bismarck, and M. Shaffer, "Removal of oxidation debris from multi-walled carbon nanotubes," *Chemical Communications*, no. 5, pp. 513–515, 2007.

[30] L. A. Tan, B. Yu, F. C. J. Sim, U. Kishore, and R. B. Sim, "Complement activation by phospholipids: the interplay of factor H and C1q.," *Protein & cell*, vol. 1, pp. 1033–49, Nov. 2010.

[31] M. S. Kojouharova, M. G. Gadjeva, I. G. Tsacheva, A. Zlatarova, L. T. Roumenina, M. I. Tchorbadjieva, B. P. Atanasov, P. Waters, B. C. Urban, R. B. Sim, K. B. M. Reid, and U. Kishore, "Mutational analyses of the recombinant globular regions of human C1q A, B, and C chains suggest an essential role for arginine and histidine residues in the C1q-IgG interaction.," *Journal of immunology*, vol. 172, pp. 4351–8, Apr. 2004.

[32] M. G. Gadjeva, M. M. Rouseva, A. S. Zlatarova, K. B. M. Reid, U. Kishore, and M. S. Kojouharova, "Interaction of human C1q with IgG and IgM: revisited," *Biochemistry*, vol. 47, pp. 13093–13102, 2008.

[33] U. Kishore, S. K. Gupta, M. V. Perdikoulis, M. S. Kojouharova, B. C. Urban, and K. B. M. Reid, "Modular organization of the carboxyl-terminal, globular head region of human C1q A, B, and C chains.," *Journal of immunology*, vol. 171, pp. 812–20, July 2003.

[34] Y.-H. Kang, B. C. Urban, R. B. Sim, and U. Kishore, "Human complement Factor H modulates C1q-mediated phagocytosis of apoptotic cells.," *Immunobiology*, vol. 217, pp. 455–64, Apr. 2012.

[35] A. Bianco, K. Kostarelos, and M. Prato, "Applications of carbon nanotubes in drug delivery," *Current Opinion in Chemical Biology*, vol. 9, pp. 674–679, Dec. 2005.

[36] W. Wu, S. Wieckowski, G. Pastorin, M. Benincasa, C. Klumpp, J. P. Briand, R. Gennaro, M. Prato, and A. Bianco, "Targeted delivery of amphotericin B to cells by using functionalized carbon nanotubes," *Angewandte Chemie-International Edition*, vol. 44, no. 39, pp. 6358–6362, 2005.

[37] N. Aoki, T. Akasaka, F. Watari, and A. Yokoyama, "Carbon nanotubes as scaffolds for cell culture and effect on cellular functions," *Dental Materials Journal*, vol. 26, no. 2, pp. 178–185, 2007.

[38] J. G. Li, W. X. Li, J. Y. Xu, X. Q. Cai, R. L. Liu, Y. J. Li, Q. F. Zhao, and Q. N. Li, "Comparative study of pathological lesions induced by multiwalled carbon nanotubes in lungs of mice by intratracheal instillation and inhalation," *Environmental Toxicology*, vol. 22, no. 4, pp. 415–421, 2007.

[39] X. F. Shi, B. Sitharaman, Q. P. Pham, F. Liang, K. Wu, W. E. Billups, L. J. Wilson, and A. G. Mikos, "Fabrication of porous ultra-short single-walled carbon nanotube nanocomposite scaffolds for bone tissue engineering," *Biomaterials*, vol. 28, no. 28, pp. 4078–4090, 2007.

[40] H. Ali-Boucetta, K. T. Al-Jamal, D. McCarthy, M. Prato, A. Bianco, and K. Kostarelos, "Multiwalled carbon nanotube-doxorubicin supramolecular complexes for cancer therapeutics.," *Chemical communications*, pp. 459–61, Jan. 2008.

[41] E. Heister, V. Neves, C. Tîlmaciu, K. Lipert, V. S. Beltrán, H. M. Coley, S. R. P. Silva, and J. McFadden, "Triple functionalisation of single-walled carbon nanotubes with doxorubicin, a monoclonal antibody, and a fluorescent marker for targeted cancer therapy," *Carbon*, vol. 47, no. 9, pp. 2152–2160, 2009.

[42] A. Yang, W. Liu, Z. Li, L. Jiang, H. Xu, and X. Yang, "Influence of polyethyleneglycol modification on phagocytic uptake of polymeric nanoparticles mediated by immunoglobulin G and complement activation," *Journal of Nanoscience and Nanotechnology*, vol. 10, no. 1, pp. 622–628, 2010.

[43] D. Pantarotto, C. D. Partidos, J. Hoebeke, F. Brown, E. Kramer, J.-P. Briand, S. Muller, M. Prato, and A. Bianco, "Immunization with peptide-functionalized carbon nanotubes enhances virus-specific neutralizing antibody responses.," *Chemistry & biology*, vol. 10, pp. 961–6, Oct. 2003.

[44] Y. Xiao, X. Gao, O. Taratula, S. Treado, A. Urbas, R. D. Holbrook, R. E. Cavicchi, C. T. Avedisian, S. Mitra, R. Savla, P. D. Wagner, S. Srivastava, and H. He, "Anti-HER2 IgY antibody-functionalized single-walled carbon nanotubes for detection and selective destruction of breast cancer cells.," *BMC cancer*, vol. 9, p. 351, Jan. 2009.

[45] K. M. Pondman, A. W. Maijenburg, F. B. Celikkol, A. A. Pathan, U. Kishore, B. ten Haken, and J. E. ten Elshof, "Au coated Ni nanowires with tuneable dimensions for biomedical applications.," *Journal of Materials Chemistry B*, vol. 1, pp. 6129–6136, 2013.

[46] U. Kishore and K. B. Reid, "Modular organization of proteins containing C1q-like globular domain," *Immunopharmacology*, vol. 42, no. 1-3, pp. 15–21, 1999.

[47] C. Salvador-Morales, E. V. Basiuk, V. A. Basiuk, M. L. H. Green, and R. B. Sim, "Effects of covalent functionalisation on the biocompatibiltiy characteristics of multi-walled carbon nanotubes," *Journal of Nanoscience and Nanotechnology*, vol. 8, no. 5, pp. 2347–2356, 2007.

[48] U. Kishore, R. Ghai, T. J. Greenhough, A. K. Shrive, D. M. Bonifati, M. G. Gadjeva, P. Waters, M. S. Kojouharova, T. Chakraborty, and A. Agrawal, "Structural and functional anatomy of the globular domain of complement protein C1q.," *Immunology letters*, vol. 95, pp. 113–28, Sept. 2004.

[49] C. Gaboriaud, J. Juanhuix, A. Gruez, M. Lacroix, C. Darnault, D. Pignol, D. Verger, J. C. Fontecilla-Camps, and G. J. Arlaud, "The crystal structure of the globular head of complement protein C1q provides a basis for its versatile recognition properties.," *The Journal of biological chemistry*, vol. 278, pp. 46974–82, Nov. 2003.

[50] R. Ghai, P. Waters, L. T. Roumenina, M. Gadjeva, M. S. Kojouharova, K. B. M. Reid, R. B. Sim, and U. Kishore, "C1q and its growing family," *Immunobiology*, vol. 212, no. 4-5, pp. 253–266, 2007.

[51] F. Balavoine, P. Schultz, C. Richard, V. Mallouh, T. W. Ebbesen, and C. Mioskowski, "Helical Crystallization of Proteins on Carbon Nanotubes: A First Step towards the Development of New Biosensors," *Angewandte Chemie International Edition*, vol. 38, pp. 1912–1915, July 1999.

[52] B. Pan and B. Xing, "Adsorption Mechanisms of Organic Chemicals on Carbon Nanotubes," *Environmental Science & Technology*, vol. 42, pp. 9005–9013, Dec. 2008.

[53] S. Jain, V. S. Thakare, M. Das, C. Godugu, A. K. Jain, R. Mathur, K. Chuttani, and A. K. Mishra, "Toxicity of multiwalled carbon nanotubes with end defects critically depends on their functionalization density," *Chemical Research in Toxicology*, vol. 24, pp. 2028–2039, 2011.

[54] K. Pulskamp, S. Diabaté, and H. F. Krug, "Carbon nanotubes show no sign of acute toxicity but induce intracellular reactive oxygen species in dependence on contaminants.," *Toxicology letters*, vol. 168, pp. 58–74, Jan. 2007.

[55] Z. Ji, D. Zhang, L. Li, X. Shen, X. Deng, L. Dong, M. Wu, and Y. Liu, "The hepatotoxicity of multi-walled carbon nanotubes in mice.," *Nanotechnology*, vol. 20, p. 445101, 2009.

[56] S. Boncel, K. H. Muller, J. N. Skepper, K. Z. Walczak, and K. K. Koziol, "Tunable chemistry and morphology of multi-wall carbon nanotubes as a route to non-toxic, theranostic systems," *Biomaterials*, vol. 32, no. 30, pp. 7677–7686, 2011.

[57] Y. Zhao, B. L. Allen, and A. Star, "Enzymatic degradation of multiwalled carbon nanotubes," *Journal of Physical Chemistry A*, vol. 115, no. 34, pp. 9536–9544, 2011.

[58] J. Muller, I. Decordier, P. H. Hoet, N. Lombaert, L. Thomassen, F. Huaux, D. Lison, and M. Kirsch-Volders, "Clastogenic and aneugenic effects of multi-wall carbon nanotubes in epithelial cells," *Carcinogenesis*, vol. 29, no. 2, pp. 427–433, 2008.

[59] R. P. Singh, M. Das, V. Thakare, and S. Jain, "Functionalization density dependent toxicity of oxidized multiwalled carbon nanotubes in a murine macrophage cell line.," *Chemical research in toxicology*, vol. 25, pp. 2127–37, Oct. 2012.

[60] P. Wick, P. Manser, L. K. Limbach, U. Dettlaff-Weglikowska, F. Krumeich, S. Roth, W. J. Stark, and A. Bruinink, "The degree and kind of agglomeration affect carbon nanotube cytotoxicity," *Toxicology Letters*, vol. 168, no. 2, pp. 121–131, 2007.

[61] E. Heister, C. Lamprecht, V. Neves, and C. Tîlmaciu, "Higher dispersion efficacy of functionalized carbon nanotubes in chemical and biological environments," *ACS Nano*, vol. 4, no. 5, pp. 2615–2626, 2010.

[62] X. Liu, R. H. Hurt, and A. B. Kane, "Biodurability of Single-Walled Carbon Nanotubes Depends on Surface Functionalization," *Carbon*, vol. 48, no. 7, pp. 1961–1969, 2010.

[63] V. E. Kagan, N. V. Konduru, W. Feng, B. L. Allen, J. Conroy, Y. Volkov, I. I. Vlasova, N. a. Belikova, N. Yanamala, A. Kapralov, Y. Y. Tyurina, J. Shi, E. R. Kisin, A. R. Murray, J. Franks, D. Stolz, P. Gou, J. Klein-Seetharaman, B. Fadeel, A. Star, A. a. Shvedova, and Vlasova II, "Carbon nanotubes degraded by neutrophil myeloperoxidase induce less pulmonary inflammation.," *Nature nanotechnology*, vol. 5, pp. 354–9, May 2010.

[64] J. Russier, C. Ménard-Moyon, E. Venturelli, E. Gravel, G. Marcolongo, M. Meneghetti, E. Doris, and A. Bianco, "Oxidative biodegradation of single- and multi-walled carbon nanotubes.," *Nanoscale*, vol. 3, pp. 893–6, Mar. 2011.

[65] M. R. McDevitt, D. Chattopadhyay, B. J. Kappel, J. S. Jaggi, S. R. Schiffman, C. Antczak, J. T. Njardarson, R. Brentjens, and D. A. Scheinberg, "Tumor targeting with antibody-functionalized, radiolabeled carbon nanotubes.," *Journal of nuclear medicine : official publication, Society of Nuclear Medicine*, vol. 48, pp. 1180–9, July 2007.

[66] M. M. Cardoso, I. N. Peca, and A. C. A. Roque, "Antibody-Conjugated Nanoparticles for Therapeutic Applications," *Current Medicinal Chemistry*, vol. 19, pp. 3103–3127, May 2012.

[67] I. H. Lee, J. M. Lee, and Y. Jung, "Controlled protein embedment onto Au/Ag core-shell nanoparticles for immuno-labeling of nanosilver surface.," *ACS applied materials & interfaces*, vol. 6, pp. 7659–64, May 2014.

Chapter 7

Magnetic drug delivery with FePd nanowires [1]

Abstract

Magnetic drug delivery is a promising method to target a drug to a diseased area while reducing negative side effects caused by systemic administration of drugs. In magnetic drug delivery a therapeutic agent is coupled to a magnetic nanoparticle. The particles are injected and at the target location withdrawn from blood flow by a magnetic field. In this study a FePd nanowire is developed with optimised properties for magnetic targeting. The nanowires have a high magnetic moment to reduce the field gradient needed to capture them with a magnet. The dimensions and the materials of the nanowire and coating are such that they are dispersable in aqueous media, non cytotoxic, easily phagocytosed and not complement activating. This is established in several in-vitro tests with macrophage and endothelial cell lines.

Along with the nanowires a magnet is designed, optimised for capture of the nanowires from the blood flow in the hind leg of a rat. The system is used in a pilot scale in-vivo experiment. No negative side effects from injection of the nanowires were found within the limited time span of the experiment. The nanowires could not be detected in the liver, spleen and kidneys of the rats indicating that the immune system is not actively trying to remove the particles from circulation. In this first pilot experiment no nanowires were found to be targeted by the magnet, most likely the particles were removed during the fixation procedure.

[1] The contents of this chapter have been submitted as K.M. Pondman, N.D. Bunt, A.W. Maijenburg, R. van Wezel, U. Kishore, L. Abelmann, J.E. ten Elshof, B. ten Haken, Magnetic Drug Delivery with FePd nanowires, Journal of Magnetism and Magnetic Materials

7.1 Introduction

Amongst many receptor dependent drug targeting methods with nanoparticles, magnetic drug delivery is a promising physical method to target pharmaceuticals. In this method, a drug is coupled to a magnetic particle and injected into blood flow. A magnet located close to the target location is used to capture the magnetic particles and therapeutics in the target area. The method is promising in modeling studies and some results in animals and a single clinical test have been published, but no magnetic drug delivery applications are used in clinics today [1–9]. The majority of magnetic particles used in biomedical applications are so called SPIONs (superparamagnetic iron oxide nanoparticles), which consist of one or multiple magnetite or maghemite cores with a biocompatible coating and active ligands [10]. The small magnetic moment of these particles makes it challenging to retain particles at the target site while withstanding the drag of blood flow. To overcome the drag force the magnetic field and gradient have to be extremely large, or the particles have to agglomerate into bundles; often causing embolisation of the vessels. Nanowires, with their elongated shape and anisotropic physical and magnetic properties, can be used to overcome some of the limitations of SPIONs in in-vivo targeting applications. Magnetic nanorods and nanowires are therefore receiving growing attention in biomedicine [11–16]. While the small diameter of nanowires makes it possible for the particle to pass through the narrow capillaries, the remnant magnetization increases the range and effectiveness of magnetic interactions at a distance from external magnets. This allows magnetic drug targeting at locations deeper inside the body [12]. Whereas spherical particles only respond to magnetic flux gradients, high aspect ratio particles allow the application of torque with a relatively weak external field to perform dynamic targeted cell therapy [13]. Due to their increased surface to volume ratio, more drugs and additional targeting ligands (e.g. ligands aiding the endocytosis of the particles) can be bound.

In this study the potential of rod-like, magnetic nanoparticles for magnetic drug delivery is investigated. First the magnetic properties of elongated nanoparticles are determined, then a magnetic nanowire is developed with optimised characteristics for magnetic drug delivery. Besides the magnetic force on the particles, the effectiveness of nanoparticles as intravenous drug delivery platforms is strongly influenced by rapid elimination of the particles from the systemic circulation by the immune cells [17]. Therefore initial tests were performed to analyse the activation of the innate immune systems complement system by the developed particles. The innate immune system plays a key role in protection against pathogens and synthetic particles including nanoparticles [17–21]. When a particle is recognised by the innate immune complement system, it will be marked for uptake by phagocytic cells (opsonised) and unable to reach its target [22]. For magnetic drug delivery not only the particles but

also the external magnet has to be specially designed with optimised characteristics for the trapping of the particles. Here we designed a magnet able to capture the developed nanowires from capillary blood flow, and of which the dimensions, field and gradient can be scaled up for application in a clinical setting. Finally the magnet-nanowire system is applied in a pilot *in-vivo* magnetic drug delivery test.

7.2 Theory

7.2.1 Magnetic properties of nanoparticles

In superparamagnetic particles thermal fluctuations allow the magnetization of a magnetic particle to cross over the energy barrier between stable directions of magnetization. The time it takes to flip the magnetisation is given by the Neel-Arrhenius equation:

$$\tau^{-1} = f_0 e^{\frac{-E_B}{k_B T}} \tag{7.1}$$

With attempt frequency $f_0 = 10^{-9} - 10^{-10}$ s^{-1} and E_B the energy barrier. For single domain ellipsoids, in which the magnetisation reverses through coherent rotation, that are well dispersed in a carrier medium the energy barrier is determined by the shape E_S and crystalline anisotropy energy E_{ca}. The crystalline anisotropy originates exclusively from intrinsic material properties:

$$E_{ca} = K_{ca} V \tag{7.2}$$

For spherical particles the orientation of the particle in the field has no influence on the magnetization direction, therefore there is no shape anisotropy and crystalline anisotropy is the dominating anisotropy factor.

Elongated particles are more easily magnetized along the long axis. This shape anisotropy energy can be described with:

$$E_S = \frac{1}{2}\mu_0 (N_a M_a^2 + N_b M_b^2 + N_c M_c^2) V \tag{7.3}$$

For a prolate ellipsoid with axis $c > a = b$, with aspect ratio $k = c/a$, the demagnetization factors N_a, N_b and N_c are given by [23, 24]:

$$N_a = N_b = \frac{k}{2(k^2-1)} \left[k - \frac{k}{2\sqrt{k^2-1}} ln \left(\frac{k + \sqrt{k^2-1}}{k - \sqrt{k^2-1}} \right) \right] \tag{7.4}$$

$$N_c = 1 - 2N_a$$

The shape anisotropy difference between the two axes is described by anisotropy constant K_S:

$$K_S = \frac{1}{2}\mu_0(3N_a - 1)M_s^2 \tag{7.5}$$

In elongated particles, the crystal anisotropy is negligible compared to the shape anisotropy. The energy barrier that has to be overcome to flip the magnetization is:

$$E_B = KV \tag{7.6}$$

For spherical particles *K* will be the crystalline anisotropy constant (K_{ca}), for elongated particles the shape anisotropy constant (K_s). Within the time constant of magnetic drug delivery we consider particles superparamagnetic if they change their magnetisation direction within one second ($\tau \simeq$ 1 sec). The maximum volume at which the particle is superparamagnetic is:

$$V_{max} = \frac{25k_BT}{K_s} \tag{7.7}$$

At high aspect ratio $k > 10$, $Nc \simeq 0$:

$$V_{max} = \frac{25k_BT}{\frac{1}{4}\mu_0 M_s^2} \tag{7.8}$$

which, for magnetite will give a maximum nanowire volume of approximately $2 \cdot 10^{-24}$ m^3 (2000 nm^3). All particles with a volume larger than V_{max} as given by equation 7.7, are ferromagnetic particles. Note that this is an upper limit, derived under the condition that the particle reverses coherently. For very long nanowires this might not be the case.

The size of single domain ferromagnetic particles is limited by the magnetic self energy which to avoid formation of a multi domain state has to be lower than the domain wall energy given by:

$$E_{DW} = 2\pi\sqrt{AK} \cdot \pi ac \tag{7.9}$$

With A the exchange stiffness constant of the material, the critical diameter is around 40 nm for spherical magnetite particles and largest for elongated particles (1 μm).

7.2.2 Forces on magnetic particles in blood flow

In the vascular system, the blood flow exerts a force on the particles dragging them along with the flow. Magnetic targeting will take place in the capillary system, were blood flow can be modelled by a slow Newtonian non-pulsating flow. The targeting is analysed by the first order forces only, which are the magnetic force (F_m) and the viscous drag force (F_d). Due to the small size and mass of the nanoparticles all second order forces such as gravitational and buoyancy forces, and inertia are neglected.

Magnetic force

The magnetic force $\boldsymbol{F}_{\mathrm{m}}$ on a small particle due to an external magnetic flux $\boldsymbol{B}$, can be assumed to be equal to the force experienced by a point-like magnetic dipole [10, 25]. The magnetic force is defined by:

$$\boldsymbol{F}_m = \bigtriangledown(\boldsymbol{m}_p \cdot \boldsymbol{B}) = \bigtriangledown(\boldsymbol{m}_p \cdot \mu_f \boldsymbol{H}_a) \tag{7.10}$$

Where μ_f is the permeability of blood. The magnetic dipole moment of the particle, m_p, depends on the magnetization and the volume:

$$m_p = V_p M \tag{7.11}$$

For ferromagnetic particles M in this equation is equal to the saturation magnetization of the particle M_s. For superparamagnetic particles the magnetization depends on the local magnetic field intensity (H_{in}), the field inside the particle, which differs from the applied field (H_a) due to the demagnetization field (H_d) that opposes H_a: $\boldsymbol{H}_{in}$ = $\boldsymbol{H}_a$ - $\boldsymbol{H}_d$. $\boldsymbol{H}_d$ depends on M and the demagnetization factor (N) which in turn depends on the shape of the particle.

$$H_{\mathrm{d},z} = N_x M_x \tag{7.12}$$

Here N_x is the demagnetization factor along the z-direction. To minimize the Zeeman energy the particle will align with the magnetic field, therefore there is only one demagnetization factor for every particle, and the internal field strength and magnetization can be determined:

$$M = M_s \mathcal{L} \left(\frac{M \mu_0 \boldsymbol{H}_{in}}{k_B T} \right) \tag{7.13}$$

With M_s the saturation magnetization of the material and $\mathcal{L}$ the Langevin function.

Drag force

The fluidic drag force can be calculated by using Stokes law for drag on a sphere in a laminar flow field with Reynolds number smaller than 1, which is a valid approximation for the flow in the microvasculature:

$$\boldsymbol{F}_d = -6\eta r_p(\boldsymbol{v}_p - \boldsymbol{v}_f) \tag{7.14}$$

In this equation η represents the viscosity of the medium ($\eta_{plasma} = 1.2 \cdot 10^{-3}$ Pa s), v_p and v_f are the velocity of the nanoparticle and the medium respectively. For prolate ellipsoids equation 7.14 can be adapted for their specific shape anisotropy [26, 27]:

$$F_d = -\eta\pi a(v_p - v_f)K_d \tag{7.15}$$

With shape factor K_d:

$$K_d = \frac{4}{ln(2k) - \frac{1}{2}} \tag{7.16}$$

when the particle is moving in the direction of the long axis and

$$K_d = \frac{8}{ln(2k) + \frac{1}{2}} \tag{7.17}$$

when the particle is moving perpendicular to the direction of the long axis.

7.3 Methods and Materials

7.3.1 FePd nanowires

FePd nanowires were synthesized by a method adapted from [28–30] by templated electrodeposition in a conventional three-electrode setup. First, an Au layer was sputtered onto a PCTE membrane with a pore size of 50 nm using a Perkin-Elmer 2400 sputtering system under argon atmosphere. The Au layer, isolated with a glass plate, was used as working electrode in the electrochemical deposition process. A small Pt mesh was used as counter electrode and Ag/AgCl in 3 M KCl (Metrohm Autolab) as reference electrode. All reported potentials are with respect to the reference electrode. The electrodes were connected to a potentiostat (Autolab PGSTAT 128N from Metrohm Autolab, Netherlands). For electrodeposition of nanowires, the electrodes were placed inside a plating solution containing 0.1

M Iron(III)sulfate pentahydrate ($Fe_2(SO_4)_3 \cdot 5\,H_2O$) (Acros organics, 97%), 0.02 M tetraamminepalladium(II)chloride monohydrate ($Pd(NH_3)_4Cl_2 \cdot H_2O$) (97% Alfa Aeser), 0.3 M 5-sulfosalicyclic acid (99%, Alfa Aesar) and 0.3 M ammonium sulfate ($(NH_4)_2SO_4$) (99%, Sigma Aldrich) at pH 5.0. Nanowires were formed by pulsed electrodeposition, using 4 cycles of 50 sec at a voltage of -1.1 V followed by 150 sec at a voltage of +0.1V. After deposition, the membranes were dissolved in dichloromethane and free nanowires washed at least 3 times in dichloromethane and 3 times in milliQ water by centrifugation.

7.3.2 Biofunctionalisation

The functionalization of the FePd nanowires was accomplished by a method inspired by [31]. FePd nanowires at 100 µg/ml were sonicated in hexane with 10 µg/ml oleic acid (OA) for 30 min, excess OA was removed by centrifugal washing (2000 g) in hexane. From this point FePds were handled in sterile conditions and sterile solutions were used. Hydrophilic coating was achieved by adding 0.5 ml 10 mg/ml FePd-OA in hexane to 20 ml of 0.5 mg/ml Pluronic-F108 (PF) (Sigma Aldrich) in H_2O. By water bath sonication a dispersion was obtained, subsequently hexane was evaporated. PF was allowed to adhere overnight under steering. Excess Pluronic-F108 was removed by washing (2000 g) in three times in sterile H_2O. To label the FePd fluorescent Nile red (NR) (Sigma Aldrich) was dissolved at 1 mg/ml in DMSO and 100 µl was added to 10 ml of FePd-OA-PF at 1 mg/ml in H_2O. To allow partitioning of the NR into the OA layer surrounding the FePd the solution was steered overnight. FePd were washed five times in sterile H_2O followed by two washings in sterile PBS (Sigma Aldrich). Labelling was analysed by fluorescence microscopy.

7.3.3 Characterization

Analysis of the nanowires was performed with a Zeiss HR-LEO 1550 FEG Scanning Electron Microscope (SEM) operating at 2.0 kV. Transmission electron microscopy (TEM) was performed on a Philips CM300ST-FEG Transmission Electron Microscope. Magnetic characterization was done using a vibrating sample magnetometer (Model 10 Mark II VSM, Microsense). Samples were either measured in the synthesis membrane or dried in a glass container before measurement; a blank measurement of the empty substrate was subtracted from the sample data.

7.3.4 Complement activation and consumption assay for the classical pathway

FePd nanowire suspensions (100 µl of 1 mg/ml, 0.5 mg/ml, 0.25 mg/ml and 0.125 mg/ml) in PBS were added to 100 µl of 1:1 diluted human serum in $DGVB^{++}$. Zymosan (0.2 mg in 100 µl PBS; Sigma) served as a positive control. The samples were incubated for 1h at 37°C

with occasional shaking, followed by centrifugation to remove the nanowires (13000 g, 10 min).

To investigate whether FePd nanowires activate (consume) complement in human serum, the sera's capacity to lyse antibody-sensitised sheep erythrocytes (EA) was tested. EA were prepared [18] using sheep erythrocytes from (TCS Biosciences) and stored in dextrose gelatin veronal buffer ($DGVB^{++}$: 2.5 mM sodium barbital, 71 mM NaCl, 0.15 mM $CaCl_2$, 0.5 mM $MgCl_2$, 2.5% w/v glucose, 0.1% w/v gelatin, pH 7.4) at 10^9 cells/ml. The serum supernatants of each sample were two-fold serially diluted (1/10 to 1/5120 in $DGVB^{++}$) and placed in microtitre wells. 100 µl of each dilution was incubated with 100 µl of EA (10^8 cells/ml in $DGVB^{++}$ in U-shaped wells (Fisher Scientific) for 1 h at 37°C. Thereafter, EA were spun down (1000 g, 10 min, RT), and released haemoglobin in 150 µl of each supernatant was read at 541 nm. Total haemolysis (100%) was measured by lysing EA with water. Background spontaneous haemolysis (0%) was determined by incubating EA with buffer only. CH50 values, which correspond to the dilution factor of the serum that results in 50% cell lysis were calculated and compared. All assays were performed in triplicates.

7.3.5 Confocal imaging

A Zeiss (Göttingen, Germany) LSM 510 confocal laser scanning microscope (CLSM) was used to image uptake of FePd nanowires by cells in bright field. 10^4 RAW264.7 or HeLa cells per well were incubated in 100 µl DMEM containing 10% heat inactivated FCS, 2 mM L-glutamine, 100 U/ml of penicillin and 100 µg/ml of streptomycin and 1 mM of sodium pyruvatein a 96-well plate. Cells were allowed to adhere for 2 h after which FePd nanowires were added with a nanowire concentration of approximately 10 nanowires/cell. This concentration was estimated by assuming the nanowires have the density of bulk FePd and average dimensions as estimated from SEM and TEM images. With ICP-MS (Inductively coupled plasma mass spectrometry) (data not shown) we found a Fe:Pd ratio of 50:50, which gives an approximate alloy density of 10^7 g/m^3. Control cell samples contained only PBS and no nanowires. Images were obtained after 24 h incubation at 37°C in 5% CO_2 atmosphere.

7.3.6 Dose dependent cell viability on phagocytotic and non phagocytotic cells

For viability testing HeLa (a human cervical carninoma epithelial cell line) and RAW264.7 (a murine macrophage cell line) were cultured in DMEM containing 10% heat inactivated FCS, 2 mM L-glutamine, 100 U/ml of penicillin and 100 µg/ml of streptomycin and 1mM of sodium pyruvate. Adherent cells, RAW264.7 and HeLa, were seeded on 96-well culture plates at $5 \cdot 10^3$ cells/well in 100 µl of complete cell medium. Cells were allowed to adhere to the plate for 24 h at 37 °C in 5% CO_2 atmosphere. Incubation of non-fluorescent labeled FePd

nanowires was done by adding 100 µl of FePd nanowire dispersion in PBS to the cells, for 48 h at 37°C in 5% CO_2 atmosphere. The final concentrations of the FePd nanowires were 1, 10, 100 and 1000 nanowires/cell. All experiments were performed in triplicates. After 48 h the cell medium was carefully removed and the cells were washed with PBS, thereafter 100 µl of cell medium was added with 10 µl of CellTiter Blue and incubated for 4 h. The fluorescence was measured on a spectrophotometer (Victor, Perkin Elmer) with an excitation wavelength of 560 nm and an emission wavelength of 590 nm. The fluorescence values were normalized by the controls and expressed as percent viability. Validity of the assay was assessed by cell counting and visual inspection of the cells.

7.3.7 In-vivo magnetic drug delivery

The animal research protocol was approved by the animal ethics committee of the de Radboud University Nijmegen. Four male Wistar rats (6-8 weeks),body weight 260 $\pm$ 10 g, were used for the studies. Animals were housed and fed according to local regulations.

Rats were kept under anesthesia with 2-3% isoflurane during the entire procedure. The animals were placed ventrally on a platform with the right hind leg between the poles of the magnet (figure 7.1). Nanowire suspensions in PBS were injected via the tail vein at 10 mg/kg. The magnet was switched on 30 sec after the injection to allow for distribution of the particles and the rats were retained in the magnet for 30 min. Thereafter, the animals were fixated by vascular perfusion through the heart with paraformaldehyde. Hind legs, liver, spleen and kidneys of the rats were sectioned, according to anatomical structures and tissue samples were measured for detection of FePd nanowires with a vibrating sample magnetometer (Quantum Design, San Diego, CA, USA) with a variable magnetic field of $\pm$ 4T. Tissue samples were kept inside quartz NMR tubes and fixated to ensure no movement occurred owing to the vibrations of the device, as described in [32].

Figure 7.1: Set-up in-vivo magnetic drug delivery

7.4 Results and discussion

7.4.1 FePd nanowires

FePd nanowires were made with tunable length depending on the number of voltage cycles (50 sec -1.1V and 150 sec +0.1V) used in the electrodeposition. Using 4 cycles nanowires were made with length 1.9 $\pm$ 0.3 μm (SEM 100 wires) and diameter 88 $\pm$ 15 nm (TEM 100 wires) (Figure 7.2) leading to an aspect ratio of 22. With their volume of $10^{-20}\,\mathrm{m}^3$ the nanowires are not small enough to be considered superparamagnetic. The magnetisation curves in figure 7.3a show the room temperature magnetization curves for uncoated FePd nanowires inside the template with magnetic field (H) applied in three different directions, 0, 45 and 90 degrees to the wire direction. The squareness ratio Mr/Ms and coercivity are known to increase significantly with aspect ratio [33]. In the case of the FePd wires the obtained hysteresis loops cannot be explained in terms of pure coherent rotation or superparamagnetic behavior. The curves show remanence in all directions, as can be seen from the nearly equal squareness ratio M_r/M_s = 0.1 $\pm$ 0.02 in all directions. Moreover, the sample is easier to saturate in the hard-axis direction (90°). The angular behavior is therefore opposite to what is expected from a simple coherent rotation model, or even more advanced micromagnetic models and experiments on Co nanowires of $50\,\mathrm{nm}$ diameter spaced by $150\,\mathrm{nm}$ [34]. Similar observations have however been made for $Co_{75}Ni_{25}$ wires [35]. At a diameter of $35\,\mathrm{nm}$ hard axis loops have lower coercity and remanence, and take longer to saturate. At $65\,\mathrm{nm}$ however, the loops are similar to our observations. The authors attribute this effect to an increased contribution of crystalline anisotropy perpendicular to the wire, which balances the shape anisotropy. Indeed, also our wires are strongly polycrystalline, as is supported by the TEM image and XRD analysis. The VSM loops of randomly oriented nanowires is shown in figure 3. With respect to the array, the remanence has increased to 0.3, which supports the assumption of a strong transverse crystal anisotropy if one assumes that the magnetic easy axis of the wires is perpendicular to their long axis. The coercivity strongly decreased to $8\,\mathrm{kA/m}$, which might be attributed to the fact that the wires become superparamagnetic. All this of course is highly speculative, and will require further magnetic characterisation.

7.4.2 Magnet design

For a magnet to be able to trap particles from the blood flow in capillaries the magnetic force on the particle has to be larger than the drag force. The drag force is mainly determined by the particles orientation and the blood flow velocity, which in small capillaries is around 1 mm/s [36]. The particles can be orientated freely in the blood flow although it is most likely the particles will align their long axis with the flow, especially when the torque caused by

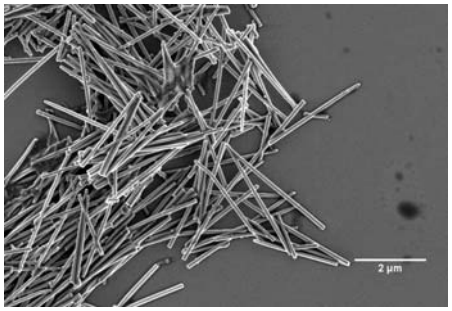

(a) SEM image of FePd nanowires

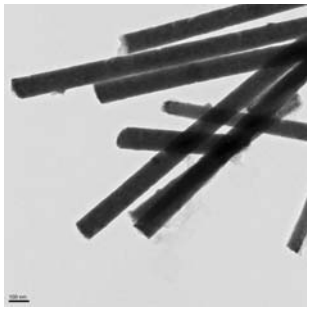

(b) TEM image of FePd nanowires

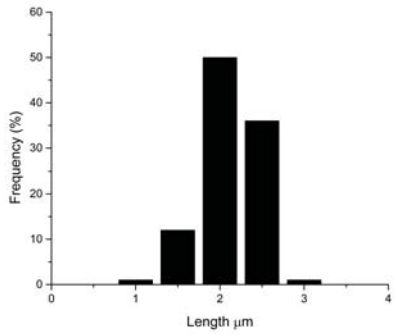

(c) Length distrigubion determined from SEM images (n=100)

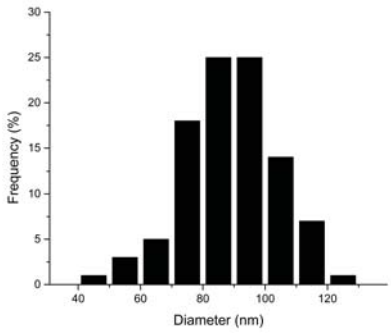

(d) Diameter distribution determined from TEM images (n=100)

Figure 7.2: Characterisation of the FePd nanowires

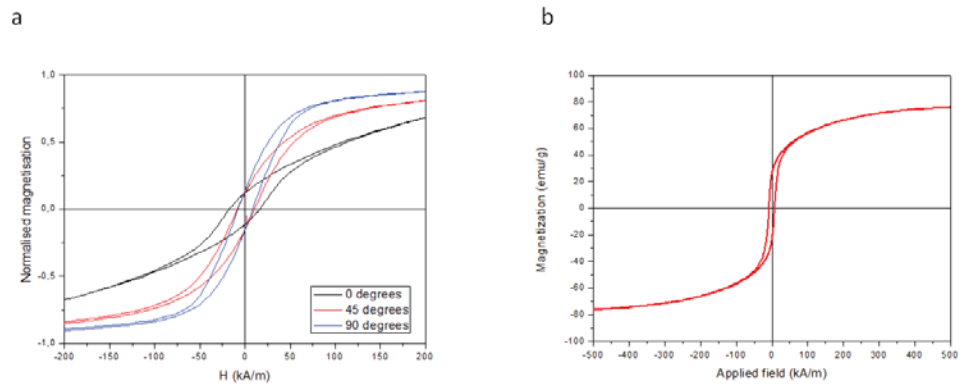

Figure 7.3: Magnetic hysteresis curves of FePd nanowires measured a) Inside the membrane under external field under 0, 45 and 90 degrees to the nanowire long axis, Mr/Ms=0.13; b) in random orientation with Ms=80 emu/g, Mr=25 emu/g and Hc= 8 kA/m

the magnet helps to align in this orientation. In a "worst case scenario" the particle will flow perpendicular to the blood flow away from the magnet which tries to capture it. For the FePd nanowires with the dimensions and characteristics described above, the drag force is 6.7 pN in this orientation. When the particle is flowing parallel to the vessel the drag force is 4.4 pN. Without the use of superconducting elements it is possible to obtain a maximum magnetic field strength of approximately 50 mT (≅400 kA/m). With the FePd density found above, we can estimate the particle magnetic moment: $10^{-15}\ \mathrm{Am}^2$. To achieve capture of these particles a magnetic field gradient of at least 0.83 T/m is needed in the perpendicular orientation and 0.55 T/m in the parallel orientation.

The magnet was developed for application in the in-vivo animal experiment (rat), with as additional requirement that the design should be scalable for use in a clinical application eg for application in breast cancer. To be able to control the field strength and the gradient a U shaped electromagnet was developed with an iron core. The gradient was obtained by using different pole sizes on either side. The inter pole distance is set to 3 cm which is the approximate size of a rats hind leg. To avoid loss of field strength at the edges the corners of the magnet were rounded. The final design of the magnet is depicted in figure 7.4a and 7.4b. The magnet core is 2 cm thick pure iron (coated to avoid oxidation), around the two arms a coil was wounded, each 480 turns in 6 layers coated with Stycast-1266 to increase heat conduction. Using a 2.5 A current the magnet had a center of gap magnet field of 70 mT and a gradient up to 2.4 T/m (measured using a Hall effect sensor CY-HS80) (figure 7.4c). These values exceed the required calculated values, as a precaution to ensure succes of this first pilot experiment. In an initial test with nanowires in a tube the FePd nanowires were easily attracted by the magnet, while in similar conditions SPIOs (Chemicell, 100nm) could not be attracted. This indicates the added value of the FePd nanowires in magnetic drug delivery.

7.4.3 In-vitro and in-vivo results

The uptake of FePd nanowires was studied by confocal microscopy (figure 7.5). After 24 h of incubation, both RAW264.7 and HeLa cells had taken up many nanowires and clusters of nanowires. RAW264.7 cells had taken up significantly more nanowires than HeLa. As RAW264.7 cells are macrophages, the uptake pathway in these cells is most likely phagocytosis. Confocal fluorescent microscopy analysis showed that the nanowires were completely taken up in the cytoplasm of these cells without signs of frustrated phagocytosis (data not shown). This indicates that macrophages will be able to remove the particles from the bloodstream within a 24 h period. In a CTB viability assay on both types of cells with 1, 10, 100 and 1000 nanowires per cell no significant reduction of viability was observed (figure 7.5) indicating the low toxicity of the nanoparticles.

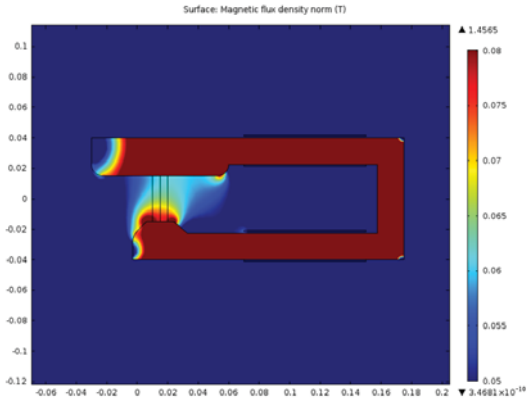

(a) Magnet design in COMSOL indication flux densities.

(b) Picture of final magnet.

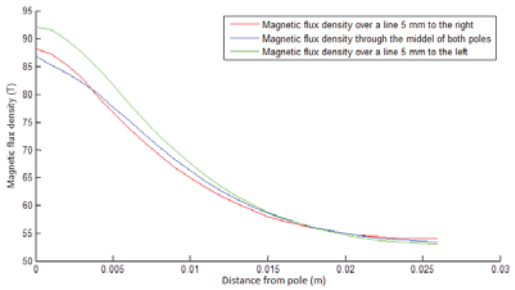

(c) Measured magnetic field strength at the locations indicated in (a)

Figure 7.4: Magnet design and characterisation

Besides toxicity also the response of the immune system was taken into account. Activation of the complement system, can lead to opsonisation of the particles, labeling them for rapid removal from the circulation by macrophages (especially in the liver). No complement activation was found even by the high (1 mg/ml) concentration of FePd nanowires (data not shown).

In the in-vivo test, the rats showed no negative side effects after the injection of the FePd nanowires compared to a control experiment with PBS only. In VSM measurements no magnetic signal could be detected in the liver, spleen and kidneys of the rats, indicating that the immune response and first pass filtration of the kidneys did not eliminate the FePd from circulation. For most SPIO particles localisation in the kidneys can be detected within a 30 min period after injection [37]. This indicates that the FePd nanowires are not rapidly recognised by the immune system and remain in circulation. In the targeted hind leg of the rat, no significant or quantifiable signal could be measured. No attempts were made to find the FePd nanowires using microscopy.

7.5 Conclusions and recommendations

Magnetic nanowires are promising new particles for magnetic drug delivery. The FePd nanowires developed in this study show very interesting properties. There length and diameter are tunable by chosing appropriate PCTE membranes and adjusting the deposition time and cycles. The magnetic properties of the nanowires cannot be explained in terms of superparamagnetic behaviour or pure coherent rotation. The measured magnetisation curves show remanence in all directions, but the sample is easier to saturate in the hard-axis direction (90°). This behaviour is opposite of what can be expected from available micromagnetic models. This effect might be caused by the polycrystalline properties, as is supported by TEM and XRD analysis and the increased remanence in randomly orientated nanowires. In the biological experiments the FePd nanowires were shown to be non-cytotoxic and non-immunotoxic in the preliminary tests presented, which is essential in order to apply the particles in any *in-vivo* application. A magnet applicable in in-vivo animal studies was designed and optimised for trapping the FePd nanowires from capillary blood flow. The dimensions can be scaled up, while keeping the field strength and gradient sufficient for targeting, for future use in a clinical relevant application as breast tumor treatment. In the pilot experiment no FePd nanowires could be found in the liver and kidneys of the rats indicating a low response of the immune system. Unfortunately also no significant amount of FePd nanowires could be detected in the target region. This was most likely caused by the fixation procedure in which the blood was removed from the rat and replaced by formaldehyde, which washed out the FePd wires. In future tests the fixation procedure should be avoided.

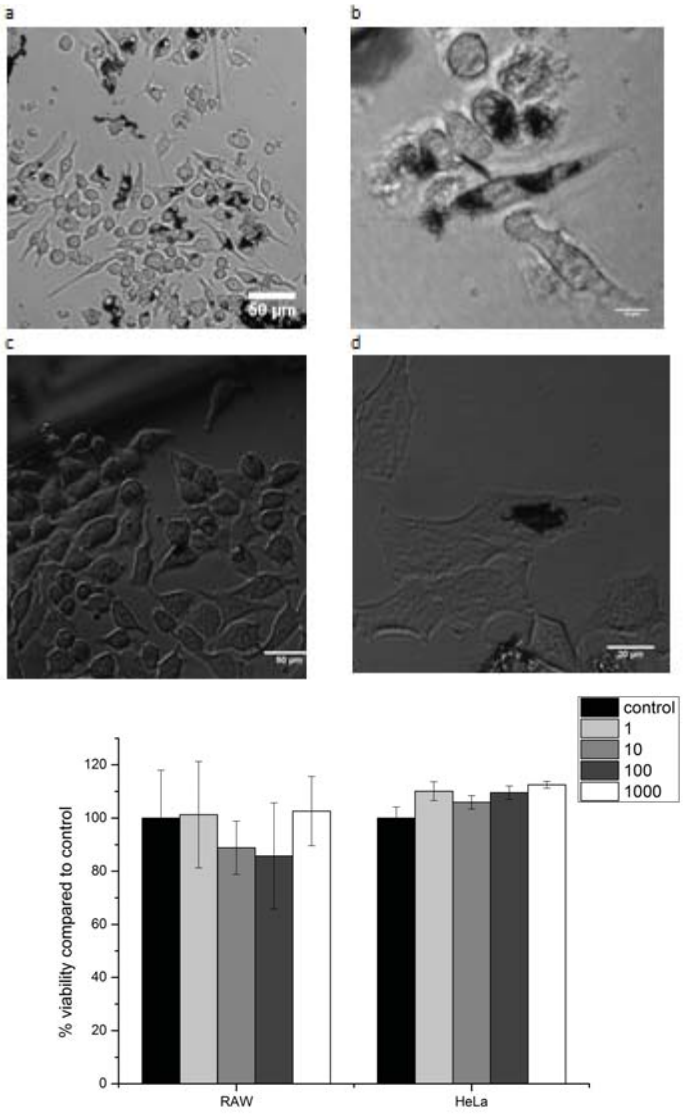

Figure 7.5: Uptake of FePd nanowires in RAW264.7 cells (A and B) and HeLa cells (C and D). E. The viability of the RAW and HeLa cells was not reduced by incubation with 1-1000 nanowires/cell over 48 h

References

[1] Y. Hirota, Y. Akiyama, Y. Izumi, and S. Nishijima, "Fundamental study for development magnetic drug delivery system," *Physica C: Superconductivity*, vol. 469, pp. 1853–1856, Oct. 2009.

[2] H. Xu, T. Song, X. Bao, and L. Hu, "Site-directed research of magnetic nanoparticles in magnetic drug targeting," *Journal of Magnetism and Magnetic Materials*, vol. 293, pp. 514–519, May 2005.

[3] O. Mykhaylyk, N. Dudchenko, and A. Dudchenko, "Doxorubicin magnetic conjugate targeting upon intravenous injection into mice: High gradient magnetic field inhibits the clearance of nanoparticles from the blood," *Journal of Magnetism and Magnetic Materials*, vol. 293, pp. 473–482, May 2005.

[4] C. Alexiou, W. Arnold, R. J. Klein, F. G. Parak, P. Hulin, C. Bergemann, W. Erhardt, S. Wagenpfeil, and a. S. Lübbe, "Locoregional cancer treatment with magnetic drug targeting.," *Cancer research*, vol. 60, pp. 6641–8, Dec. 2000.

[5] C. Alexiou, R. Jurgons, R. Schmid, A. Hilpert, C. Bergemann, F. Parak, and H. Iro, "In vitro and in vivo investigations of targeted chemotherapy with magnetic nanoparticles," *Journal of Magnetism and Magnetic Materials*, vol. 293, pp. 389–393, 2005.

[6] S. Goodwin, C. Peterson, C. Hoh, and C. Bittner, "Targeting and retention of magnetic targeted carriers (MTCs) enhancing intra-arterial chemotherapy," *Journal of Magnetism and Magnetic Materials*, vol. 194, pp. 132–139, Apr. 1999.

[7] A. S. Lübbe, C. Bergemann, W. Huhnt, T. Fricke, and H. Riess, "Predinical Experiences Drug Targeting : Tolerance and Efficacy," *Cancer research*, vol. 56, pp. 4694–4701, 1996.

[8] Y. Yoshida, S. Fukui, S. Fujimoto, F. Mishima, S. Takeda, Y. Izumi, S. Ohtani, Y. Fujitani, and S. Nishijima, "Ex vivo investigation of magnetically targeted drug delivery system," *Journal of Magnetism and Magnetic Materials*, vol. 310, pp. 2880–2882, Mar. 2007.

[9] J. . A. Dobson, "Magnetic Nanoparticles for Drug Delivery," *Drug development research*, vol. 60, pp. 55–60, 2006.

[10] Q. a. Pankhurst, J. Connolly, S. K. Jones, and J. Dobson, "Applications of magnetic nanoparticles in biomedicine," *Journal of Physics D: Applied Physics*, vol. 36, pp. R167–R181, July 2003.

[11] A. Hultgren, M. Tanase, C. S. Chen, G. J. Meyer, D. H. Reich, and L. A. Bauer, "Cell manipulation using magnetic nanowires," *Journal of Applied Physics*, vol. 93, no. 10, pp. 7275–7280, 2003.

[12] A. Prina-Mello, Z. Diao, and J. M. D. Coey, "Internalization of ferromagnetic nanowires by different living cells.," *Journal of nanobiotechnology*, vol. 4, p. 9, Jan. 2006.

[13] A. O. Fung, V. Kapadia, E. Pierstorff, D. Ho, and Y. Chen, "Induction of cell death by magnetic actuation of nickel nanowires internalized by fibroblasts," *Journal of Physical Chemistry C*, vol. 112, no. 39, pp. 15085–15088, 2008.

[14] F. K. Keating, M. K. Fung, and D. J. Schneider, "Induction of platelet white blood cell (WBC) aggregate formation by platelets and WBCs in red blood cell units," *Transfusion*, vol. 48, no. 6, pp. 1099–1105, 2008.

[15] Q. I. N. Hu, Y. Q. I. LIU, N. Li, C. Cheng, S. G. Xu, N. Wang, W. E. I. Qin, and B. Z. E. N. Z. TANG, "Ni-NTA-Coated nanowire materials for protein enrichment and the application in a medical device used for blood glucose degradation," *Nano*, vol. 8, no. 3, p. 1350029, 2013.

[16] K. M. Pondman, A. W. Maijenburg, F. B. Celikkol, A. A. Pathan, U. Kishore, B. ten Haken, and J. E. ten Elshof, "Au coated Ni nanowires with tuneable dimensions for biomedical applications.," *Journal of Materials Chemistry B*, vol. 1, pp. 6129–6136, 2013.

[17] S. Hussain, J. A. J. Vanoirbeek, and P. H. M. Hoet, "Interactions of nanomaterials with the immune system," *Wiley Interdisciplinary Reviews-Nanomedicine and Nanobiotechnology*, vol. 4, no. 2, pp. 169–183, 2012.

[18] C. Salvador-Morales, E. Flahaut, E. Sim, J. Sloan, M. L. Green, and R. B. Sim, "Complement activation and protein adsorption by carbon nanotubes," *Molecular Immunology*, vol. 43, no. 3, pp. 193–201, 2006.

[19] C. Salvador-Morales, E. V. Basiuk, V. A. Basiuk, M. L. H. Green, and R. B. Sim, "Effects of covalent functionalisation on the biocompatibiltiy characteristics of multi-walled carbon nanotubes," *Journal of Nanoscience and Nanotechnology*, vol. 8, no. 5, pp. 2347–2356, 2007.

[20] C. Salvador-Morales, M. L. H. Green, and R. B. Sim, "Interaction between carbon nanotubes and biomolecules.," in *Chemistry of carbon nanotubes* (E. V. Basiuk and V. A. Basiuk, eds.), ch. 27, American Scientific Publishers, 2007.

[21] M. Rybak-Smith, K. Pondman, E. Flahaut, C. Salvador-Morales, R. Sim, and ., "Recognition of Carbon Nanotubes by the Human Innate Immune System.," in *Carbon Nanotubes for Biomedical Applications* (R. Klingeler and R. B. Sim, eds.), pp. 183–210, Springer, 2011.

[22] K. M. Pondman, M. Sobik, A. Nayak, A. G. Tsolaki, A. Jäkel, E. Flahaut, S. Hampel, B. Ten Haken, R. B. Sim, and U. Kishore, "Complement activation by carbon nan-

otubes and its influence on the phagocytosis and cytokine response by macrophages.," *Nanomedicine : nanotechnology, biology, and medicine*, vol. 10, pp. 1287–1299, Mar. 2014.

[23] L. Sun, Y. Hao, C. L. Chien, and P. C. Searson, "Tuning the properties of magnetic nanowires," *IBM Journal of Research and development*, vol. 49, no. 1, pp. 79–102, 2005.

[24] A. Aharoni, "Elongated superparamagnetic particles," *Journal of Applied Physics*, vol. 75, no. 10, pp. 5891–5893, 1994.

[25] B. Hallmark, N. J. Darton, T. James, P. Agrawal, and N. K. H. Slater, "Magnetic field strength requirements to capture superparamagnetic nanoparticles within capillary flow," *Journal of Nanoparticle Research*, vol. 12, pp. 2951–2965, Mar. 2010.

[26] J. Ahmadi and G. McLaughlin, *Transport, Deposition, and Removal of Fine Particles: Biomedical Applications.* Springer, 2008.

[27] H. C. Berg, *Random walks in Biology*. 1993.

[28] V. Haehnel, S. Fähler, L. Schultz, and H. Schlörb, "Electrodeposition of Fe70Pd30 nanowires from a complexed ammoniumsulfosalicylic electrolyte with high stability," *Electrochemistry Communications*, vol. 12, pp. 1116–1119, Aug. 2010.

[29] V. Haehnel, C. Mickel, S. Fa, and L. Schultz, "Structure , Microstructure , and Magnetism of Electrodeposited Fe 70 Pd 30 Nanowires," *Journal of Physical Chemistry C*, vol. 114, pp. 19278–19283, 2010.

[30] H. Schlörb, V. Haehnel, M. S. Khatri, A. Srivastav, A. Kumar, L. Schultz, and S. Fähler, "Magnetic nanowires by electrodeposition within templates," *physica status solidi (b)*, vol. 247, pp. 2364–2379, Aug. 2010.

[31] T. K. Jain, M. A. Morales, S. K. Sahoo, D. L. Leslie-Pelecky, and V. Labhasetwar, "Iron oxide nanoparticles for sustained delivery of anticancer agents," *Molecular Pharmaceutics*, vol. 2, no. 3, pp. 194–205, 2005.

[32] M. Visscher, J. J. Pouw, J. Van Baarlen, J. M. Klaase, and B. T. Haken, "Quantitative analysis of superparamagnetic contrast agent in sentinel lymph nodes using ex vivo vibrating sample magnetometry," *IEEE Transactions on Biomedical Engineering*, vol. 60, pp. 2594–2602, 2013.

[33] L. A. Bauer, D. H. Reich, and G. J. Meyer, "Selective functionalization of two-component magnetic nanowires," *Langmuir*, vol. 19, no. 17, pp. 7043–7048, 2003.

[34] R. Lavín, C. Gallardo, J. Palma, J. Escrig, and J. Denardin, "Angular dependence of the coercivity and remanence of ordered arrays of Co nanowires," *Journal of Magnetism and Magnetic Materials*, vol. 324, pp. 2360–2362, Aug. 2012.

[35] M. Vázquez and L. G. Vivas, "Magnetization reversal in Co-base nanowire arrays," *Physica Status Solidi (B)*, vol. 248, pp. 2368–2381, Oct. 2011.

[36] K. P. Ivanov, M. K. Kalinina, and Levkovich YuI, "Blood flow velocity in capillaries of brain and muscles and its physiological significance.," *Microvascular research*, vol. 22, pp. 143–155, 1981.

[37] Y.-X. J. Wang, "Superparamagnetic iron oxide based MRI contrast agents: Current status of clinical application.," *Quantitative imaging in medicine and surgery*, vol. 1, pp. 35–40, 2011.

Chapter 8

Conclusions and Perspectives

The research presented in this thesis shows that the application of nanotechnology has the potential to overcome important hurdles in medicine. One of the biggest challenges is to deliver a therapeutic entity to its target location, an organ, cell or even a cell nucleus. Therefore, nanoparticles have been actively explored as drug delivery vehicles for targeted organ-specific as well as systemic therapy. Carbon nanotubes (CNTs) specifically have many advantageous properties for drug delivery applications that include the ease of functionalization of the carbon shells, the possibility for filling up the inner tubes, and their ability to traverse through cellular and nuclear membranes. Although there are many studies suggesting applications of CNTs, no clinical applications have been approved until this day. There are still many questions that remain unanswered with respect to interactions between the human body and CNTs.

The effectiveness of nanoparticles as intravenous drug delivery platforms is strongly influenced by interactions with immune cells, as rapid elimination of the particles from the systemic circulation prevents the drug from reaching the target location. Furthermore, immune system activation can lead to severe inflammatory reactions and long-term potentiation of the adaptive immunity. Therefore, understanding the interactions between the nanoparticles and the immune system is of utmost importance. In particular, how CNTs are dealt with by the innate immune system is essential for their strategic and specific in vivo use, since CNTs are most likely to encounter cellular and humoral components of the innate immune wing immediately after their entry into the human body. Several studies have shown that CNTs activate the innate immune complement system, predominantly through the classical pathway, and to a lesser extent through the alternative pathway. However, the mode of the recognition of CNTs, pristine or functionalized, by the classical pathways first subcomponent C1q, and subsequent mechanism of the activation of the classical pathway

remained unclear. This thesis sets out to elucidate the nature of interaction between CNTs and C1q using a panel of native, recombinant and mutant versions of human C1q. C1q binds via ionic interactions onto charge patterns on the target which we considered are likely to be readily available on derivatized CNTs, in addition to several other nanoparticles.

In chapter 3, we show that human C1q binds in an orientation that activates the classical pathway of complement activation, and the complement cascade continues up to the consumption of C3 and C5, indicating the formation of the membrane attack complex. We also demonstrate that the recombinant individual globular heads of C1q (ghA, ghB and ghC) are able to bind onto the surface of CMC coated CNTs. In chapter 6, we identified the Arg162 of ghA, and the Lys136 and Arg129 of ghB modules as essential residues involved in C1q interaction with CNTs (both CMC coated and oxidised CNTs). This appears to suggest an ionic/charge pattern interaction reminiscent of C1q-IgG binding since similar residues have been shown to be involved in C1q-IgG interaction. This proves that binding of C1q is not simply absorbed onto the surface but a true interaction directed towards a non-self. In chapter 4, we developed a particle suitable for magnetic drug delivery. The Au-Ni nanowire has similar dimensions to CNTs, but with magnetic properties and a PEGylated gold surface which was shown to be non-cytotoxic. The Au-Ni nanowires did not activate the complement system and therefore gave us an opportunity to analyse the effect of complement activation on the subsequent immune response evoked by nanoparticles.

We first showed that complement activation and deposition on the surface of CNTs enhanced their uptake by macrophages (U937 cell line) and human monocytes in a time dependent manner. Complement opsonisation of CNTs also led to modulation (mostly downregulation) of pro-inflammatory and anti-inflammatory cytokine production by U937 cells and human monocytes. In order to understand how complement-activating and non-activating nanoparticles are dealt not only by phagocytic and antigen presenting macrophages, but also with B and T cells of the adaptive immunity, CMC-CNTs, RNA-CNTs and Au-Ni nanowires were challenged against U937 (macrophage cell line), Raji (B cell line) and Jurkat (T cell line) cells with and without complement deposition and examined for phagocytosis and cytokine response. Our results suggest that complement deposition on CNTs determines the balance between pro-inflammatory and anti-inflammatory immune responses. In the absence of complement activation and deposition, the pro-inflammatory cytokine response was dramatically upregulated. We suggest that complement deposition can sequester CNTs towards a non-inflammatory uptake by immune cells that express complement receptors on their surfaces, such as macrophages and B lymphocytes. We also report here that complement deposition also alters IL-10 and IL-12, which is likely to raise the threshold of adaptive immune response and subsequent antigen presentation and T cell response. The downregulation of pro-inflammatory cytokines can be attributed to higher IL-10 production via complement

whereas IL-12 is likely to promote helper T cell 1 (Th1) response leading to IFN-γ secretion by Th 1 cells. Thus, our work suggests a model to work on deciphering nanoparticles that can be Th2 or Th1 polarising. These issues become paramount if the drug delivery is designed for chronic pathological conditions/syndromes.

After establishing the importance of the presence of complement proteins on the surface of the nanoparticles, we targeted a set of key innate immune humoral factors to examine the contributions of pattern recognition proteins to phagocytosis and cytokine response seen by complement deposition. We found that the individual globular heads of C1q were able to dampen complement activation by the CNTs, suggesting specificity of the classical pathway activation. Other humoral factors, C1q and factor H did not have this complement inhibitory effect. All individual humoral soluble factors were able to influence the cytokine expression by U937 cells to various degrees. However, the large cytokine dampening effect appears to be dependent on full complement activation. Therefore, other pattern recognition molecules are likely to modulate CNT-immune cell interaction and its outcome locally in the tissues and organs. However, systemic delivery of nanoparticles that attract highest complement deposition will lead to the best opsonic and anti-inflammatory effect: an idea that needs to tested in vivo now.

Chapter 7 presents a method by which magnetism can be used in combination with specially designed magnetic nanowires to move a bound therapeutic to the target area. In the design of the particle we pay attention to the dimensions and the coating of the particles to render them bio-compatible, non-cytotoxic and not easily recognised by the immune system to avoid rapid elimination of the particles before the target location is reached. The FePd nanowire has high magnetisation with low remnant magnetisation to avoid within macrophages (RAW264.7) and epithelial cells (HeLa). This promising method requires further optimisation for capturing at the target location.

The thesis highlights the importance of a multi-disciplinary approach in order to realise the intended objectives of the nanomedicine application. Whereas good chemistry and physics are required to synthesise and characterise application-oriented nanoparticles, to ensure its biocompatibility the particles need to undergo a range of tests including cytotoxicity. How these particles are viewed and responded to by the immune system can alter the intended use. Small alterations, e.g. in the molecular patterns presented on the surface of nanoparticles, can trigger completely altered immune responses. Therefore, each newly developed nanotechnology should be evaluated individually and extensively using a range of cell biological, immunological and pharmacological parameters. It remains to be said that a strong partnership is required between biologist, chemists and nanoengineers.

Summary

Over the last years, nanoparticles have been actively explored as drug delivery vehicles for targeted as well as systemic therapy. Especially carbon nanotubes (CNTs) have many advantageous properties for drug delivery applications. The main advantages are the easy functionalization of the carbon shells, the possibility for filling of the inner tubes and their capability of passing through cellular and nuclear membranes. Although there are many studies suggesting applications of CNTs, no clinical applications are approved until this day. There are still many questions about interactions between the human body and CNTs. The effectiveness of nanoparticles as an intravenous drug delivery platform is strongly influenced by interactions with immune cells, as rapid elimination of the particles from the systemic circulation prevents the drug from reaching the target location. Furthermore, immune system activation can lead to severe inflammatory reactions. Therefore, understanding the interactions between nanoparticles and immune system, particularly the innate immune system, is essential for their strategic and specific use for in vivo delivery. In literature (chapter 2) several studies show that CNTs activate the innate immune complement system, but there were still many questions about the recognition pathways involved. Therefore, in this thesis we set out to elucidate some of the fundamental interactions.

In chapter 3 we find that CNTs coated with various dispersants activate the complement system predominantly through the classical pathway and for a minor extent through the alternative pathway. The interactions between CNTs and C1q; the recognition molecule of the classical pathway of the complement system, were studied in detail. We found that C1q binds through its individual globular head regions ghA, ghB and ghC. Pre-coating CNTs with these proteins inhibits complement activation by the CNTs. We confirmed that complement activation by the CNTs used continues up to C3 and C5, indicating that the entire complement system is activated including the formation of membrane-attack complexes. The phagocytosis of CNTs by U937 cells is enhanced significantly in the presence of serum compared to serum free conditions, with concomitant downregulation of pro-inflammatory cytokines and upregulation of anti-inflammatory cytokines in both U937 cells and human monocytes. We propose that CNT-mediated complement activation may cause recruitment of

cellular infiltration, followed by phagocytosis without inducing a pro-inflammatory immune response.

In chapter 4 a new high aspect ratio nanoparticle is developed for biomedical applications especially magnetic drug delivery. Due to their shape anisotropy, high aspect ratio magnetic nanoparticles offer many advantages in biomedical applications. For biocompatibility, it is essential to have full control over the dimensions and surface chemistry of the particles. The particle was made by electrodeposition of nickel inside the pores of a polycarbonate membrane, the length of the particles was controlled by adjusting the deposition time. To assure biocompatibility, a continuous gold coating was deposited onto the Ni wires by a newly developed electroless deposition method, leading to an Au-Ni nanowire. The coating was analysed using electron microscopy and X-ray diffraction. The particles show high saturation magnetisation and remanence as can be expected from elongated particles. After functionalization of 2 μm long Au-Ni nanowires with poly(ethylene glycol), no significant cytotoxic effects were found in studies involving a diverse range of primary and tumour cells exposed to increasing concentrations of Au-Ni nanowires for up to 7 days. These nanowires may thus be used for in-vivo applications such as magnetic drug delivery.

In chapter 5 the influence of complement deposition onto the surface of nanoparticles on further immune response was studied. The Au-Ni nanowires developed in chapter 4 did not induce any complement activation. This offered an opportunity to compare these particles with similarly dimensionalised CNTs (coated with RNA or CMC) which are potent complement activators. The extent of complement activation seems to impact upon phagocytosis and cytokine secretion by U937 (a macrophage cell line), Raji (a B cell line) and Jurkat (a T cell line) cells. We suggest that complement deposition directs CNTs away from other potential PAMP-PRR interactions, modulating the pattern of cytokine secretion. Wherever nanoparticles fail to deposit complement on their surfaces, the opsonisation by other serum proteins give rise to potentially deleterious pro-inflammatory immune response.

In chapter 6 we examined the interactions of various pattern recognition soluble factors with CNTs. The binding of the globular heads of C1q was analysed in detail by means of single amino acid mutated forms of the globular head regions and the Arg162 of ghA, and the Lys136 and Arg129 of ghB were identified as essential amino acids in the binding onto CNTs (both CMC coated and oxidised CNTs). We found that coating of individual innate immune humoral factors reduced the cytokine storm evoked by uncoated CNTs, but the effect is not as pronouced as when we allow full complement activation to take place (as in chapter 3). Complement deposition on the nanoparticles appears to skew the pro-inflammatory towards anti-inflammatory response, suggesting beneficial effects of complement. It is unclear how complement deposition enhances anti-inflammatory immune response. We find that various pattern recognition soluble factors interact differentially with CNTs, exerting overlapping

effects in a complement-independent manner. These results have implications on regulating complement activation prior to designing therapeutic strategies based on nanoparticles.

In chapter 7 a potential application of nanomedicine is magnetic drug delivery is proposed. Magnetic drug delivery uses a magnetic field with high gradient to capture magnetic nanoparticles in a diseased area. Thereapeutics are coupled to the nanoparticles. The current magnetic drug delivery systems use spherical superparamagnetic particles, unfortunately the fields and gradients needed to capture these particles inside the human body are very difficult to achieve. Therefore we proposed the use of elongated magnetic particles. A FePd nanowire was developed, with high magnetisation and low remanence magnetisation. The nanowires are 2 μm in length and 80 nm in diameter. In cytotoxicity tests in macrophages and epithelial cells no negative effects were found, the cells were all capable of internalising the particles. The particles did not activate the complement system. A magnet was developed, in theory capable of capturing the particles over a distance of 3 cm. The system was used in a pilot scale in-vivo experiment. No FePd nanowires were found in the liver, spleen and kidneys of the rats indicating that the immune system does not rapidly remove the particles from circulation. Unfortunately we could not find FePd nanowires in the targeted leg of the rats. We assume the particles are removed in the fixation procedure.

Samenvatting

Nanodeeltjes worden al enkele jaren actief bestudeerd als medicijn afgifte systeem voor zowel gerichte als systemische therapie. Vooral koolstof nanobuisjes (CNT) hebben vele gunstige eigenschappen in medicatie toepassingen. De koolstof schillen zijn gemakkelijk te functionaliseren en het is mogelijk de binnenste buis te vullen met medicijnen. Ook is aangetoond dat CNTs door cel- en kernmembranen kunnen gaan.

Hoewel er veel geschreven is over medische toepassingen van CNTs, zijn er op dit moment geen goedgekeurde klinische toepassingen. Eén van de redenen daarvoor is dat er nog veel vragen zijn over de (mogelijk schadelijke) interacties tussen het menselijk lichaam en CNTs.

De effectiviteit van nanodeeltjes als intraveneus medicijn afgifte platform wordt sterk beïnvloed door immuuncellen. De medicatie kan de doellocatie niet bereiken wanneer de nanodeeltjes uit de systemische circulatie worden verwijderd door fagocytische immuuncellen. Bovendien kan activering van het immuunsysteem leiden tot ernstige ontstekingsreacties. Begrip van de interacties tussen nanodeeltjes en het immuunsysteem, met name het aspecifieke (aangeboren) immuunsysteem, is essentieel voor de toepassing van CNTs voor medicijnafgifte. In de literatuur (samengevat in hoofdstuk 2) blijkt uit verschillende studies dat CNTs het complement systeem van het aspecifieke immuunsysteem activeren, maar er zijn nog veel vragen over de manier waarop dit gebeurt. In dit proefschrift proberen we om een aantal van de fundamentele interacties te verhelderen.

In hoofdstuk 3 toonden we aan dat CNTs gefunctionaliseerd met verschillende dispergeermiddelen het complementsysteem voornamelijk via de klassieke route en in mindere mate via de alternatieve route activeren. De interacties tussen CNTs en C1q (het herkenningseiwit van de klassieke route van het complementsysteem) werden bestudeerd. Wij vonden dat C1q bindt door zijn individuele globulaire regio's ghA, ghB en ghC. Wanneer CNTs met deze eiwitten gecoat zijn, onderdrukt dit de complement activatie door de CNTs. We bevestigden dat complement activering door de CNTs via de aangegeven routes doorgaat tot activatie van C3 en C5, wat aangeeft dat het gehele complementsysteem wordt geactiveerd tot en met de vorming van het "membrane attack complex ". De fagocytose van CNTs

door U937 (macrofaag) cellen nam significant toe in aanwezigheid van serum vergeleken met serum-vrije omstandigheden. Tegelijkertijd nam de productie van pro-inflammatoire cytokines af en was er een toename van productie van anti-inflammatoire cytokines in zowel U937-cellen als humane monocyten. Wij stelden dat CNT-gemedieerde complement activatie cellulaire infiltratie kan veroorzaken, welke wordt gevolgd door fagocytose zonder dat een pro-inflammatoire immuunrespons wordt geïnduceerd.

In hoofdstuk 4 werd een nieuw nanodeeltje ontwikkeld met een grote aspect ratio. Door de vorm-anisotropie bieden langwerpige magnetische nanodeeltjes bieden vele voordelen in biomedische toepassingen. Voor biocompatibiliteit, is het essentieel om volledige controle te hebben over de afmetingen en oppervlaktechemie van de deeltjes. Daarom werd ervoor gekozen om de deeltjes te maken met behulp van elektrodepositie in polycarbonaat membranen, waarbij de depositietijd werd gecontroleerd. Om biocompatibiliteit te bewerkstelligen werden de gemaakte nikkel deeltjes gecoat met goud via een nieuw ontwikkelde depositie methode, hierdoor ontstond een Au-Ni nanostaafje. De coating werd geanalyseerd door middel van elektronenmicroscopie en röntgendiffractie. De deeltjes hebben een hoge verzadigings magnetisatie en remanentie zoals kan worden verwacht van langwerpige deeltjes. Na functionalisering van de 2 μm lange Au-Ni nanostaafjes met poly(ethyleenglycol), werden geen significante cytotoxische effecten gevonden in studies met diverse primaire cellen en tumorcellen, die waren blootgesteld aan Au-Ni nanostaafjes voor maximaal 7 dagen. De Au-Ni nanostaafjes kunnen worden gebruikt voor in-vivo toepassingen zoals magnetische geneesmiddelafgifte.

In hoofdstuk 5 werd de invloed van complement afzetting op het oppervlak van nanodeeltjes op de verdere immuunrespons bestudeerd. De Au-Ni nanostaafjes, beschreven in hoofdstuk 4, wekken geen complement activatie op. Dit bood de mogelijkheid om deze deeltjes te vergelijken met gelijk gedimensionaliseerde CNTs (gecoat met RNA of CMC) welke krachtiger complement activatoren zijn. De mate van complement activatie lijkt van invloed te zijn op fagocytose en cytokine secretie door U937 (een macrofaag cellijn), Raji (een B-cellijn) en Jurkat (een T-cellijn) cellen. Wij concludeerden dat complement afzetting op CNTs door het moduleren van het patroon van cytokine secretie andere potentiële PAMP-PRR interacties voorkomt. Wanneer geen complement depositie plaatsvindt op het oppervlak van nanodeeltjes, leidt de opsonisatie door andere serumeiwitten tot een mogelijk schadelijke pro-inflammatoire immuunrespons.

In hoofdstuk 6 onderzochten we de interacties van verschillende patroonherkennings humorale factoren met CNTs. De binding van de globulaire regio's van C1q werd in detail geanalyseerd met behulp van op een enkele aminozuur gemuteerde vormen van de globulaire regio's. De Arg162 van ghA en de Lys136 en Arg129 van ghB werden gedentificeerd als essentiële aminozuren in de binding met CNTs (zowel CMC gecoat als geoxideerde CNTs).

Wij vonden dat het coaten van CNTs met individuele humorale factoren de “cytokine storm” verminderde die wordt opgeroepen door niet gecoate CNTs, maar het effect is niet zo uitgesproken als wanneer we volledige complement activatie laten plaatsvinden (zoals in hoofdstuk 3). Complement depositie op de nanodeeltjes lijkt de pro-inflammatoire responsie om te buigen naar een anti-inflammatoire respons, dit suggereert de gunstige effecten van complement depositie. Het is nog onduidelijk hoe complement depositie de anti-inflammatoire immuunrespons verbeterd. We zagen dat verschillende patroonherkennings eiwitten verschillende interacties hebben met CNTs; ze oefenen overlappende effecten uit op een complement-onafhankelijke wijze. Deze resultaten hebben implicaties voor het reguleren van complement activatie bij het ontwerpen van therapeutische strategieën op basis van nanodeeltjes.

In hoofdstuk 7 werd een mogelijke toepassing van nanomedicine voorgesteld: magnetische medicijnafgifte. Magnetische medicijn afgifte maakt gebruik van een magnetisch veld met een hoge gradiënt om magnetische nanodeeltjes vast te houden in een aangedaan gebied (tumor). Medicijnen worden gekoppeld aan de nanodeeltjes. In de huidige magnetische geneesmiddel-afgiftesystemen worden bolvormige superparamagnetische deeltjes gebruikt, helaas zijn de velden en gradiënten die nodig zijn om deze deeltjes af te vangen in het menselijk lichaam zeer moeilijk te bereiken. Daarom stelden wij het gebruik van langwerpige magnetische deeltjes voor. Voor dit onderzoek werd een FePd nanostaafje ontwikkeld, met een hoge magnetisatie en lage remanentie. De nanostaafjes zijn 2 μm lang en 80 nm in diameter. In cytotoxiciteit testen met macrofagen en epitheelcellen werden geen negatieve effecten gevonden, de cellen waren in staat de deeltjes op te nemen. De staafjes activeren het complementsysteem niet. Een magneet werd ontwikkeld die in theorie de deeltjes over een afstand van 3 cm kon afvangen. Het systeem werd gebruikt in een pilot-schaal in vivo experiment. Geen FePd nanostaafjes werden gevonden in de lever, milt en nieren van de ratten. Dit geeft aan dat het immuunsysteem de deeltjes niet snel verwijderd uit de circulatie. Helaas konden we geen FePd nanostaafjes vinden in de getargette poot van de ratten. We veronderstellen dat de deeltjes werden verwijderd in de fixatie procedure.

Acknowledgements

At the end of this thesis and the four years of research it represents, I would like to thank the many people who contributed to this work. As mentioned before, this was a very multidisciplinary study, therefore I often looked for information, help and sources outside my own group, therefore I had a chance to work with many people in various groups in Twente, Oxford, Brunel, Utrecht and Aalborg. I will try to acknowledge everyone who helped me, but please forgive me if I forgot to mention you, I highly appreciate all the help I got.

First I'm grateful to Bennie ten Haken for giving me the opportunity to do a PhD in the NIM (Neuroimaging) group and giving me the freedom and trust to find my own way. I would like to thank my promotor, professor Andre ten Elshof for welcoming me in the IMS (inorganic material science) group, and for sharing his knowledge and ideas. Also I like to express my gratitude to my second promotor, professor Bob Sim, from Oxford University. Bob, all I know about biochemistry is thanks to your teaching and I am very thankful that you were always available to give me advice on any subject. I also greatly appreciate your eye for detail in finalising the papers we wrote and this thesis. Dr Uday Kishore, thank you for inviting me to work in your lab in Brunel. While you had no prior experience with nanoparticles you were always very interested and many of the chapters and papers in this thesis are based on your ideas, furthermore I really appreciated the many long discussions on the research and drafts.

Although finally not the main topic of this thesis, magnetic drug delivery was the original starting point of my work. I would like to thank the BNT/MNF (Biomolecular nanotechnolgy/ molecular nanofabrication) and NBP (Nanobiophysics) labs for allowing me to use their facilities. Also I like to thank professor Richard van Wezel, professor Leon Abelmann and his student Garud Snoep for their help with the calculations and in-vivo testing. In this field I appreciated the opportunity to work with the group at Aalborg University of professor Torben Moos and Louiza Bohn Thomson, a collaboration initiated by Gerben Visser (Utrecht University).

I would like to thank my students Evelyn de Jong, Ellis Markink and Nathan Bunt and the other people in the NIM group. Although I was always an outsider, you always showed interest in my work. It was fun to be ”the biologist” or ”the chemist” amongst you, while everywhere else I was always ”the physicist” or ”the engineer”. Martin Sobik, I had a great time sharing an office and a fume hood with you, furthermore you were a great colleague and friend, your passion for research and perseverance was an inspiration to me.

In the last few years I had many collegues and labmates who helped me with various experiments, or who made the long lab hours more enjoyable. I won't even try to name everyone, but it was great to work with all of you. I only want to mention a few people who I have worked with very closely over the last years. I would like to thank Wouter Maijenburg for teaching me all I needed to know about electrodeposition. Benjamin Matt, I really enjoyed working with you on a friday-afternoon experiment that turned into a nice and now published paper. Also I like to thank Nathalie Katsonis for her guidance in this project.

It was great to see how research can progress when people work together, I am very thankful for all the proteins and samples that my labmates in Brunel prepared, so I would be able to ”stick” them on my nanotubes. You all kept my cells alive while I went back to the Netherlands and performed some essential experiments in my absence. Specially I would like to thank Eswari Dodagatta-Marri for making sure I would never go a day without home cooked lunch and dinner, you made my stay away from home very easy and made me love Indian cooking.

Work is not all there is in life, although I would be the first to admit I often lose this sense of perspective. I like to thank my family, friends and housemates for the good talks, walks, swims, runs, city tours, dinners, midnight tea's (without milk!), also thank you for listening to my often so boring work stories.

Ewoud, I want to thank you especially, although I was often away from home for long times (even when I was working in Twente), you were always very supportive. Thank you for your support, correcting all the silly mistakes in this thesis, your patience, trust and love.

List of publications

1. B. Matt, **K.M. Pondman**, S.J. Asshoff, B. ten Haken, B. Fleury, N. Katsonis, ”Soft magnets from the self-organization of magnetic nanoparticles in chiral liquid crystals”, *Angewandte*, in press

2. **K.M. Pondman**, M. Sobik, A. Nayak, A.G. Tsolaki, A. Jäkel, E. Flahaut, S. Hampel, B. ten Haken, R.B. Sim, U. Kishore, “Complement activation by carbon nanotubes and its influence on the phagocytosis and cytokine response by macrophages”, *Nanomedicine: Nanotechnology, Biology, and Medicine*, vol. 10, no. 6, p. 1287-1299, 2014

3. **K.M. Pondman**, A.W. Maijenburg, F.B. Celikkol, A.A. Pathan, U. Kishore, B. ten Haken and J.E. ten Elshof, “Au coated Ni nanowires with tuneable dimensions for biomedical applications”, *Journal of Materials Chemistry B*, vol. 1, p. 6129-6136, 2013

4. L.B. Thomsen, T. Linemann, **K.M. Pondman**, J. Lichota, K.S. Kim, R.J. Pieters, G.M Visser, T. Moos, “Uptake and transport of superparamagnetic iron oxide nanoparticles through human brain capillary endothelial cells”, *ACS Chemical Neuroscience*, vol. 4, no. 10, p. 1352-1360, 2013

5. M. Sobik, **K.M. Pondman**, B. Erné, B. Kuipers, B. ten Haken, H. Rogalla, “Magnetic nanoparticles for diagnosis and medical therapy”, in *Carbon nanotubes for biomedical applications*, eds: Klingeler and Sim, p. 85-95, 2011

6. M.J. Rybak-Smith, **K.M. Pondman**, E. Flahaut, C. Salvador-Morales, R.B. Sim, “Recognition of carbon nanotubes by the human innate immune system”, in *Carbon nanotubes for biomedical applications*, eds: Klingeler and Sim, p. 183-210, 2011

7. **K.M. Pondman**, J.J. Fütterer, B. ten Haken, L.J. Schultze Kool, J.A. Witjes, T. Hambrock, K.J. Macura, J.O. Barentsz, “MR-Guided Biopsy of the Prostate: An Overview of Techniques and a Systematic Review”, *European Urology*, vol. 54, no. 3, p. 517-527, 2008

Submitted papers

8. **K.M. Pondman**, A.G. Tsolaki, M.H. Shamji, A. Switzer, B. ten Haken, R.B. Sim, U. Kishore, "Complement deposition on nanoparticles can modulate immune responses by macrophage, B and T cells", *Journal of Biomedical Nanotechnology*, submitted.

9. **K.M. Pondman**, A.G. Tsolaki, L. Pednekar, E. Dodagatta-Marri, L. Kouser, M. Sobik, B. ten Haken, R.B. Sim, U. Kishore, "Innate immune humoral factors, C1q and factor H, with differential pattern recognition properties alter macrophage response to carbon nanotubes", *Small*, submitted.

10. **K.M.Pondman**, N.D. Bunt, A.W. Maijenburg, R. van Wezel, U. Kishore, L. Abelmann, J.E. ten Elshof, B. ten Haken, "Magnetic Drug Delivery with FePd nanowires", *Journal of Magnetism and Magnetic Materials*, submitted

11. **K.M. Pondman**, E. Dodagatta-Marri, A.G. Tsolaki, M. Sobik, B. ten Haken, R.B. Sim, U Kishore, "Pulmonary surfactant protein SP-D opsonises carbon nanotubes and modulates immune response by macrophage and alveolar epithelial cells", *Nanotoxicology*, submitted.

12. **K.M.Pondman**, M. Sobik, R.B. Sim, U. Kishore, "Interactions of the innate immune system with carbon nanotubes", *Nanomedicine: Nanotechnology, Biology, and Medicine*, in preparation.

Abbreviations

Ala	Alanine
APC	Antigen Presenting Cell
Arg	Arginine
Asp	Aspartic acid
BALF	Bronchoalveolar lavage fluid
BSA	Bovine serum albumin
CD	Cluster of differentiation
cDNA	Complementary DNA
CMC	Carboxymethyl cellulose
CNT	Carbon Nanotube
CR	Complement receptor
CRP	C-reactive protein
Ct	Cycle threshold
CTB	CellTiter Blue
DC	Dendritic cell
DMEM	Dulbecco's modified Eagle's medium
DNA	Deoxyribonucleic acid
$DVGB^{++}$	Dextrose gelatin veronal buffer, with Ca^{2+} and Mg^{2+} ions
DWNT	Double Walled Carbon Nanotube

EA	Antibody-sensitised sheep erythrocytes
EDC	1-Ethyl-3-(3-dimethylaminopropyl) carbodiimide
EDTA	Ethylenediaminetetraacetic acid
EGFR	Epidermal Growth Factor Receptor
EGTA	ethylene glycol tetraacetic acid
EPR	Enhanced Permeability and Retention
ESF	European Science Foundation
FBG	Fibrinogen
FCS	Fetal calf serum
Fe-MWNTs	Iron filled multi walled carbon nanotubes
FR	Folate Receptor
gC1q	Globular regions of human C1q
ghA, ghB, ghC	Recombinant globular head domain of C1q: A, B or C polypeptides
Gln	Glutamine
Glu	Glutamic acid
HEPES	4-(2-hydroxyethyl)-1-piperazineethanesulfonic acid
HER2	Human Epidermal Growth Factor Receptor 2
His	Histidine
HRP	Horseradish peroxidase
HSA	Human serum albumin
Ig	Immunoglobulin
IL	Interleukin
iNOS	cytokine inducible nitric oxide synthase
Leu	Leucine
Lys	Lysine

MAC	Membrane attack complex
MASP	MBL-associated serine protease
MES	2-(N-morpholino) ethanesulfonic acid
MHC	Major histocompatibility complex
MRI	Magnetic Resonance Imaging
mRNA	Messenger RNA
MWNT	Multi Walled Carbon Nanotube
NF-kβ	nuclear factor kappa-light-chain-enhancer of activated B cells
NLRP3	Nucleotide-binding oligomerization domain-like receptors family, pyrin domain containing 3
NOD2	Nucleotide-binding oligomerization domain-containing protein 2
OPD	O-Phenylenediamine dihydrochloride
PBMC	Peripheral blood mononuclear cell
PBS	Phosphate buffered saline
PCR	Polymerase chain reaction
PCTE	Polycarbonate
PEG	Poly ethylene glycol
PL-PEG-NH2	Phospholipid polyethylene glycol amine
PTX3	Pentraxin-related protein
PVP	Polyvinylpyrrolidone
qPCR	Quantitative polymerase chain reaction
rhSP-D	recombinant human SP-D
RNA	Ribonucleic acid
ROI	Reactive oxigen intermediate
RPMI	Roswell Park Memorial Institute medium

RQ	Relative Quantification
RT	Room temperature
SAP	Serum amyloid P
SDS-PAGE	Sodium dodecyl sulfate - Polyacrylamide gel electrophoresis
SEM	Scanning electron microscope
SPIO	Superparamagnetic Iron Oxide Nanoparticle
SRBC	Sheep red blood cell
SWNT	Single Walled Carbon Nanotube
Tc	Cytotoxic T-cell
TGF	Transforming growth factor
Th	Helper T-cell
TLR	Toll-like receptor
TNF	Tumor necosis factor
Tyr	Tyrosine
VSM	Vibrating sample magnetometer
WHO	World Health Organisation
XRD	X-ray diffraction